Ph.D. Thesis

Exotic ordering and multipole excitations in anisotropic systems

Judit Romhányi

Thesis Advisor: Karlo Penc

Department of Physics

Budapest University of Technology and Economics

BME

2012

Acknowledgments

I wrote this part in the hope that it would be easy after finishing more than 150 pages. Alas, thanking everybody in a fair way turned out to be nearly impossible.

As a conclusion of my doctoral studies, I would like to express my sincere gratitude to my supervisor Karlo Penc. His kindness and support followed me throughout my Ph.D. I'm indebted to him for the possibility to see a large bit of the world, from the United States to Japan, and I remember the multitude of workshops and conferences we attended together with rejoicing. I'm also honestly grateful to Keisuke Totsuka for his kind hospitality during our three months stay in Kyoto. It feels appropriate to tell how much I appreciate the first year of Ph.D., when I was lucky to be the student of Patrik Fazekas. Although he cannot be with us today, his memory inspires me unceasingly. In the field of magnetism Karlo and Patrik taught me everything I know, yet sometimes I wish they had taught me everything they know.

I feel truly lucky that I had Miklós Lajkó and Annamária (Ani) Kiss as collaborators. They are not only excellent colleagues but also very valuable friends. I prize the jokes and jests of Miklós which made my days at the office really joyful and left me breathless with laughter so many times. I am very happy that I could share my enthusiasm for Japanese culture and language with Ani. The Japanese language summer camps we attended together remain dear and unforgettable memories to me.

I'm very thankful to my friends for their continuous support during these years. Although I couldn't possibly list each one of them here, I have to thank Zsófia Nagy for being there for me all the way. Her persistent encouragement helped me when things were not exactly looking up and I enjoyed immensely the conversations we had – often to all hours. I'm obliged to Péter (Pöcök) Balla for the enlightening discussions and for introducing me, among many others, to Terry Pratchett, of whom I became a huge fan. I am especially grateful to Gøran Nilsen whose friendship I hold very dear. His wits and wonderful sense of humor cheered me more times than I could count. I consider myself very fortunate for meeting him in Trieste four years ago and treasure every day I could spend in his company ever since.

Finally, I will try to express how much I'm indebted to my family for the constant support and love. My gentle and caring Father and my spirited, clever Mother stand as the best role models in my life. I would like to thank Andris for being such a jolly good brother and for believing in me unconditionally. I feel it is impossible to put in words how much I owe to my twin sister Ági. Although we are biologically identical, I firmly believe that she is without an equal. I'm beholden to both of my Grannies for their tireless care, especially to Rozália for the long visits, delicious feasts and endless anecdotes. Going home to them fills me with genuine happiness.

Preface

The study of strongly-correlated electron systems is a rapidly evolving, fundamental area of research in contemporary condensed-matter physics. Its beauty lies where its difficulty does; while the properties of weakly correlated systems can be accounted for by band theory, in strongly correlated materials the interactions between the electrons cannot be treated in a perturbative manner. Most f and d-electron systems provide as worthy examples for the manifestation of strong correlations. As electron-electron interaction becomes important several interesting phenomena; such as metal-insulator transition, or structural distortion can occur, which is often accompanied by magnetic ordering. For instance, in some rare earth heavy fermion superconductors the magnetic order coexists with unconventional superconductivity, manganites exhibit metal-insulator transition, charge or orbital ordering, giant magnetoresistance or ferromagnetic ordering depending on the applied magnetic field and pressure, or organic metals can be tuned between the antiferromagnetic insulator and superconducting phases.

Magnetism, in the traditional sense, means that a given material shows finite magnetization when exposed to an external field and the emerging magnetic order can be explained as a result of small perturbation. In more interesting cases though, a spontaneous magnetization arises without the effect of applied field. Such is the case with magnetite, the very first example in the history of magnetism. In contrast to the deceivingly logical explanation that the ferromagnetic order arises from the tiny atomic dipole moments sitting in each other's magnetic field, spontaneous magnetization has quantum mechanical origins and emerges as a display of strong electron-electron interaction.

Low dimensionality, geometrical frustration, and strong anisotropies add further complications, yet without them the field of condensed matter physics would not be near as rich as it is; on their account a multitude of new novel quantum phases occur: gapless algebraic spin liquids, gapped spontaneous and explicit valence bond solids, their fluctuating analog the resonating valence bond liquid, or nematic phases that are often related to multipolar ordering.

As it usually takes a considerable effort to deal with correlations theoretically, the experimental means to explore the physical properties of strongly correlated systems require in most cases extreme low temperature, high pressure or very high magnetic field, dividing the difficulties equally between theorists and experimentalists. Despite of the remarkable advances in the last couple of decades the thorough understanding of such systems remains a challenging task to this day.

Nonetheless, within this work we attempt to find a minimal, yet sufficient model to study the ground state properties and dynamics of some representatives of the strongly correlated materials. Our investigations are motivated by the cutting edge experiments carried out on the frustrated orthogonal dimer system $SrCu_2(BO_3)_2$ and the multiferroic compound $Ba_2CoGe_2O_7$. This work is structured in the following way: chapter 1 provides a very brief introduction to what we are dealing with here, including the nowadays popular spin liquid, supersolid and multiferroic states

of matter. $SrCu_2(BO_3)_2$ and $Ba_2CoGe_2O_7$ will be discussed in more detail accompanied by experimental results. However, these reviews should not by any means considered to be complete, they merely aim to acquaint the reader with some of the important properties of these substances. Chapter 2 is dedicated to the symmetry considerations; we will classify the order parameters that are later used to identify the appearing phases, and build the suitable Hamiltonians based on symmetry properties. In chapter 3 a short discussion will be given on the mathematical framework of our main approach, the generalized spin wave technique. The following chapters 4, 5 and 6 comprehend the essence of this thesis. They serve as a detailed report of the variational phase diagrams and excitation spectra of the materials in question, including quantitative comparison to the experimental findings where possible. Finally, the last chapter attempts to sum it all up.

Contents

Chapter 1

Introduction

Everything starts somewhere, although many physicists disagree.

– *Terry Pratchett, Hogfather*

Customarily, the quantum theory of solids distinguishes between two dominant phases, the metal and insulator phases. Band theoretical considerations imply that if the number of electrons per unit cell is odd, we necessarily have a partially filled band and a metallic state is formed. While, at even number of electrons, we usually are in a band insulator phase. The arising of spontaneous magnetic order is closely related to the phenomena of metal-insulator transition. When studying substances characterised by narrow conduction band, most of the d- and f-electron systems are such, we often find that what is expected to be a metal behaves as a magnetic insulator instead.

Strong electron-electron correlations in ionic d- and f-electron compounds tend to localize the electrons onto the ions, inducing a metal-insulator transition even in a half-filled band. This correlation-driven collective localization of the electrons is the Mott transition.[1] The simplest many-body Hamiltonian which includes the spin degrees of freedom and grasps the essential aspects of the ongoing physics is the Hubbard model. It has been introduced basically at the same time by Gutzwiller, Hubbard, and Kanamori [Gutzwiller 1963, Hubbard 1963, Kanamori 1963]

$$\mathcal{H} = -t \sum_{\langle i,j \rangle} \sum_{\sigma} (c^{\dagger}_{i\sigma} c_{j\sigma} + \text{h.c.}) + U \sum_{j} \hat{n}_{j\uparrow} \hat{n}_{j\downarrow} \,. \tag{1.1}$$

The first term represents the kinetic energy of the electrons which favors the itinerant Bloch states, thus a metallic ground state. The second term stands for the electron-electron interaction which is approximated as the on-site Coulomb repulsion that wants to localize the electrons onto the ions, thus inducing a Mott insulator state. At half filling, when we consider one electron with a spin $\uparrow$ or $\downarrow$ per lattice site, the electrons become localized when the Coulomb repulsion is large enough and the Mott insulator ground state emerges. In this limit, various low-energy effective spin Hamiltonians can be used to describe the subsequent magnetic ordering depending on the interactions of the underlying fermionic model. Starting from (1.1), in the

[1] We shall emphasis however, that strong interaction between the electrons is not necessarily enough to induce a Mott insulator state, the band filling for example plays a crucial role. Fractional filling arising from doping and the overlapping of bands might stabilize metallic states even when the correlations are strong.

limit $U/t \to \infty$ and at exactly half filling, the effective spin Hamiltonian is the celebrated Heisenberg model

$$\mathcal{H} = J \sum_{\langle i,j \rangle} \mathbf{S}_i \cdot \mathbf{S}_j \ , \tag{1.2}$$

with the parameter $J = 4t^2/U$. The expression (1.2) is the result of a second order perturbation in t, however going further, e.g. to the fourth-order terms, we will find next nearest neighbour interactions and terms that are higher order in spin operators, such as the plaquette exchange. Had we begun with a degenerate Hubbard model which is suitable to describe materials with higher ($S > 1/2$) spins, even more terms become possible to include. For instance the fourth-order process can bring in the nearest neighbour biquadratic interaction $\sim (\mathbf{S}_i \mathbf{S}_j)^2$.

The interplay between spin and orbital orderings can lead to ferromagnetic exchange coupling due to Hund's rule, according to which spins tend to align parallel on partially filled atomic levels.[2]

The relativistic spin-orbit interaction couples the direct space with the spin space leading to the emergence of anisotropies which can be deduced from microscopic models as e.g in Ref. [Moriya 1960] or on the basis of symmetry considerations as shown in Ref. [Dzyaloshinsky 1958].

Once the suitable Hamiltonian is derived, numerous techniques can be carried out to investigate the physical properties of the given system; mean field theory and spin wave approximation are widely known examples and will be used as the main apparatuses in this work. Depending on the details of the interactions, the geometry of the lattice and the lengths of the participating spins, many different ground states can occur. Some of these are possible to understand classically, while there are other, more interesting, states of matter which are essentially of quantum mechanical origins.

In most of the situations, below a critical temperature, the system exhibits magnetic long range order. That is, the relative orientation of the spins does not change even at large distances. For instance, such magnetically ordered state is the helical state with the correlation function

$$\langle \mathbf{S}_i, \mathbf{S}_j \rangle \sim m_s^2 \cos(\mathbf{q}(\mathbf{r}_i - \mathbf{r}_j)) \ . \tag{1.3}$$

The pitch vector $\mathbf{q}$ can be determined by minimizing the Fourier transform of the coupling constant $J(\mathbf{k}) = \sum_j J e^{i\mathbf{k}(\mathbf{r}_i - \mathbf{r}_j)}$. As special cases, ferromagnetic and antiferromagnetic order can be described by $\mathbf{q} = \mathbf{0}$ and $\mathbf{q} = (\pi, \pi, \pi)$, respectively. In the classical limit, choosing $\mathbf{S}_j = (S\cos(\mathbf{q} \cdot \mathbf{r_j}), S\sin(\mathbf{q} \cdot \mathbf{r_j}), 0)$, we can write $\mathbf{S}_i \cdot \mathbf{S}_j = S^2 \cos(\mathbf{q}(\mathbf{r}_i - \mathbf{r}_j))$ and the quantum fluctuations can be accounted for in the

[2] When there is only one orbital degree of freedom, the hopping of electrons with parallel spins onto the same atom is forbidden by Pauli's principle. However, if we have more than one orbital states, the electrons can occupy the same lattice point with parallel spins, which is in fact favoured by Hund's rule reducing the intra-atomic Coulomb repulsion compared to an antiparallel spin configuration.

context of a $1/S$ expansion, vanishing as the spin length $S \to \infty$ [Mila 2000]. Conventionally, spin wave theory provides a systematic method to calculate the quantum fluctuations whenever a classical long range order is realized as the ground state. These magnetic orders spontaneously break the spin rotational invariance, resulting in the appearance of a Goldstone mode which corresponds to a gapless excitation. To illustrate this dynamical property, in Fig. 1.1 we show the neutron spectroscopy measurement along with the spin wave result for La_2CuO_4 [Coldea 2001] which is a fairly isotropic Heisenberg antiferromagnet with next nearest neighbour coupling and plaquette exchange.

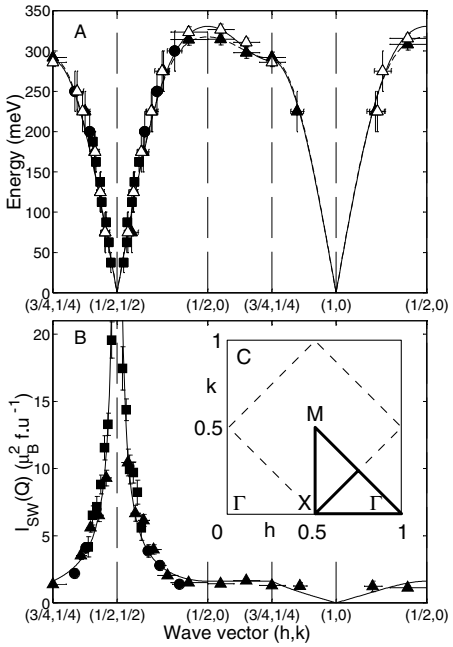

Figure 1.1: (a) Dispersion relation of the $S = 1/2$ square lattice Néel antiferromagnet La_2CuO_4 along high symmetry directions measured by neutron scattering at $T = 10$ K (open symbols) and at $T = 295$ K (solid symbols). The solid line corresponds to spin wave dispersion relation. (b) Wave vector dependence of the spin wave intensity at $T = 295$ K compared with the prediction of linear spin wave theory shown by solid line [Coldea 2001].

The presence of anisotropy, in most cases easy-axis anisotropy, can lift the continuous degeneracy of the ground state, inducing a gap in the excitation spectrum. In the case of easy-plane anisotropy the spins are confined in the 'easy' plane with a relative angle determined by the exchange interactions. Their collective rotation in the plane, however, does not cost energy, therefore we expect the presence of a gapped and a gapless (Goldstone) mode. Typically antiferromagnetic bipartite lattices are of this kind with quite a few physical realizations.

Further investigations lead to the question whether (isotropic) Heisenberg mod-

els with antiferromagnetic exchange couplings can exhibit collective spin states of different kind. In fact, we find many examples where the ground state has quantum mechanical character, i.e. it has no classical analogue. These disordered states usually do not break the spin rotational symmetry, in contrast to the magnetically ordered phases.

We shall point out that the nature of (quantum) antiferromagnetism and ferromagnetism is fundamentally different. Taking a finite system of spins coupled antiferromagnetically, it turns out that the Néel state is not even an eigenstate of the Hamiltonian (1.2). Rather, the ground state is a singlet ($S_{\text{tot}} = 0$) in which $\langle S_j^\alpha \rangle = 0$ for any spin component α and for all sites j. Inspecting a ferromagnetic cluster on the other hand, retains the expected nature of aligned spins; the ground state is the fully polarized state similarly to an infinitely large system. The explanation for the difference between the world of antiferromagnets and ferromagnets can be understood by considering the order parameters. The ferromagnetic order parameter S_{tot}^z commutes with the Hamiltonian (1.2) indicating that these two operators can be diagonalized simultaneously. However, the antiferromagnetic order parameter, that is, the staggered magnetization $\sum_{i\in A} S_i^z - \sum_{j\in B} S_j^z$, does not commute with $\mathcal{H}$, the alternating antiferromagnetic order cannot be the ground state (or any eigenstate). The Néel order can only be realized in an infinitely large system. Although, one has to be aware that even in the thermodynamical limit, antiferromagnetic interactions do not necessarily lead to antiferromagnetic ground states; there are examples where the singlet ground state is manifested even for an infinitely large system.

A natural way of constructing non-magnetic quantum ground state is covering the lattice with the singlet state of spin pairs. This state is known as the valence-bond solid (VBS) that usually breaks the translation invariance of the lattice. VBS states are characterised by exponentially decaying correlation function

$$\langle \mathbf{S}_i \mathbf{S}_j \rangle \sim S^2 e^{-|\mathbf{r}_i - \mathbf{r}_j|/\xi} \tag{1.4}$$

where ξ is the correlation length. VBS states regularly exhibit spin gap to the lowest lying magnetic excitations which can be of different nature.

In the J_1-J_2 antiferromagnetic spin-half chain the next nearest neighbour coupling J_2 introduces frustration and a two-fold degenerate, translational symmetry breaking dimer singlet ground state is realized [Majumdar 1969] as illustrated in Fig. 1.2(a). The $S = 1/2$ chain is characterized by fractional excitations, the so called spinons which are neutral in charge and carry a spin $S = 1/2$. The spinons are gapped for they are excited via the breaking of a singlet bond. The integer-spin Heisenberg chain, or in other words the Haldane chain, however, exhibits a singlet ground state that does not break the translational invariance (see Fig. 1.2(b)) and the excitations are gapped $S = 1$ magnons.

In two dimensional systems VBS states can arise spontaneously when third nearest neighbour coupling or ring-exchange is present, forming ground states of dimer- or plaquette-singlet covering of the lattice. Fig. 1.2(c) shows a possible realization of spontaneous VBS state on a square lattice. Among the two dimensional systems

the Shastry-Sutherland model provides a unique example with 'explicit' VBS state, where the dimer covering of the lattice is straightforward as shown in Fig. 1.2(d). It is worth to mention that this dimer singlet state does not break the translational symmetry of the lattice, therefore, in a broader sense we can think about it as a spin liquid state.

Spin gaps were found for example in the spin-1 Haldane chain Y_2BaNiO_5 [Darriet 1993], in one-dimensional dimerized $S = 1/2$ systems such as $CuGeO_3$ [Hase 1993a] and Sr_2CuO_3 [Motoyama 1996], or in the quasi two-dimensional compound CaV_4O_9 which attracted much interest as the origin of the observed spin gap might be a resonating plaquette order [Taniguchi 1995]. A very recent and remarkable example is the quasi two-dimensional orthogonal dimer compound $SrCu_2(BO_3)_2$ [Kageyama 1999a] which is the experimental equivalent of the Shastry-Sutherland model. $SrCu_2(BO_3)_2$ provides as one of the main subjects of our investigations and will be introduced in more detail, although without the aim of completeness, in the upcoming sections. When the quantum fluctuations allow for the transition between different singlet coverings we can speak of valence bond 'liquid', or as usually referred to, resonating valence bond (RVB) state [Anderson 1973] which can be thought of as a superposition of various valence bond configurations. While VBS states, aside from some exceptions, break the translational symmetry the RVB state does not, therefore one can think about it as a spin liquid state that is characterized by exponentially decaying spin-spin correlations and exhibit translational invariance. The bonds belonging to sites far from each other are weaker, thus breaking them leads to the appearance of low lying excitations. However, quantum spin liquids support other, more exotic excitations with fractional quantum number. Such is the already introduced spinon, that can appear in the system when one spin is not paired in a valence bond and can move at low energy cost by adjusting the surrounding valence bonds (see Fig. 1.2(e)). RVB states were studied in terms of dimerized square and triangle lattices, however an experimental realization is yet to be found.

Frustration, i.e. the inability of the system to simultaneously satisfy the competing interactions, enhances fluctuations and supports the emergence of a quantum spin liquid state. The prototype of frustrated systems was the antiferromagnetic triangular lattice with Ising-like spins, where after aligning two spins on a triangle oppositely, we cannot set the direction of the third spin so that all the bonds have antiparallel spins. The system can exhibit a macroscopic number of equally 'bad' ground states, the fluctuations become more important and the magnetic order is suppressed. As a consequence, a residual entropy characterises the frustrated systems. Frustrated lattices built of triangular motifs, such as the triangular, kagomé, hyperkagomé or pyrochlore lattices with $S = 1/2$ spins are promising candidates to realize spin liquid state.

The experimental detection of quantum spin liquids is rather challenging as they are characterized by properties they do not show, as in long range order or symmetry breaking. Nonetheless, nuclear magnetic resonance and muon spin resonance measurements can test whether there is ordering down to very small temperatures,

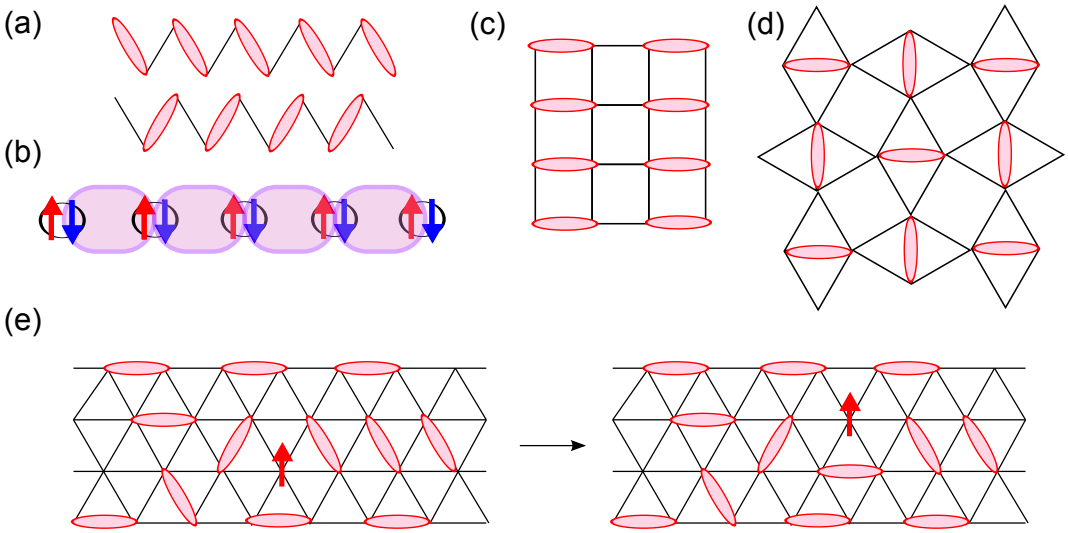

Figure 1.2: (a) The doubly degenerate Majumdar-Ghosh ground state of the $S = 1/2$ Heisenberg chain with antiferromagnetic nearest and next nearest neighbour couplings. (b) The Haldane state of an $S = 1$ Heisenberg chain which can be constructed by breaking the $S = 1$ state into two spin-halves, each of which participate in a singlet with one of the $S = 1/2$ spins of the neighbouring lattice point. In this way a translational invariant singlet covering of the chain is achieved. (c) A possible dimer-singlet configuration on the square lattice. (d) The Shastry-Sutherland lattice with the explicit VBS state. Here the singlet covering is unambiguous. Panel (e) shows one of the VBS configuration in the RVB state of a triangular lattice with a spinon (neutral spin-half) excitation that can propagate almost freely via the rearranging of the dimer configuration into a new one that is already superposed in the RVB state.

if not, the spin liquid state can be present, although by no means conclusively. Comparing the low temperature susceptibility measurements to the theoretically predicted exponentially vanishing form of $\chi \sim e^{-\Delta/k_B T}$ can also give us a hint. Furthermore, neutron scattering can reveal the nature of correlations and excitations, with a possible detection of spinons.

The spin-half antiferromagnetic kagomé lattices, such as $ZnCu_3(OH)_6Cl_2$ (herbertsmithite) [Helton 2007, Olariu 2008, Zorko 2008, de Vries 2009], $Cu_3V_2O_7(OH)_2 \cdot 2H_2O$ (volborthite) [Bert 2005, Yoshida 2009, Nilsen 2011] and $Cu_3Ba(VO_5H)_2$ (vesignieite) [Quilliam 2011, Colman 2011], the $S = 1/2$ organic triangular lattice κ-(BEDT-TTF)$_2$Cu$_2$(CN)$_3$ [Shimizu 2003] and the spin-half hyperkagomé compound $Na_4Ir_3O_8$ [Okamoto 2007] are possible candidates for experimental realization of the quantum spin liquid state, although the complete clarification of the ground states of these materials remains the subject of further investigations.

In this work we study the physical properties of two compounds: the above mentioned orthogonal dimer system, $SrCu_2(BO_3)_2$ and the strongly anisotropic spin-3/2 multiferroic material $Ba_2CoGe_2O_7$. While the former shows an interesting dimer singlet ground state and is characterised by a spin gap of quantum mechanical origin, the latter exhibits a magnetic long range order [Miyahara 1999], where the spins are aligned antiferromagnetically in the cobalt plane due to the strong easy-plane anisotropy [Zheludev 2003]. Although $Ba_2CoGe_2O_7$ seems to be less interesting at first glance, we will show that due to its non-centrosymmetric crystal structure, the strong anisotropy and the large spins, peculiar high energy excitations can occur in this compound. As we will see, the larger Hilbert space of a spin $S = 3/2$ allows for quadrupole and octupole degrees of freedom, and as a consequence of the lack of inversion symmetry the electric polarization can directly couple to quadratic spin operators (i.e. quadrupoles). It will be shown that the higher order excitations observed in the light absorption spectrum are electromagnons, in other words magnetic excitations active for the electric component of the exciting light.

In the following sections we give a brief introduction to these materials introducing, by no means all, the main experimental and theoretical work that has been done so far. A section will be devoted to the introduction of the magnetic supersolid state which will be discussed in terms of bipartite lattices with anisotropic interactions in chapter 5.

Our general strategy is the following: we build the Hamiltonian according to the symmetry properties as detailed in chapter 2 then we map out the variational phase diagram and based on the variational ground state using the generalized spin wave approach of chapter 3 we calculate the dispersion relation and the field dependent excitation spectrum. When possible we compare our findings with the experimental results.

1.1 The Shastry-Sutherland model and its physical analogue: $SrCu_2(BO_3)_2$

Based purely on theoretical interest, the Shastry-Sutherland model was constructed more than 30 years ago, following the example of the spin-1/2 zig-zag Heisenberg chain with antiferromagnetic nearest (J) and next nearest (J') neighbour interactions [Shastry 1981]. In the zig-zag model at $J'/J \approx 0.2411$ a quantum phase transition takes place [Okamoto 1992] and above this critical point the ground state is nonmagnetic, characterized by a spin gap. In particular, when $J'/J = 0.5$ the Hamiltonian can be rewritten as the sum of terms that measure the total spin of three consecutive sites and the Hamiltonian becomes minimal when every other spin-pair forms a singlet. This two-fold degenerate dimer singlet ground state is called the Majumdar-Ghosh state [Majumdar 1969] and is illustrated in Fig. 1.2(a). The Shastry-Sutherland model is the two dimensional analogue to the spin-half Heisenberg chain. Conveniently, one can think about it as a model, built of corner and edge sharing triangles of $S = 1/2$ spins, in which the singlet bonds occur along

the shared edges as shown in Figs. 1.2(d) and 1.3(a,b). The singlet dimers form an orthogonal network which, as we will see, is responsible for many of the interesting physical properties of this system.

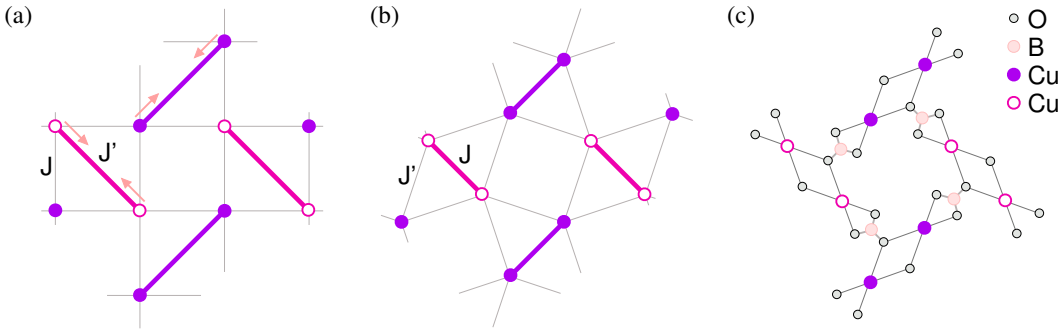

Figure 1.3: (a) The original Shastry-Sutherland model which is in fact a square lattice where one of the diagonal couplings is present on every second square. The pink arrows along the diagonals represent the shortening of these bonds that leads to the topologically equivalent orthogonal dimer model of (b). Note that the role of first and second neighbour interactions is reversed compared to the original model. (c) The schematic figure of the $CuBO_3$ layer. The different colouring of the Cu^{2+} ions means only to distinguish between the orthogonal dimers so that it is easier to associate with the theoretical model shown in panel (b).

The Hamiltonian of the Shastry-Sutherland model has the form

$$\mathcal{H} = J \sum_{n.n.} \mathbf{S}_i \cdot \mathbf{S}_j + J' \sum_{n.n.n.} \mathbf{S}_i \cdot \mathbf{S}_j \ , \tag{1.5}$$

where J represents the first and J' the second nearest neighbour interaction. In the case of $J' = 0$ the model is reduced to a lattice of independent dimers, where the ground state is the product of dimer-singlets. Due to the particular geometry of the lattice, the singlet product state is an exact eigenstate of the Hamiltonian (2.13) even for finite values of the J' [Shastry 1981].
An experimental realization, the quasi two-dimensional antiferromagnetic compound $SrCu_2(BO_3)_2$ [Kageyama 1999a], was found almost two decades after the construction of the Shastry-Sutherland model. This compound has tetragonal unit cell and is characterized by the alternating layers of $CuBO_3$ molecules and Sr^{2+} ions. In the former, the magnetic spin-1/2 Cu^{2+} ions occupy crystallographically equivalent sites and form a lattice of orthogonal dimers. These dimers are connected by triangular-shaped BO_3 molecules as shown in Fig. 1.3(c) [Smith 1991, Kageyama 1999a]. Magnetic susceptibility measurements, NMR relaxation rate and magnetization measurements indicated the presence of a spin-singlet ground state with a gap of about 30 K. [Kageyama 1999a] as shown in Fig. 1.4(a).

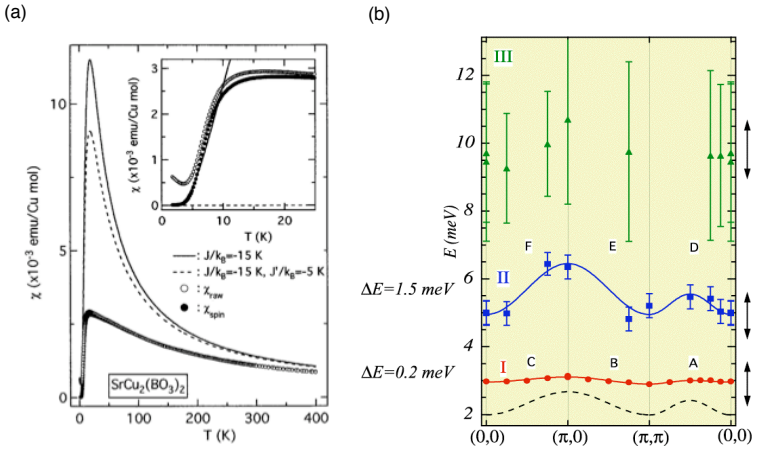

Figure 1.4: (a) Magnetic susceptibility measurement in Ref. [Kageyama 2000]. At low temperature we can observe the exponentially vanishing susceptibility that is an indicator of the spin liquid ground state. From fitting $e^{-\Delta/k_BT}$ one can estimate a spin gap of 30 K. (b) Momentum dependence of the excitations observed by neutron scattering at 1.7 K. Form Ref. [Kageyama 2000]. The triplet excitations, shown by red line and labelled as I, have almost completely flat dispersion.

Miyahara and Ueda showed that the $SrCu_2(BO_3)_2$ can be satisfyingly described by the Shastry-Sutherland model.[3] Performing variational calculations and exact numerical diagonalization they determined the quantum critical point $(J'/J)_c = 0.7$ that separates the singlet dimer phase and the magnetically ordered Néel state. Furthermore, using the experimental findings of Ref. [Kageyama 1999a] they estimated the Heisenberg couplings to be $J = 100$ K and $J' = 68$ K which gives $J'/J = 0.68$, placing the $SrCu_2(BO_3)_2$ in the vicinity of the transition point [Miyahara 1999].

Later works, such as series expansion [Koga 2000] and numerical exact diagonalization [Läuchli 2002a] suggested the presence of a new plaquette-singlet phase between the singlet and antiferromagnetic phases, furthermore that the transition from the dimer phase to the plaquette-singlet occurs at $(J'/J)_c = 0.68$. The coupling constants have also been updated to $J = 7.3$ meV with $J'/J = 0.635$ [Miyahara 2000] and $J = 6.16$ meV with $J'/J = 0.603$ [Knetter 2000]. A word should be added on the interlayer coupling J'' which is present in the real compound additionally to the intraplane interactions J and J'. The distance between the interlayer coppers is shorter than that of the next nearest neighbour distance in the plane, however, the super-exchange of J' is realized through the molecular orbital of the BO_3 triangles (as shown in Fig. 1.3(c)) while the $CuBO_3$ layers are well isolated by the Sr^{2+} ions which have closed shell. Therefore, we expect the interlayer coupling J'' to be negligible compared to J'.

[3] In the following by Shastry-Sutherland model we mean the orthogonal dimer model in Fig. 1.3(b) and not the original model.

One of the unusual properties of the $SrCu_2(BO_3)_2$ is the localized nature of its excitations. Early neutron scattering measurements revealed an essentially dispersionless single-triplet branch, indicating that the lowest excitations are almost completely localized. On the other hand, higher- energy excitations exhibit a dispersive character [Kageyama 2000] as shown in Fig. 1.4(b). Perturbational approach, performed in the dimer-singlet state, suggested that the hopping of triplet excitations occurs only in the sixth order of J'/J [Miyahara 1999, Miyahara 2003]. The localized property of the triplet excitations is strongly related to the formation of plateau states. At certain values of the magnetization the excitations localize into a superlattice structure to minimize the energy [Miyahara 1999]. Momoi and Totsuka [Momoi 2000a, Momoi 2000b] explained the emergence of such states in the context of Mott-insulator transition where the triplet excitations were regarded as interacting bosonic particles. In this scenario, at dominant repulsive interaction, the triplet excitations crystalize into commensurate patterns, into so called superlattices, developing the plateau states. Experimentally the first plateaus have been observed

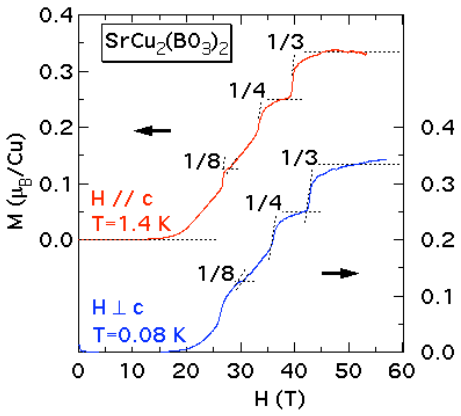

Figure 1.5: Magnetization plateaus measured in Ref. [Kageyama 2002]

in high field magnetization measurements at the 1/8th, 1/4th [Kageyama 1999a, Kageyama 1999b] and later at the 1/3rd [Onizuka 2000, Kageyama 2002] of the saturated magnetization. Uniquely, these plateau states break the translational symmetry of the lattice. The theoretically expected superlattice structure at the $m/m_{\mathrm{sat}} = 1/8$ plateau has been confirmed directly by NMR spectroscopy [Kodama 2002]. More recent theoretical works suggested the presence of new magnetization plateaus. Non-perturbative Contractor–Renormalization (CORE) method predicted plateaus at 1/9, 1/6 and 2/9 of the saturation [Abendschein 2008], and perturbative continuous unitary transformation (PCUT) analysis [Dorier 2008] at $m/m_{\mathrm{sat}} = 2/15$.

In the past few years various experiments were carried out aiming at a better understanding of excitations in $SrCu_2(BO_3)_2$. Inelastic neutron scattering measurements [Cépas 2001], electron spin resonance (ESR) [Nojiri 1999], and Raman scat-

tering [Gozar 2005] revealed anisotropic behavior, in contrast with the the Shastry-Sutherland model (2.13) which is fully isotropic in spin space. The experimentally observed Γ-point splitting of the triplet excitations suggested the presence of the out-of-plane interdimer Dzyaloshinskii-Moriya (DM) interaction [Cépas 2001]. The other, $\mathbf{q} = (\pi, 0)$, splitting observed with higher-resolution neutron scattering [Gaulin 2004] (see Fig. 1.6(a)) and the anti-level crossing at the critical magnetic field[4] detected with ESR spectroscopy [Nojiri 2003], posed the relevance of the in-plane components of the DM interaction (Fig. 1.6(b)). These splittings and the

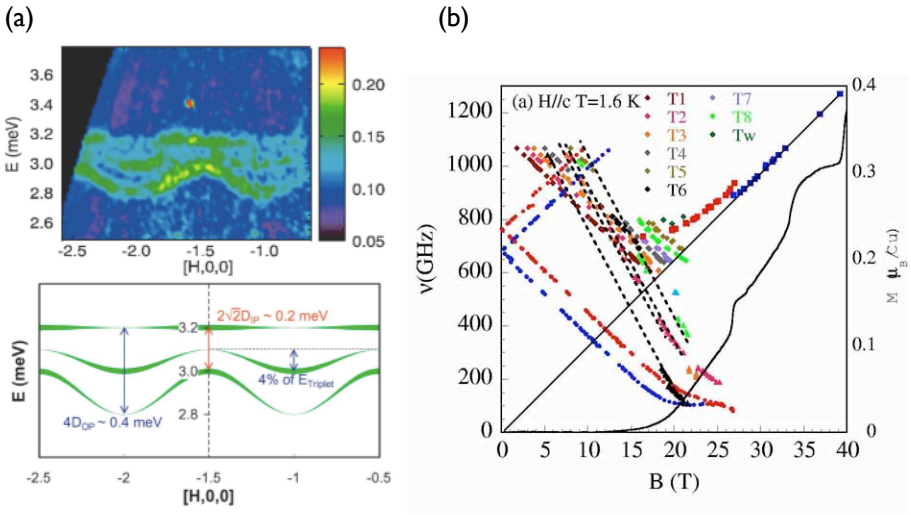

Figure 1.6: (a) High resolution neutron spectroscopy measurement form Ref. [Gaulin 2004]. The triplet excitations split even in zero magnetic field indicating the presence of anisotropy. (b) ESR measurement of Ref. [Nojiri 2003] confirmed the zero field splitting of the triplet excitations, furthermore it indicated an anti-level crossing about the critical field that implies the presence of an in-plane DM coupling.

anti-level crossing mean that states of different symmetry properties, i.e. singlets and triplets, are mixed in the ground state and S^z is no longer a good quantum number. A finite intradimer anisotropy, such as the intradimer DM vector, can account for such mixing of triplet and singlet states.

An enthusiastic reader may find more detailes on the Shastry-Sutherland model and $SrCu_2(BO_3)_2$ in the reviewing articles Ref. [Miyahara 2003] from a theoretical point of view and in Ref. [Takigawa 2010] regarding the experiments.

[4]This denotes the point in the magnetic field at which the lowest-lying triplet excitation would cross the singlet level.

1.2 The multiferroic $Ba_2CoGe_2O_7$

Conventionally, in multiferroic materials the ferroelectric and ferromagnetic long-range order is simultaneously realized [Fiebig 2005, Cheong 2007, Arima 2011]. The quest to discover materials, in which magnetism and ferroelectricity coexists, is fueled by the idea of spintronic devices, in other words the possibility to control spins by applied voltages, or electric charges by external magnetic field. Due to the fact that a ferroelectric order breaks the (space) inversion symmetry but it is invariant under time-reversion while a magnetic order behaves in the opposite way, the concurrent presence of electric and magnetic order is rather difficult. Additionally, the coupling between these two order parameters proves to be very weak. After almost fifty years, the discovery of the giant magnetoelectric response in $TbMnO_3$ [Kimura 2003] has launched a new concept, namely the spin driven ferroelectricity. The ferroelectricity induced in complicated spin structures is much smaller than a usual ferroelectric order in ferroelectrics, besides the magnetoelectric interaction is weak, yet the cross-coupling effects are strong due to the sensibility of the magnetic order, and subsequently the induced electric polarization, to the applied magnetic field.

Recently, new theoretical explanations have been suggested as the source of such phenomena. Electric polarization induced by noncollinear chiral spin configuration was explained through 'spin chirality' [Katsura 2005] or inverse Dzyaloshinskii-Moriya mechanism [Sergienko 2006], alongside with the experimental realizations such as $TbMnO_3$ [Kimura 2003], $Ni_3V_2O_8$ [Lawes 2005], $CuFeO_2$ [Kimura 2006], $MnWO_4$ [Taniguchi 2006], $CoCr_2O_4$ [Yamasaki 2006], $LiCu_2O_2$ [Park 2007] and CuO [Kimura 2008]. Exchange striction was shown to be the origin of electric polarization in the case of the perovskite $R MnO_3$ materials [Mochizuki 2010], with R being a rare earth ion. This and spin chirality may induce polarization jointly, as predicted in the case of $R Mn_2O_5$ materials [Chapon 2006, Noda 2008, Fukunaga 2009]. The aforementioned mechanisms all involve a pair of spins, however, in materials that are non-centrosymmetric, the spin dependent metal-ligand hybridization [Jia 2006, Jia 2007] has been proposed to induce polarization involving a single spin. Murakawa and collaborators suggested that this mechanism explains the induced ferroelectric polarization in $Ba_2CoGe_2O_7$ [Murakawa 2010].

The reviewing articles Refs. [Cheong 2007] and [Arima 2011] provide a committed reader with additional information on multiferroics.

$Ba_2CoGe_2O_7$ is a quasi two-dimensional material, characterized by layers of square lattices formed by the magnetic Co^{2+} ions [Zheludev 2003, Sato 2003, Yi 2008]. As the neighboring cobalts are positioned in differently oriented tetrahedral environments of four oxygen atoms, the unit cell contains two of them. A schematic view of the cobalt layer in $Ba_2CoGe_2O_7$ is shown in Fig. 1.7. The magnetization measurements performed in fields applied parallel and perpendicular to the cobalt layers indicated the presence of anisotropy. The magnetization curves, shown in Fig. 1.8, reveal that for a field setting parallel to the plane, the magnetization is twice as big as in the perpendicular field direction [Sato 2003].

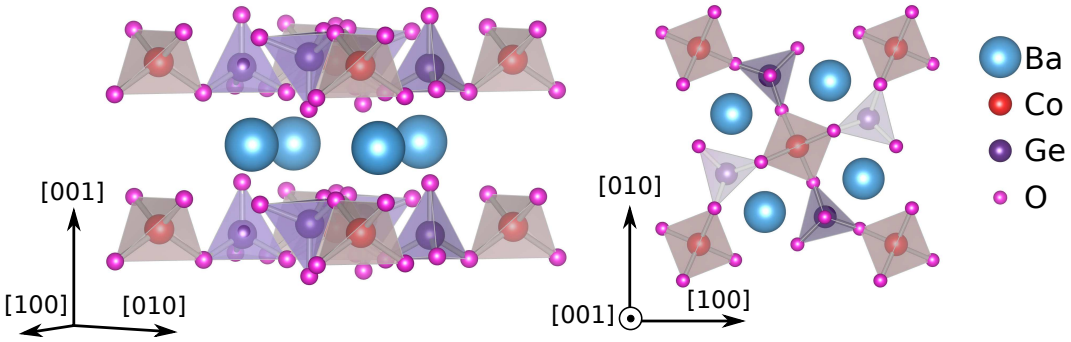

Figure 1.7: The crystal structure of $Ba_2CoGe_2O_7$. The cobalt ions are surrounded by the tetrahedra of four oxygens thus violating the inversion symmetry and allowing for a direct coupling between the spin and polarization of the CoO_4 complexes. (The crystal structure was constructed with VESTA using the lattice and structure parameters of Ref. [Hutanu 2011])

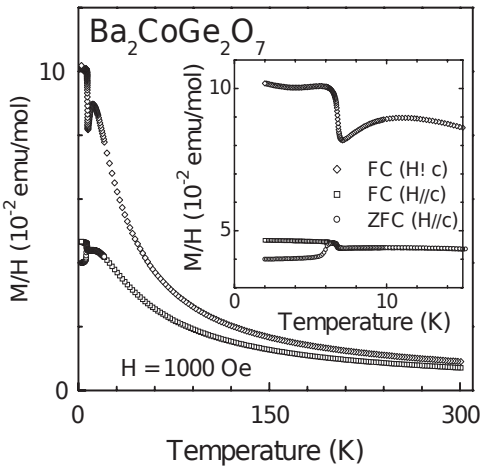

Figure 1.8: The temperature dependence of magnetization measured in Ref [Sato 2003]. Below 6.7 K there is a phase transition to the planar antiferromagnetic phase, in which the multiferroic behaviour is realized.

As a result of strong easy-plane anisotropy, below $T_N = 6.7$ K the $S = 3/2$ moments order into a canted antiferromagnetic pattern that is confined in the Co–plane [Zheludev 2003]. This canted planar antiferromagnetic phase is in fact a multiferroic phase, in which magnetoelectric behavior has been observed. Ascribed to the symmetry properties of $Ba_2CoGe_2O_7$ the sum over the vector

spin chirality $\mathbf{S_i} \times \mathbf{S_j}$ vanishes and the exchange interaction $\mathbf{S_i} \cdot \mathbf{S_j}$ is uniform for all the bonds. Therefore the induced polarization cannot be explained by the concept of spin chirality or exchange striction as it was the case in the previously listed frustrated spin systems with complex magnetic order. The spin dependent hybridization mechanism, however, recovers the sinusoidal response of electric polarization to the rotating magnetic field and describes the nature of induced polarization in magnetic field qualitatively well [Murakawa 2010]. The experimental results are shown in Fig. 1.9. In this scenario, due to the spin-orbit coupling, the spin state of the cobalts determine the hybridization between the O^{2-} and Co^{2+} ions. The local polarization takes the form of $\mathbf{P} \propto \sum_{i=1}^{4} (\mathbf{S} \cdot \mathbf{e_i})^2 \mathbf{e_i}$, where $\mathbf{e_i}$ vectors point from the Co^{2+} ions toward the surrounding four O^{2-} ions. On the other hand, the spin-dependent hybridization model does not capture

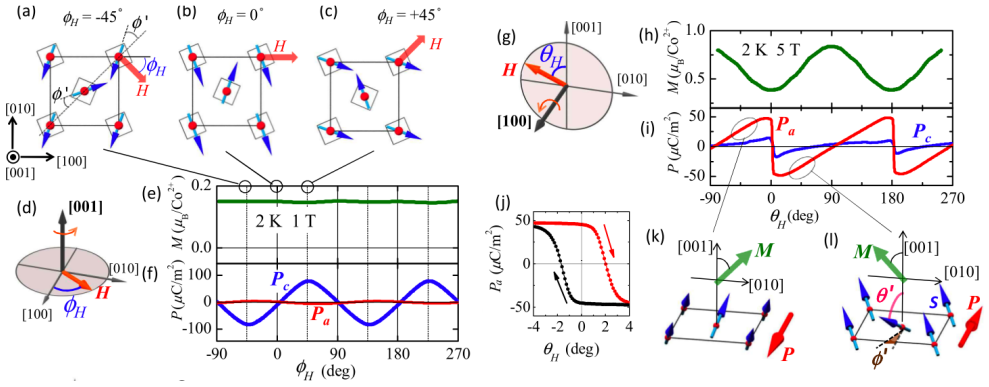

Figure 1.9: Panels (a)-(c) illustrate the canted AFM states for a rotating field about the [001] direction as shown in (d). (e) and (f) reveals the modulation of the in-plane component of the magnetization and polarization, respectively. (h) and (i) displays the angular dependence of the in-plane magnetization and polarization when the external field is rotating about the [100] axis as indicated in (g). (j) represents the hysteresis of P_a in the vicinity of $h||[001]$, finally a schematic figure of the canted AFM spin state and the induced polarization is shown in (k) and (j) under out-of-plane field setting. (From Ref. [Murakawa 2010])

the curious field and temperature dependence of the magnetization and induced polarization measured in Ref. [Murakawa 2010]. In external magnetic field applied parallel to the [110] axis, the magnetization hardly changes with the temperature (Fig. 1.10(b)), while the induced polarization drastically does so (Fig. 1.10(c)).

The zero field dispersion relation has been measured by means of inelastic neutron scattering and explained through an effective model which, based on the strong easy-plane anisotropy, introduces effective spin-1/2 objects corresponding to the lowest-energy Kramers doublets of the Co^{2+} ions [Zheludev 2003]. The neutron spectrum and the calculated low energy excitations are shown in Fig. 1.11.

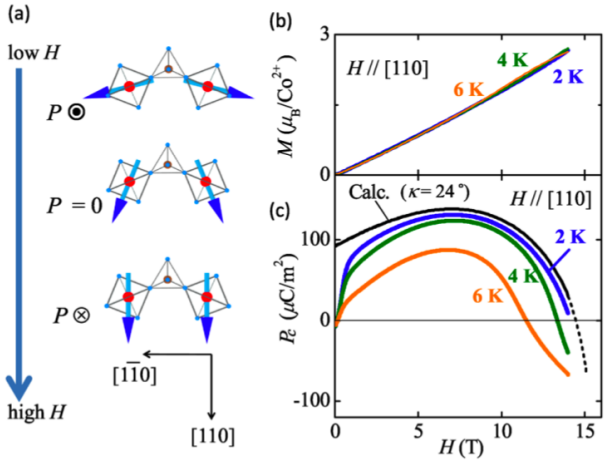

Figure 1.10: (a) The illustration of spin configuration and induced polarization for increasing $h||[110]$. (b) and (c) reveals the field dependence of the magnetization and electric polarization for various temperature values. (From Ref. [Murakawa 2010])

Although the low-energy physics, that is the excitations at 0 and ≈2 meV, can

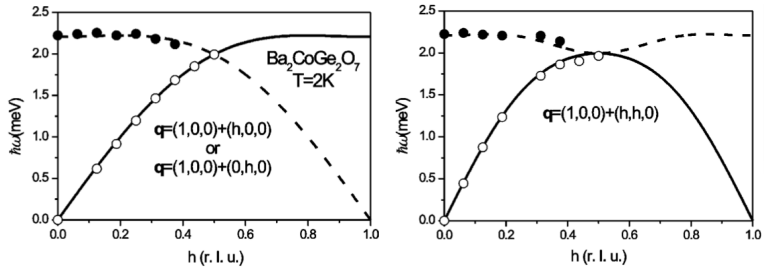

Figure 1.11: The zero field dispersion along the (100) and (110) reciprocal-space direction at $T = 2$ K. The solid and dashed lines indicate the two modes obtained from spin wave calculation starting from the effective model (Ref. [Zheludev 2003])

be satisfyingly described via the anisotropic effective spin-1/2 model proposed in Ref. [Zheludev 2003], as well as the spin-dependent hybridization can account for the periodic modulation of induced electric polarization under a rotating external field, there are properties yet to understand. As it turns out, there are higher energy excitation that cannot be described by the magnons of a conventional spin wave theory. Recent optical spectroscopy measurements suggested that the excitation observed at about 4 meV is in fact a so called electromagnon [Kézsmárki 2011], i.e. a magnetic excitation active for the electric component of the exciting electromagnetic field. A systematic measurement for different sets of electromagnetic polarisations (E^ω, H^ω) revealed the selection rules for the different modes. At zero external field, two distinct absorption bands, at about 0.5 and 1 THz, can be ob-

served. The strength of the 0.5 THz mode is independent of the orientation of the exciting electric polarization, the 1 THz mode, however, is sensitive to both the magnetic and electric components of the exciting light, as indicated in Fig. 1.12. This tells us that the lower mode has a dominant magnetic character, while the 1 THz mode is excited by the electric and magnetic components of the light at the same time. Therefore we can say that this higher energy magnetic excitation, being electrically active, corresponds to an electromagnon.

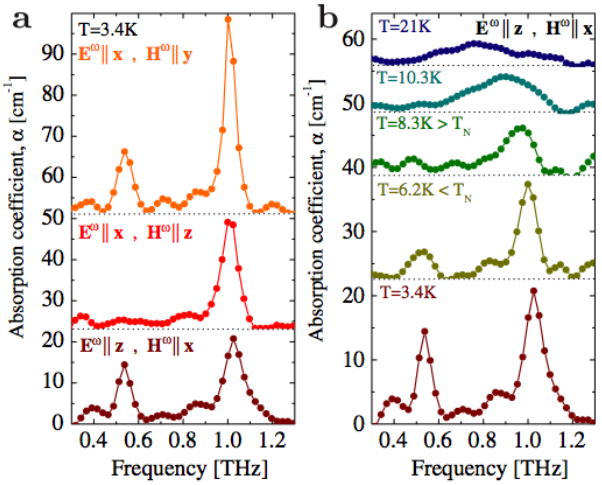

Figure 1.12: (a) Electromagnetic polarization dependence of the absorption spectrum in zero external magnetic field from Ref. [Kézsmárki 2011]. The 0.5 THz mode is excited by the magnetic H^ω component of the exciting light and is insensitive to the electric component E^ω, while the 1 THz mode is affected by both components, H^ω and E^ω. (b) The temperature dependence of the modes. The purely magnetic excitation disappears above the Néel temperature $T_N = 6.7$ K. The electromagnon, however survives even at about 20 K.

In chapter 6 we will discuss the properties of induced polarization in the multiferroic phase, with distinct heed to the effect of Dzyaloshinky-Moriya interaction, reproducing quantitatively the findings of Ref. [Murakawa 2010]. Based on variational approach and generalized spin wave technique, which will be introduced in chapter 3, we will study the nature of the excitations and quantitatively reproduce the dispersion relation measured by inelastic neutron scattering in Ref. [Zheludev 2003] as well as the field dependent spectrum observed by optical spectroscopy in Ref. [Penc 2012].

1.3 A very brief introduction to magnetic supersolids

Quantum phenomena manifesting at macroscopical scale attracted the interest in the scientific community for almost a century. Superconductors, superfluid helium, semiconductor lasers and quasi-one-dimensional conductors that undergo a Peierls

transition, all exhibit unusual macroscopic properties governed by quantum mechanics. What is common in these systems is the macroscopic occupation of a single quantum state.[5] As a remarkable example, the concept of Bose-Einstein condensation was introduced in 1924 revealing that below a critical temperature an ideal Bose gas undergoes a phase transition and the lowest energy single-paricle state will be occupied by a macroscopic number of particles [Einstein 1924]. However, this concept was believed to have little physical relevance and was considered purely as a mathematical accomplishment, until the discovery of superfluidity in liquid ^{4}He [Kapitza 1938, Allen 1938]. The analogy between liquid helium of isotopic mass 4 and Bose-Einstein condensate was pointed out by London in the same year [London 1938]. As the superfluid ^{4}He is a strongly interacting system and the theory of Bose-Einstein condensate involved ideal non-interacting bosons, it was necessary to formulate a microscopic theory of interacting bosonic particles [Bogoliubov 1947]. In the theoretical understanding of superfluid phase, the concept of broken symmetry, the idea that the phase transitions occur by way of symmetry reduction, played an important role. The unsymmetrical, or less symmetric, phase can be characterised by an order parameter. Generally speaking, the order parameter is simply a parameter that is zero in the symmetric state and nonzero when the symmetry is broken. Penrose, Onsager and Yang proposed that the superfluid state can be characterised by a two-particle density matrix which can be factorized as:

$$\rho(r,r') = \langle \hat{\psi}^\dagger(r)\hat{\psi}\ (r')\rangle = \psi^*(r)\psi(r) + \text{small terms}\ , \tag{1.6}$$

where $\hat{\psi}^\dagger(r)$ is a field operator. The parameter $\psi(r) = \langle\hat{\psi}(r)\rangle$ is the complex order parameter of the superfluid phase [Penrose 1951, Penrose 1956, Yang 1962]. In a normal, non-superfluid system the gauge symmetry ensures that the superfluid order parameter $\psi(r)$ is zero, but when this symmetry is broken we reach the superfluid phase with a finite value of $\psi(r)$:

$$\psi(r) = \sqrt{\rho_s}e^{i\phi} = \langle N-1|\hat{\psi}(r)|N\rangle\ , \tag{1.7}$$

where ρ_s is the density of the superfluid and ϕ the phase of the condensate. When $\psi(r)$ is finite, we say that off-diagonal long-range order (ODLRO) is present. Later, the concept of ODLRO became generalized to fermionic systems in the framework of the BCS theory of superconductivity where the off-diagonal orderparameter corresponds to the wave function of the Cooper pair [Bardeen 1957].

In other words, we can say that in the superfluid (or superconducting) state there is a correlation between the particles even infinitely far from each other. In a normal state the two-particle correlation function approaches zero as the distance of the particles goes to infinity, however, in the superfluid (or superconducting) state the $\langle\hat{\psi}^\dagger(r)\hat{\psi}\ (r')\rangle \approx \psi^*(r)\psi(r)$ converges to a finite value, namely the superfluid density ρ_s (see Eq. 1.7), even at infinite distances.

[5] In superfluid helium the zero momentum state, in supersolid materials a given momentum state of the electron pairs, in lasers a mode of the electromagnetic radiation, while in one-dimensional metals under the Peierls transition point it is a phonon mode that is macroscopically occupied.

Next to superfluidity and superconductivity, a new exotic phase was theoretically proposed, namely the supersolid state. As quantum crystals can be characterized by diagonal long-range order (DLRO) and superfluids by ODLRO, it is straightforward to think about the supersolid as a state in which ODLRO and DLRO coexists.

Apparently various bosonic lattice models are of good use in the understanding of supersolid phases [Batrouni 2000, Sengupta 2005, Yamamoto 2009].

Matsuda and Tsuneto, and independently Liu and Fisher showed that the quantum lattice picture of supersolid state can be mapped onto a model of magnetic supersolid where the magnetic order breaks the spin rotational symmetry and the translational invariance at the same time [Matsuda 1970, Liu 1973]. They considered the following model of bosonic particles

$$\mathcal{H} = \sum_{ij} v_{ij}\mathbf{n}_i\mathbf{n}_j + \frac{1}{2}\sum_{ij} u_{ij}(\mathbf{a}_i^\dagger\mathbf{a}_j + \mathbf{a}_i\mathbf{a}_j^\dagger) \tag{1.8}$$

where $\mathbf{a}_i^\dagger$ and $\mathbf{a}_i$ are the creation and annihilation operators of a boson—satisfying the bosonic commutation relations—and $\mathbf{n}_i = \mathbf{a}_i^\dagger\mathbf{a}_i$ represents the boson number at the lattice point i. The real parameters v_{ij} and u_{ij} denote the potential and the hopping between a pair of bosons, respectively. They showed that this model is isomorphic to a model of localized spins of $S = 1/2$ through the following transformation:

$$\mathbf{a}_j = \mathbf{S}_j^x + i\mathbf{S}_j^y\,, \tag{1.9a}$$

$$\mathbf{a}_j^\dagger = \mathbf{S}_j^x - i\mathbf{S}_j^y\,, \tag{1.9b}$$

$$\mathbf{n}_j = \mathbf{a}_j^\dagger\mathbf{a}_j = \frac{1}{2} - \mathbf{S}_j^z\,. \tag{1.9c}$$

The spin model then has the form of

$$\mathcal{H}_{spin} = \sum_{i<j}\left[v_{ij}\mathbf{S}_i^z\mathbf{S}_j^z + u_{ij}(\mathbf{S}_i^x\mathbf{S}_j^x + \mathbf{S}_i^y\mathbf{S}_j^y)\right]\,. \tag{1.10}$$

The diagonal long-range order (DLRO) in the spin system can be rephrased as $Tr(\rho\mathbf{a}_i^\dagger\mathbf{a}_i) = \langle\mathbf{S}_i^z\rangle$. Therefore, there is no DLRO in the paramagnetic and ferromagnetic phases, where $\langle\mathbf{S}_i^z\rangle$ does not depend on i. However the antiferromagnetic state exhibits DLRO. The definition of ODLRO can be given similarly: $Tr(\rho\mathbf{a}_i^\dagger\mathbf{a}_j) = \langle\mathbf{S}_i^x\mathbf{S}_j^x + \mathbf{S}_i^y\mathbf{S}_j^y\rangle$, that is, we can speak of ODLRO only if the order parameter $\langle\mathbf{S}_i^x\mathbf{S}_j^x + \mathbf{S}_i^y\mathbf{S}_j^y\rangle$ is finite, even when the lattice sites i and j are infinitely far from each other [Matsuda 1970].

Such magnetic analogs of supersolid state were observed in triangular lattice via Quantum Monte Carlo (QMC) simulations [Wessel 2005, Melko 2005, Heidarian 2005] where frustration and order-by-disorder mechanism is considered to play an important role in the emergence of supersolid phase. Classical Monte Carlo simulation on triangular lattice supported by mean-field calculation and Landau theory suggested that strong anisotropy can stabilize supersolid phases [Seabra 2011]. Amongst quasi two dimensional systems, strong

frustration and/or anisotropy were found to stabilize supersolid states on bilayer dimer models [Ng 2006, Sengupta 2007a, Laflorencie 2007, Picon 2008] and orthogonal dimer models [Schmidt 2008]. Supersolid states have also been reported in the spin-1 Heisenberg chain with strong exchange and uniaxial single-ion anisotropies [Sengupta 2007b, Peters 2009, Peters 2010, Rossini 2011], furthermore in spin and hard-core Bose-Hubbard model [Ueda 2010] in three dimensions.

In chapter 5 we show that a simple model of bipartite lattices with single-ion and exchange anisotropies and larger ($S = 1$ and $S = 3/2$) spins supports the emergence of magnetic supersolid phase. Our variational calculations are strengthen with exact diagonalization and, in the one-dimensional case, Density Matrix Renormalization Group technique.

Chapter 2

Symmetry

It's still magic even if you know how it's done.

– *Terry Pratchett, A Hat Full of Sky*

The concept of symmetry appears in natural sciences as early as the classical antiquity. Its meaning, however, was strictly related to harmony, beauty and unity; and it played little role until the arising of modern physics at the turn of the twentieth century. Although, the unity of various elements was related to symmetry in the ancient sense as well, in contemporary physics the symmetry of objects, even abstract ones; like mathematical equations, is defined in terms of their invariance under certain groups of transformations. This definition was widely accepted and used in physics, yet the fundamental significance of symmetries was not acknowledged until Einstein's special relativity. It was not until then, that the way of thinking about symmetry has essentially changed. While earlier the laws of physics were thought to exhibit certain symmetries, now the concept is reversed: the laws of nature follow from the principles of invariance.

Symmetry groups became especially effective in quantum physics. The main reason of this roots in the possibility of superposing quantum states, and in the capacity of representation theory to describe the action of a group transformation on such states. Conventionally, when a physical system is invariant under the transformations of a given group, then its eigenstates transform into each other according to the group's representations. That is, the group transformations can be represented in the state space by operators corresponding to physical observables. The operators that represent the action of symmetries commute with the Hamiltonian of the system, thus are conserved quantities. Additionally, the eigenvalues of invariant operators are suitable to label the irreducible representations of the symmetry group of the system. Rotational invariance and the conservation of angular momentum demonstrate these properties beautifully. The invariance of the Hamiltonian $\mathcal{H}$ under the proper rotation R about the axis $\mathbf{n}$ through the angle φ can be expressed as

$$[R_{\mathbf{n}}(\varphi), \mathcal{H}] = 0 \tag{2.1}$$

for any $R_{\mathbf{n}}(\varphi)$. In fact, it means that the equation of motion is rotationally invariant. Because of the invariance of $\mathcal{H}$, if $|\Psi\rangle$ is an eigenvector with the eigenvalue E, then $R_{\mathbf{n}}(\varphi)|\Psi\rangle$ is also an eigenvector with the same eigenvalue.[1] The group that contains

[1] $\mathcal{H}\left(R_{\mathbf{n}}(\varphi)|\Psi\rangle\right) = R_{\mathbf{n}}(\varphi)\mathcal{H}|\Psi\rangle = R_{\mathbf{n}}(\varphi)E|\Psi\rangle = E\left(R_{\mathbf{n}}(\varphi)|\Psi\rangle\right)$

all proper three dimensional rotations is the group SO(3). It can be shown that its infinitesimal generators (up to a factor $\hbar$) are the angular momentum operators $\mathbf{J}$, therefore the invariance under rotations can be expressed as the invariance under infinitesimal rotations:

$$[\mathbf{J}, \mathcal{H}] = 0 \tag{2.2}$$

The components of $\mathbf{J}$ are thus conserved quantities, and the operators $\mathcal{H}$, $\mathbf{J}^2$ and J_z commute with each other; meaning that they can be simultaneously diagonalized. This considerably simplifies the eigenvalue problem of the Hamiltonian. The eigenvectors corresponding to the same value of J belong to the $(2J+1)$-dimensional irreducible representation $D^{(J)}$ of SO(3), and can be rotated into each other by the application of the operators J_- or J_+.[2] Together they span a rotational invariant irreducible subspace, that is, an orthogonal basis for the $(2J+1)$-fold degenerate eigenvalue E_J of $\mathcal{H}$.

Studying the symmetry properties of a system we inevitably encounter mechanisms that are governed by approximate, hidden or broken symmetries. In the case of approximate symmetries the symmetry breaking forces are very small, therefore the symmetry violation can be treated as a perturbation.[3] The breaking of the symmetry does not mean that there is no symmetry present at all, rather it is characterized by a lower symmetry, that is a subgroup of the initial symmetry group. Symmetry breaking can be explicit or spontaneous. When it is explicit the dynamical equations are not invariant, consequently there are terms in the Hamiltonian that lower the symmetry of the system. A more interesting phenomenon is the spontaneous symmetry breaking. We say that the symmetry is spontaneously broken when the laws are symmetric but not the states of the system. In quantum mechanics, as a consequence of superposition, the systems with finite degrees of freedom always have symmetric ground state. Although, when the system is characterized by infinite number of degrees of freedom there are cases when the ground state does not exhibit the symmetry of the Hamiltonian, but is asymmetric, leading to spontaneous symmetry breaking [Gross 1995]. Such mechanism is responsible for the existence of crystals, magnetism, or superconductivity. The prototype example is the ferromagnetic Heisenberg model exhibiting rotational invariance, however below the critical temperature the ground state is magnetically ordered by which a direction is selected thus breaking the rotational symmetry spontaneously. As a consequence of spontaneous symmetry breaking; for each violated global symmetry a fluctuation, characterized by very small energy, appears. This property was formulated in the celebrated Goldstone theorem, according to which for each broken generator of the symmetry group – i.e. that does not preserve the ground state – a massless[4] bosonic particle, a so called Goldstone boson occurs.

[2] J_+ can be expressed as $J_x + iJ_y$ and J_- as $J_x - iJ_y$ providing a usually more convenient basis than J_x and J_y.

[3] A good example is the isotopic symmetry of the nuclear forces where the electromagnetic force is rather weak and the masses of up and down quarks are very small.

[4] or very light when the symmetry of the system is not exact.

2.1 Crystal structures and point groups

Although $SrCu_2(BO_3)_2$ and $Ba_2CoGe_2O_7$ both serve – for different reasons – as unique and interesting examples among the strongly correlated materials, they do not share much of their properties. $SrCu_2(BO_3)_2$ provide a rare example of the two dimensional frustrated spin gap antiferromagnets, whereas $Ba_2CoGe_2O_7$ is a member of the popular family of multiferroic materials. Nevertheless, this section attempts to discuss their symmetry properties more or less simultaneously. As for the common properties, both compounds are quasi two dimensional and have tetragonal structure. $Ba_2CoGe_2O_7$ is characterized by the space group $P\bar{4}2_1m$, while regarding $SrCu_2(BO_3)_2$ we will distinguish the high and low temperature cases. In the former the space group is I4/mcm, in the latter, though, the loss of the inversion lowers the symmetry to the subgoup $I\bar{4}2m$. In this work we shall restrict ourselves to the physically interesting layers in which the important interactions take place. Within them, we primarily focus on the translational invariant phases, where the ordering can be characterized by symmetry breaking inside the unit cell. Therefore, a symmetry analysis based only on the symmetry groups of the physically important layers will serve our investigations satisfyingly.

$SrCu_2(BO_3)_2$ is characterized by alternating layers of $CuBO_3$ molecules and Sr^{2+} ions. The strontium layers isolate well the $CuBO_3$ planes from each other; allowing us to neglect the inter-layer coupling between the copper ions. The magnetic Cu^{2+} ions have a spin $S = 1/2$ and are coupled to one another via the BO_3 molecules of triangular shape. The neighbouring coppers form bonds and together they build up an orthogonal dimer lattice [Smith 1991, Kageyama 1999a] as shown in Fig 2.1(a). This type of lattice structure (with the spins $S = 1/2$) is called the Shastry-Sutherland model and has a great importance as it is the only exactly solvable two dimensional problem.[5]
At high temperature, when $T_s > 395$ K, the dimers are all laying in the same plane preserving the reflection symmetry about it [Smith 1991, Sparta 2001]. However, below T_s a structural distortion takes place and in the buckled layer the two types of dimers shift in opposite directions perpendicular to the plane [Sparta 2001]. We will concentrate mainly on this low symmetry – that is to say low temperature case – for it has more experimental relevance. Nonetheless, we consider the high symmetry case shortly too; as we believe that a lot can be learned from paralleling the two of them.

In $Ba_2CoGe_2O_7$ the magnetic Co^{2+} ions have 3/2-spins and are surrounded by the tetrahedral environment of four oxygen atoms. The alternating orientation of the neighbouring CoO_4 tetrahedra is responsible for many interesting properties of this material and can be pictured as it follows. The oxygen bonds below the Co-plane are tilted by the angle $\pm\kappa$ with respect to the [110] crystallographic direction.[6] Due to the different environment of the neighbours the unit cell contains two Co^{2+}

[5] Hereby we mean that the exact ground state is available, though not the excitations.

[6] Naturally selecting the oxygen bond above the plane would suffice too, as long as we remain consistent.

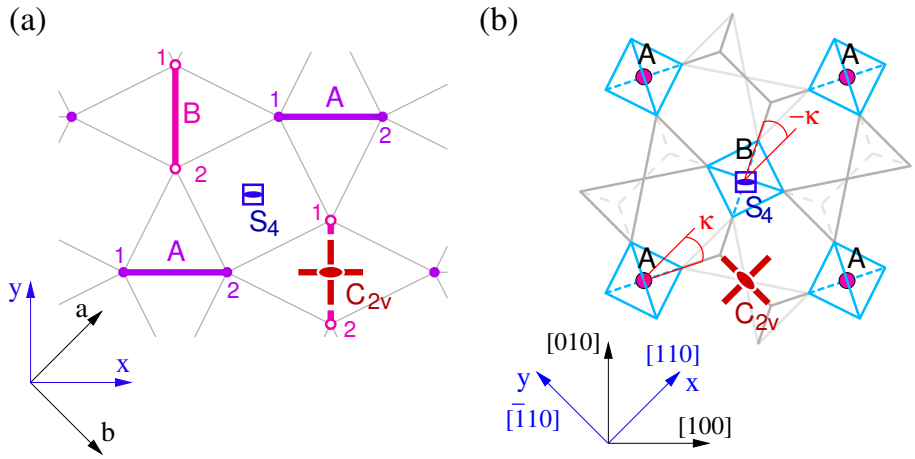

Figure 2.1: Schematic figures of $SrCu_2(BO_3)_2$ and $Ba_2CoGe_2O_7$. (a) There are two site symmetries in the buckled $CuBO_3$ layer: $\mathcal{S}_4$ in the middle of four dimer and $\mathcal{C}_{2v}$ acting on the dimers. Copper ions below and above the layer are indicated by open or closed circles, respectively. This buckled property is emphasized by the different colouring of the orthogonal dimers. (b) The site symmetries of $Ba_2CoGe_2O_7$ are $\mathcal{S}_4$ and $\mathcal{C}_{2v}$ too, acting on the Co sites and in the middle of four sites, respectively. The Co^{2+} ions are located at the center of the tetrahedra and are represented by magenta circles. The unit cell contains two Co^{2+} ions that we denote by A and B (note that the neighbouring tetrahedra are oriented differently)

ions. A schematic figure of the CoO_4 structure is shown in Fig. 2.1(b).

The symmetry group of the unit cell for both compounds is isomorphic to $\mathcal{D}_{2d}$.[7] In the case of $SrCu_2(BO_3)_2$ the rotation axis of $\mathcal{S}_4$ is pinned to the center of four sites, while the mirror planes are determined by the directions of the dimers as illustrated in Fig. 2.1(a). As for $Ba_2CoGe_2O_7$, the fourfold rotation axis is located on the Co^{2+} sites, while $\mathcal{C}_{2v}$ acts in the center of the four Co^{2+} ions, the way it is indicated in Fig. 2.1(b).

2.2 Construction of Hamiltonian and symmetry classification of order parameters

The symmetry properties of the lattices determine the terms that can be included in the Hamiltonian, i.e. the terms that transform as the fully symmetric irreducible representation (A_1) of the symmetry group. In this part we derive the symmetry-allowed terms of the Hamiltonian, such as the components of the symmetric and antisymmetric exchanges and that of the g-tensor anisotropy. A word shall be added about the order parameters that become important when discussing the phase diagram of the above models.

[7] Note that here we mean the low temperature structure of $SrCu_2(BO_3)_2$.

Conventionally, when discussing the magnetic properties of a correlated system one relies on Hamiltonians built of purely spin terms. Depending on the problem this Hamiltonian can be linear, bilinear, biquadratic and of even higher order in spin operators. The first principle derivation of such models, however, is a rather enormous task, thus following a pragmatic approach is usually preferred. The restricted length of this work prevents us from a detailed introduction of the microscopic origins of the occurring spin terms, nevertheless, once we acknowledge the concept of pure spin models, we shall build a suitable Hamiltonian based on symmetry considerations.

Generally, we can argue that when the orbital degrees of freedom are unaffected, we can project onto the subspace of spin configurations leaving out the orbital components. Within this subspace the electron-electron interaction can be expressed using spin operators, usually in the fashion of an effective model. The most prevailing example for this would be the Heisenberg model. This can be derived starting with a Mott-insulating state, in which the electrons are localized due to the large Coulomb-repulsion. The Heisenberg model has the following form:

$$\mathcal{H} = \sum_{\langle i,j \rangle} J_{ij} \hat{\mathbf{S}}_i \hat{\mathbf{S}}_j \ , \tag{2.3}$$

with $\hat{\mathbf{S}}_i$ denoting the spin operator on site i and J_{ij} the coupling strength between the sites i and j. Taking relativistic effects, and thereby spin-orbit coupling into account, additional anisotropic terms appear. Among them, the single-ion and g-tensor anisotropies as well as the antisymmetric exchange, that is often referred to as the Dzyaloshinsky-Moriya interaction, are the most frequently occurring ones. Based on symmetry arguments, it was shown that due to the spin-orbit coupling an anisotropic part is present in the exchange interaction [Dzyaloshinsky 1958], and that it can be derived microscopically as a linear correction to the standard superexchange mechanism [Moriya 1960]. At the same time, single-ion anisotropy appears in the second order of perturbation of the same procedure. The DM interaction and g-tensor anisotropy have the following form:

$$\mathcal{H}^{\mathrm{DM}} = \sum_{\langle i,j \rangle} \mathbf{D_{ij}} (\hat{\mathbf{S}}_i \times \hat{\mathbf{S}}_j) \tag{2.4}$$

$$\mathcal{H}^{\mathrm{Zeeman}} = \sum_{i} \mathbf{h} \mathbf{g} \hat{\mathbf{S}}_i \tag{2.5}$$

where $\hat{\mathbf{S}}_i$ represents the i-th spin operator, $\mathbf{D}_{ij}$ is the Dzyaloshinsky-Moriya vector between the sites i and j, $\mathbf{h}$ is the magnetic field and $\mathbf{g}$ is a tensor with elements determined by the symmetry properties.

Another way to introduce the symmetric and antisymmetric terms is to think about the spin-spin interaction as a rank-2 tensor D in $\sum_{\alpha\beta} D_{\alpha\beta} \hat{S}_i^{\alpha} \hat{S}_j^{\beta}$, that can be decomposed into a symmetric and a traceless antisymmetric part. Dividing the symmetric part further into a diagonal and a traceless symmetric tensor we obtain the usual forms of the above discussed terms [A. Bencini 1990]. The DM interaction and the on-site anisotropies break the SU(2) invariance of the symmetric Heisenberg

exchange, and are responsible for many interesting physical phenomena. On their account the ground state degeneracy of frustrated systems can be lifted and they can open a small gap in the excitation spectrum of an otherwise gapless system. Additionally, they can lead to the development of a transverse magnetization available for torque measurements.

2.2.1 Symmetry considerations for $SrCu_2(BO_3)_2$

We will first consider the symmetry properties of $SrCu_2(BO_3)_2$, or rather, that of the $CuBO_3$ layer. The unit cell consists of two orthogonal dimers: dimer A which is parallel to the x-axis, and dimer B parallel to the y-axis as indicated in Fig. 2.1(a). In the low temperature case, the symmetry group of the unit cell is $\mathcal{D}_{2d}$ consisting of 8 symmetry elements: E, σ_{xz}, σ_{yz}, C_2, S_4, S_4^3, $\sigma_{xz}S_4$ and $\sigma_{yz}S_4$. Here we should point out that for the conjugation class typically denoted by $2C_2'$ we use the notation $2\sigma S_4$ throughout this work (see the character table 2.1). When the ground state is ordered, usually a symmetry breaking follows, therefore it is practical to consider the proper subgroups of $\mathcal{D}_{2d}$, which are $\mathcal{S}_4 = \{E, S_4, C_2, S_4^3\}$, $\mathcal{D}_2 = \{E, C_2, \sigma_{xz}S_4, \sigma_{yz}S_4\}$, $\mathcal{C}_{2v} = \{E, C_2, \sigma_{xz}, \sigma_{yz}\}$, $\mathcal{C}_2 = \{E, C_2\}$, and $\mathcal{C}_s = \{E, \sigma_h\}$. Later on these will serve to characterize the symmetry groups of the various ordered phases. The effects of the symmetry elements on the sites $A1$, $A2$, $B1$ and $B2$, as well as on the spin components are given in Table 2.2. It is worth to mention here that the spin – similarly to the magnetic field – transforms as an axial vector.

	E	$2S_4$	$C_2(z)$	$2\sigma S_4$	$2\sigma_d$
$\mathsf{A_1}$	1	1	1	1	1
$\mathsf{A_2}$	1	1	1	-1	-1
$\mathsf{B_1}$	1	-1	1	1	-1
$\mathsf{B_2}$	1	-1	1	-1	1
E	2	0	-2	0	0

Table 2.1: Character table of the point group $\mathcal{D}_{2d}$. Here we use $2\sigma_d = \{\sigma_{xz}, \sigma_{yz}\}$ and $2\sigma S_4 = \{\sigma_{xz}S_4, \sigma_{yz}S_4\}$ to denote the conjugation classes.

Discussing symmetry breaking in the presence of magnetic field somewhat adds to the difficulties. We shall not forget that the magnetic field breaks the time reversal symmetry, or in other words, the time reversal operation T changes the direction of the magnetic field. When the field is perpendicular to the $CuBO_3$ plane, that is $\mathbf{h} = (0, 0, h_z)$, the reflections σ_{xz} and σ_{yz} reverse its direction to $\mathbf{h} = (0, 0, -h_z)$, just like they reverse the z component of a spin as shown in Table 2.2. Similarly, the field applied in the x direction is reversed under the action of σ_{xz} and is rotated by the symmetry class S_4. Classifying the components of the magnetic field yields that h_z transforms as the irrep $\mathsf{A_2}$, whereas the components (h_x, h_y) belong to the two-dimensional irreducible representation E of the group $\mathcal{D}_{2d}$.

E	σ_{xz}	σ_{yz}	C_2	S_4	S_4^3	$\sigma_{xz}S_4$	$\sigma_{yz}S_4$
S^x	$-S^x$	S^x	$-S^x$	$-S^y$	S^y	$-S^y$	S^y
S^y	S^y	$-S^y$	$-S^y$	S^x	$-S^x$	$-S^x$	S^x
S^z	$-S^z$	$-S^z$	S^z	S^z	S^z	$-S^z$	$-S^z$
A1	A1	A2	A2	B2	B1	B1	B2
A2	A2	A1	A1	B1	B2	B2	B1
B1	B2	B1	B2	A1	A2	A1	A2
B2	B1	B2	B1	A2	A1	A2	A1

Table 2.2: The transformation of axial vector (spin) components and sites under the symmetry transformations of the point group of the unit cell in the low symmetry case.

2.2.1.1 Order parameters for magnetic field along the z direction

irrep	notation	order parameter
A_1	m^z	$S^z_{A1} + S^z_{A2} + S^z_{B1} + S^z_{B2}$
	n_{S_4}	$S^x_{A1} - S^x_{A2} + S^y_{B1} - S^y_{B2}$
A_2	$\tilde{n}_{\mathcal{S}_4}$	$S^y_{A1} - S^y_{A2} - S^x_{B1} + S^x_{B2}$
B_1	$\tilde{n}_{\mathcal{C}_4}$	$S^y_{A1} - S^y_{A2} + S^x_{B1} - S^x_{B2}$
B_2	$n_{\mathcal{C}_4}$	$S^x_{A1} - S^x_{A2} - S^y_{B1} + S^y_{B2}$
	$m^z_{\text{Néel}}$	$S^z_{A1} + S^z_{A2} - S^z_{B1} - S^z_{B2}$
E	m^x	$S^x_{A1} + S^x_{A2} + S^x_{B1} + S^x_{B2}$
	m^y	$S^y_{A1} + S^y_{A2} + S^y_{B1} + S^y_{B2}$
	$m^x_{\text{Néel}}$	$S^x_{A1} + S^x_{A2} - S^x_{B1} - S^x_{B2}$
	$m^y_{\text{Néel}}$	$-S^y_{A1} - S^y_{A2} + S^y_{B1} + S^y_{B2}$
	n^z_A	$S^z_{A1} - S^z_{A2}$
	n^z_B	$S^z_{B1} - S^z_{B2}$

Table 2.3: Symmetry classification of the order parameters according to the magnetic point group $\mathcal{D}_{2d}(\mathcal{S}_4)$ when the field is parallel to the z-axis.

In case of a field parallel to the z-axis, the application of the σ_{xz} followed by the time reversion T leaves the magnetic field invariant. Thus, the actual symmetry group of the system in magnetic field is correctly taken into account if we consider the so called magnetic point groups, where the time reversal operation T is included as well. For finite h_z the symmetry group under which the Hamiltonian is invariant will be the magnetic group $\mathcal{S}_4 + T\sigma_{xz} \times \mathcal{S}_4$. Note that this group is isomorphic to $\mathcal{D}_{2d}$, and in Schönflies notation it is denoted by $\mathcal{D}_{2d}(\mathcal{S}_4)$. Therefore, we use the

character table of $\mathcal{D}_{2d}$ to classify the order parameters according to the irreducible representations of the magnetic point group. The classified operators which are linear in spin, along with their notation, are summarized in Table 2.3. m denotes the total magnetic moment of the unit cell, the indices Néel, S_4 and C_4 indicate that the given operator has a finite expectation value in case of classical Néel order, or in the case of a spin configuration that is invariant under the operation S_4 and C_4, respectively. The notation n stands for the staggered magnetic moment of a bond when the spin operators are parallel to the dimer, while $\tilde{n}$ represent the perpendicular staggered components.

2.2.1.2 Order parameters for h_x

The magnetic field along the x-axis breaks the symmetry $\mathcal{S}_4 = \left\{E, S_4, C_2(z), S_4^3\right\}$ and also the time reversal invariance. The remaining symmetry group that leaves the Hamilton operator unchanged is the magnetic group $\{E, \sigma_{yz}\} + TC_2(z) \times \{E, \sigma_{yz}\}$ which is isomorphic to the group $\mathcal{C}_{2v}$ and has four one dimensional irreducible representations, namely $\mathsf{A_1}$, $\mathsf{A_2}$, $\mathsf{B_1}$ and $\mathsf{B_2}$ as shown in Table 2.4. Proceeding with this group, the x component of the magnetic field, h_x is invariant, i.e. it transforms as the fully symmetric irreducible representation $\mathsf{A_1}$ of $\mathcal{C}_{2v}$.

	E	$C_2(z)$	σ_{xz}	σ_{yz}
$\mathsf{A_1}$	1	1	1	1
$\mathsf{A_2}$	1	1	-1	-1
$\mathsf{B_1}$	1	-1	1	-1
$\mathsf{B_2}$	1	-1	-1	1

Table 2.4: Character table of the point group $\mathcal{C}_{2v}$.

irrep	order parameter
$\mathsf{A_1}$	m^x, $m^x_{\text{Néel}}$, n^z_A
$\mathsf{A_2}$	m^y, $m^y_{\text{Néel}}$, n^z_B
$\mathsf{B_1}$	m^z, $m^z_{\text{Néel}}$, $n_{\mathcal{C}_4}$, $n_{\mathcal{S}_4}$
$\mathsf{B_2}$	$\tilde{n}_{\mathcal{C}_4}$, $\tilde{n}_{\mathcal{S}_4}$

Table 2.5: The symmetry classification of order parameters for $h||x$. Here we do not show the form of the operators only their notations used in Table 2.3.

The order parameters in this case have the same form as in the case of $h||z$ but now they are labelled with the irreducible representations of the point group $\mathcal{C}_{2v}$. Table 2.5 summarizes the classified linear operators for the field applied parallel to the x axis.

2.2.1.3 The anisotropic terms

Following the symmetry transformations of the spins under the relevant point groups we can construct the invariant combinations of the spin operators that can be included in the Hamiltonian. Thus we can derive the possible components of g-tensor anisotropy; collecting the invariants we have determined above for the two settings of magnetic field, we can write

$$\mathcal{H}^{Zeeman} = -(g_z m^z + g_s n_{\mathcal{S}_4}) h_z \tag{2.6}$$

for $h||z$, whereas for a field along the x-axis the Zeeman term reads

$$\mathcal{H}^{Zeeman} = -\left[\frac{1}{2}(g_x + g_y)m^x + \frac{1}{2}(g_x - g_y)m^x_{\text{Néel}} - g_s n^z_A\right] h_x \tag{2.7}$$

Introducing the intradimer ($\mathbf{D}$) and interdimer ($\mathbf{D}'$) DM vectors, we can extend our model with the following terms:

$$\mathcal{H}_{\text{DM}} = \mathbf{D}\sum_{nn}(\mathbf{S}_i \times \mathbf{S}_j) + \mathbf{D}'\sum_{nnn}(\mathbf{S}_i \times \mathbf{S}_j) \tag{2.8}$$

The symmetry properties of the lattice determine the allowed components of the vectors $\mathbf{D}$ and $\mathbf{D}'$ as it was shown in Ref. [Kodama 2005]. For completeness, here we shortly present the relevant terms and introduce a way to derive them.The intradimer interaction on the bond type A has the form of $\mathbf{D}_A(\mathbf{S}_{A1} \times \mathbf{S}_{A2})$ that can be written as a determinant:

$$\begin{vmatrix} D^x_A & D^y_A & D^z_A \\ S^x_A & S^y_A & S^z_A \\ S^x_A & S^y_A & S^z_A \end{vmatrix} \tag{2.9}$$

This determinant has to be invariant under all the symmetry elements of $\mathcal{D}_{2d}$. Applying C_2 for instance, we get:

$$C_2 \begin{vmatrix} D^x_A & D^y_A & D^z_A \\ S^x_{A1} & S^y_{A1} & S^z_{A1} \\ S^x_{A2} & S^y_{A2} & S^z_{A2} \end{vmatrix} = \begin{vmatrix} D^x_A & D^y_A & D^z_A \\ -S^x_{A2} & -S^y_{A2} & S^z_{A2} \\ -S^x_{A1} & -S^y_{A1} & S^z_{A1} \end{vmatrix} = \begin{vmatrix} D^x_A & D^y_A & -D^z_A \\ S^x_{A1} & S^y_{A1} & S^z_{A1} \\ S^x_{A2} & S^y_{A2} & S^z_{A2} \end{vmatrix} \tag{2.10}$$

The original determinant and the one after applying C_2 has to be equal, therefore it follows that $D^z_A = 0$. Similarly one can consider the application of σ_{xz}, σ_{yz}, S_4, S_4^3, $\sigma_{xz}S_4$ and $\sigma_{yz}S_4$:

$$\sigma_{xz} \begin{vmatrix} D^x_A & D^y_A & D^z_A \\ S^x_{A1} & S^y_{A1} & S^z_{A1} \\ S^x_{A2} & S^y_{A2} & S^z_{A2} \end{vmatrix} = \begin{vmatrix} D^x_A & D^y_A & D^z_A \\ -S^x_{A1} & S^y_{A1} & -S^z_{A1} \\ -S^x_{A2} & S^y_{A2} & -S^z_{A2} \end{vmatrix} = \begin{vmatrix} -D^x_A & D^y_A & -D^z_A \\ S^x_{A1} & S^y_{A1} & S^z_{A1} \\ S^x_{A2} & S^y_{A2} & S^z_{A2} \end{vmatrix}$$

resulting in $D^x_A = 0$. The effect of σ_{yz} will not give a new condition, however, applying the rotation S_4:

$$S_4 \begin{vmatrix} D^x_A & D^y_A & D^z_A \\ S^x_{A1} & S^y_{A1} & S^z_{A1} \\ S^x_{A2} & S^y_{A2} & S^z_{A2} \end{vmatrix} = \begin{vmatrix} D^x_A & D^y_A & D^z_A \\ -S^y_{B2} & S^x_{B2} & S^z_{B2} \\ -S^y_{B1} & S^x_{B1} & S^z_{B1} \end{vmatrix} = \begin{vmatrix} -D^y_A & D^x_A & -D^z_A \\ S^x_{B1} & S^y_{B1} & S^z_{B1} \\ S^x_{B2} & S^y_{B2} & S^z_{B2} \end{vmatrix}$$

provides $D_A^y = -D_B^x$, $D_A^x = D_B^y$ and $D_A^z = D_B^z$. For we have already established that $D_A^x = 0$ and $D_A^z = 0$, consequently $D_B^y = 0$ and $D_B^z = 0$ must be fulfilled. Performing the rest of the transformations we will not obtain new equations, thus we can conclude that the form of the intradimer Dzyaloshinsky-Moriya interaction per unit cell is:

$$\mathcal{H}_{\mathrm{DM}}^{\mathrm{intra}} = D\left(\mathbf{S}_{A1} \times \mathbf{S}_{A2}\right)_y - D\left(\mathbf{S}_{B1} \times \mathbf{S}_{B2}\right)_x \tag{2.11}$$

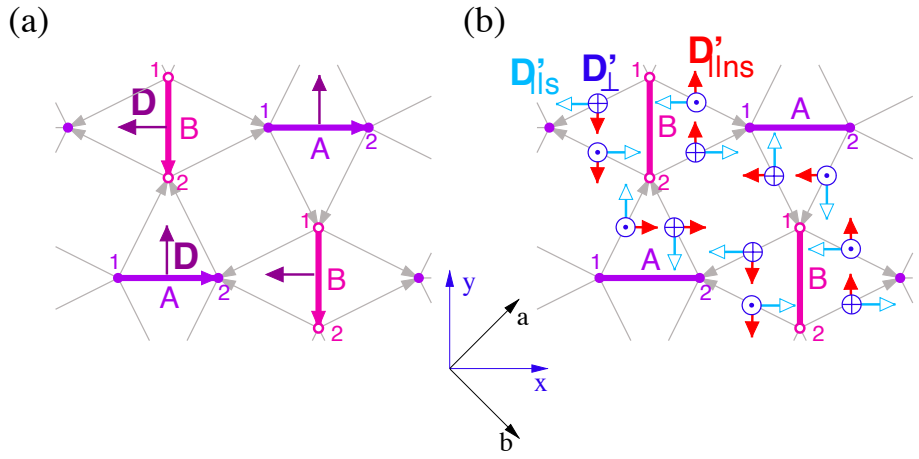

Figure 2.2: Symmetry allowed components of the DM vector in the low symmetry case. (a) The intradimer DM vectors: $\mathbf{D}_A = (0, D, 0)$ and $\mathbf{D}_B = (-D, 0, 0)$. (b) The interdimer DM vector can have any component, once we specify its direction on a given bond, though, the DM interactions on the remaining bonds in the unit cell follow from the symmetry properties.

Similar argument leads to the symmetry allowed components of the inter-dimer DM interaction. While the intradimer DM vector is laying in the plane of the dimer network in the direction perpendicular to the dimers: $\mathbf{D}_A = (0, D, 0)$ and $\mathbf{D}_B = (-D, 0, 0)$[8], the interdimer DM interaction is a vector with arbitrary direction: $\mathbf{D}' = (D'_{||ns}, D'_{||s}, D'_{\perp})$, although fixing this vector on one bond, the direction of the rest within the unit cell is determined by the symmetry. The allowed DM components in the low temperature system are illustrated in Fig. 2.2. Note that the dimers are directed; changing the order of the sites in the DM interaction would result in a minus sign.

2.2.1.4 High symmetry case

Restricting ourselves to the symmetries of the $CuBO_3$ layer, above T_s, the two mutually perpendicular sets of dimers lay in the same plane. The $CuBO_3$ plane

[8]Naturally the choice $\mathbf{D}_A = (0, -D, 0)$ would be right too, with $\mathbf{D}_B = (D, 0, 0)$ to preserve the symmetry.

	E	$2C_4(z)$	$C_2(z)$	$2\sigma_d S_4$	$2I\sigma_d$	I	$2S_4$	σ_h	$2\sigma_d C_4$	$2\sigma_d$
$\mathsf{A_{1g}}$	1	1	1	1	1	1	1	1	1	1
$\mathsf{A_{2g}}$	1	1	1	-1	-1	1	1	1	-1	-1
$\mathsf{B_{1g}}$	1	-1	1	1	-1	1	-1	1	1	-1
$\mathsf{B_{2g}}$	1	-1	1	-1	1	1	-1	1	-1	1
$\mathsf{E_g}$	2	0	-2	0	0	2	0	-2	0	0
$\mathsf{A_{1u}}$	1	1	1	1	1	-1	-1	-1	-1	-1
$\mathsf{A_{2u}}$	1	1	1	-1	-1	-1	-1	-1	1	1
$\mathsf{B_{1u}}$	1	-1	1	1	-1	-1	1	-1	-1	1
$\mathsf{B_{2u}}$	1	-1	1	-1	1	-1	1	-1	1	-1
$\mathsf{E_u}$	2	0	-2	0	0	-2	0	2	0	0

Table 2.6: Character table of $\mathcal{D}_{4h}$ point group. $\sigma_d = \{\sigma_{xz}, \sigma_{yz}\}$. $2I\sigma_d$, $2\sigma_d S_4$ and $2\sigma_d C_4$ correspond to C_2'', C_2' and σ_v in the conventional notation.

becomes a mirror plane, and the inversion appears among the symmetry elements. The symmetry group is $\mathcal{D}_{4h}$ which has 16 group elements. The combinations $\sigma_{yz}S_4$ and $\sigma_{xz}S_4$, that correspond to the C_2' two-fold axis in the standard $\mathcal{D}_{4h}$ group, are actually 2_1 screw axes. Furthermore the combinations $\sigma_{yz}C_4$ and $\sigma_{xz}C_4$ are glide planes, corresponding to the σ_v mirror planes in $\mathcal{D}_{4h}$. In the character table 2.6 we use the notation suitable for the present case.

irrep	notation	order parameter
$\mathsf{A_{1g}}$	m^z	$S^z_{A1} + S^z_{A2} + S^z_{B1} + S^z_{B2}$
$\mathsf{A_{1u}}$	$\tilde{n}_{\mathcal{C}_4}$	$S^y_{A1} - S^y_{A2} + S^x_{B1} - S^x_{B2}$
$\mathsf{A_{2u}}$	$n_{\mathcal{C}_4}$	$S^x_{A1} - S^x_{A2} - S^y_{B1} + S^y_{B2}$
$\mathsf{B_{1u}}$	n_{S_4}	$S^x_{A1} - S^x_{A2} + S^y_{B1} - S^y_{B2}$
$\mathsf{B_{2g}}$	$m^z_{\text{Néel}}$	$S^z_{A1} + S^z_{A2} - S^z_{B1} - S^z_{B2}$
$\mathsf{B_{2u}}$	$\tilde{n}_{\mathcal{S}_4}$	$S^y_{A1} - S^y_{A2} - S^x_{B1} + S^x_{B2}$
$\mathsf{E_g}$	m^x	$S^x_{A1} + S^x_{A2} + S^x_{B1} + S^x_{B2}$
	m^y	$S^y_{A1} + S^y_{A2} + S^y_{B1} + S^y_{B2}$
$\mathsf{E_g}$	$m^x_{\text{Néel}}$	$S^x_{A1} + S^x_{A2} - S^x_{B1} - S^x_{B2}$
	$m^y_{\text{Néel}}$	$-S^y_{A1} - S^y_{A2} + S^y_{B1} + S^y_{B2}$
$\mathsf{E_u}$	n^z_A	$S^z_{A1} - S^z_{A2}$
	n^z_B	$S^z_{B1} - S^z_{B2}$

Table 2.7: The symmetry classification of order parameters when $h||z$.

The classified linear operators are collected in Tab. 2.6. In the high symmetry

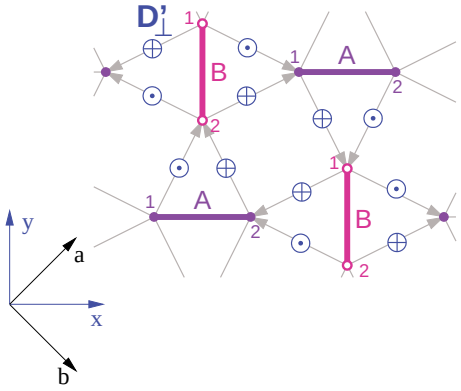

Figure 2.3: Symmetry allowed components of the DM vector in the high symmetry case. The in-plane DM vector components vanish and only the perpendicular component $D'_\perp$ of the inter-dimer DM interaction survives.

case the only invariant – that is, the only order parameter transforming as the $\mathsf{A_{1g}}$ irrep of $\mathcal{D}_{4h}$ – is the total magnetization along the field, in this case along the z–axis:

$$m^z = S^z_{A1} + S^z_{A2} + S^z_{B1} + S^z_{B2} \tag{2.12}$$

The staggered operators (n) are all odd with respect to the inversion which is the new symmetry element in the high temperature phase. The allowed DM components will be considerably simplified too. It is easy to show that for the dimers have inversion symmetry, all the intradimer DM components vanish. The inversion changes the sign of a polar vector, whereas it leaves an axial vector (like the spin and the magnetic filed) unaffected. As for the sites, inversion acts in the following way: $A1 \leftrightarrow A2$ and $B1 \leftrightarrow B2$.

$$I \begin{vmatrix} D^x_A & D^y_A & D^z_A \\ S^x_{A1} & S^y_{A1} & S^z_{A1} \\ S^x_{A2} & S^y_{A2} & S^z_{A2} \end{vmatrix} = \begin{vmatrix} D^x_A & D^y_A & D^z_A \\ S^x_{A2} & S^y_{A2} & S^z_{A2} \\ S^x_{A1} & S^y_{A1} & S^z_{A1} \end{vmatrix} = \begin{vmatrix} -D^x_A & -D^y_A & -D^z_A \\ S^x_{A1} & S^y_{A1} & S^z_{A1} \\ S^x_{A2} & S^y_{A2} & S^z_{A2} \end{vmatrix}$$

Thus $\mathbf{D} = 0$. Due to the reflexion plane and the inversion, all the in-plane DM terms must be zero. Therefore, regarding the interdimer components $\mathbf{D}' = (0, 0, D'_\perp)$. The only DM component in the high symmetry case is the out-of-plane interdimer term as shown in Fig. 2.3.

Table 2.8 intends to give a short summary on the invariant DM components for $SrCu_2(BO_3)_2$.

Based on this analysis, regarding $SrCu_2(BO_3)_2$, we will consider the usual Shastry-Sutherland model

$$\mathcal{H} = J \sum_{n.n.} \mathbf{S}_i \cdot \mathbf{S}_j + J' \sum_{n.n.n.} \mathbf{S}_i \cdot \mathbf{S}_j \ . \tag{2.13}$$

including the DM interactions:

$$\mathcal{H}_D = \sum_{\mathrm{NN}} \mathbf{D}_{ij} \cdot (\mathbf{S}_i \times \mathbf{S}_j) \tag{2.14}$$

	high-symmetry	low-symmetry
symmetry (unit cell)	$\mathcal{D}_{4h}$	$\mathcal{D}_{2d}$
DM (intra-dimer)	forbidden	$\mathbf{D} \parallel (ab) \wedge \mathbf{D} \perp$ dimer
DM (inter-dimer)	$\mathbf{D}' \parallel c$	arbitrary
spin ($h \parallel z$)	$O(2)$-sym	–
spin ($h \parallel x$)	–	–

Table 2.8: Summary of the symmetry analysis. If the g-tensor anisotropy is taken into account, the spin $O(2)$-symmetry is lost.

$$\mathcal{H}_{D'} = \sum_{\mathrm{NNN}} \mathbf{D'}_{ij} \cdot (\mathbf{S}_i \times \mathbf{S}_j) \tag{2.15}$$

and–when we compare our findings with the experiments–also the g-tensor anisotropy:

$$\begin{aligned} \mathcal{H}_{h_z} = &- g_z \mu_{\mathrm{B}} h_z \left(S^z_{\mathrm{A}1} + S^z_{\mathrm{A}2} + S^z_{\mathrm{B}1} + S^z_{\mathrm{B}2}\right) \\ &+ g_{\mathrm{s}} \mu_{\mathrm{B}} h_z \left(S^x_{\mathrm{A}1} - S^x_{\mathrm{A}2} + S^y_{\mathrm{B}1} - S^y_{\mathrm{B}2}\right) \ , \end{aligned} \tag{2.16a}$$

and

$$\mathcal{H}_{h_x} = -g_x \mu_B h_x \left(S^x_{\mathrm{A}1} + S^x_{\mathrm{A}2}\right) - g_y \mu_B h_x \left(S^x_{\mathrm{B}1} + S^x_{\mathrm{B}2}\right) + g_{\mathrm{s}} \mu_B h_x \left(S^z_{\mathrm{A}1} - S^z_{\mathrm{A}2}\right) \ . \tag{2.16b}$$

2.2.2 Symmetry properties of $Ba_2CoGe_2O_7$

In this part we follow a slightly different approach when constructing the Hamiltonian; namely we classify the bilinear spin operators as well and select the invariant terms. We also discuss which of the linear and bilinear operators can couple to the magnetic and electric field based on symmetry properties. Before we go on, however, the multipole characteristics of a larger spin deserves a few thoughts.

2.2.2.1 Multipole operators

Generally, when introducing a local basis in the Hilbert space of a spin S, we choose the eigenstates of the z component of the spin operator: $\hat{S^z}$. Any operator acting on this $2S+1$-dimensional space can be written in terms of Hubbard operators $|i\rangle\langle j|$

$$\hat{\mathcal{C}} = \sum_{i,i} c_{ij} |i\rangle\langle j| \ , \tag{2.17}$$

where $|i\rangle$ and $|j\rangle$ are basis elements of the Hilbert space of S.
For simplicity, let us begin with the story of a spin $S = 1/2$. Usually, its basis is selected as $|\hat{S^z} = \frac{1}{2}\rangle = |\uparrow\rangle$ and $|\hat{S^z} = -\frac{1}{2}\rangle = |\downarrow\rangle$. For this space is two-dimensional, we have four linearly independent operators: $|\uparrow\rangle\langle\uparrow|$, $|\uparrow\rangle\langle\downarrow|$, $|\downarrow\rangle\langle\uparrow|$ and $|\downarrow\rangle\langle\downarrow|$. Of

course, these are not hermitian as the operator of a proper physical quantity should be, therefore we need to take a suitable linear combination, such as: $|\uparrow\rangle\langle\uparrow|$, $|\uparrow\rangle\langle\downarrow| + |\downarrow\rangle\langle\uparrow|$, $-i\,|\uparrow\rangle\langle\downarrow| + i\,|\downarrow\rangle\langle\uparrow|$ and $|\downarrow\rangle\langle\downarrow|$. Due to the small size of the Hilbert space there is no other independent operator acting on a spin-half object.

A more elegant way to find the on-site order parameters of a spin S, is to involve the SU(2) symmetry classification. The $|\uparrow\rangle$, $|\downarrow\rangle$ states of a spin-half transform as the two-dimensional irreducible representation $\mathsf{D}^{(1/2)}$ of SU(2). Therefore the operator space they span must belong to the irrep $\mathsf{D}^{(1/2)} \otimes \mathsf{D}^{(1/2)}$. Recalling that the decomposition of the direct product of two irreps can be given by the Clebsh-Gordan series:

$$\mathsf{D}^{(j_1)} \otimes \mathsf{D}^{(j_2)} = \sum_{|j_1 - j_2|}^{j_1+j_2} \oplus \mathsf{D}^{(j)} \tag{2.18}$$

we can write $\mathsf{D}^{(1/2)} \otimes \mathsf{D}^{(1/2)} = \mathsf{D}^{(0)} \oplus \mathsf{D}^{(1)}$, meaning that the four operators will be decomposed into a one-dimensional scalar operator which is the identity and a 3-dimensional vector operator corresponding to the components of the spin (see Table 2.9). The spin operators belong together in the sense that they transform

irrep	spin-half operator
$\mathsf{D}^{(0)}$	$\hat{I} = \|\uparrow\rangle\langle\uparrow\| + \|\downarrow\rangle\langle\downarrow\|$
$\mathsf{D}^{(1)}$	$\hat{S}^x = \frac{1}{2}\,\|\uparrow\rangle\langle\downarrow\| + \frac{1}{2}\,\|\downarrow\rangle\langle\uparrow\|$
	$\hat{S}^y = -\frac{i}{2}\,\|\uparrow\rangle\langle\downarrow\| + \frac{i}{2}\,\|\downarrow\rangle\langle\uparrow\|$
	$\hat{S}^z = \frac{1}{2}\,\|\uparrow\rangle\langle\uparrow\| - \frac{1}{2}\,\|\downarrow\rangle\langle\downarrow\|$

Table 2.9: SU(2) classification of the linearly independent operators acting on a single $S = 1/2$ spin.

among each other as the components of a rank-1 tensor. This is true in general; the operators that belong to the irrep $\mathsf{D}^{(j)}$ span a $2j+1$ dimensional subspace of SU(2) and transform as a rank-j tensor operator. Had we consider a spin-one, its Hilbert space would be 3-dimensional, furthermore it would transform as the irreducible representation $\mathsf{D}^{(1)}$. The operator space of a spin-one is then $3 \times 3 = 9$ dimensional. According to (2.18) $\mathsf{D}^{(1)} \otimes \mathsf{D}^{(1)} = \mathsf{D}^{(0)} \oplus \mathsf{D}^{(1)} \oplus \mathsf{D}^{(2)}$. $\mathsf{D}^{(0)}$ stands for a scalar operator, namely the identity operator, $\mathsf{D}^{(1)}$ is a rank-1 tensor operator corresponding to the spin components $\hat{S}^x$, $\hat{S}^y$ and $\hat{S}^z$, and $\mathsf{D}^{(2)}$ is a rank-2 tensor with five elements each of them a quadrupole operator. The quadrupoles can be expressed in quadratic terms of spin operators and are time reversal-invariant. Conventionally, the $2k+1$ components $\hat{T}^{(k)}_n$ $(n = -k, \ldots, k)$ of a rank-k tensor operator $\hat{\mathbf{T}}^{(k)}$ can be rotated into one another through the following commutation relations:

$$\left[\hat{S}^z, \hat{T}^{(k)}_n\right] = n\hat{T}^{(k)}_n\,, \tag{2.19a}$$

$$\left[\hat{S}^{\pm}, \hat{T}^{(k)}_n\right] = \sqrt{k(k+1) - n(n \pm 1)}\,\hat{T}^{(k)}_{n\pm 1}\,. \tag{2.19b}$$

With the help of (2.19) one can systematically construct the components of $\hat{\mathbf{T}}^{(k)}$. Further increasing the spin length, and the Hilbert space along with it, we find additional multipole operators.

In our case, the Co^{2+} ions have spin $S = \frac{3}{2}$ that displays octupole characteristics beside the quadrupole and dipole ones. $\mathsf{D}^{(3/2)} \otimes \mathsf{D}^{(3/2)}$ can be decoupled as $\mathsf{D}^{(0)} \oplus \mathsf{D}^{(1)} \oplus \mathsf{D}^{(2)} \oplus \mathsf{D}^{(3)}$ where the octupole operators define a basis of the 7-dimensional subspace of $\mathsf{D}^{(3)}$. For completeness, the multipole operators, that are suitable on-site order parameter for a spin $S = 3/2$ are listed in Table 2.10.

irrep	operator	T
$\mathsf{D}^{(0)}$	$\hat{I} \sim (\hat{S}^x)^2 + (\hat{S}^y)^2 + (\hat{S}^z)^2$	✓
$\mathsf{D}^{(1)}$	$\hat{S}^x$ $\hat{S}^y$ $\hat{S}^z$	×
$\mathsf{D}^{(2)}$	$\hat{Q}^{xy} = \overline{\hat{S}^x\hat{S}^y}$ $\hat{Q}^{yz} = \overline{\hat{S}^y\hat{S}^z}$ $\hat{Q}^{zx} = \overline{\hat{S}^z\hat{S}^x}$ $\hat{Q}^{z^2} = 3(\hat{S}^z)^2 - S(S+1)$ $\hat{Q}^{x^2-y^2} = (\hat{S}^x)^2 - (\hat{S}^y)^2$	✓
$\mathsf{D}^{(3)}$	$\hat{T}^{xyz} = \overline{\hat{S}^x\hat{S}^y\hat{S}^z}$ $\hat{T}^x = \overline{\hat{S}^x\hat{S}^y\hat{S}^y} - \overline{\hat{S}^z\hat{S}^z\hat{S}^x}$ $\hat{T}^y = \overline{\hat{S}^y\hat{S}^z\hat{S}^z} - \overline{\hat{S}^y\hat{S}^x\hat{S}^x}$ $\hat{T}^z = \overline{\hat{S}^z\hat{S}^x\hat{S}^x} - \overline{\hat{S}^y\hat{S}^y\hat{S}^z}$ $\hat{T}^{x^3} = 2(\hat{S}^x)^3 - (\overline{\hat{S}^x\hat{S}^y\hat{S}^y} + \overline{\hat{S}^z\hat{S}^z\hat{S}^x})$ $\hat{T}^{y^3} = 2(\hat{S}^y)^3 - (\overline{\hat{S}^y\hat{S}^z\hat{S}^z} + \overline{\hat{S}^x\hat{S}^x\hat{S}^y})$ $\hat{T}^{z^3} = 2(\hat{S}^z)^3 - (\overline{\hat{S}^z\hat{S}^x\hat{S}^x} + \overline{\hat{S}^y\hat{S}^y\hat{S}^z})$	×

Table 2.10: SU(2) classification of the on-site multipole order parameters up to cubic order in spin operators. The over-line indicates a symmetric sum: for example $\overline{\hat{S}^x\hat{S}^y} = \hat{S}^x\hat{S}^y + \hat{S}^y\hat{S}^x$, $\overline{\hat{S}^y\hat{S}^x\hat{S}^x} = \hat{S}^y\hat{S}^x\hat{S}^x + \hat{S}^x\hat{S}^y\hat{S}^x + \hat{S}^x\hat{S}^x\hat{S}^y$ and $\overline{\hat{S}^x\hat{S}^y\hat{S}^z}$ consists of six terms. The last column indicates the transformation under time reversal transformation.

2.2.2.2 Order parameters of the unit cell in $Ba_2CoGe_2O_7$

Let us begin our investigations with the linear order parameters. We have 6 spin components altogether from the sites A and B. Using the character table of $\mathcal{D}_{2d}$

shown in Table 2.1 and the group actions listed in Table 2.11, this 6 dimensional representation can be decoupled as $\Gamma = \mathsf{A}_1 + \mathsf{A}_2 + 2\mathsf{E}$. The linear order parameters are collected in Table 2.12.

E	σ_{xz}	σ_{yz}	C_2	S_4	S_4^3	$\sigma_{xz}S_4$	$\sigma_{yz}S_4$
x	x	$-x$	$-x$	$-y$	y	$-y$	y
y	$-y$	y	$-y$	x	$-x$	$-x$	x
z	z	z	z	$-z$	$-z$	$-z$	$-z$
S^x	$-S^x$	S^x	$-S^x$	$-S^y$	S^y	S^y	$-S^y$
S^y	S^y	$-S^y$	$-S^y$	S^x	$-S^x$	S^x	$-S^x$
S^z	$-S^z$	$-S^z$	S^z	S^z	S^z	$-S^z$	$-S^z$
A	B	B	A	A	A	B	B
B	A	A	B	B	B	A	A

Table 2.11: The transformation of polar vectors (polarization), axial vectors (spin) and sites under the symmetry elements of the unit cell.

irrep	linear operators
A_1	$S_A^z - S_B^z$
A_2	$S_A^z + S_B^z$
E	$S_A^x + S_B^x$ $S_A^y + S_B^y$
E	$S_A^y - S_B^y$ $-S_A^x + S_B^x$

Table 2.12: The symmetry classification of linear order parameters.

For the z component of the magnetic field transforms as the irreducible representation A_2 and breaks the time reversal symmetry, just like the total magnetization $S_A^z + S_B^z$, coupling these two together will provide an invariant term. That is, the expression $h_z(S_A^z + S_B^z)$ is invariant under the time reversal operator T, and because $\mathsf{A}_2 \otimes \mathsf{A}_2 = \mathsf{A}_1$, it transforms as a fully symmetric representation of $\mathcal{D}_{2d}$. Similarly, the in-plane components of the magnetic field (h_x, h_y) violate the time reversal invariance, and transform as the two-dimensional irrep E of the point group, in the same way as the spin operators: $(S_A^x + S_B^x, S_A^y + S_B^y)$. Keeping in mind that $\mathsf{E} \otimes \mathsf{E} = \mathsf{A}_1 \oplus \mathsf{A}_2 \oplus \mathsf{E}$; the scalar product of (h_x, h_y) and $(S_A^x + S_B^x, S_A^y + S_B^y)$ will belong to the symmetric representation A_1. Based on this simple argument we can

include the following term in our model:[9]

$$\mathcal{H}^{Zeeman} = -h_z g_z m^z - g_{\parallel}(h_x m^x + h_y m^y) \tag{2.20}$$

Let us continue with the classification of the bilinear spin operators $\hat{\mathbf{S}}_i^{\alpha}\hat{\mathbf{S}}_j^{\beta}$, where $i,j \in \{A,B\}$ and $\alpha,\beta \in \{x,y,z\}$. Of these we have 21 that are different; and the 21-dimensional representation Γ can be reduced as $\Gamma = 5\mathsf{A}_1 + 2\mathsf{A}_2 + 3\mathsf{B}_1 + 3\mathsf{B}_2 + 4\mathsf{E}$ according to the irreducible representations of $\mathcal{D}_{2d}$.

irrep	bilinear operators
A_1	$S_A^z S_B^z$
	$S_A^x S_B^x + S_A^y S_B^y$
	$S_A^x S_B^y - S_A^y S_B^x$
	$(S_A^z)^2 + (S_B^z)^2$
	$(S_A^x)^2 + (S_B^x)^2 + (S_A^y)^2 + (S_B^y)^2$
A_2	$(S_A^z)^2 - (S_B^z)^2$
	$(S_A^x)^2 - (S_B^x)^2 + (S_A^y)^2 - (S_B^y)^2$
B_1	$(S_A^x)^2 - (S_B^x)^2 - (S_A^y)^2 + (S_B^y)^2$
	$\overline{S_A^x S_A^y} + \overline{S_B^x S_B^y}$
	$S_A^x S_B^y + S_A^y S_B^x$
B_2	$(S_A^x)^2 + (S_B^x)^2 - (S_A^y)^2 - (S_B^y)^2$
	$\overline{S_A^x S_A^y} - \overline{S_B^x S_B^y}$
	$S_A^x S_B^x - S_A^y S_B^y$
E	$\begin{pmatrix} \overline{S_A^z S_A^x} + \overline{S_B^z S_B^x} \\ \overline{S_A^y S_A^z} + \overline{S_B^y S_B^z} \end{pmatrix}$
	$\begin{pmatrix} \overline{S_A^y S_A^z} - \overline{S_B^y S_B^z} \\ -\overline{S_A^z S_A^x} + \overline{S_B^z S_B^x} \end{pmatrix}$
	$\begin{pmatrix} S_A^z S_B^x + S_A^x S_B^z \\ S_A^y S_B^z + S_A^z S_B^y \end{pmatrix}$
	$\begin{pmatrix} S_A^y S_B^z - S_A^z S_B^y \\ -S_A^z S_B^x + S_A^x S_B^z \end{pmatrix}$

Table 2.13: The symmetry classification of the bilinear order parameters according to the point group of the lattice.

[9] Naturally there are other terms that could be included, e.g. the $h_x(S_A^y - S_B^y) + h_y(-S_A^x + S_B^x)$ is also an invariant operator. For an exhaustive study one would need to examine the term $\mathbf{h}\cdot\mathbf{g}\cdot\hat{\mathbf{S}}$ under the symmetry operation and deduce the components of the tensor $\mathbf{g}$.

We find that there are five terms that transform as the fully symmetric representation A_1, though one of them corresponds to the identity, thus we are left with four independent terms that can be included in the Hamiltonian.[10] Among these we find the single-ion easy-plane anisotropy:

$$\mathcal{H}_{\text{ani}} = \Lambda \left((S_A^z)^2 + (S_B^z)^2 \right), \tag{2.21}$$

and the z component of $\hat{\mathbf{S}}_A \times \hat{\mathbf{S}}_B$ resulting in the Dzyaloshinsky-Moriya term:

$$\mathcal{H}_{\text{DM}} = D \left(S_A^x S_B^y - S_A^y S_B^x \right). \tag{2.22}$$

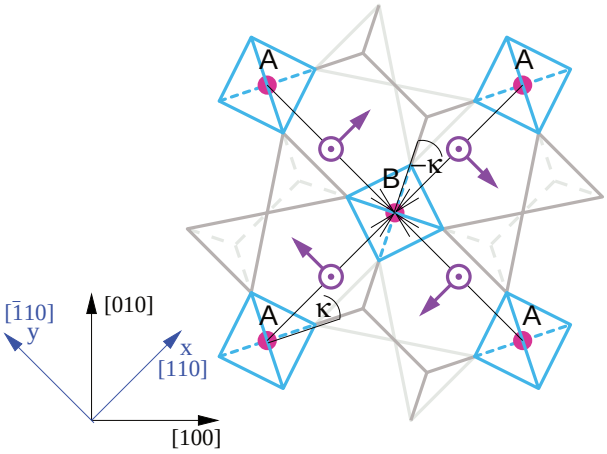

Figure 2.4: Symmetry allowed components of the DM vector. Note that we only include the z component in our discussion, because we confine ourselves only to the translational invariant, i.e. two-sublattice ordering and the in-plane components of DM vector would cancel out in such cases.

The in-plane components of the DM vector can also be deduced, either from the product of two E irreps[11] like in the case of the in-plane magnetic field above, or similarly to the investigations in section 2.2.1.3. However, we only consider the translational invariant states, for which the in-plane DM terms cancel each other. The allowed components of the DM vector are illustrated in Fig. 2.4.
Furthermore, the fact that the operators $S_A^z S_B^z$ and $S_A^x S_B^x + S_A^y S_B^y$ belong to A_1 by themselves, means that any linear combination of them would transform as A_1 too. This allows us to include exchange anisotropy in the following way:

$$\mathcal{H}_{\text{ex}} = J \left(S_A^x S_B^x + S_A^y S_B^y \right) + J_z S_A^z S_B^z. \tag{2.23}$$

Collecting these terms, the Hamiltonian of the unit cell looks as it follows:

$$\begin{aligned} \mathcal{H}_{\text{u.c.}} \;=\; & J \left(S_A^x S_B^x + S_A^y S_B^y \right) + J_z S_A^z S_B^z + \Lambda \left[(S_A^z)^2 + (S_B^z)^2 \right] + D \left(S_A^x S_B^y - S_A^y S_B^x \right) \\ & - g_z h_z (\hat{S}_A^z + \hat{S}_B^z) - g_{\parallel} \left[h_x (\hat{S}_A^x + \hat{S}_B^x) + h_y (\hat{S}_A^y + \hat{S}_B^y) \right]. \end{aligned} \tag{2.24}$$

[10] The sum of $(S_A^x)^2 + (S_B^x)^2 + (S_A^y)^2 + (S_B^y)^2$ and $(S_A^z)^2 + (S_B^z)^2$ gives the identity operator.
[11] The x and y components of the DM vector belongs to the irrep E

For we would like to discuss the spin order induced electric polarization, it is useful to shortly discuss the connection between electric polarization and the order parameters introduced above. The polarization vector is a polar vector and is unchanged by the time reversal operator T. The z component of the polarization vector p^z transforms as the irreducible representation B_2 of $\mathcal{D}_{2d}$. Consequently, we need to find order parameters with the same properties. As a start, we consider only the quadratic spin terms, for they are invariant under T, then select those that belong to B_2. Although, there are 3 such operators, we restrict ourselves to the on-site induced polarization, therefore the operators $(S_A^x)^2+(S_B^x)^2-(S_A^y)^2-(S_B^y)^2$ and $\overline{S_A^xS_A^y}-\overline{S_B^xS_B^y}$ will be sufficient. An arbitrary linear combination can be written as:

$$\begin{aligned}\hat{P}^z_{\text{u.c.}} &= \cos(2\kappa)\left((S_A^x)^2+(S_B^x)^2-(S_A^y)^2-(S_B^y)^2\right)\\ &\quad+\sin(2\kappa)\left(\overline{S_A^xS_A^y}-\overline{S_B^xS_B^y}\right).\end{aligned} \tag{2.25}$$

Collecting the terms according to site indices we get

$$\begin{aligned}\hat{P}^z_{\text{u.c.}} &= \cos(2\kappa)\left((S_A^x)^2-(S_A^y)^2\right)+\sin(2\kappa)\overline{S_A^xS_A^y}\\ &\quad+\cos(2\kappa)\left((S_B^x)^2-(S_B^y)^2\right)-\sin(2\kappa)\overline{S_B^xS_B^y}\end{aligned} \tag{2.26}$$

and as further simplification the minus sign in the term of site B can be included in the κ angle as:

$$\hat{P}^z_j = \cos(2\kappa_j)\left((S_j^x)^2-(S_j^y)^2\right)+\sin(2\kappa_j)\overline{S_j^xS_j^y} \tag{2.27}$$

where j belongs to either sublattice A or B, and the different orientation of the tetrahedra around the two types of sites can be accounted for by choosing $\kappa_{j\in A}=\kappa$ and $\kappa_{j\in B}=-\kappa$. Similar logic leads to the form of the operators $\hat{P}^x$ and $\hat{P}^y$:

$$\begin{aligned}\hat{P}^x_j &\propto -\cos 2\kappa_j\left(\hat{S}_j^x\hat{S}_j^z+\hat{S}_j^z\hat{S}_j^x\right)-\sin 2\kappa_j\overline{\hat{S}_j^y\hat{S}_j^z}\\ \hat{P}^y_j &\propto \cos 2\kappa_j\left(\hat{S}_j^y\hat{S}_j^z+\hat{S}_j^z\hat{S}_j^y\right)-\sin 2\kappa_j\overline{\hat{S}_j^z\hat{S}_j^x}\end{aligned} \tag{2.28}$$

It is worth to note that the polarization operators defined in (2.27) and (2.28) are actually quadrupole operators.

Chapter 3

Generalized spin waves

It is at this point that normal language gives up, and goes and has a drink.

– *Terry Pratchett, The Color of Magic*

Spin wave theory is recognized as a landmark in the quest to understand the nature of elementary magnetic excitations. It was formulated more than half a century ago [Holstein 1940, Anderson 1952, Kubo 1952], and remains to be of fundamental importance. The basic idea of spin wave theory is that the classical ground state is assumed to exhibit long range magnetic order and the excitations are related to the dynamical quantum fluctuations about it. We should remark that spin waves can be considered as an analogue of lattice waves. In solid systems the lattice vibrations are accounted for the presence of phonons, in other words quantized lattice waves, and these fluctuations are responsible for the broadening of Bragg peaks. Similarly, quantum fluctuations reduce magnetic ordering, and the excitations can be described, in the fashion of phonons, as bosonic quasiparticles known as magnons.

Probably the most common quantum mechanical way of treating spin waves is the Holstein-Primakoff transformation when the creation and annihilation of magnons are related to the lowering and raising spin operators: $\hat{S}^-$ and $\hat{S}^+$. In the following we attempt to introduce a more general, yet very similar method to this, where we allow for multipolar fluctuations and a non-magnetically ordered ground state as well. Strictly speaking the multipole excitations are not (all) spin waves, nonetheless we keep this name, and refer to the method as generalized spin wave approach.

3.1 Mathematical formulation

This section is devoted to the mathematical formulation of the generalized spin waves method, following mainly Ref. [Shiina 2003] with regards to the construction of the spin wave Hamiltonian. As for its solution though a subsection is committed to the generalized Bogoliubov transformation based primarily on private communications with Totsuka Keisuke. For simplicity we assume a two-sublattice order to be the ground state and introduce the procedure accordingly. The method for a ground state with larger (magnetic) unit cell can be derived without much effort using the two-sublattice approach.

In a general case the Hamiltonian contains interactions between the multipole operators $\hat{C}^\alpha$, where α denotes one of the $2k+1$ components if $\hat{C}$ transforms as a

rank-k tensor. For example $\hat{C}^{\alpha}$ might stand for the three spin operators, the five quadrupoles and the seven octupole operators with $k = 1, 2$ and 3, respectively, as introduced earlier. Additionally, terms that couple the multipole operators to some kind of external field can be present in the Hamiltonian, such as an external magnetic field or the anisotropy field Λ in the single-ion anisotropy term $\Lambda(S_j^z)^2$.

$$\mathcal{H} = \sum_{\substack{(ij)\\ i\in A\\ j\in B}} \sum_{\alpha,\beta} J_{ij}^{\alpha\beta} \hat{C}_i^{\alpha} \hat{C}_j^{\beta} - \sum_i \sum_{\alpha} h_i^{\alpha} \hat{C}_i^{\alpha} \tag{3.1}$$

where (i, j) denotes the summation for the neighbouring unit cells. $J_{ij}^{\alpha\beta}$ stands for the coupling strength between the α and β components of the multipole operators $\hat{C}_i$ and $\hat{C}_j$. Furthermore h_i^{α} represents the component of the external field that couples to $\hat{C}_i^{\alpha}$.

3.1.1 Variational approach – setting the generalized spin waves into motion

Let $\{|\phi_{\xi,0}(l)\rangle, \ldots, |\phi_{\xi,N}(l)\rangle\}$ be a basis for the local Hilbert space of the site $l \in \xi$ on the sublattice $\xi \in \{A, B\}$. Conventionally, it is selected to contain the eigenvectors of the spin operator $\hat{S}^z$. For we would like to apply the spin wave method to a general ground state, let us begin with a sublattice-dependent unitary transformation of the initial basis:

$$|\psi_{A,n}(i)\rangle = \sum_m U_{mn}(A)|\phi_{A,m}(i)\rangle, \tag{3.2}$$

$$|\psi_{B,n}(j)\rangle = \sum_m U_{mn}(B)|\phi_{B,m}(j)\rangle \tag{3.3}$$

and we assume that the ground state of the system is factorized in the following way:

$$|\Psi\rangle = \prod |\psi_{A,0}(i)\rangle|\psi_{B,0}(i)\rangle \tag{3.4}$$

where $\prod$ indicates a product over the unit cells. We can express any multipole operator in terms of Hubbard operators using the above basis

$$\hat{C}_l^{\alpha} = \sum_{nm} c_{nm}^{\alpha}(\xi)|\psi_{\xi,n}(l)\rangle\langle\psi_{\xi,m}(l)| \tag{3.5}$$

where $\xi \in \{A, B\}$ depending on which sublattice l belongs. The matrix elements correspond to

$$c_{nn'}^{\alpha}(\xi) = \sum_{mm'} U_{nm}(\xi)\langle\phi_{\xi,m}(l)|C_l^{\alpha}|\phi_{\xi,m'}(l)\rangle U_{m'n'}(\xi). \tag{3.6}$$

This rotation of the basis is closely related to a variational approach where $|\Psi\rangle = \prod |\psi_{A,0}(i)\rangle|\psi_{B,0}(i)\rangle$ plays the role of the variational wave function. We will choose

the transformation matrices $\mathbf{U}(A)$ and $\mathbf{U}(B)$ so that their first column contains $2n-2$ independent variational parameters and the wave functions $|\psi_{A,0}(i)\rangle$ and $|\psi_{B,0}(i)\rangle$ have the form of

$$|\psi_{A,0}(i)\rangle \propto |\phi_{A,0}(i)\rangle + u_1 e^{i\varphi_1}|\phi_{A,1}(i)\rangle + \cdots + u_n e^{i\varphi_n}|\phi_{A,n}(i)\rangle \tag{3.7}$$

where the parameters u_m are reals and a similar expression holds for $|\psi_{B,0}(i)\rangle$ with different coefficients. (3.7) is the most general linear variational state, where we reduced the n complex coefficients to $2n-2$ real parameters by the condition that the new state is normed and by neglecting a general phase factor. One can construct the other columns of $\mathbf{U}(A)$ and $\mathbf{U}(B)$ to be orthogonal with the same parameters u_m and φ_m where $m \in \{1,\ldots,n\}$.
We can determine the variational parameters by minimizing the energy

$$E = \frac{\langle\Psi|\mathcal{H}|\Psi\rangle}{\langle\Psi|\Psi\rangle}\,. \tag{3.8}$$

3.1.2 The spin wave Hamiltonian

It becomes useful to introduce the boson operators $a^\dagger_{\xi,n}(l)$ and $a_{\xi,n}(l)$ for $|\psi_{n,\xi}(l)\rangle$ and $\langle\psi_{\xi,n}(l)|$ so that the Hubbard operators $|\psi_{\xi,n}(l)\rangle\langle\psi_{\xi,m}(l)|$ take the form of $a^\dagger_{\xi,n}(l)a_{\xi,m}(l)$. Since the bosonic occupation number can be arbitrarily large, but the Hilbert space of a site on sublattice ξ is only $N+1$ dimensional, the following constraint needs to be fulfilled:

$$\sum_{n=0}^{N} a^\dagger_{\xi,n}(l)a_{\xi,n}(l) = M. \tag{3.9}$$

Note that in the physical system $M=1$, however, we shall forget about this for now and perform the $1/M$ -expansion as if M would be a large parameter. This corresponds to the usual Holstein-Primakoff transformation where the number of bosons is restricted by the fact that a spin-S can be rotated only $2S$ times, and the expansion is performed in the parameter $\frac{1}{2S}$. Apparently, this works fine for large spins, although when the spin is small, especially when $S=1/2$, the approximation seems to break down. Fortunately, this is not the case. For example, in the ferromagnetic spin wave theory, the excitation energy of a single-magnon calculated for a spin-1/2 system via Holstein-Primakoff transformation is in fact exact. To verify this statement one needs only to check that the one-magnon state is an eigenstate and that its eigenvalue corresponds to that of given by the spin wave approach.[Fazekas 1999]
Using the constraint (3.9) we can eliminate the diagonal term $a^\dagger_{\xi,0}(l)a_{\xi,0}(l)$ replacing

$$a^\dagger_{\xi,0}(l)a_{\xi,0}(l) = M - \sum_{n=1}^{N} a^\dagger_{\xi,n}(l)a_{\xi,n}(l) \tag{3.10}$$

and we can rid ourselves of the off-diagonal Hubbard operators: $a^\dagger_{\xi,n}(l)a_{\xi,0}(l)$ and $a^\dagger_{\xi,0}(l)a_{\xi,n}(l)$ by introducing the following transformation similar to the Holstein-

Primakoff approach:

$$a^\dagger_{\xi,n}(l)a_{\xi,0}(l) \;\rightarrow\; a^\dagger_{\xi,n}(l)\cdot\sqrt{M-\sum_{m=1}^{N}a^\dagger_{\xi,m}(l)a_{\xi,m}(l)}, \tag{3.11}$$

$$a^\dagger_{\xi,0}(l)a_{\xi,n}(l) \;\rightarrow\; \sqrt{M-\sum_{m=1}^{N}a^\dagger_{\xi,m}(l)a_{\xi,m}(l)}\cdot a_{\xi,n}(l). \tag{3.12}$$

Now we can express the operators in terms of $a^\dagger_{\xi,n}(l)a_{\xi,m}(l)$ where $n,m\in\{1,\dots,N\}$:

$$\begin{aligned}\hat{C}^\alpha_l \;=\; & Mc^\alpha_{00}(\xi)-c^\alpha_{00}(\xi)\sum_{n=1}^{N}a^\dagger_{\xi,n}(l)a_{\xi,n}(l)+\sum_{n=1}^{N}\sum_{n'=1}^{N}c^\alpha_{nn'}(\xi)a^\dagger_{\xi,n}(l)a_{\xi,n'}(l)\\ & +\sum_{n=1}^{N}c^\alpha_{0n}(\xi)\sqrt{M-\sum_{m=1}^{N}a^\dagger_{\xi,m}(l)a_{\xi,m}(l)}\cdot a_{\xi,n}(l)\\ & +\sum_{n=1}^{N}c^\alpha_{n0}(\xi)a^\dagger_{\xi,n}(l)\cdot\sqrt{M-\sum_{m=1}^{N}a^\dagger_{\xi,m}(l)a_{\xi,m}(l)}\end{aligned} \tag{3.13}$$

We shall emphasize that this transformation is exact in the sense that expressing the spin operators following (3.13), they will fulfill the usual spin commutation relations: $[\hat{S}^\alpha,\hat{S}^\beta]=i\varepsilon_{\alpha\beta\gamma}\hat{S}^\gamma$.

Performing the $\frac{1}{M}$ expansion:

$$\sqrt{M-\sum_{n=1}^{N}a^\dagger_{\xi,n}a_{\xi,n}}\approx\sqrt{M}-\frac{1}{2\sqrt{M}}\sum_{n=1}^{N}a^\dagger_{\xi,n}a_{\xi,n}+\dots \tag{3.14}$$

and collecting the terms according to the order in boson operators we can write the Hamiltonian (3.1) as

$$\mathcal{H}=M^2\mathcal{H}^{(0)}+M^{3/2}\mathcal{H}^{(1)}+M\mathcal{H}^{(2)}+O(\sqrt{M}) \tag{3.15}$$

The lowest order term $\mathcal{H}^{(0)}$ is a scalar and it is equal to the mean-field energy: $\langle\Psi|\mathcal{H}|\Psi\rangle/\langle\Psi|\Psi\rangle$, where the ground state $|\Psi\rangle$ has been defined in (3.4)

$$\mathcal{H}^{(0)}=\sum_{\alpha\beta}\sum_{\substack{(i,j)\\ i\in A\\ j\in B}}J^{\alpha\beta}_{ij}c^\alpha_{00}(A)c^\beta_{00}(B)-\sum_{\alpha}\sum_{\substack{i\in A\\ j\in B}}(h^\alpha_i c^\alpha_{00}(A)+h^\alpha_j c^\alpha_{00}(B)). \tag{3.16}$$

For simplicity we consider only first neighbour coupling thus we can replace $J^{\alpha\beta}_{ij}$ with $J^{\alpha\beta}$ and we assume that the field h depends only on the sublattices, so that we can write h_A and h_B instead of h_i and h_j. The zeroth order term then takes the form of

$$\mathcal{H}^{(0)}=\frac{zL}{2}\sum_{\alpha\beta}J^{\alpha\beta}c^\alpha_{00}(A)c^\beta_{00}(B)-\frac{L}{2}\sum_{\alpha}(h^\alpha_A c^\alpha_{00}(A)+h^\alpha_B c^\alpha_{00}(B)) \tag{3.17}$$

where L denotes the system size and z stands for the coordination number. Minimizing the ground state energy (3.17) we obtain $c^{\alpha}_{00}(\xi)$, in other words the ground state wave function, as $c^{\alpha}_{00}(\xi)$ is the function of the $2n-2$ variational parameters. The first order term $\mathcal{H}^{(1)}$ has the following form

$$\begin{aligned}\mathcal{H}^{(1)} = \sum_{\substack{i\in A\\ j\in B}}\sum_{\alpha\beta}\sum_{n=1}^{N}\Big[&(J^{\alpha\beta}c^{\beta}_{00}(B) - h^{\alpha}_{A})c^{\alpha}_{n0}(A)\cdot a^{\dagger}_{A,n}(i) + h.c.\\ &+(J^{\alpha\beta}c^{\beta}_{00}(A) - h^{\alpha}_{B})c^{\alpha}_{n0}(B)\cdot a^{\dagger}_{B,n}(j) + h.c.\Big]\end{aligned} \tag{3.18}$$

Note that the conjugate of a coefficient $c^{\alpha}_{n0}(\xi)$ would be $c^{\alpha}_{0n}(\xi)$ as a consequence of its definition. $\mathcal{H}^{(1)}$ is identically zero when $\mathcal{H}^{(0)}$ is minimal and the first quantum corrections appear in $\mathcal{H}^{(2)}$.

$$\begin{aligned}\mathcal{H}^{(2)} = \sum_{\alpha\beta}\sum_{(ij)}\sum_{\substack{n=1\\ m=1}}^{N} J^{\alpha\beta}\Big[&c^{\beta}_{00}(B)\left(c^{\alpha}_{nm}(A) - \delta_{nm}c^{\alpha}_{00}(A)\right)\cdot a^{\dagger}_{A,n}(i)a_{A,m}(i)\\ &+c^{\alpha}_{00}(A)\left(c^{\beta}_{nm}(B) - \delta_{nm}c^{\beta}_{00}(B)\right)\cdot a^{\dagger}_{B,n}(j)a_{B,m}(j)\\ &+c^{\alpha}_{n0}(A)c^{\beta}_{0m}(B)\cdot a^{\dagger}_{A,n}(i)a_{B,m}(j) + h.c.\\ &+ c^{\alpha}_{n0}(A)c^{\beta}_{m0}(B)\cdot a^{\dagger}_{A,n}(i)a^{\dagger}_{B,m}(j) + h.c.\Big]\\ -\sum_{\alpha}\sum_{i\in A}\sum_{\substack{n=1\\ m=1}}^{N} &h^{\alpha}_{A}(c^{\alpha}_{nm}(A) - \delta_{nm}c^{\alpha}_{00}(A))\cdot a^{\dagger}_{A,n}(i)a_{A,m}(i)\\ -\sum_{\alpha}\sum_{j\in B}\sum_{\substack{n=1\\ m=1}}^{N} &h^{\alpha}_{B}(c^{\alpha}_{nm}(B) - \delta_{nm}c^{\alpha}_{00}(B))\cdot a^{\dagger}_{B,n}(j)a_{B,m}(j).\end{aligned} \tag{3.19}$$

As the next step we perform a Fourier transformation according to

$$\begin{aligned}a^{\dagger}_{\xi,n}(\mathbf{k}) &= \frac{1}{\sqrt{L}}\sum_{i} a^{\dagger}_{\xi,n}(i)e^{i\mathbf{k}\mathbf{r}_i}\\ a_{\xi,n}(\mathbf{k}) &= \frac{1}{\sqrt{L}}\sum_{i} a_{\xi,n}(i)e^{-i\mathbf{k}\mathbf{r}_i}\end{aligned} \tag{3.20}$$

and introduce the geometrical factor $\gamma_{\mathbf{k}}$

$$\gamma_{\mathbf{k}} = \frac{1}{z}\sum_{\boldsymbol{\delta}} e^{i\mathbf{k}\boldsymbol{\delta}} \tag{3.21}$$

with $\boldsymbol{\delta}$ denoting the translation vectors and z being the coordination number so that

the second order Hamiltonian $\mathcal{H}^{(2)}$ becomes:

$$\begin{aligned}\mathcal{H}^{(2)} = \sum_{\mathbf{k}} \sum_{\substack{n=1\\m=1}}^{N} \sum_{\alpha\beta} & (zJ^{\alpha\beta} c_{00}^{\beta}(B) - h_A^{\alpha}) \left(c_{nm}^{\alpha}(A) - \delta_{nm} c_{00}^{\alpha}(A)\right) \cdot a_{A,n}^{\dagger}(\mathbf{k}) a_{A,m}(\mathbf{k}) \\ & + (zJ^{\alpha\beta} c_{00}^{\alpha}(A) - h_B^{\alpha})(c_{nm}^{\beta}(B) - \delta_{nm} c_{00}^{\beta}(B)) \cdot a_{B,n}^{\dagger}(\mathbf{k}) a_{B,m}(\mathbf{k}) \\ & + J^{\alpha\beta} z \gamma_{\mathbf{k}} c_{n0}^{\alpha}(A) c_{0m}^{\beta}(B) \cdot a_{A,n}^{\dagger}(\mathbf{k}) a_{B,m}(\mathbf{k}) + h.c. \\ & + J^{\alpha\beta} z \gamma_{\mathbf{k}} c_{n0}^{\alpha}(A) c_{m0}^{\beta}(B) \cdot a_{A,n}^{\dagger}(\mathbf{k}) a_{B,m}^{\dagger}(-\mathbf{k}) + h.c\end{aligned} \tag{3.22}$$

In order to obtain a mathematically tractable form we introduce the vector notations $\mathbf{a}_{\xi}^{\dagger}(\pm\mathbf{k}) = \left\{a_{\xi,1}^{\dagger}(\pm\mathbf{k}), \ldots, a_{\xi,N}^{\dagger}(\pm\mathbf{k})\right\}$ and $\mathbf{a}_{\xi}(\pm\mathbf{k}) = \left\{a_{\xi,1}(\pm\mathbf{k}), \ldots, a_{\xi,N}(\pm\mathbf{k})\right\}$, furthermore we symmetrize the terms

$$\begin{aligned}\gamma_{\mathbf{k}} a_{\xi,n}^{\dagger}(\mathbf{k}) a_{\zeta,m}(\mathbf{k}) &\rightarrow \frac{\gamma_{\mathbf{k}}}{2} a_{\xi,n}^{\dagger}(\mathbf{k}) a_{\zeta,m}(\mathbf{k}) + \frac{\gamma_{-\mathbf{k}}}{2} a_{\zeta,m}(-\mathbf{k}) a_{\xi,n}^{\dagger}(-\mathbf{k}) \\ \gamma_{\mathbf{k}} a_{\xi,n}^{\dagger}(\mathbf{k}) a_{\zeta,m}^{\dagger}(-\mathbf{k}) &\rightarrow \frac{\gamma_{\mathbf{k}}}{2} a_{\xi,n}^{\dagger}(\mathbf{k}) a_{\zeta,m}^{\dagger}(-\mathbf{k}) + \frac{\gamma_{-\mathbf{k}}}{2} a_{\zeta,m}^{\dagger}(-\mathbf{k}) a_{\xi,n}^{\dagger}(\mathbf{k}) \\ \gamma_{\mathbf{k}} a_{\xi,n}(\mathbf{k}) a_{\zeta,m}(-\mathbf{k}) &\rightarrow \frac{\gamma_{\mathbf{k}}}{2} a_{\xi,n}(\mathbf{k}) a_{\zeta,m}(-\mathbf{k}) + \frac{\gamma_{-\mathbf{k}}}{2} a_{\zeta,m}(-\mathbf{k}) a_{\xi,n}(\mathbf{k}).\end{aligned} \tag{3.23}$$

so that, aside from a constant, we can write (3.22) in the form of

$$\mathcal{H}^{(2)}(\mathbf{k}) = \begin{pmatrix} \mathbf{a}_A^{\dagger}(\mathbf{k}) \\ \mathbf{a}_B^{\dagger}(\mathbf{k}) \\ \mathbf{a}_B(-\mathbf{k}) \\ \mathbf{a}_A(-\mathbf{k}) \end{pmatrix}^T \begin{pmatrix} \mathbf{H}_{11}(\mathbf{k}) & \mathbf{H}_{12}(\mathbf{k}) & \mathbf{H}_{13}(\mathbf{k}) & \mathbf{H}_{14}(\mathbf{k}) \\ \mathbf{H}_{21}(\mathbf{k}) & \mathbf{H}_{22}(\mathbf{k}) & \mathbf{H}_{23}(\mathbf{k}) & \mathbf{H}_{24}(\mathbf{k}) \\ \mathbf{H}_{31}(\mathbf{k}) & \mathbf{H}_{32}(\mathbf{k}) & \mathbf{H}_{33}(\mathbf{k}) & \mathbf{H}_{34}(\mathbf{k}) \\ \mathbf{H}_{41}(\mathbf{k}) & \mathbf{H}_{42}(\mathbf{k}) & \mathbf{H}_{43}(\mathbf{k}) & \mathbf{H}_{44}(\mathbf{k}) \end{pmatrix} \begin{pmatrix} \mathbf{a}_A(\mathbf{k}) \\ \mathbf{a}_B(\mathbf{k}) \\ \mathbf{a}_B^{\dagger}(-\mathbf{k}) \\ \mathbf{a}_A^{\dagger}(-\mathbf{k}) \end{pmatrix} \tag{3.24}$$

where $\mathbf{H}_{ij}(\mathbf{k})$ are $N \times N$ dimensional matrices. Due to the hermiticity of the Hamiltonian $\mathbf{H}^{(2)}(\mathbf{k})$ the matrices $\mathbf{H}_{ij}(\mathbf{k})$ are not independent. In appendix A we show that following some simple arguments the Hamiltonian can be brought to the following form

$$\mathcal{H}^{(2)}(\mathbf{k}) = \begin{pmatrix} \mathbf{a}_A^{\dagger}(\mathbf{k}) \\ \mathbf{a}_B^{\dagger}(\mathbf{k}) \\ \mathbf{a}_B(-\mathbf{k}) \\ \mathbf{a}_A(-\mathbf{k}) \end{pmatrix}^T \begin{pmatrix} \mathbf{H}_{11}(\mathbf{k}) & \mathbf{H}_{12}(\mathbf{k}) & \mathbf{H}_{13}(\mathbf{k}) & \mathbf{H}_{14}(\mathbf{k}) \\ \mathbf{H}_{12}^{\dagger}(\mathbf{k}) & \mathbf{H}_{22}(\mathbf{k}) & \mathbf{H}_{23}(\mathbf{k}) & \mathbf{H}_{13}^{T}(-\mathbf{k}) \\ \mathbf{H}_{13}^{\dagger}(\mathbf{k}) & \mathbf{H}_{23}^{\dagger}(\mathbf{k}) & \mathbf{H}_{22}^{T}(-\mathbf{k}) & \mathbf{H}_{12}^{T}(-\mathbf{k}) \\ \mathbf{H}_{14}^{\dagger}(\mathbf{k}) & \mathbf{H}_{13}^{*}(-\mathbf{k}) & \mathbf{H}_{12}^{*}(-\mathbf{k}) & \mathbf{H}_{11}^{T}(-\mathbf{k}) \end{pmatrix} \begin{pmatrix} \mathbf{a}_A(\mathbf{k}) \\ \mathbf{a}_B(\mathbf{k}) \\ \mathbf{a}_B^{\dagger}(-\mathbf{k}) \\ \mathbf{a}_A^{\dagger}(-\mathbf{k}) \end{pmatrix} \tag{3.25}$$

The hermiticity of $\mathbf{H}^{(2)}(\mathbf{k})$ requires conditions related to the form of $\mathbf{H}_{11}(\mathbf{k})$, $\mathbf{H}_{22}(\mathbf{k})$, $\mathbf{H}_{14}(\mathbf{k})$ and $\mathbf{H}_{23}(\mathbf{k})$ as well. The first two must be hermitian for they are in the diagonal part of $\mathbf{H}^{(2)}(\mathbf{k})$: $\mathbf{H}_{ii}(\mathbf{k}) = \mathbf{H}_{ii}^{\dagger}(\mathbf{k})$, the other two on the other hand has to fulfill the following equations: $\mathbf{H}_{14}(\mathbf{k}) = \mathbf{H}_{14}^{T}(-\mathbf{k})$ and $\mathbf{H}_{23}(\mathbf{k}) = \mathbf{H}_{23}^{T}(-\mathbf{k})$. The proof of these relationships is given in appendix A.

In our simple model there are no such terms as $\hat{C}^{\alpha}_{\xi}\hat{C}^{\beta}_{\xi}$, in other words terms that couple sites belonging to the same sublattice. Therefore the coefficients of $a^{\dagger}_{A,n}(\mathbf{k})a^{\dagger}_{A,m}(-\mathbf{k})$ and $a^{\dagger}_{B,n}(\mathbf{k})a^{\dagger}_{B,m}(-\mathbf{k})$, equivalently the matrices $\mathbf{H}_{14}(\mathbf{k})$ and $\mathbf{H}_{23}(\mathbf{k})$, are zero. The six independent matrices in (3.25) can be given as

$$
\begin{aligned}
[\mathbf{H}_{11}(\mathbf{k})]_{nm} &= \frac{1}{2}\sum_{\alpha\beta}(zJ^{\alpha\beta}c^{\beta}_{00}(B) - h^{\alpha}_{A})(c^{\alpha}_{nm}(A) - \delta_{nm}c^{\alpha}_{00}(A)) \\
[\mathbf{H}_{22}(\mathbf{k})]_{nm} &= \frac{1}{2}\sum_{\alpha\beta}(zJ^{\alpha\beta}c^{\alpha}_{00}(A) - h^{\beta}_{B})(c^{\beta}_{nm}(B) - \delta_{nm}c^{\beta}_{00}(B)) \\
[\mathbf{H}_{12}(\mathbf{k})]_{nm} &= \frac{1}{2}\sum_{\alpha\beta}J^{\alpha\beta}z\gamma_{\mathbf{k}}c^{\alpha}_{n0}(A)c^{\beta}_{0m}(B) \qquad (3.26) \\
[\mathbf{H}_{13}(\mathbf{k})]_{nm} &= \frac{1}{2}\sum_{\alpha\beta}J^{\alpha\beta}z\gamma_{\mathbf{k}}c^{\alpha}_{n0}(A)c^{\beta}_{m0}(B) \qquad (3.27) \\
[\mathbf{H}_{14}(\mathbf{k})]_{nm} &= 0 \qquad (3.28) \\
[\mathbf{H}_{23}(\mathbf{k})]_{nm} &= 0 \qquad (3.29)
\end{aligned}
$$

Nonetheless, in the following subsection we present the solution for (3.25) regardless the shape of the independent matrices $\mathbf{H}_{11}(\mathbf{k})$, $\mathbf{H}_{12}(\mathbf{k})$, $\mathbf{H}_{13}(\mathbf{k})$, $\mathbf{H}_{14}(\mathbf{k})$, $\mathbf{H}_{22}(\mathbf{k})$ and $\mathbf{H}_{23}(\mathbf{k})$.

3.1.3 Generalized Bogoliubov transformation

In order to obtain the excitation spectrum we need to bring (3.25) into the diagonal form:

$$
\mathcal{H}^{(2)} = \sum_{\mathbf{k}} \tilde{\mathbf{a}}^{\dagger}(\mathbf{k})\mathbf{\Omega}(\mathbf{k})\tilde{\mathbf{a}}\ (\mathbf{k}) \qquad (3.30)
$$

where the components of $\tilde{\mathbf{a}}^{(\dagger)}(\mathbf{k})$ are new field operators in the vector notation: $\tilde{\mathbf{a}}^{(\dagger)}(\mathbf{k}) = \left\{\tilde{a}^{(\dagger)}_{1}(\mathbf{k}), \ldots, \tilde{a}^{(\dagger)}_{2N}(\mathbf{k})\right\}$ and $\mathbf{\Omega}$ is a diagonal matrix with the excitation energies. The new operators satisfy the usual boson commutation relations

$$
\begin{aligned}
&\left[\tilde{a}^{(\dagger)}_{n}(\mathbf{k}), \tilde{a}^{(\dagger)}_{n'}(\mathbf{k}')\right] = 0 \quad \text{and} \\
&\left[\tilde{a}_{n}(\mathbf{k}), \tilde{a}^{\dagger}_{n'}(\mathbf{k}')\right] = \delta_{nn'}\delta_{\mathbf{k}\mathbf{k}'}, \qquad (3.31)
\end{aligned}
$$

furthermore they are constructed so that they are eigenmodes with energy $\omega_l(\mathbf{k})$:

$$
i\dot{\tilde{a}}_{n}(\mathbf{k}) = \left[\tilde{a}_{n}(\mathbf{k}), \mathcal{H}(\mathbf{k})\right] = \omega_{l}(\mathbf{k})\tilde{a}_{n}(\mathbf{k}) \qquad (3.32)
$$

(3.32) is equivalent to the requirement that the new operators $\tilde{a}^{(\dagger)}_{n}(\mathbf{k})$ diagonalize the Hamiltonian. Let us write the equation of motion for the operators $a_{A,n}(\mathbf{k})$,

$a_{B,n}(\mathbf{k})$, $a^{\dagger}_{B,n}(-\mathbf{k})$ and $a^{\dagger}_{A,n}(-\mathbf{k})$ in the vectorial form of

$$\dot{\mathbf{a}}^{(\dagger)}_{\xi}(\pm\mathbf{k}) = i\left[\mathcal{H}^{(2)}, \mathbf{a}^{(\dagger)}_{\xi}(\pm\mathbf{k})\right] = \begin{pmatrix} \dot{a}^{(\dagger)}_{\xi,1}(\pm\mathbf{k}) \\ \vdots \\ \dot{a}^{(\dagger)}_{\xi,N}(\pm\mathbf{k}) \end{pmatrix} = i \begin{pmatrix} \left[\mathcal{H}^{(2)}, a^{(\dagger)}_{\xi,1}(\pm\mathbf{k})\right] \\ \vdots \\ \left[\mathcal{H}^{(2)}, a^{(\dagger)}_{\xi,N}(\pm\mathbf{k})\right] \end{pmatrix} \tag{3.33}$$

where $\xi \in \{A, B\}$. In the following we show in detail how the equation of motion for a selected component of $\dot{\mathbf{a}}_A(\mathbf{k})$ can be given, and omit the derivation for the rest of the operators which can be done in the same way.

$$\begin{aligned}
\dot{a}_{A,n}(\mathbf{k}) &= i\left[\sum_{\mathbf{k}} \mathcal{H}^{(2)}(\mathbf{k}), a_{A,n}(\mathbf{k})\right] \\
&= i\sum_{\mathbf{k}}\sum_{j=1}^{N} \Big\{ \Big[[\mathbf{H}_{11}(\mathbf{k})]_{nj} \cdot a^{\dagger}_{A,n}(\mathbf{k}) a_{A,j}(\mathbf{k}), a_{A,n}(\mathbf{k}')\Big] \\
&\quad + \Big[[\mathbf{H}_{12}(\mathbf{k})]_{nj} \cdot a^{\dagger}_{A,n}(\mathbf{k}) a_{B,j}(\mathbf{k}), a_{A,n}(\mathbf{k}')\Big] \\
&\quad + \Big[[\mathbf{H}_{13}(\mathbf{k})]_{nj} \cdot a^{\dagger}_{A,n}(\mathbf{k}) a^{\dagger}_{B,j}(-\mathbf{k}), a_{A,n}(\mathbf{k}')\Big] \\
&\quad + \Big[[\mathbf{H}_{14}(\mathbf{k})]_{nj} \cdot a^{\dagger}_{A,n}(\mathbf{k}) a^{\dagger}_{A,j}(-\mathbf{k}), a_{A,n}(\mathbf{k}')\Big] \\
&\quad + \Big[[\mathbf{H}_{14}(\mathbf{k})]_{jn} \cdot a^{\dagger}_{A,j}(\mathbf{k}) a^{\dagger}_{A,n}(-\mathbf{k}), a_{A,n}(\mathbf{k}')\Big] \\
&\quad + \Big[\big[\mathbf{H}^{T}_{13}(-\mathbf{k})\big]_{jn} \cdot a^{\dagger}_{B,j}(\mathbf{k}) a^{\dagger}_{A,n}(-\mathbf{k}), a_{A,n}(\mathbf{k}')\Big] \\
&\quad + \Big[\big[\mathbf{H}^{T}_{12}(-\mathbf{k})\big]_{jn} \cdot a_{B,j}(-\mathbf{k}) a^{\dagger}_{A,n}(-\mathbf{k}), a_{A,n}(\mathbf{k}')\Big] \\
&\quad + \Big[\big[\mathbf{H}^{T}_{11}(-\mathbf{k})\big]_{jn} \cdot a_{A,j}(-\mathbf{k}) a^{\dagger}_{A,n}(-\mathbf{k}), a_{A,n}(\mathbf{k}')\Big] \Big\}
\end{aligned} \tag{3.34}$$

the rest of the terms are zero due to the bosonic commutation relations

$$\begin{aligned}
&[a^{(\dagger)}_{\xi,n}(\mathbf{k}), a^{(\dagger)}_{\zeta,m}(\mathbf{k})] = 0 \quad \text{and} \\
&[a_{\xi,n}(\mathbf{k}), a^{\dagger}_{\zeta,m}(\mathbf{k}')] = \delta_{nm}\delta_{\xi\zeta}\delta_{\mathbf{k}\mathbf{k}'}.
\end{aligned} \tag{3.35}$$

Relying on these and the relation $[ab,c]=a[b,c]+[a,c]b$ we can write

$$\begin{aligned}\dot{a}_{A,n}(\mathbf{k}) &= -i\sum_{j=1}^{N}\Big\{[\mathbf{H}_{11}(\mathbf{k})]_{nj}\cdot a_{A,j}(\mathbf{k})+[\mathbf{H}_{12}(\mathbf{k})]_{nj}\cdot a_{B,j}(\mathbf{k})\\ &\quad+[\mathbf{H}_{13}(\mathbf{k})]_{nj}\cdot a^{\dagger}_{B,j}(-\mathbf{k})+[\mathbf{H}_{14}(\mathbf{k})]_{nj}\cdot a^{\dagger}_{A,j}(-\mathbf{k})\\ &\quad+[\mathbf{H}_{14}(-\mathbf{k})]_{jn}\cdot a^{\dagger}_{A,j}(-\mathbf{k})+\left[\mathbf{H}^{T}_{13}(\mathbf{k})\right]_{jn}\cdot a^{\dagger}_{B,j}(-\mathbf{k})\\ &\quad+\left[\mathbf{H}^{T}_{12}(\mathbf{k})\right]_{jn}\cdot a_{B,j}(\mathbf{k})+\left[\mathbf{H}^{T}_{11}(\mathbf{k})\right]_{jn}\cdot a_{A,j}(\mathbf{k})\Big\}\\ &= -2i\sum_{j=1}^{N}\Big\{[\mathbf{H}_{11}(\mathbf{k})]_{nj}\cdot a_{A,j}(\mathbf{k})+[\mathbf{H}_{12}(\mathbf{k})]_{nj}\cdot a_{B,j}(\mathbf{k})\\ &\quad+[\mathbf{H}_{13}(\mathbf{k})]_{nj}\cdot a^{\dagger}_{B,j}(-\mathbf{k})+[\mathbf{H}_{14}(\mathbf{k})]_{nj}\cdot a^{\dagger}_{A,j}(-\mathbf{k})\Big\} \qquad (3.36)\end{aligned}$$

where we used that $\left[\mathbf{H}^{T}_{ab}(\mathbf{k})\right]_{jn}=[\mathbf{H}_{ab}(\mathbf{k})]_{nj}$ and $\mathbf{H}_{14}(\mathbf{k})=\mathbf{H}^{T}_{14}(-\mathbf{k})$. For simplicity let us use the vectorial form:

$$\begin{aligned}\dot{\mathbf{a}}_{A}(\mathbf{k}) &= -2i\mathbf{H}_{11}(\mathbf{k})\mathbf{a}_{A,j}(\mathbf{k})-2i\mathbf{H}_{12}(\mathbf{k})\mathbf{a}_{B,j}(\mathbf{k})\\ &\quad-2i\mathbf{H}_{13}(\mathbf{k})\mathbf{a}^{\dagger}_{B,j}(-\mathbf{k})-2i\mathbf{H}_{14}(\mathbf{k})\mathbf{a}^{\dagger}_{A,j}(-\mathbf{k}). \qquad (3.37)\end{aligned}$$

The equation of motion for the other three types of operators can be derived similarly and they read as follows

$$\begin{aligned}\dot{\mathbf{a}}_{B}(\mathbf{k}) &= -2i\mathbf{H}^{\dagger}_{12}(\mathbf{k})\mathbf{a}_{A,j}(\mathbf{k})-2i\mathbf{H}_{22}(\mathbf{k})\mathbf{a}_{B,j}(\mathbf{k})\\ &\quad-2i\mathbf{H}_{23}(\mathbf{k})\mathbf{a}^{\dagger}_{B,j}(-\mathbf{k})-2i\mathbf{H}^{T}_{13}(-\mathbf{k})\mathbf{a}^{\dagger}_{A,j}(-\mathbf{k}), \qquad (3.38)\end{aligned}$$

$$\begin{aligned}\dot{\mathbf{a}}^{\dagger}_{B}(-\mathbf{k}) &= 2i\mathbf{H}^{\dagger}_{13}(\mathbf{k})\mathbf{a}_{A,j}(\mathbf{k})+2i\mathbf{H}^{\dagger}_{23}(\mathbf{k})\mathbf{a}_{B,j}(\mathbf{k})\\ &\quad+2i\mathbf{H}^{T}_{22}(-\mathbf{k})\mathbf{a}^{\dagger}_{B,j}(-\mathbf{k})+2i\mathbf{H}^{T}_{12}(-\mathbf{k})\mathbf{a}^{\dagger}_{A,j}(-\mathbf{k}), \qquad (3.39)\end{aligned}$$

$$\begin{aligned}\dot{\mathbf{a}}^{\dagger}_{A}(-\mathbf{k}) &= 2i\mathbf{H}^{\dagger}_{14}(\mathbf{k})\mathbf{a}_{A,j}(\mathbf{k})+2i\mathbf{H}^{*}_{13}(-\mathbf{k})\mathbf{a}_{B,j}(\mathbf{k})\\ &\quad+2i\mathbf{H}^{*}_{12}(-\mathbf{k})\mathbf{a}^{\dagger}_{B,j}(-\mathbf{k})+2i\mathbf{H}^{T}_{11}(-\mathbf{k})\mathbf{a}^{\dagger}_{A,j}(-\mathbf{k}). \qquad (3.40)\end{aligned}$$

Collecting (3.37)-(3.40) in a matrix form we obtain

$$\begin{pmatrix}\dot{\mathbf{a}}_{A}(\mathbf{k})\\ \dot{\mathbf{a}}_{B}(\mathbf{k})\\ \dot{\mathbf{a}}^{\dagger}_{B}(-\mathbf{k})\\ \dot{\mathbf{a}}^{\dagger}_{A}(-\mathbf{k})\end{pmatrix}=-2i\begin{pmatrix}\mathbf{H}_{11}(\mathbf{k}) & \mathbf{H}_{12}(\mathbf{k}) & \mathbf{H}_{13}(\mathbf{k}) & \mathbf{H}_{14}(\mathbf{k})\\ \mathbf{H}^{\dagger}_{12}(\mathbf{k}) & \mathbf{H}_{22}(\mathbf{k}) & \mathbf{H}_{23}(\mathbf{k}) & \mathbf{H}^{T}_{13}(-\mathbf{k})\\ -\mathbf{H}^{\dagger}_{13}(\mathbf{k}) & -\mathbf{H}^{\dagger}_{23}(\mathbf{k}) & -\mathbf{H}^{T}_{22}(-\mathbf{k}) & -\mathbf{H}^{T}_{12}(-\mathbf{k})\\ -\mathbf{H}^{\dagger}_{14}(\mathbf{k}) & -\mathbf{H}^{*}_{13}(-\mathbf{k}) & -\mathbf{H}^{*}_{12}(-\mathbf{k}) & -\mathbf{H}^{T}_{11}(-\mathbf{k})\end{pmatrix}\begin{pmatrix}\mathbf{a}_{A}(\mathbf{k})\\ \mathbf{a}_{B}(\mathbf{k})\\ \mathbf{a}^{\dagger}_{B}(-\mathbf{k})\\ \mathbf{a}^{\dagger}_{A}(-\mathbf{k})\end{pmatrix} \qquad (3.41)$$

In order to gain a simpler form of the equation of motion we introduce the matrix

$$\mathbf{J}=\begin{pmatrix}\mathbf{I} & \mathbf{0}\\ \mathbf{0} & -\mathbf{I}\end{pmatrix} \qquad (3.42)$$

where $\mathbf{0}$ is a $2N \times 2N$ dimensional nullmatrix and $\mathbf{I}$ is the $2N \times 2N$ dimensional identity matrix. With this we can write (3.41) as

$$\dot{\mathbf{a}} = -2i\mathbf{JHa} \tag{3.43}$$

where $\mathbf{H}$ corresponds to the original Hamiltonian matrix of (3.25) and $\mathbf{a} := (\mathbf{a}_A(\mathbf{k}), \mathbf{a}_B(\mathbf{k}), \mathbf{a}_B^\dagger(-\mathbf{k}), \mathbf{a}_A^\dagger(-\mathbf{k}))$. Recalling that the diagonalization of the original Hamiltonian $\mathcal{H}^{(2)}(\mathbf{k})$ is equivalent to the problem of finding a rotated basis $\tilde{\mathbf{a}}$ for which (3.32) is realized, that is $\dot{\tilde{a}}_j = -i\omega_j \tilde{a}_j$. From (3.43) it follows that we need only to diagonalize the matrix $2\mathbf{JH}$. Let $\mathbf{V}$ be the unitary transformation that brings $2\mathbf{JH}$ into a diagonal form, the rotated basis then is $\tilde{\mathbf{a}} = \mathbf{V}^\dagger\mathbf{a}$ and multiplying (3.43) by $\mathbf{V}^\dagger$ from the left hand side

$$\mathbf{V}^\dagger\dot{\mathbf{a}} = \dot{\tilde{\mathbf{a}}} = -i\mathbf{V}^\dagger(2\mathbf{JH})\mathbf{a} \tag{3.44}$$

then inserting $\mathbf{a} = \mathbf{V}\tilde{\mathbf{a}}$ we get

$$\dot{\tilde{\mathbf{a}}} = -i\mathbf{V}^\dagger(2\mathbf{JH})\mathbf{V}\tilde{\mathbf{a}} = -i\mathbf{D}\tilde{\mathbf{a}} \tag{3.45}$$

where $\mathbf{D}$ is a diagonal matrix containing the excitation energies. We shall note that the unitary transformation $\mathbf{V}$ is $4N \times 4N$ dimensional and so is the matrix $\mathbf{D}$, however we only have $2N$ excitations. $\mathbf{D}$ can be written as

$$\mathbf{D} = \begin{pmatrix} \boldsymbol{\Omega}/2 & \\ & -\boldsymbol{\Omega}/2 \end{pmatrix} \tag{3.46}$$

where the eigenvalues in the diagonal matrix $\boldsymbol{\Omega}$, that is the values $[\boldsymbol{\Omega}]_{ii} = \omega_i$ are all positive. Naturally the negative values in the lower half cannot correspond to excitation energies thus are not physical eigenvalues and we obtain the desired form:

$$\mathcal{H}^{(2)} = \sum_{\mathbf{k}} \tilde{\mathbf{a}}^\dagger(\mathbf{k})\boldsymbol{\Omega}(\mathbf{k})\tilde{\mathbf{a}}\ (\mathbf{k}) \tag{3.47}$$

Chapter 4

From the Shastry-Sutherland model to $SrCu_2(BO_3)_2$

Fantasy is an exercise bicycle for the mind. It might not take you anywhere, but it tones up the muscles that can.

– *Terry Pratchett, Eric*

Spin gap systems, among them the antiferromagnetic ones with gap of purely quantum mechanical origins, have long been the subject of interest in the field of condensed matter physics. The study of the high-temperature-superconducting cuprates led to the discovery of many low-dimensional systems with (magnetically) disordered singlet ground states. Well known examples are the spin-Peierls materials like $CuGeO_3$ [Hase 1993b] and α'-NaV_2O_5 [Ueda 1998], the Haldane chains such as Y_2BaNiO_5 [Ramirez 1994, Alet 2000] or $PbNi_2V_2O_8$ [Masuda 2002, Smirnov 2002], the two-leg spin ladders with dimer singlet ground state like $SrCu_2O_3$ [Ishida 1994] and CaV_2O_5 [Ueda 1998] furthermore the spin plaquette systems such as CaV_4O_9 which was the first among the two-dimensional spin gap materials [Taniguchi 1995]. In low dimensions the role of frustration is enhanced, resulting in the formation of disordered ground state which is usually referred to as a quantum spin liquid [Misguich 2005, Balents 2010].
This phenomenon is well illustrated in the two-dimensional spin-1/2 quantum antiferromagntes exhibiting spontaneously dimerized phases [Gelfand 1989]. Among the two-dimensional frustrated systems the Shastry-Sutherland model serves as a unique example.

The aim of this chapter is to present a simple theoretical framework to investigate the ground-state phases and the magnetic excitations above them. We will use the Shastry-Sutherland model extended with anisotropy terms such as the antisymmetric exchange (DM) and g-tensor anisotropy as introduced on the basis of symmetry consideration in chapter 2. When calculating the excitation spectrum we will rely upon the general spin wave method discussed in chapter 3. In the form of a suitable bond-wave approximation we examine the momentum and field dependent excitation spectrum of $SrCu_2(BO_3)_2$ below the plateaus and compare our results with the observation of neutron-scattering and the ESR spectroscopy. As already revealed in chapter 2 we shall distinguish between the high and low temperature cases. The relevancy of this differentiation is that in the high symmetry case, due to the inversion symmetry of the dimers (and the presence of the reflection plane)

the in-plane components of DM vector vanish, while in the low symmetry case we need to include those components as well (see chapter 2). We shall start our investigations with the introduction of the variational approach and the definition of the bond basis. We shortly summarize the crucial steps in the bond wave approach and attempt to point out its relation to the generalized spin wave theory of chapter 3. Then we discuss the low and high symmetry phase diagrams as the function of magnetic field and DM anisotropy. A separate section will be devoted to the zero-field momentum dependent spectrum as well as to the cases when the field is applied perpendicular and parallel to the $CuBO_3$-plane.

4.1 The variational approach and the bond–wave theory

Based on the symmetry analysis presented in chapter 2 the Hamiltonian has the following form

$$\begin{aligned}\mathcal{H} &= J\sum_{n.n.}\mathbf{S}_i\cdot\mathbf{S}_j + J'\sum_{n.n.n.}\mathbf{S}_i\cdot\mathbf{S}_j + \sum_{n.n.}\mathbf{D}_{ij}\cdot(\mathbf{S}_i\times\mathbf{S}_j) + \sum_{n.n.n.}\mathbf{D'}_{ij}\cdot(\mathbf{S}_i\times\mathbf{S}_j)\\ &\quad -h_z\sum_{u.c.}\left[g_z\left(S^z_{\mathrm{A1}}+S^z_{\mathrm{A2}}+S^z_{\mathrm{B1}}+S^z_{\mathrm{B2}}\right)-g_{\mathrm{s}}\left(S^x_{\mathrm{A1}}-S^x_{\mathrm{A2}}+S^y_{\mathrm{B1}}-S^y_{\mathrm{B2}}\right)\right]\\ &\quad -h_x\sum_{u.c.}\left[g_x\left(S^x_{\mathrm{A1}}+S^x_{\mathrm{A2}}\right)+g_y\left(S^x_{\mathrm{B1}}+S^x_{\mathrm{B2}}\right)-g_{\mathrm{s}}\left(S^z_{\mathrm{A1}}-S^z_{\mathrm{A2}}\right)\right] \qquad (4.1)\end{aligned}$$

Due to the geometry and the known dimer-sinlet ground state of the Shastry-Sutherland model, instead of the conventional basis defined on the sites, we will use a more convenient dimer basis. That is, we will think about the orthogonal bonds as the elementary building units of the lattice, therby allowing for the quantum mechanical entanglement on them.
In the spirit of Sachdev and Bhatt [Sachdev 1990], we introduce the singlet and the triplet states on each bond as it follows

$$|s\rangle = \frac{1}{\sqrt{2}}(|\uparrow\downarrow\rangle - |\downarrow\uparrow\rangle) \qquad (4.2a)$$

$$|t_x\rangle = \frac{i}{\sqrt{2}}(|\uparrow\uparrow\rangle - |\downarrow\downarrow\rangle) \qquad (4.2b)$$

$$|t_y\rangle = \frac{1}{\sqrt{2}}(|\uparrow\uparrow\rangle + |\downarrow\downarrow\rangle) \qquad (4.2c)$$

$$|t_z\rangle = -\frac{i}{\sqrt{2}}(|\uparrow\downarrow\rangle + |\downarrow\uparrow\rangle)\,. \qquad (4.2d)$$

This definition of $|t_x\rangle$, $|t_y\rangle$, and $|t_z\rangle$ is different from that in Ref. [Sachdev 1990] by an additional phase factor $(-i)$, ensuring the time-reversal invariance of (4.2).[1] In fact, the triplets with the above definition are quadrupole states.

[1] The action of the antiunitary time-reversal operator on spin-1/2 states flips the spin and adds minus sign only to $|\downarrow\rangle$-state, thus leaves the states $|s\rangle$, $|t_x\rangle$, $|t_y\rangle$, and $|t_z\rangle$ invariant.

In the presence of magnetic field along the z-axis, it will be more convenient to use the usual triplet states that are the eigenstates of the z component of the spin operator:

$$|t_1\rangle = |\uparrow\uparrow\rangle \tag{4.3a}$$
$$|t_0\rangle = i|t_z\rangle \tag{4.3b}$$
$$|t_{\bar{1}}\rangle = |\downarrow\downarrow\rangle\,. \tag{4.3c}$$

In this way we introduced the four dimensional local Hilbert space defined on a dimer of two $S = 1/2$ spins. In the introductory chapter 3, we considered a the general form of the local basis: $\{|\phi_{\xi,0}(l)\rangle, \ldots, |\phi_{\xi,N}(l)\rangle\}$, where l denoted the site index on sublattice ξ. This basis corresponds now to $\{|s_\xi(l)\rangle, |t_{\alpha,\xi}(l)\rangle, |t_{\beta,\xi}(l)\rangle, |t_{\gamma,\xi}(l)\rangle\}$ with $\xi \in \{A, B\}$.

4.1.1 Variational wave function

Using the above basis, below the critical value $(J'/J)_c = 0.68$, the ground state of the pure Shastry-Sutherland model (2.13) can be written as a product of singlets $|s\rangle$ over the dimer bonds, $|\Psi\rangle = \prod_{\text{dimers}} |s\rangle$. However, in the presence of the DM interactions and/or finite magnetic fields, we need to allow for a linear combination of the singlet and triplet states on each dimer, still keeping the dimer wave function entangled, while retaining the product form over the dimer bonds:

$$|\Psi\rangle = \prod_{\text{A dimers}} |\psi_{A,0}\rangle \prod_{\text{B dimers}} |\psi_{B,0}\rangle\,, \tag{4.4}$$

where

$$|\psi_{A,0}\rangle = U_{00}(A)|s\rangle + \sum_{\alpha=1}^{3} U_{\alpha 0}(A)|t_\alpha\rangle\,, \tag{4.5a}$$
$$|\psi_{B,0}\rangle = U_{00}(B)|s\rangle + \sum_{\alpha=1}^{3} U_{\alpha 0}(B)|t_\alpha\rangle\,, \tag{4.5b}$$

with $|t_\alpha\rangle$ denoting the three components of the triplets in the basis (4.2) or (4.3). This wave function can describe the phases that do not break the translational symmetry. Since we have two (i.e. A and B) dimers in the unit cell, the entire wave function $|\Psi\rangle$ is translationally invariant even when the wave functions of the two dimers are different. Certainly, this wave function cannot describe the plateau states, except for the translationally invariant 1/2-plateu. To consider the other plateaus as well one needs to take a larger unit cell. The complex variational parameters $U_{\alpha 0}(A)$ and $U_{\alpha 0}(\mathrm{B})$ ($\alpha = 1, 2, 3$) are to be determined by minimizing the energy

$$E = \frac{\langle\Psi|\mathcal{H}|\Psi\rangle}{\langle\Psi|\Psi\rangle}\,. \tag{4.6}$$

We perform the minimization numerically, except for some simple cases when the analytical solution is available.

4.1.2 Auxiliary boson formalism for the Hamiltonian

In order to find the excitation spectrum, we introduce the auxiliary bosons which create the singlet and the triplet states on each bond. The operator $s^\dagger|0\rangle = |s\rangle$ creates the singlet state, while the operators $t^\dagger_\alpha$, $t^\dagger_\beta$, and $t^\dagger_\gamma$ create the triplets $|t_\alpha\rangle$, $|t_\beta\rangle$, and $|t_\gamma\rangle$, respectively. In order to faithfully represent the four states, the number of bosons per dimer needs to be constrained:

$$s^\dagger s \; + \sum_\alpha t^\dagger_\alpha t_\alpha = 1 \; . \tag{4.7}$$

In the basis (4.2) the components of the spin operators on bond j can be given as

$$S^\alpha_{j,1} = \frac{i}{2}\left(t^\dagger_{\alpha,j} s_j - s^\dagger_j t_{\alpha,j}\right) - \frac{i}{2}\epsilon_{\alpha,\beta,\gamma} t^\dagger_{\beta,j} t_{\gamma,j} \; , \tag{4.8a}$$

$$S^\alpha_{j,2} = -\frac{i}{2}\left(t^\dagger_{\alpha,j} s_j - s^\dagger_j t_{\alpha,j}\right) - \frac{i}{2}\epsilon_{\alpha,\beta,\gamma} t^\dagger_{\beta,j} t_{\gamma,j} \; . \tag{4.8b}$$

The indices 1 and 2 correspond to the two sites belonging to the dimer j.
The intradimer Heisenberg exchange of the Hamiltonian (2.13) in this bond representation reads

$$\mathcal{H}_J = -\frac{3J}{4}\sum_j s^\dagger_j s_j + \frac{J}{4}\sum_j \sum_{\alpha=x,y,z} t^\dagger_{\alpha,j} t_{\alpha,j} \; , \tag{4.9}$$

while the intradimer DM-interaction has the form of

$$\mathcal{H}_D = \frac{D}{2}\sum_{j\in A}\left(t^\dagger_{y,j} s_j + s^\dagger_j t_{y,j}\right) - \frac{D}{2}\sum_{j\in B}\left(t^\dagger_{x,j} s_j + s^\dagger_j t_{x,j}\right) \; . \tag{4.10}$$

The rest of the terms in the Hamiltonian can be expressed similarly in the bond basis.

In the presence of magnetic field along the z axis we use the triplet states defined in (4.3) which leads to the following form of the spin operators:

$$S^+_{j,l} = \frac{t^\dagger_{1,j} t_{0,j} + t^\dagger_{0,j} t_{\bar{1},j}}{\sqrt{2}} \pm \frac{s^\dagger_j t_{\bar{1},j} - t^\dagger_{1,j} s_j}{\sqrt{2}} \; , \tag{4.11a}$$

$$S^-_{j,l} = \frac{t^\dagger_{\bar{1},j} t_{0,j} + t^\dagger_{0,j} t_{1,j}}{\sqrt{2}} \mp \frac{s^\dagger_j t_{1,j} - t^\dagger_{\bar{1},j} s_j}{\sqrt{2}} \; , \tag{4.11b}$$

$$S^z_{j,l} = \frac{t^\dagger_{1,j} t_{1,j} - t^\dagger_{\bar{1},j} t_{\bar{1},j}}{2} \pm \frac{s^\dagger_j t_{0,j} + t^\dagger_{0,j} s_j}{2} \; . \tag{4.11c}$$

The upper sign belongs to the site $l = 1$ and the lower to the site 2 on the dimer j.

4.1.3 Bond wave method

After rewriting the Hamiltonian (4.1) in terms of the bond operators using Eq. (4.8) or (4.11), we perform a bond wave approximation on the basis of the general spin

wave theory introduced in chapter 3. As the first step, we extend the number of bosons per dimer from 1 to M, so that the constraint (4.7) reads

$$s^\dagger s \; + \sum_{\alpha=x,y,z} t_\alpha^\dagger t_\alpha = M \; . \tag{4.12}$$

The variational approach introduced in Sec. 4.1.1 is equivalent to finding the classical ($S \to \infty$) ground state. $M \to \infty$ corresponds to the classical solution where the quantum fluctuations between the dimers are neglected. To understand this, let us rotate the 'quantization axis' on both dimers through the unitary transformations $\mathbf{U}(A)$ and $\mathbf{U}(B)$. This is in accordance with writing the ground state wave function in the variational form of (4.5a) and (6.3). Now, the variational solution $|\psi_{A,0}\rangle$ can be expressed in terms of the 'rotated' bosons as $|\psi_{A,0}\rangle = a_{A,0}^\dagger|0\rangle$, where according to (4.5a) $a_{A,0}^\dagger = U_{00}(A)s^\dagger + \sum_{\alpha=1}^3 U_{\alpha 0}(A)t_\alpha^\dagger$ and similarly, $|\psi_{B,0}\rangle = a_{B,0}^\dagger|0\rangle$ with $a_{B,0}^\dagger = U_{00}(B)s^\dagger + \sum_{\alpha=1}^3 U_{\alpha 0}(B)t_\alpha^\dagger$.
When M is arbitrary, we promote $|\psi_{A,0}\rangle = a_{A,0}^\dagger|0\rangle$ and $|\psi_{B,0}\rangle = a_{B,0}^\dagger|0\rangle$ to $|\psi_{A,0}\rangle = (a_{A,0}^\dagger)^M|0\rangle$ and $|\psi_{B,0}\rangle = (a_{B,0}^\dagger)^M|0\rangle$, which are directly connected to the Bloch coherent states of an $S = M/2$ spin system. In the classical limit $M \to \infty$ and we can think about the coherent states $|\psi_{A,0}\rangle$ and $|\psi_{B,0}\rangle$ as the condensate of the bosons $a_{A,0}$ and $a_{B,0}$.

Naturally, the unitary transformations $\mathbf{U}(A)$ and $\mathbf{U}(B)$ rotate the triplet bosons into $a_{A,\alpha}$ and $a_{B,\alpha}$ ($\alpha = 1, 2, 3$) so that they fulfil the usual commutation relations and the local constraint Eq. (4.12) remains true as

$$a_{\xi,0}^\dagger a_{\xi,0} + \sum_{\alpha=1}^3 a_{\xi,\alpha}^\dagger a_{\xi,\alpha} = M \; . \tag{4.13}$$

with $\xi \in \{A, B\}$. Correspondingly, we need to express the spin operators (4.8) or (4.11) in the rotated basis as defined in (3.5) and (3.6).

To consider the small 'transverse' fluctuations around the classical solution, we solve the constraint (4.13) explicitly for $a_{\xi,0}$ and treat $a_{\xi,1}$, $a_{\xi,2}$ and $a_{\xi,3}$ as the Holstein-Primakoff bosons. Replacing

$$\begin{aligned} a_{\xi,0}^\dagger \quad &\to \quad \sqrt{M - \sum_\alpha a_{\xi,\alpha}^\dagger a_{\xi,\alpha}} \approx \sqrt{M} - \frac{1}{2\sqrt{M}} \sum_\alpha a_{\xi,\alpha}^\dagger a_{\xi,\alpha} + \cdots \quad \text{and} \\ a_{\xi,0} \quad &\to \quad \sqrt{M - \sum_\alpha a_{\xi,\alpha}^\dagger a_{\xi,\alpha}} \approx \sqrt{M} - \frac{1}{2\sqrt{M}} \sum_\alpha a_{\xi,\alpha}^\dagger a_{\xi,\alpha} + \cdots \end{aligned} \tag{4.14}$$

we perform the $1/M$-expansion in the spin operators and subsequently in the Hamiltonian. Then, performing a Fourier transformation, the Hamilton operator can be written as

$$\mathcal{H} = \mathcal{H}^{(0)} + \mathcal{H}^{(1)} + \mathcal{H}^{(2)} + \cdots \tag{4.15}$$

where $\mathcal{H}^{(0)} = E_0$ corresponds to the variational energy (4.6) and $\mathcal{H}^{(1)}$ consists of the terms linear in

$$\mathbf{a_k} = \Big(a_{A,1}(\mathbf{k}), a_{A,2}(\mathbf{k}), a_{A,3}(\mathbf{k}), a_{B,1}(\mathbf{k}), a_{B,2}(\mathbf{k}), a_{B,3}(\mathbf{k})\Big) \tag{4.16}$$

as well as in $\mathbf{a}^\dagger_{\mathbf{k}}$ defined similarly. Furthermore, $\mathcal{H}^{(1)}$ is identically zero at the variational solution and the first correction appears in the quadratic order:

$$\mathcal{H}^{(2)} = \frac{1}{2}\sum_{\mathbf{k}\in \mathrm{BZ}} \begin{pmatrix} \mathbf{a}^\dagger_{\mathbf{k}} \\ \mathbf{a}_{-\mathbf{k}} \end{pmatrix}^T \begin{pmatrix} M & N \\ N^* & M \end{pmatrix} \begin{pmatrix} \mathbf{a}_{\mathbf{k}} \\ \mathbf{a}^\dagger_{-\mathbf{k}} \end{pmatrix} . \tag{4.17}$$

$\mathcal{H}^{(2)}$ can be diagonalized by the generalized Bogoliubov transformation introduced in chapter 3, and we obtain three excitations, one for each $a_{\xi,\alpha}(\mathbf{k})$ boson, per dimer.

4.2 Phase diagram in a field parallel to z axis

In this section we will consider the variational ground state phase diagram in the presence of an external field along the z-axis. For clarity, we will investigate the high-symmetry case, where $D = 0$ and the low-symmetry case, where the in-plane DM component is allowed, separately. In the whole discussion we neglect the effect of the g-tensor anisotropy: $g_s = 0$.

4.2.1 High symmetry case

At temperatures higher than $T_\mathrm{s} = 395$ K, the symmetry group of the two–dimer unit cell is $\mathcal{D}_{4h}$ and only the out-of-plane inter-dimer $D'_\perp$ term is allowed. With this type of anisotropy the z component of the spin is a conserved quantity which greatly simplifies the form of the variational ground states and that of the bond wave Hamiltonian.

Numerically minimizing the variational energy (4.6) in the presence of a magnetic field along the z direction, we have found three gapped phases: the dimer–singlet (DS), the one–half magnetization plateau, and the fully polarized phase. Furthermore, there are four gapless phases associated with the rotational ($O(2)$) symmetry breaking, namely the Néel, the $O(2)[\mathcal{C}_4]$, the $O(2)[\mathcal{S}_4]$, and the $O(2)\times Z_2$ phases. In these $O(2)$-type phases, the rotational symmetry in the plane perpendicular to the field h_z is spontaneously broken. We show the phase digrams as the function of magnetic field and $D'_\perp$, and as of the field and the ratio J'/J in Fig. 4.1 (a) and (b), respectively. A separate section will be devoted to the more important phases, and an interested reader may find the rest of them in appendix B.1.

4.2.1.1 Dimer–singlet phase

As we mentioned earlier, the exact ground state of the SU(2) symmetric Shastry–Sutherland model is the product of singlets: $|\psi_{A,0}\rangle = |\psi_{B,0}\rangle = |s\rangle$ for $0 \le J' \lesssim 0.68J$, as shown in Ref. [Koga 2000]. In the variational approach this ground state turns out to be stable for finite values of $D'_\perp$ and for magnetic fields $h < h_\mathrm{c}$, where the critical field can be given as

$$h_\mathrm{c} = \sqrt{J^2 - 4|D'_\perp|J}\,. \tag{4.18}$$

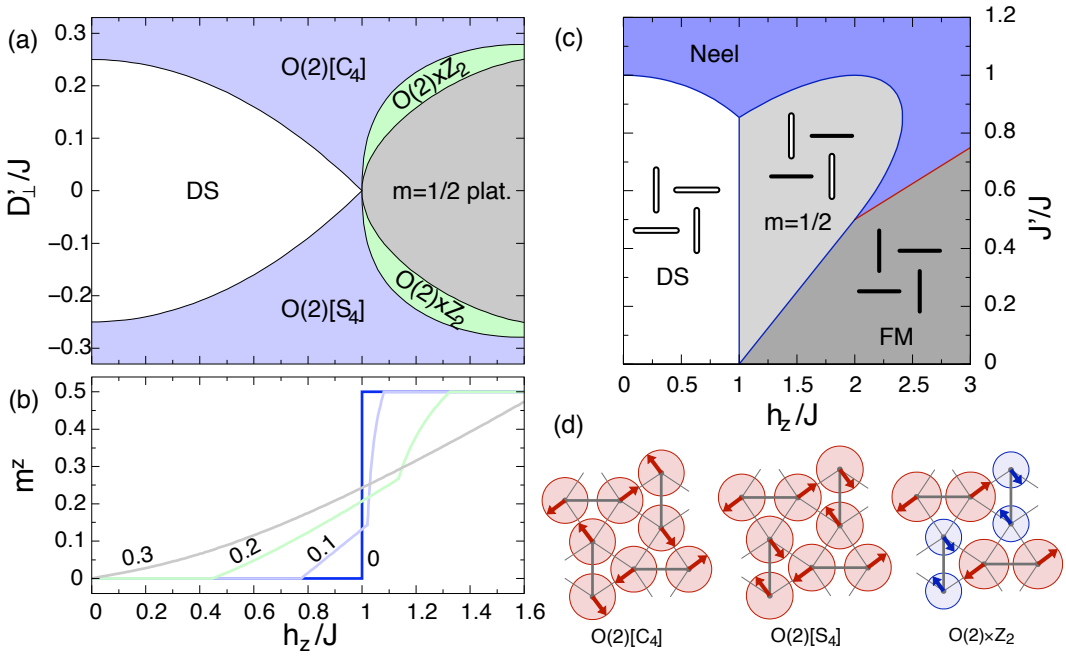

Figure 4.1: (a) Phase diagram in the h_z–$D'_\perp$ plane for $D = 0$ and $J'/J = 0.6$. DS denotes the dimer singlet phase that remains a variational ground state even for finite values of $D'_\perp$. 'm=1/2 plat.' denotes the half–magnetization plateau phase, with a singlet and a magnetized triplet in each unit cell. (b) The magnetization curves for different values of $|D'_\perp|/J$ as a function of the magnetic field. (c) Phase diagram as the function of the field and interdimer exchange J'. The white dimers represent the singlet, the black the $S^z = 1$ triplet state. (d) The spin configurations in the $O(2)$ symmetry breaking phases. For S^z is a conserved quantity, the spins can be arbitrarily rotated by a global $O(2)$ rotation in the plane. The blue and red arrows represent spins with unequal length.

The ground state energy is coming purely from the exchange within a dimer:

$$E_{\mathrm{DS}} = -\frac{3J}{2}\,, \tag{4.19}$$

and the bond energies between the dimers are identically zero.

4.2.1.2 The rotational symmetry breaking phases

Between the dimer singlet and the one-half magnetization plateau the $O(2)$ symmetry breaking phases emerge as indicated in Fig. 4.1(a). In them the magnetization increases continuously between 0 and 1/2 per dimer, or equivalently between 0 and 1 per unit cell (see Fig. 4.1(b)). S^z being a conserved quantity, the Hamiltonian does not break the rotational symmetry about the z-axis. This symmetry is spon-

taneously broken in the $O(2)$ phases. From numerical minimization we found that the wave functions can be written as

$$|\psi_{A,0}\rangle \propto |s\rangle + ue^{i\varphi}|t_1\rangle + de^{-i\varphi}|t_{\bar{1}}\rangle \,, \tag{4.20a}$$
$$|\psi_{B,0}\rangle \propto |s\rangle \pm iue^{i\varphi}|t_1\rangle \mp ide^{-i\varphi}|t_{\bar{1}}\rangle \,, \tag{4.20b}$$

where the upper sign belongs to the case $D'_\perp > 0$ and the lower sign to $D'_\perp < 0$. This wave function is continuously connected to the dimer–singlet phase: as the (real) parameters u and d become 0, the singlet-product state is recovered. In these phases the S^z expectation values are equal for all the spins

$$\langle S^z\rangle \propto |u|^2 - |d|^2 \tag{4.21}$$

and the spin components in the xy plane along the dimers are perpendicular to each other, so that going around on a square of sites belonging to different dimers, the spins make a full turn too, as shown in Fig. 4.1(d). In other words, the spin configurations are invariant with respect to either the rotation C_4 or the S_4. The sign of $D'_\perp$ will select between the two types of rotations and thus between the two phases. To make a clear distinction, we use the symmetry group that leaves the given variational ground state invariant to label the phases. $O(2)[\mathcal{C}_4]$ and $O(2)[\mathcal{S}_4]$ are realized for positive and negative values of $D'_\perp$, respectively. The ground state energy of the states (4.20a) and (4.20b) reads

$$\begin{aligned} E_{O(2)} &= \frac{u^2+d^2-3}{u^2+d^2+1}\frac{J}{2} + \frac{2(u^2-d^2)^2}{(u^2+d^2+1)^2}J' \\ &\quad - \frac{4(u-d)^2}{(u^2+d^2+1)^2}|D'_\perp| - \frac{2(u^2-d^2)}{u^2+d^2+1}h_z \,, \end{aligned} \tag{4.22}$$

and the minimization gives a set of polynomial equations that can be solved numerically. Close to the phase boundary (4.18) of the dimer singlet phase, we can perform a series expansion in the parameter $\delta h = h_z - h_\mathrm{c}$. The variational parameters then, in the lowest order of δh, can be expressed as:

$$u = -\frac{(J+h_\mathrm{c})\sqrt{2h_\mathrm{c}}}{2\sqrt{4JJ'h_\mathrm{c}^2 + J^4 - h_\mathrm{c}^4}}\sqrt{\delta h} \,, \tag{4.23a}$$
$$d = \frac{(J-h_\mathrm{c})\sqrt{2h_\mathrm{c}}}{2\sqrt{4JJ'h_\mathrm{c}^2 + J^4 - h_\mathrm{c}^4}}\sqrt{\delta h} \,. \tag{4.23b}$$

The magnetization below the critical field h_c is 0, and above it increases as

$$m^z = \frac{(J-4|D'_\perp|)\delta h}{2J|D'_\perp| - 4{D'_\perp}^2 + J'(J-4|D'_\perp|)} + O\left(\delta h^2\right) \,. \tag{4.24}$$

In the absence of the magnetic field the absolute values of the parameters u and d – that is the contribution of the two triplet components to the ground state –

become equal and using the notation $v/\sqrt{2} = u = -d$, the wave function can be written as

$$|\psi_{A,0}\rangle \propto |s\rangle + \frac{v}{\sqrt{2}}\left(e^{i\varphi}|t_1\rangle - e^{-i\varphi}|t_{\bar{1}}\rangle\right) , \tag{4.25a}$$

$$|\psi_{B,0}\rangle \propto |s\rangle \pm \frac{v}{\sqrt{2}} i\left(e^{i\varphi}|t_1\rangle + e^{-i\varphi}|t_{\bar{1}}\rangle\right) . \tag{4.25b}$$

Again, the lower and upper sign is determined by that of $D'_\perp$. The minimum of the energy (4.22) in this case is achieved for

$$v = \sqrt{\frac{4|D'_\perp| - J}{4|D'_\perp| + J}} , \tag{4.26}$$

and has the form of

$$E = -\frac{J}{2} - 2|D'_\perp| - \frac{J^2}{8|D'_\perp|} . \tag{4.27}$$

We can conclude that in zero field the $O(2)$ phases are realized for $|D'_\perp| > J/4$ which is consistent with the instability of the dimer singlet phase given in (4.18).

phase	$2\Theta\sigma$	$C_2(z)$	$2S_4$	$2\Theta\sigma S_4$	I	$\mathcal{G}_H$
DS	✓	✓	✓	✓	✓	$\mathcal{D}_{4h}$
$O(2)[\mathcal{C}_4]$	–	✓	–	–	–	$\mathcal{C}_4$
$O(2)[\mathcal{S}_4]$	–	✓	✓	–	–	$\mathcal{S}_4$
$O(2) \times Z_2$	–	✓	–	–	–	$\mathcal{C}_2$
plateau	✓	✓	–	–	✓	$\mathcal{D}_{2h}$
Néel	–	–	–	–	✓	$\mathcal{C}_i$

Table 4.1: A summary of symmetry properties of the high–symmetry phases when the field is perpendicular to the xy-plane. A checkmark indicates the symmetry class under which the given state is invariant. The last column shows the subgroup of $\mathcal{D}_{4h}$ that characterises the phases.

The $O(2)[\mathcal{S}_4]$ and similarly the $O(2)[\mathcal{C}_4]$ phases are separated by two continuous phase transitions from the one–half magnetization plateau phase. The intermediate phase exhibits both the Z_2-symmetry breaking of the plateau phase – that is, the different z-component of the magnetization on the dimers A and the B – and the rotational symmetry breaking of $O(2)[\mathcal{S}_4]$ and $O(2)[\mathcal{C}_4]$. The variational wave function of this phase can be written as

$$|\psi_{A,0}\rangle \propto |s\rangle + (u \pm v)e^{i\varphi}|t_1\rangle + (d \pm e)e^{-i\varphi}|t_{\bar{1}}\rangle , \tag{4.28a}$$

$$|\psi_{B,0}\rangle \propto |s\rangle - i(u \mp v)e^{i\varphi}|t_1\rangle + i(d \mp e)e^{-i\varphi}|t_{\bar{1}}\rangle \tag{4.28b}$$

and a schematic figure of the in-plane spin configuration is shown in Fig. 4.1(d). As we approach the boundary of the one-half magnetization plateau the in-plane components of the spins decrease, and eventually vanish at the phase boundary.

Though the translational symmetry is not broken in this phase, the fact that the magnetization along the field is not equal on the two types of dimers means that some kind of discrete symmetry is violated. At the same time, due to the $O(2)$ characteristics, a continuous symmetry is broken as well, therefore we may call this phase a (magnetic) supersolid [Matsuda 1970, Liu 1973].

4.2.2 Low–symmetry case

At low temperatures, specifically at $T < T_s = 395$ K, the symmetry of two–dimer unit cell is reduced to $\mathcal{D}_{2d}$ as the $CuBO_3$ layer becomes buckled and the inversion symmetry vanishes. The loss of inversion symmetry allows for a finite value of the in-plane DM interactions of which there are three components: one intradimer term D, and two interdimer DM components: $D'_{||,ns}$ and $D'_{||,s}$. As D is much larger than $D'_{||,ns}$ and $D'_{||,s}$ we consider only the effect of the intradimer DM component D and that of the out-of-plane interdimer component $D'_{\perp}$.

4.2.2.1 The symmetric phase

Numerical minimization indicated that in low field and within the experimentally relevant parameter region the ground state does not break any of the symmetries of the Hamiltonian, therefore we shall refer to this phase as $Z_1[\mathcal{D}_{2d}]$. In addition to this symmetric phase, two-fold degenerate Z_2 phases appear in the low symmetry phase diagram which will be discussed in appendix B.2. The schematic figures of the spin configurations and the phase diagrams as the function of magnetic field and exchange couplings are shown in Fig. 4.2. As the in-plane DM vector becomes finite, S^z ceases to be a good quantum number and the continuous symmetry of the $O(2)$ phases reduces to discrete symmetries. Due to the absence of continuous symmetry all the phases become gapped. This symmetry reduction shows in the expectation values of the energy; the inclusion of the intra-dimer DM component D introduces an additional anisotropy term to Eq. (4.22)

$$E_{Z_1[\mathcal{D}_{2d}]} = E_{O(2)} + \sqrt{2}D\frac{u+d}{u^2+d^2+1}\cos\varphi\,. \tag{4.29}$$

This extra term determines the preferred direction of the xy components. Assuming $D > 0$ and positive u and v, the DM energy on the dimers, that is the second term in (4.29) is minimal when $\varphi = \pi$. The variational wave function in the phase $Z_1[\mathcal{D}_{2d}]$ can be given as

$$|\psi_{A,0}\rangle \propto |s\rangle - u\,|t_1\rangle - d\,|t_{\bar{1}}\rangle\,, \tag{4.30a}$$
$$|\psi_{B,0}\rangle \propto |s\rangle + iu\,|t_1\rangle - id\,|t_{\bar{1}}\rangle\,. \tag{4.30b}$$

This phase is adiabatically connected to the dimer-singlet product phase as $u \to 0$ and $d \to 0$, and in general the intra-dimer DM interaction D mixes the triplet components to the singlet, as expected from Eq. (4.10). Recalling the (4.20) expression of the $O(2)[\mathcal{S}_4]$ wave function (with the lower sign) we can say that locking the phase

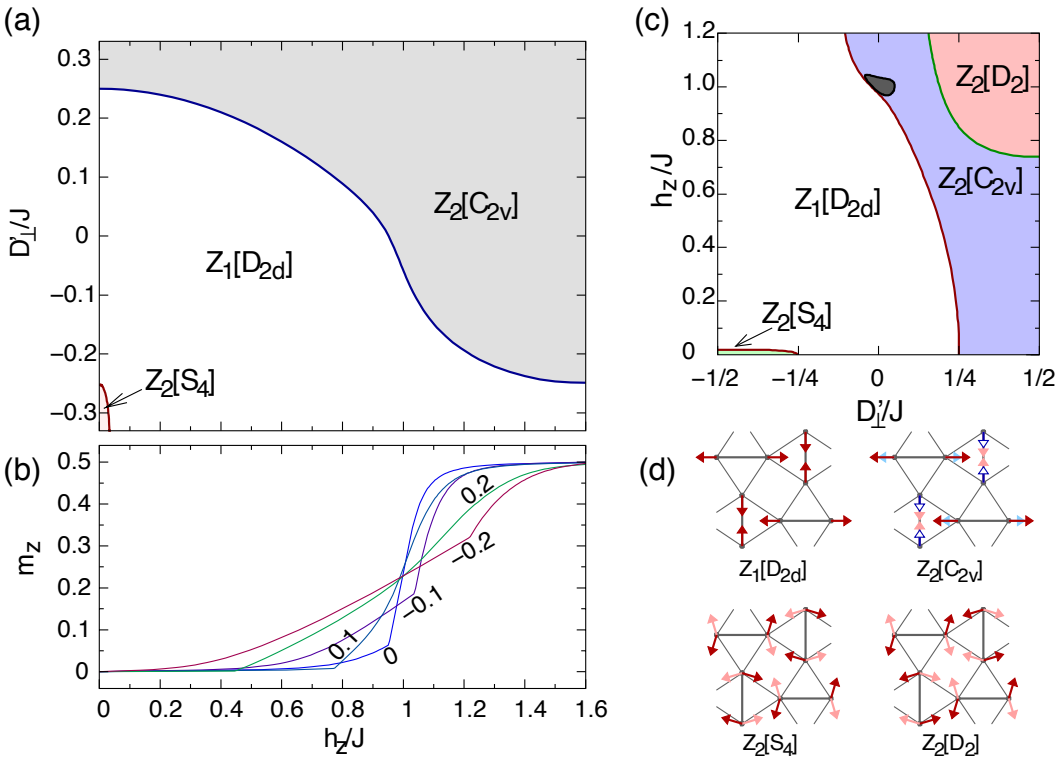

Figure 4.2: (a) Phase diagram in h_z–$D'_\perp$ plane the for $J'/J = 0.6$ and $D/J = 0.1$. In comparison to the $D = 0$ case in Fig. 4.1, in a large region of the phase space the dimer-singlet and the $O(2)[S_4]$ essentially merged to create the $Z_1[D_{2d}]$ phase, a small part of the $O(2)[S_4]$ phase become a twofold degenerate $Z_2[S_4]$, and the $O(2)[C_4]$ merged with the $m = 1/2$ magnetization plateau phase into the $Z_2[C_{2v}]$ phase. (b) Magnetization curves for a few selected values of $D'_\perp$. (c) Phase diagram for $J'/J = 0.3$ and $D/J = 0.1$. (d) Schematic figure of the spin configurations.

to $\varphi = 0$ corresponds to the wave function of $Z_1[\mathcal{D}_{2d}]$. In other words, when $D' < 0$, an infinitesimal value of D removes the phase boundary between the dimer-singlet phase and the $O(2)[\mathcal{S}_4]$ phase. For $D' > 0$, the $O(2)[\mathcal{C}_4]$ phase becomes frustrated with respect to D, and will give rise to a Z_2-symmetry breaking.

The conditions $\partial E_{Z_1[\mathcal{D}_{2d}]}/\partial u = 0$ and $\partial E_{Z_1[\mathcal{D}_{2d}]}/\partial d = 0$ lead to a set of polynomial equations of high degree that one can solve only numerically. However, for small values of D, a series expansion in the parameter D/J is possible. When $h_z < h_c$ (h_c was defined in Eq. (4.18)) we can expand the energy as

$$E_{Z_1[\mathcal{D}_{2d}]} = -\frac{3J}{2} + 2J(d^2 + u^2) + 4D'_\perp(u - d)^2 - 2h_z(u^2 - d^2) - \sqrt{2}D(u + d) \tag{4.31}$$

and in the lowest order in D the minimum is achieved when

$$u = \frac{1}{2\sqrt{2}} \frac{D(J + 4D'_\perp + h_z)}{J^2 + 4JD'_\perp - h_z^2} , \tag{4.32a}$$

$$d = \frac{1}{2\sqrt{2}} \frac{D(J + 4D'_\perp - h_z)}{J^2 + 4JD'_\perp - h_z^2} . \tag{4.32b}$$

To be more precise, the expansion is actually performed in $D/(J^2 + 4JD'_\perp - h_z^2) = D/(h_c^2 - h_z^2)$, and the denominator becomes 0 at the $D = 0$ boundary between the dimer–singlet and the $O(2)[\mathcal{S}_4]$ phase. The magnetization per dimer in this limit grows quadratically with the anisotropy

$$m^z = \frac{h_z}{J} \frac{h_c^2}{(h_c^2 - h_z^2)^2} (D - 2\tilde{g}_s J)^2 + O\left(D^4\right) , \tag{4.33}$$

Finally, we shall note that J' enters only in the next order in the expansion.

Table 4.2: Symmetry properties of the low–symmetry phases when $h||z$. Similarly to the high symmetry case, we show the symmetry classes which leave the given phase unaffected, as well as the subgroup $\mathcal{G}_L$ characterizing them.

phase	$2\Theta\sigma$	$C_2(z)$	$2S_4$	$2\Theta\sigma S_4$	$\mathcal{G}_L$
$Z_1[\mathcal{D}_{2d}]$	✓	✓	✓	✓	$\mathcal{D}_{2d}$
$Z_2[\mathcal{D}_2]$	–	✓	–	✓	$\mathcal{D}_2$
$Z_2[\mathcal{S}_4]$	–	✓	✓	–	$\mathcal{S}_4$
$Z_2[\mathcal{C}_{2v}]$	✓	✓	–	–	$\mathcal{C}_{2v}$

4.3 Bond wave spectrum in zero field, in the low symmetry case

Early neutron scattering results [Kageyama 2000] indicated that the lowest excitation spectrum is essentially dispersionless as the consequence of the orthogonal dimer structure. More recent higher-resolution neutron scattering experiments [Gaulin 2004], however, revealed that the first triplet excitations split into 3 subbands with well-defined dispersions indicating the importance of anisotropies. In the following, we will calculate the zero field momentum dependent spectrum based on the bond-wave theory. As the zero field splitting will be related to the different components of the DM vector we carry out our investigations in the low symmetry case, and we shall include the interdimer in-plane components ($D'_{||,s}$ and $D'_{||,ns}$) of DM interaction as well.

Based on our preceding numerical findings, we search for the variational solution in zero magnetic field in the following form:

$$|\psi_{A,0}\rangle \propto |s\rangle + w|t_y\rangle , \tag{4.34a}$$

$$|\psi_{B,0}\rangle \propto |s\rangle - w|t_x\rangle , \tag{4.34b}$$

assuming that the singlet dimer ground state in only modified by the intradimer DM couplin D. On dimer A which is parallel to the x-axis, the intradimer DM vector has the form $(0, D, 0)$ while on dimer B it is $(-D, 0, 0)$, thus always perpendicular to the dimers as it was introduced in chapter 2. For simplicity the different DM components are repeated here in Fig. 4.3. Choosing the basis (4.2), the intradimer DM term has the form of (4.10) and it is plausible that a finite D mixes the singlet state with a $|t_y\rangle$ triplet on dimer A and with a $|t_x\rangle$ triplet on dimer B. Minimizing the variational energy for the parameter w, we obtain

$$w = -\frac{D}{J + \sqrt{J^2 + D^2}} = -\frac{D}{2J} + O(D^3/J^3) \tag{4.35}$$

and the ground state energy can be given as

$$E_{Z_1[\mathcal{D}_{2d}]} = -\frac{J}{2} - \sqrt{D^2 + J^2}\,. \tag{4.36}$$

We shall note that the wave function (4.34) is directly related to that of $Z_1[\mathcal{D}_{2d}]$ defined in (4.30) with the parameters (4.32) when $h \to 0$. Furthermore, (4.34) is time-reversal invariant and does not break any of the symmetries of the point group $\mathcal{D}_{2d}$, as it was pointed out in the discussion of the symmetric phase in section 4.2.2.1.

To obtain the excitation spectrum, following the recipe outlined in section 4.1.3 and in chapter 3, we rotate the states on each bond of type A as

$$\begin{pmatrix} a^\dagger_{A,0} \\ a^\dagger_{A,1} \\ a^\dagger_{A,2} \\ a^\dagger_{A,3} \end{pmatrix} = \begin{pmatrix} \frac{1}{\sqrt{1+w^2}} & 0 & \frac{w}{\sqrt{1+w^2}} & 0 \\ 0 & 1 & 0 & 0 \\ -\frac{w}{\sqrt{1+w^2}} & 0 & \frac{1}{\sqrt{1+w^2}} & 0 \\ 0 & 0 & 0 & 1 \end{pmatrix} \begin{pmatrix} s^\dagger_{\mathrm{A}} \\ t^\dagger_{x,\mathrm{A}} \\ t^\dagger_{y,\mathrm{A}} \\ t^\dagger_{z,\mathrm{A}} \end{pmatrix}, \tag{4.37}$$

and similarly on bonds B according to:

$$\begin{pmatrix} a^\dagger_{B,0} \\ a^\dagger_{B,1} \\ a^\dagger_{B,2} \\ a^\dagger_{B,3} \end{pmatrix} = \begin{pmatrix} \frac{1}{\sqrt{1+w^2}} & -\frac{w}{\sqrt{1+w^2}} & 0 & 0 \\ \frac{w}{\sqrt{1+w^2}} & \frac{1}{\sqrt{1+w^2}} & 0 & 0 \\ 0 & 0 & 1 & 0 \\ 0 & 0 & 0 & 1 \end{pmatrix} \begin{pmatrix} s^\dagger_{B} \\ t^\dagger_{x,B} \\ t^\dagger_{y,B} \\ t^\dagger_{z,B} \end{pmatrix} \tag{4.38}$$

so that the variational wave functions in Eqs. (4.34) can be written as $|\psi_{A,0}\rangle = a^\dagger_{A,0}|0\rangle$ and $|\psi_{B,0}\rangle = a^\dagger_{B,0}|0\rangle$. The expression of the bond-wave Hamiltonian is complicated at an arbitrary point in the Brillouin-zone, however at the Γ point it

has the form of:

$$\begin{aligned}\mathcal{H}^{(2)} &= \frac{\Omega}{2}\left(a^\dagger_{A,3}a_{A,3}+a^\dagger_{B,3}a_{B,3}+a_{A,3}a^\dagger_{A,3}+a_{B,3}a^\dagger_{B,3}\right)\\ &+\frac{1}{2}\begin{pmatrix} a^\dagger_{B,2}\\ a^\dagger_{A,1}\\ a_{A,1}\\ a_{B,2}\end{pmatrix}^T\begin{pmatrix}\Omega&\Lambda&\Lambda&0\\ \Lambda&\Omega&0&\Lambda\\ \Lambda&0&\Omega&\Lambda\\ 0&\Lambda&\Lambda&\Omega\end{pmatrix}\begin{pmatrix} a_{B,2}\\ a_{A,1}\\ a^\dagger_{A,1}\\ a^\dagger_{B,2}\end{pmatrix}\\ &-\begin{pmatrix} a^\dagger_{B,1}\\ a^\dagger_{A,2}\\ a_{A,2}\\ a_{B,1}\end{pmatrix}^T\begin{pmatrix}\frac{J}{2}-\Omega&D'_\perp&D'_\perp&0\\ D'_\perp&\frac{J}{2}-\Omega&0&D'_\perp\\ D'_\perp&0&\frac{J}{2}-\Omega&D'_\perp\\ 0&D'_\perp&D'_\perp&\frac{J}{2}-\Omega\end{pmatrix}\begin{pmatrix} a_{B,1}\\ a_{A,2}\\ a^\dagger_{A,2}\\ a^\dagger_{B,1}\end{pmatrix}\end{aligned} \tag{4.39}$$

with

$$\Lambda = \frac{2(D'_\perp + wD'_{||} + J'w^2)}{1+w^2}\,, \tag{4.40}$$

$$\Omega = \frac{J+\sqrt{J^2+D^2}}{2}\,. \tag{4.41}$$

For simplicity, we have introduced the quantity

$$D'_{||} = D'_{||,\mathrm{ns}} - D'_{||,\mathrm{s}}\,, \tag{4.42}$$

which includes the in-plane components of the interdimer DM interaction.[2]

After diagonalizing the Hamiltonian (4.39) we obtain the excitation energies:

$$\omega_{1,2} = \Omega\,, \tag{4.43a}$$

$$\omega_3^\pm = \sqrt{\Omega(\Omega\pm 2\Lambda)}\,, \tag{4.43b}$$

$$\omega_4^\pm = \sqrt{J^2+D^2\pm 4D'_\perp\sqrt{J^2+D^2}}\,. \tag{4.43c}$$

For small values of $D'_\perp/J$: $\omega_3^\pm \approx J\pm 2D'_\perp$ and $\omega_4^\pm \approx J\pm 2D'_\perp$. Thus the excitations ω_3 and ω_4 are essentially indistinguishable. Furthermore, the splitting between the plus-minus branches of ω_3 and ω_4 at the Γ point is $4D'_\perp + O({D'_\perp}^2/J)$, which is in good agreement with the findings of Ref. [Cheng 2007] and Fig. 1.6.

Let us note that for larger values of $|D'_\perp|$ the dispersion becomes comparable to the gap, and new phases appear. The branches $\omega_3^\pm$ become gapless when $\sqrt{J^2+D^2} = \mp 4(D'_\perp + wD'_{||} + J'w^2)$, while $\omega_4^\pm = 0$ for $4D'_\perp = \mp\sqrt{J^2+D^2}$. Assuming that $D'_{||}$ is absent and keeping only the leading term in D/J, we find that the phase $Z_1[\mathcal{D}_{2d}]$ is stable for

$$-\frac{J}{4}-\frac{D^2}{8J} < D'_\perp < \frac{J}{4}-\frac{D^2}{8J^2}\left(2J'-J\right)\,. \tag{4.44}$$

[2] Actually, the matrices in the Hamiltonian (4.39) can be reduced to 2×2 ones by using the symmetries of the $\mathcal{S}_4$ point group.

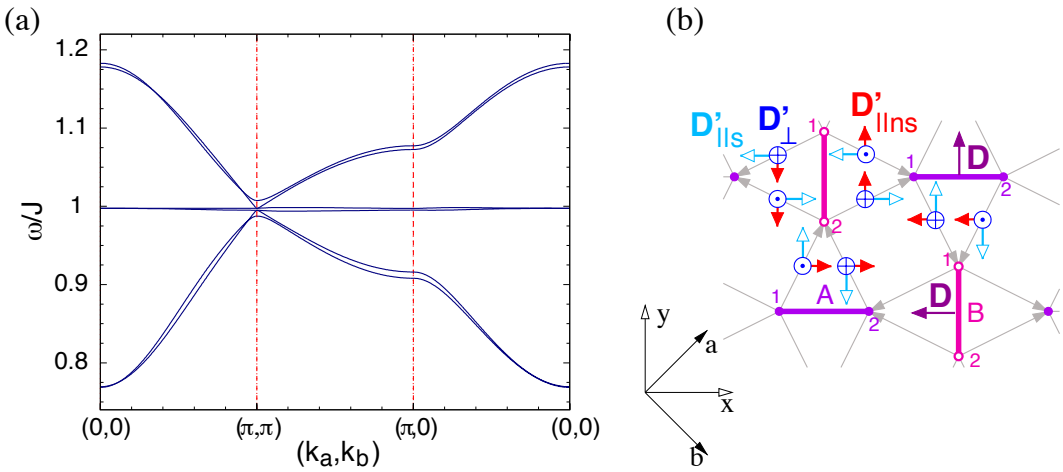

Figure 4.3: (a)Dispersion of the quasi–triplet excitations in zero magnetic field with $D = D'_{\perp} = 0.1J$, $D'_{\parallel} = 0.05J$ and $J' = 0.6J$. $\omega^{-}_{3,4}$ (bottom), $\omega_{1,2}$ (middle), and $\omega^{+}_{3,4}$ (top).(b) The different components of the inter- and intradimer DM vector.

in the zero field. Beyond these boundaries, the twofold degenerate (Z_2) phases emerge, with the symmetry group $\mathcal{C}_{2v}$, when $\omega^{-}_{3} \to 0$ for $D'_{\perp} > 0$ and $\mathcal{S}_4$, when $\omega^{+}_{4} \to 0$ for $D'_{\perp} < 0$, as it was introduced in section 4.2.2 and represented in Fig. 4.2.

After a first order expansion with respect to the parameters D/J, $D'_{\perp}/J$, $D'_{||,s}/J$, and $D'_{||,ns}/J$, it is possible to solve the eigenvalue problem analytically. In this limit we get three two-fold degenerate branches: a dispersionless one with the eigenvalue $\omega_{1,2} = J$ and two branches with

$$\omega^{+}_{3,4}(\mathbf{k}) = \sqrt{J^2 + J\Omega_{\mathbf{q}}} \approx J + \frac{1}{2}\Omega_{\mathbf{k}} \tag{4.45a}$$

$$\omega^{-}_{3,4}(\mathbf{k}) = \sqrt{J^2 - J\Omega_{\mathbf{q}}} \approx J - \frac{1}{2}\Omega_{\mathbf{k}}\,, \tag{4.45b}$$

where

$$\Omega_{\mathbf{k}} = \left[\left(\frac{J'D}{J} - 2D'_{\parallel,s}\right)^2 (1 - \cos q_a \cos q_b) + 16 D'^2_{\perp} \cos^2\frac{q_a}{2}\cos^2\frac{q_b}{2}\right]^{1/2}. \tag{4.46}$$

and the splitting between the + and − branches is just $\Omega_{\mathbf{k}}$. At the Γ point $\Omega_{(0,0)} = 4|D'_{\perp}|$, while at $\mathbf{k} = (\pi,\pi)$ and $(\pi,0)$ the splitting is 0 and $\sqrt{2}|\frac{J'D}{J} - 2D'_{\parallel,s}|$ in agreement with Ref. [Cheng 2007].

We shall note that a more precise calculation at the point (π,π) leads to the dispersion relations $\frac{J^2}{\sqrt{J^2+D^2}}$ and $\frac{J}{2} + \frac{J^2}{2\sqrt{J^2+D^2}}$ with a splitting quadratic in DM $\frac{J}{2} - \frac{J^2}{2\sqrt{J^2+D^2}} \approx \frac{D^2}{4J^2}$. The numerically calculated dispersion of the quasi triplet excitations is shown in Fig. 4.3(a).

4.4 Bond–wave spectrum in magnetic field $h||z$

In this section, we calculate the bond-wave excitation spectrum in the presence of an external magnetic field applied perpendicular to the $CuBO_3$ layer, that is $h \parallel z$, and examine the effect of the intra- and interdimer DM interactions in detail.

4.4.1 High symmetry case

As earlier, we start our investigations with the high symmetry case where the in-plane DM vectors are all vanishing. In the dimer–singlet product phase, the singlet state is condensed on both dimers, and there is no need to rotate the quantization axis along with the triplet bosons: $a^\dagger_\alpha = t^\dagger_\alpha$. Up tho a constant term the energy can be written as

$$\mathcal{H} = E_{\rm DS} + \sum_{\mathbf{q}\in \rm BZ} \mathcal{H}_2(\mathbf{k}) \,, \tag{4.47}$$

Although the rotation is not necessary for the condensation of the right ground state, introducing the following linear combinations

$$\tilde{t}^\dagger_{1,\pm}(\mathbf{k}) = \frac{1}{\sqrt{2}}\left(t^\dagger_{1,A}(\mathbf{k}) \mp i t^\dagger_{1,B}(\mathbf{k})\right) \tag{4.48a}$$

$$\tilde{t}^\dagger_{\bar{1},\pm}(\mathbf{k}) = \frac{1}{\sqrt{2}}\left(t^\dagger_{\bar{1},A}(\mathbf{k}) \pm i t^\dagger_{\bar{1},B}(\mathbf{k})\right) \tag{4.48b}$$

together with the corresponding annihilation operators, will decompose the otherwise 4 by 4 block in $\mathcal{H}_2(\mathbf{k})$ into two 2 by 2 blocks. The Hamiltonians of these blocks then have the form of

$$\begin{aligned}\mathcal{H}^{(2)}_\pm(\mathbf{k}) &= (J - h_z \pm D'_\perp)\cdot \tilde{t}^\dagger_{1,\pm}(\mathbf{k})\tilde{t}_{1,\pm}(\mathbf{k}) + (J + h_z \pm D'_\perp)\cdot \tilde{t}^\dagger_{\bar{1},\pm}(\mathbf{k})\tilde{t}_{\bar{1},\pm}(\mathbf{k}) \\ &\quad \pm 2D'_\perp\gamma\left(\tilde{t}^\dagger_{1,\pm}(\mathbf{k})\tilde{t}^\dagger_{\bar{1},\pm}(\mathbf{k}) + \tilde{t}_{1,\pm}(\mathbf{k})\tilde{t}_{\bar{1},\pm}(\mathbf{k})\right) \,,\end{aligned} \tag{4.49}$$

with the geometrical factor

$$\gamma = \cos\frac{k_a}{2}\cos\frac{k_b}{2} \,. \tag{4.50}$$

The Hamiltonian matrix can be diagonalized following the procedure outlined in chapter 3. We find that bond wave spectrum consists of six modes, namely a twofold degenerate non-dispersive excitation with $\omega(\mathbf{k}) = J$ which we denote by $T^{\rm e,o}_0$ and four dispersive modes:

$$\omega_{e,\pm} = \sqrt{J^2 + 4JD'_\perp\gamma} \pm h_z \tag{4.51a}$$

$$\omega_{o,\pm} = \sqrt{J^2 - 4JD'_\perp\gamma} \pm h_z \tag{4.51b}$$

which come from $\mathcal{H}^{(2)}_+(\mathbf{k})$ and $\mathcal{H}^{(2)}_-(\mathbf{k})$ and will be referred to as $T^{\rm e}_{\pm1}$ and $T^{\rm o}_{\pm1}$, respectively. To emphasise the even-odd parity of the lines we indicate $T^{\rm e}_{\pm1}$ by a

blue and $T^{o}_{\pm 1}$ by a red line in Fig. 4.4. Let us mention that for $h_z = 0$ we recover the excitation spectrum (4.45) when the in-plane DM terms D and $D'_{||}$ are zero.

The dispersions have a finite gap in the dimer-singlet phase which closes at $\mathbf{k} = 0$ when the magnetic field reaches h_c defined by Eq. (4.18) and we enter into the $O(2)$ phases. Due to the complicated form of the bond-wave Hamiltonians $\mathcal{H}_2(\mathbf{k})$ in the $O(2)$ phases, we discuss only the numerical solution. When $D'_{\perp} > 0$, the closing of the gap leads to the emergence of a Goldstone mode as the consequence of the continuous symmetry breaking. The Goldstone mode appears as a continuation of the $\omega_{o,-}$ excitation, furthermore the condensation of a linear combination of the $\tilde{t}^{\dagger}_{1,-}(\mathbf{k} = 0)$ and $\tilde{t}^{\dagger}_{\bar{1},-}(\mathbf{k} = 0)$ bosons results in the $O(2)[\mathcal{C}_4]$ phase described by the wave function (4.20) with the upper sign (see also Fig. 4.1). For $D'_{\perp} < 0$, on the other hand, the Goldstone mode evolves from the $\omega_{e,-}$ mode, and the $O(2)[\mathcal{S}_4]$ phase is realized (Fig. 4.1). As we can see in Fig. 4.4, the lowest gapped mode for $\mathbf{k} = 0$ in

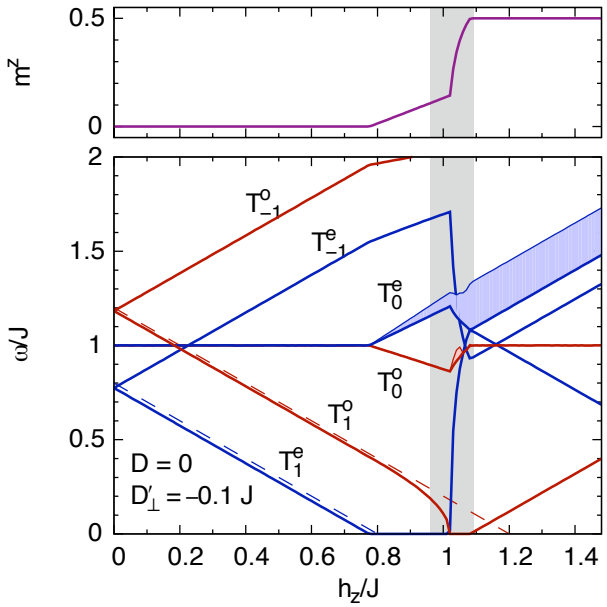

Figure 4.4: Bond wave spectrum at the Γ point in the high temperature case. The magnetic field is parallel to z-axis, $J' = 0.6J$, and $D'_{\perp} = 0.1J$. The transition into the $O(2)$ phase happens at $h_z \approx 0.77J$, and into the plateau phase at $h_z \approx 1.1J$. For $0.77 \lesssim h_z/J \lesssim 1.03$ and $1.03 \lesssim h_z/J \lesssim 1.1$ a Goldstone mode is present in the excitation spectrum of the $O(2)[\mathcal{S}_4]$ phase and $O(2) \times Z_2$ phase, respectively. The 2–dimer variational solution is unstable in the shaded region - the dispersion goes to 0 at some wave vector away from the Γ-point at $h_z = 0.96$ and 1.08. The filled area above the dispersion line shows the strength of the spin structure factor $S^{xx} + S^{yy}$. The dashed line represents the approximation from Ref. [Miyahara 2005].

the dimer–singlet phase remains gapless while the $O(2)$ symmetry is broken which is the case until we reach the half magnetization plateau.

Also, from the **k**-dependent excitation spectrum we learn that the spectrum may become gapless not only at the $\mathbf{k} = 0$, but also at some other **k** values in the Brillouin zone, thus announcing a helical instability of the $O(2)$ phases. In Fig. 4.4 a shaded area indicates the boundary of this instability obtained from the numerical calculations of the spectra.

The strength of the magnetic probe response is closely related to the structure factor $S^{\alpha\alpha}(\mathbf{k}, \omega)$. In particular, the $S^{xx}(\mathbf{k} = \mathbf{0}, \omega)$ and $S^{yy}(\mathbf{k}{=}\mathbf{0}, \omega)$ determines the strength of the ESR lines in first approximation, when the static magnetic field is along the z axes. The structure factor is given by

$$S^{\alpha\alpha}(\mathbf{k}, \omega) \propto \sum |\langle f|S^{\alpha}_{\mathbf{k}}|0\rangle|^2 \, \delta(\omega - E_f + E_0) \, , \tag{4.52}$$

where $|0\rangle$ stands for the ground state (in our case the variational wave function $|\Psi\rangle$), $|f\rangle$ represents the excited states, and E_0 and E_f are the energies corresponding to them.

As a first step, it is instructive to look at the ω-integrated, in other words static, structure factor, $S^{\alpha\alpha}(\mathbf{k}) = \int d\omega S^{\alpha\alpha}(\mathbf{k}, \omega)$, which is actually the sum of the (positive) matrix elements, and is equal to $\langle\Psi|S^{\alpha}_{-\mathbf{k}} S^{\alpha}_{\mathbf{k}}|\Psi\rangle$. In the pure dimer-singlet ground state, $\lim_{\mathbf{k}\to 0} S^{\alpha}_{\mathbf{k}}|0\rangle \to 0$, so we expect no response in ESR experiments, unless there are anisotropies which mix the triplet components with the singlet.

In the $O(2)$ phase (discussed in Sec. 4.2.1.2), the static structure factor has the following form

$$S^{\alpha\alpha}(\mathbf{k} = \mathbf{0}) = \frac{u^2 + d^2}{1 + u^2 + v^2} \approx \frac{(J^2 + h_{\mathrm{c}}^2) h_{\mathrm{c}}}{4JJ' h_{\mathrm{c}}^2 + J^4 - h_{\mathrm{c}}^4} \delta h \tag{4.53}$$

for $\alpha = x, y$, and z. As it turns out, the matrix elements for the S^{xx} and S^{yy} are all vanishing except for the T_0^{e} line. On the other hand, the matrix elements for S^{zz} are nonzero for T_1^{e} and T_{-1}^{e}. Since the ESR line width is proportional to S^{xx} and S^{yy} when the field is along the z-direction, we expect a strong signal for the T_0^{e} line. The intensity of the excitations is indicated by a filled curve above the given lines in Fig. 4.4.

4.4.2 Low symmetry case

As it has been stressed in earlier sections, in the low symmetry case the in-plane DM components are allowed as well. For simplicity however, we shall regard only the most important components of the DM coupling: the out-of-plane interdimer DM term $D'_{\perp}$ and the in-plane intradimer component D. In order to study the effect of these on the excitation spectrum, we shall distinguish between two cases: $D'_{\perp} = 0$ and $D \neq 0$ and when both $D'_{\perp}$ and D are finite. The case when $D'_{\perp} \neq 0$ and $D = 0$ corresponds to the high symmetry case and was discussed in section 4.4.1.

Let us start with the case $D'_{\perp} = 0$. At low fields, the spectrum, shown in Fig. 4.5, looks like the usual single-triplet excitations, Zeeman-splitted by the magnetic field.

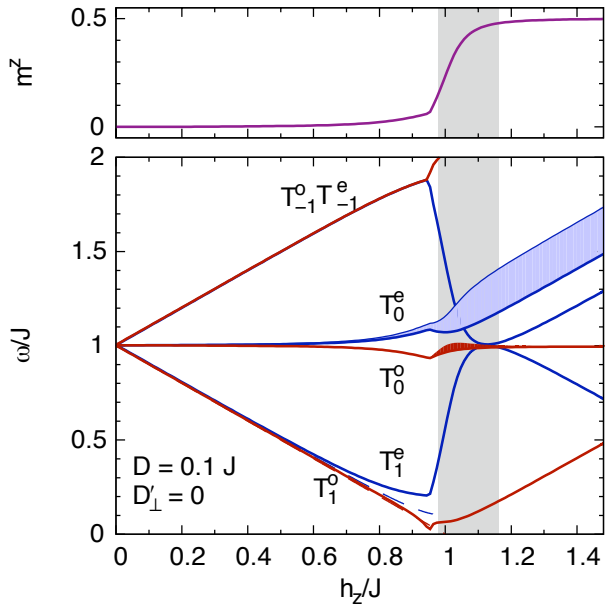

Figure 4.5: Excitation spectrum in magnetic field parallel to z-axis when $D'_\perp = 0$, $J'/J = 0.6$. The instabilities toward helical states are at $h_z/J = 0.9421$ and 1.1002, while the $\mathbf{k} = 0$ instability into the Z_2 phase is at 0.9515. The dashed line represents the approximation from Ref. [Miyahara 2005].

Without any kind of anisotropies, these excitations would correspond to the pure single-triplet excitations. However, the finite intradimer DM coupling D mixes the singlets with these excitations. From the zero-field equations Eqs. (4.43) we obtained that the splitting is of the order of D^2 for small values of D/J, which is much smaller than the linear splitting caused by $D'_\perp$. On the other hand, the effect of D is much more pronounced at higher fields, where the gap becomes small and the singlet-triplet mixing is enhanced. Instead of the Goldstone mode, the anisotropy induces a level repulsion, and we can observe a finite gap that is roughly proportional to $\sqrt{D/J}$, consistently with the usual form of the anisotropy gaps. We note that the level repulsion happens only to one of the two almost degenerate branches descending with the applied field, and it depends crucially on the symmetry of those state. Considering the dispersion of a single-triplet bond moving in the singlet background by the standard perturbation theory, this property has been suggested by Miyahara and Mila [Miyahara 2005]. As we increase the field, the gap closes for the T_1^{o} level at the phase boundary of the $Z_2[\mathcal{C}_{2v}]$ phase (see Fig. 4.2).

For finite inter- and intradimer DM interactions, we perceive both the zero-field splitting observed for $D'_\perp \neq 0$ and $D = 0$ in section 4.4.1 and the anti level-crossing characteristic for finite D around the critical field. In section 4.3, we presented a detailed calculation for the zero-field dispersion and estimated the $h = 0$ splitting in the first order of DM interactions to be $4D'_\perp$. This is in excellent agreement

with the findings of Cheng *et al* [Cheng 2007]. The two descending modes in Fig. 4.6(a) and (b) curve differently in the $O(2)$ phases: only one of them crosses the ground state, while the other is gapped. This can be explained by that only one low lying excitation, namely T_1^e is coupled to D which is proportional to the gap [Miyahara 2005]. Due to the effect of quantum fluctuations, in the case of the bond wave aproximation, the gap opens as $\sqrt{D}$. This property is discussed in Appendix C.1 in more detail. Flipping the sign of the inter-dimer DM coupling $D'_\perp$ changes the lowest-lying mode (compare Fig. 4.6(a) and (b)). The singlet-triplet mixing is different according to the symmetry of the lowest-lying mode and the anti level-crossing occurs only for $D'_\perp < 0$.

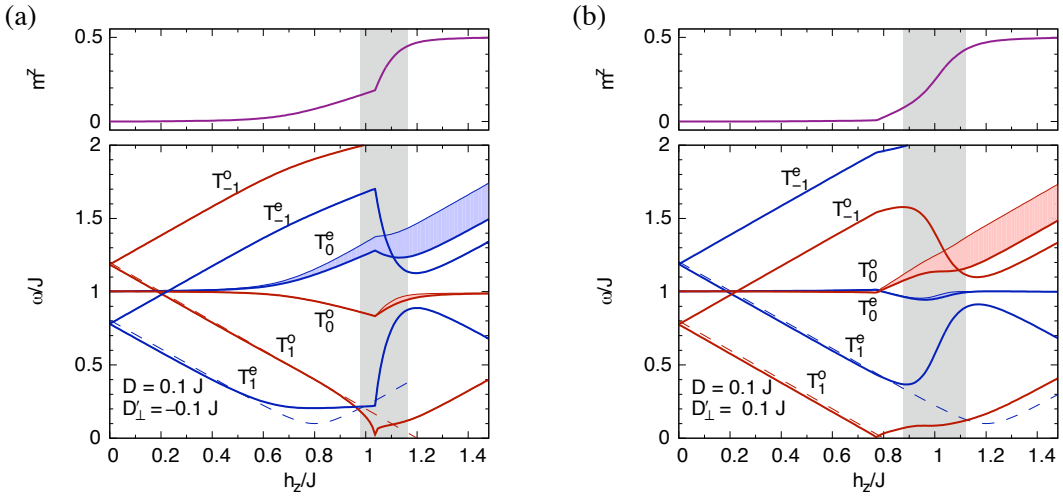

Figure 4.6: (a) Excitation spectrum in magnetic field parallel to z-axis for $D'_\perp < 0$ and (b) for $D'_\perp > 0$. In both cases $D/J = 0.1$, $J' = 0.6J$ and the notations are the same as in Fig. 4.4. The dashed lines represent the approximation from Ref. [Miyahara 2005].

The (4.53) expression of the static structure factor is valid also for finite D values if the variational parameters u and v are those of the wave function (4.30) and take values that minimize the (4.29) energy of $Z_1[\mathcal{D}_{2d}]$. In the limit of small D/J, we can use the values that are given by Eqs. (4.32), and at $\mathbf{q} = \mathbf{0}$ we get

$$S^{xx} = S^{yy} = \frac{D^2}{4} \frac{(J + 4D'_\perp)^2 + h_z^2}{(J^2 + 4JD'_\perp - h_z^2)^2} \tag{4.54}$$

in lowest order in D/J and for small values of the field.[3] Similarly to the $D = 0$ case, the weight of the spin correlation function $S^{xx}(\mathbf{q} = \mathbf{0}, \omega)$ in the $Z_1[\mathcal{D}_{2d}]$-phase is concentrated on the T_0^e line. As we enter the $Z_2[\mathcal{C}_{2v}]$ phase, $S^{xx}(\mathbf{q} = \mathbf{0}, \omega)$ is

[3]The apparent singularity at the critical field $h_z = h_c = \sqrt{J^2 - 4|D'_\perp|J}$ is an artifact of the expansion

distributed among the T_0^{e} and T_0^{o} lines. The strengths of the modes are represented in Figs. 4.5, 4.6(a), and 4.6(b) by the filled area above the T_0^{e} and T_0^{o} lines.

4.5 Phase diagram and excitation spectrum for $h||x$

In this shorter section we intend to discuss the effect of a magnetic field applied in the $CuBO_3$ plane, parallel to the bond A, i.e. parallel to the x-axis. With this field setting the equivalency of the two dimers is violated and so is the rotational symmetry S_4. Consequently, the symmetry is reduced to the magnetic group $\{E, \sigma_{yz}\} + TC_2(z) \times \{E, \sigma_{yz}\}$ which is isomorphic to the point group $\mathcal{C}_{2v}$ as introduced in chapter 2. Unlike the $h||z$ case, the finite value of intradimer DM interaction does not lower the symmetry any further. The operator S^x (or any other dipole operator) ceases to commute with the Hamiltonian.

In the following, we map out the phase diagram as the function of $D'_\perp$ and h_x and give a short discussion on the appearing phases. We also study the excitation spectrum at the end of this section.

4.5.1 Phase diagram

In the absence of DM interaction (and other anisotropies) the spin and real space are not coupled and the situation for $h||z$ and $h||x$ is basically the same. At low field the dimer singlet covering is the ground state and at $h = J$ a first order phase transition occurs to the 1/2 plateau phase (see Fig. 4.7(a)). The introduction of a non-zero interdimer DM coupling ($D'_\perp$) leads to the emergence of a coexisting $Z_2[\mathcal{C}_s^{(y)}]$ and $Z_2[\mathcal{C}_s^{(x)}]$ phase between the dimer singlet and the 1/2 magnetization plateau. The schematic phase diagram for $D = 0$ is shown in Fig. 4.7(a).
The ground state wave functions in the $Z_2[\mathcal{C}_s^{(y)}]$ phase reads

$$\begin{aligned} |\psi_{A,0}\rangle &= |s\rangle \mp i u_y |t_y\rangle \pm v_z |t_z\rangle, \\ |\psi_{B,0}\rangle &= |s\rangle \pm i u_x |t_x\rangle. \end{aligned} \tag{4.55}$$

Note that now we use the quadrupole basis defined in 4.2. The energy, as the function of variational parameters, has the form of

$$\begin{aligned} E_0 = &-J\left[\frac{1-u_x^2}{2(1+u_x^2)^2} + \frac{1}{(1+u_y^2+v_z^2)^2}\right] - 2h_x \frac{u_y v_z}{(1+u_y^2+v_z^2)^2} \\ &+8D'_\perp \frac{u_x u_y}{(1+u_x^2)^2(1+u_y^2+v_z^2)^2}\,. \end{aligned} \tag{4.56}$$

The ground state wave function of the phase $Z_2[\mathcal{C}_s^{(x)}]$ is the same as (4.55) with the indices A and B interchanged. The spin components that characterize the phases $Z_2[\mathcal{C}_s^{(y)}]$ and $Z_2[\mathcal{C}_s^{(x)}]$ are shown in Fig. 4.7(c), only here the S^z components are all zero. Let us briefly refer to the invariance of the phases $Z_2[\mathcal{C}_s^{(y)}]$ and $Z_2[\mathcal{C}_s^{(x)}]$ under the reflexions σ_{yz} and $T\sigma_{xz}$, respectively which is why we chose these notations of

the phases. In the dimer singlet phase the variational solution becomes unstable when

$$h_x = \sqrt{J^2 - 16{D'_\perp}^2}\,. \tag{4.57}$$

This is the second-order phase boundary between the dimer-singlet and the co-existing $Z_2[\mathcal{C}_s^{(y)}]$ and $Z_2[\mathcal{C}_s^{(x)}]$ phases, as shown in Fig. 4.7(a). Similarly, the boundary of the plateau phase according to the variational calculation is given by $h_x = J + 8{D'_z}^2/J$. The finite intradimer coupling D destroys the singlet state of the

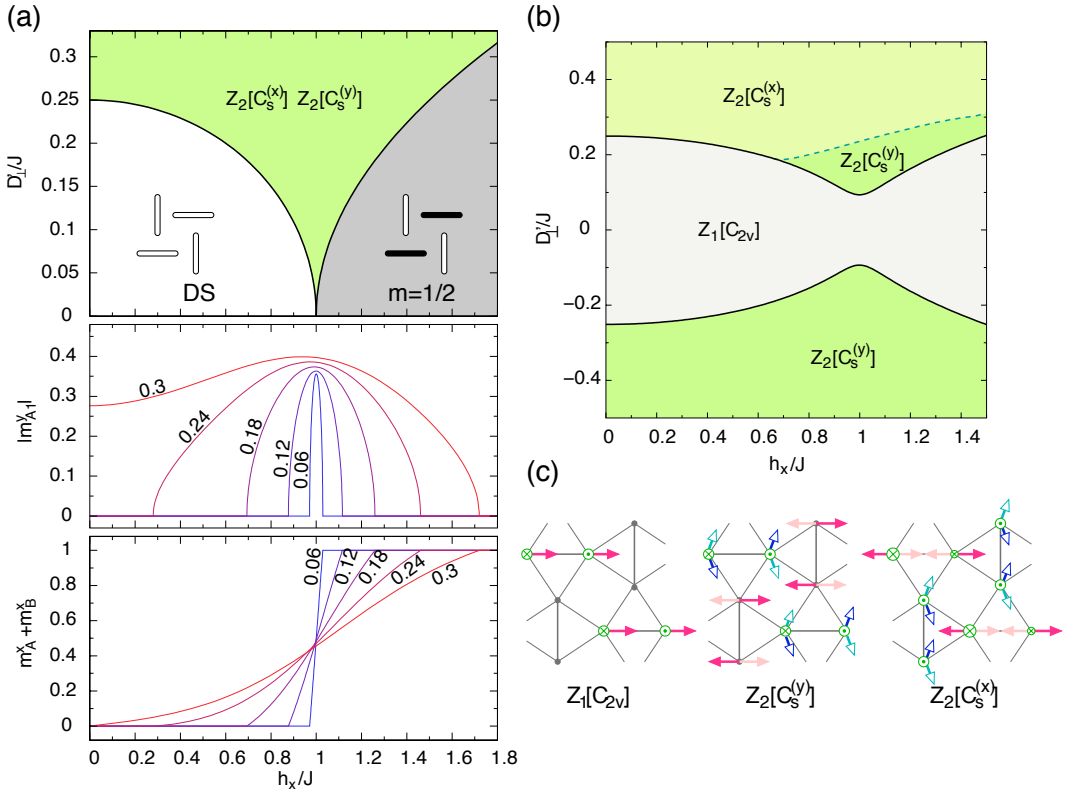

Figure 4.7: (a) Phase diagram for $D = 0$ and $J'/J = 0.6$ as the function of magnetic field applied along the x-axis. (b) Phase diagram in the case of finite intradimer DM coupling: $D/J = 0.1$. (c) Schematic figure of the spin configurations in the phases $Z_1[\mathcal{C}_{2v}]$, $Z_2[\mathcal{C}_s^{(x)}]$ and $Z_2[\mathcal{C}_s^{(y)}]$. The darker and lighter arrow represent the two degenerate states of the Z_2 phases.

dimers by mixing triplets to them. From numerical minimization we learn that the dimer-singlet ground state evolves into:

$$|\psi_{A,0}\rangle \propto |s\rangle - v_y|t_y\rangle - iu_z|t_z\rangle\,, \tag{4.58a}$$
$$|\psi_{B,0}\rangle \propto |s\rangle + v_x|t_x\rangle\,, \tag{4.58b}$$

when D is finite and the energy expectation value has the form of

$$E_{Z_1[\mathcal{C}_{2v}]} = -\frac{J(1-v_x^2)+2Dv_x}{2(1+v_x^2)} - \frac{J+2h_xu_zv_y+Du_z}{1+u_z^2+v_y^2}. \tag{4.59}$$

The ground state (4.58) exhibits the full $\mathcal{C}_{2v}$ symmetry of the unit cell thus we denote this phase by $Z_1[\mathcal{C}_{2v}]$.

In general, the DM interaction $\mathbf{D}(\mathbf{S}_i \times \mathbf{S}_j)$ prefers states with dipole expectation values perpendicular to the vector $\mathbf{D}$. The in-plane intradimer DM vector is parallel to the axis y on dimer A and to the axis x on dimer B, therefore a magnetic field along x will select a momentum orientation on dimer A and introduces frustration on dimer B. More precisely, on dimer A, both the DM vector and h_x supports the development of a finite magnetization $m_A^x = S_{A,1}^x + S_{A,2}^x$ as well as the emergence of a staggered magnetization $n_A^z = S_{A,1}^z - S_{A,2}^z$. The y component of the momentum, either staggered or uniform, is suppressed by the DM vector. On the other hand, in the case of dimer B, the finite field results in a competition with the DM interaction D which here is parallele to the field h_x. As a consequence, the arising state is non-magnetic: $\langle \mathbf{S}_{1,2} \rangle = \mathbf{0}$ and time reversal invariant. However, $|\psi_B\rangle$ breaks the rotational symmetry, as the vector chirality is finite: $\langle \mathbf{S}_1 \times \mathbf{S}_2 \rangle = -v_x/(1+v_x^2)$. In the literature this state is often referred to as p-type nematic state [Andreev 1984, Läuchli 2005]. The parameter v_x does not depend on the magnetic filed, and minimizing the energy (4.59) we find that $v_x = D/2J$.

The finite D splits the degeneracy of the phases $Z_2[\mathcal{C}_s^{(y)}]$ and $Z_2[\mathcal{C}_s^{(x)}]$ as shown in the phase diagram 4.7(b). For sufficiently large negative values of $D'_\perp$, the phase $Z_2[\mathcal{C}_s^{(y)}]$ is realized with the wave function

$$|\psi_{A,0}\rangle \propto |s\rangle - (v_y \pm iu_y)|t_y\rangle - (iu_z \mp v_z)|t_z\rangle \,, \tag{4.60a}$$
$$|\psi_{B,0}\rangle \propto |s\rangle + (v_x \pm iu_x)|t_x\rangle \,. \tag{4.60b}$$

Note that when the parameters v_y, u_z and v_x are approaching zero, we continuously recover Eq. (4.55), although, the symmetry remains the same as it was for $D = 0$. Furthermore, as the other three parameters, u_y, v_z and u_x approach zero, we adiabatically reach the symmetric phase $Z_1[\mathcal{C}_{2v}]$ (see Eq. 4.58). The magnetization on dimer A consist of a uniform part $m_A^x = S_{A,1}^x + S_{A,2}^x$ as well as the staggered components $n_A^y = S_{A,1}^y - S_{A_2}^y$ and $n_A^z = S_{A,1}^z - S_{A,2}^z$, as shown in Fig. 4.7(b). While in the phase $Z_1[\mathcal{C}_{2v}]$ there were no dipole components on dimer B, here the expectation value of the staggered magnetization $n_B^x = S_{B,1}^x - S_{B,2}^x$ becomes finite. The magnetization pattern is invariant under the reflexion σ_{yz}, as it was for $D = 0$.

At large enough positive $D'_\perp$, we reach the phase $Z_2[\mathcal{C}_s^{(x)}]$ where the ground state has the following form

$$|\psi_{A,0}\rangle \propto |s\rangle \pm iu_x|t_x\rangle - v_y|t_y\rangle - iu_z|t_z\rangle \,, \tag{4.61a}$$
$$|\psi_{B,0}\rangle \propto |s\rangle + v_x|t_x\rangle \mp iu_y|t_y\rangle \pm v_z|t_z\rangle \,. \tag{4.61b}$$

When the parameters v_y, u_z and v_x are zero we recover the $Z_2[\mathcal{C}_s^{(x)}]$ wave function of $D = 0$ (see Eq. 4.55 with the interchange of A and B). Similarly to the case

$D = 0$, the spin expectation values are invariant under the reflexion $T\sigma_{xz}$ in this phase. We note that in the limit $D \to 0$ the symmetric $Z_1[\mathcal{C}_{2v}]$-phase is continuously connected to the dimer-singlet phase. This phase is also adiabatically connected to one of the ground states of the twofold-degenerate $m = 1/2$ plateau phase, namely where the singlets are located on the bonds B. The symmetry properties of the occurring phase are collected in table 4.3.

Table 4.3: Symmetry properties of the different phases in the case of $h||x$.

	$TC_2(z)$	$T\sigma_{xz}$	σ_{yz}	$\mathcal{G}_L$
DS, plateau	✓	✓	✓	$\mathcal{C}_{2v}$
$Z_2[\mathcal{C}_s^{(y)}]$	–	–	✓	$\mathcal{C}_s^{(y)}$
$Z_2[\mathcal{C}_s^{(x)}]$	–	✓	–	$\mathcal{C}_s^{(x)}$

4.5.2 ESR spectrum

We continue our investigations with the discussion of the excitation spectrum in magnetic filed $h||x$. Let us recall that in the absence of the DM interactions the dimer singlet is the ground state for fields $h_x < J$ and the excitations are the pure, Zeeman-split triplets with the energies $J - h_x$, J, and $J + h_x$. Each of the triplets is twofold degenerate corresponding to the two dimers in the unit cell. The exclusion of DM components is the reason why the triplet excitations are not mixed with singlets. Introducing the intradimer DM interaction D, the two-fold degeneracy of the triplet branches splits and the spectrum consists of three pairs of almost degenerate levels[4] and the modes split only at higher fields, near to the transition point. This can be explained by the mixing of triplet and singlet states. As discussed previously for finite D, but $D'_\perp = 0$ the $Z_1[\mathcal{C}_{2v}]$ phase is realized, as indicated in the phase diagram 4.7(b). Increasing the field from zero, the value of parameter u_z in the wave function (4.58) increases continuously, developing a finite magnetization m^x at dimer A. The magnetization of dimer B however remains zero. The singlet-triplet mixing varies on the two type of dimers causing the small splitting of the originally degenerate branches and the different behavior of the two low lying excitations around the critical field. The excitation spectrum for $D'_\perp = 0$ and finite D is shown in Fig. 4.8(a).

When the interdimer DM interaction $D'_\perp$ is finite, we observe the zero field splitting $4D'_\perp$ discussed in section 4.3 and 4.4. The ground state is the pure singlet for magnetic field values $h_x < J$ and the triplet excitations are two fold degenerate corresponding to the two-dimer unit cell. At $h_x = J$ a first order phase transition occurs to the coexisting phase of $Z_2[\mathcal{C}_s^{(x)}]$ and $Z_2[\mathcal{C}_s^{(x)}]$ and the magnetization increases linearly with the field. With further increase of the magnetic field we reach

[4] Note that in the absence of D each pair is exactly degenerate in the dimer singlet phase

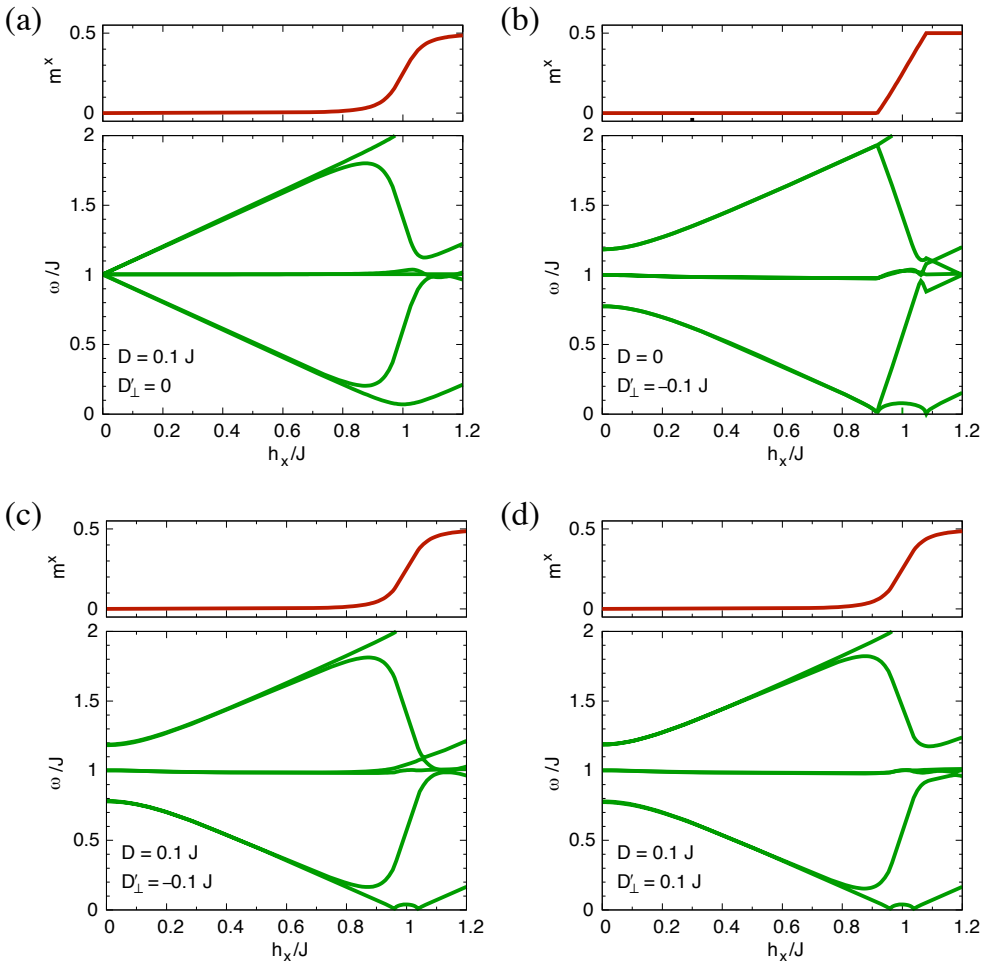

Figure 4.8: Excitation spectrum in magnetic field parallel to x-axis. ($J' = 0.6J$)

the 1/2 plateau. The excitation spectrum and the magnetization for $D = 0$ and finite $D'_\perp$ is plotted in Fig. 4.8(b).

We can conclude from the above two cases that the zero field splitting is due to $D'_\perp$ while the anti-level crossing around the critical field is caused by D. The excitation spectrum is shown for two cases: $D'_\perp/J = -0.1$ and $D'_\perp/J = 0.1$ in Figs. 4.8(c) and 4.8(d), respectively.

4.6 Comparison with the experimental spectrum

The ESR spectrum has been considered earlier by perturbation theory [Cépas 2001] for $\mathbf{D} = \mathbf{0}$ and by exact diagonalization [El Shawish 2005]. Our approach makes it straightforward to take all the experimentally relevant anisotropies into account. Therefore, in the following, we consider the ESR spectrum in a more realistic setting to test our theoretical framework.

There have been various attempts to determine the values of the different couplings in the Hamiltonian. Among the most important estimates on the strength of the DM components we shall remark $D'_\perp/J = -0.02$ from perturbational approach [Cépas 2001], $D/J = 0.034$ from exact diagonalization [Kodama 2005], $D'_\perp = 0.18$ meV and $D'_{||,\mathrm{s}} + J'D/2J = 0.07$ meV [Cheng 2007] from fitting the zero field neutron scattering data of [Gaulin 2004], furthermore $D = 0.35$ meV, $D'_\perp = 0.1$ meV, $D'_{||,\mathrm{s}} = 0.06$ meV and $D'_{||,\mathrm{ns}} = 0.04$ meV from LSDA+U calculation [Mazurenko 2008].

The values of the g-tensor anisotropies were estimated by ESR and NMR measurements with the results: $g_x = g_y = 2.05$ and $g_z = 2.28$ in Ref. [Nojiri 1999], and $g_\mathrm{s} = 0.023$ in Ref. [Kodama 2005].

Although Raman scattering is also a powerful method to investigate the excitation spectrum, we will mainly compare our results with the ESR [Nojiri 1999, Nojiri 2003], far-infrared (FIR) [Rõõm 2000, Rõõm 2004] and neutron-scattering measurements [Kageyama 2000, Cépas 2001, Gaulin 2004].[5]

4.6.1 Quantitative comparison to experiments at zero field

More specifically, two triplet excitations were observed with ESR measurement at 679 ± 2GHz and 764 ± 2GHz [Nojiri 2003], furthermore FIR spectroscopy [Rõõm 2004] indicated three triplet modes at 22.72 ± 0.05 cm^{-1} ($\approx$ 681GHz), 24.11 ± 0.05cm^{-1} ($\approx$723GHz), and at 25.51 ± 0.05cm^{-1} ($\approx$765GHz). The origin of the middle signal at 24.11cm^{-1} is the $\Delta S_z = 0$ triplet excitation that does not appear in the zero field ESR spectrum. From Eq. (4.46) we can deduce that the splitting between the $\Delta S^z = 1$ and $\Delta S^z = -1$ triplet lines gives $4D'_\perp \approx 85$ GHz, that is $D'_\perp \approx 21$ GHz.

High resolution inelastic neutron scattering measurements carried out in zero field [Gaulin 2004] revealed that the dispersion above the gap consist of three distinct branches of triplet excitations. The exact diagonalization to fit the observed splitting [Cheng 2007] provided a result which is identical to our Eq. (4.46). From these dispersions, the splitting between the triplets at $\mathbf{k} = 0$ is $\Omega_{(0,0)} = 4D'_\perp \approx 0.4$meV (that is $\approx$95 GHz, close to the above result 85 GHz), while at $\mathbf{k} = (\pi, 0)$ it is $\Omega_{(\pi,0)} = \sqrt{2}\left(2D'_{||,s} - \frac{DJ'}{J}\right) = 0.2$meV.

We need to mention here that in our approach the dispersion of the triplets originating from the interdimer coupling J' is altogether missing; this is why in the estimate of $D'_\perp$ we used the 'bare' value J as the single-triplet gap, instead of using the renormalized value which is actually observed in ESR measurements.[6]

[5] For clarity, our mode denoted by $T^{\mathrm{o}}_{\pm 1}$ corresponds to $T_{0p}(\pm)$ in the FIR spectrum in Ref. [Rõõm 2004] and to O_1 in the ESR spectrum in Ref. [Nojiri 2003], the lines $T^{\mathrm{e}}_{\pm 1}$ correspond to $T_{0m}(\pm)$ in Ref. [Rõõm 2004] and to O_2 in Ref. [Nojiri 2003], while T^{e}_0 and T^{o}_0 are $T_{0p,m}(0)$ in Ref. [Rõõm 2004].

[6] This value may be renormalized if we go beyond the linear bond-wave approximation. Although, numerical diagonalization of Ref. [Cheng 2007] indicated that the splittings remain independent of the J'.

4.6.2 Quantitative comparison of the spectra at finite magnetic field

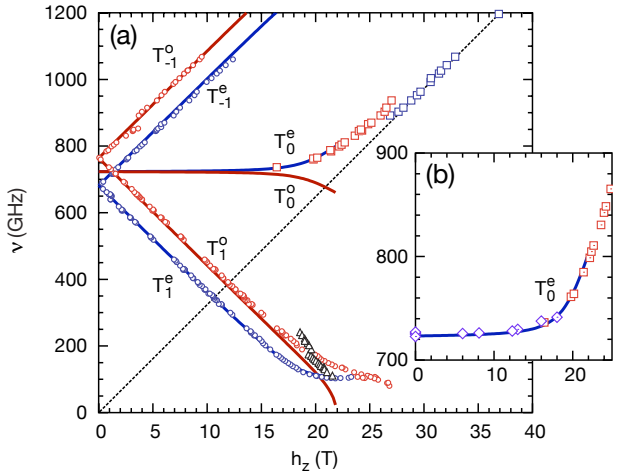

Figure 4.9: Qualitative comparison of excitation spectrum with the $h\|z$ ESR spectrum shown in Fig. 1.6(b) from Ref. [Nojiri 2003]. The solid lines represent our theoretical results. In the inset (b) the dimanonds indicate the far-infrared data from Ref. [Rõõm 2004], while the squares correspond to the ESR data from Ref. [Nojiri 2003].

At last we fit the ESR spectrum of Ref. [Nojiri 2003] by using the bond wave method starting with the variational ground state. To obtain a quantitatively good fit, we need to include the DM interactions as well as the g-tensor anisotropies. By the fitting, we use the values of the anisotropy constants $g_z = 2.28$ estimated in Ref. [Nojiri 1999], and $g_s = 0.023$ in Ref. [Kodama 2005]. The value of the intra-dimer DM coupling $D = 0.034J \approx 60$ GHz is obtained in Ref. [Kodama 2005], assuming that $J = 85$K [Miyahara 1999, Miyahara 2000].[7] The inter-dimer coupling constant is given by $D'_\perp = 21$ GHz, as determined previously. For the reason described above, we choose J to be equal to 722 GHz, the value of the experimentally observed gap[Nojiri 1999]. Furthermore, we find that the spectrum is essentially independent of the value of J' as long as we are in the $Z_1[\mathcal{D}_{2d}]$ phase, thus we selected $J'/J = 0.6$ for internal consistency of the calculation. The calculated bond wave spectrum with the parameters mentioned above is shown in Fig. 4.9. We find a surprisingly good quantitative agreement with the high field ESR and FIR spectroscopy results of Ref. [Nojiri 2003] and Ref. [Rõõm 2004], respectively. Our spectrum reproduces the value of the high-field gap in the T^e_1-excitation above 20 T, furthermore the behavior of the T^e_0 mode which follows nicely the main (i.e. largest-intensity) peak in the ESR spectrum, thus clearly identifying the modes originating from triplet excitations (see Fig. 4.9(b)).

[7] A similar value, $D = 1.8$ cm$^{-1} = 54$ GHz is reported in Ref. [Rõõm 2004].

Chapter 5

Magnetic supersolid

Everyone may be right, all at the same time. That's the thing about quantum.

– *Terry Pratchett, Lords and Ladies*

Supersolid phases were first predicted in the context of strongly interacting bosons of ^{4}He [Chester 1970, Leggett 1970, Andreev 1971] that can simultaneously Bose condense and order in crystalline solid. An experimental indication, however, was found only fifty years later [Kim 2004, Rittner 2006, Kondo 2007, Aoki 2007], suggesting that theoretical interpretation might be more difficult than the first ideas [Leggett 2004, Anderson 2007, Anderson 2008, Anderson 2009].
In the early study of supersolidity, it was believed that perfect crystals cannot exhibit supersolid phases [Penrose 1956] and that defects, like atomic delocalization could lead to long range phase correlation in solids [Yang 1962]. The exchange process has also been considered as the origin of superflow [Leggett 1970, Leggett 2004], along with the idea, that the Bose-Einstein condensation of vacancies might play an important role in the superfluidity of solids [Andreev 1971]. As opposed to these works, Anderson suggested that supersolidity is an intrinsic property of quantum crystals which is only enhanced by disorder [Anderson 2007, Anderson 2008, Anderson 2009]. Although a general agreement in the theory of supersolidity is yet wanting, this intriguing subject evolves quickly.

In this chapter we investigate the spin-1 and spin-3/2 quantum antiferromagnetic models on bipartite lattices, including both easy-plane, $\Lambda(\hat{S}_i^z)^2$, and exchange anisotropies. By the exchange anisotropy we mean that the off-diagonal coupling J in the term $\frac{J}{2}(\hat{S}_i^+\hat{S}_j^- + \hat{S}_i^-\hat{S}_j^+)$ can differ from the diagonal coupling J_z of $J_z\hat{S}_i^z\hat{S}_j^z$. Our model is inspired by the quasi two-dimensional compound, $Ba_2CoGe_2O_7$, where the magnetic spin-3/2 Co^{2+} ions form layers of strongly anisotropic square lattices [Zheludev 2003, Yi 2008, Murakawa 2010, Miyahara 2011].
The case of $Ba_2CoGe_2O_7$, however is a bit different: due to the crystal structure the unit cell contains two cobalt ions, while here the neighbouring cobalts are equivalent. This difference is important when we talk about the translational symmetry of a given state. Let us consider the following Hamiltonian based on the symmetry analysis of chapter 2:

$$\mathcal{H} = J\sum_{\langle i,j\rangle}\left(\hat{S}_i^x\hat{S}_j^x + \hat{S}_i^y\hat{S}_j^y\right) + J_z\sum_{\langle i,j\rangle}\hat{S}_i^z\hat{S}_j^z + \Lambda\sum_i\left(\hat{S}_i^z\right)^2 - h\sum_i\hat{S}_i^z \tag{5.1}$$

where $\langle i, j \rangle$ indicates nearest neighbor sites. Note that in this chapter we neglect the effect of the Dzyaloshinsky-Moriya interaction, although it is allowed by the symmetries.

In the following sections we determine the phase diagram in the Ising limit, when the off-diagonal exchange J is zero, furthermore we discuss the instabilities of the plateaus using perturbation theory. We will map out the variational phase diagram for a finite but smaller J, namely when $J/J_z = 0.2$ as well as in the Heisenberg limit which we associate with the case of isotropic exchange interaction $J = J_z$.[1] In order to check the reliability of the variational method, we calculate the phase diagram of the spin-1 model and compare it to the known results in the literature. The variational results will be supported by a variant of the Density Matrix Renormalization Group in one-dimension as well as by exact diagonalization on a square lattice.

5.1 The Ising limit

The existence of the gapped phases in our model is due to the anisotropic terms, thus turning off the off-diagonal Heisenberg term, $\hat{S}_i^x \hat{S}_j^x + \hat{S}_i^y \hat{S}_j^y$, what remains are the plateau states. For brevity, we call this $J \to 0$ limit the Ising limit as indicated previously.

5.1.1 The Ising limit and the degeneracy of the phase boundaries

Since we consider lattices that are bipartite and we only include nearest neighbor interactions, the spins are not frustrated and all the ground states are either uniform or exhibit two-sublattice order. The wave functions and the properties of the emerging phase in the Ising limit are listed in Table 5.1. The phase diagram as the function of magnetic field and single-ion anisotropy is mapped out in Figure 5.1. We find two uniform phases in finite magnetic field: the fully polarized state with $S^z = 3/2$ ($\Uparrow$) and the partially polarized state with $S_z = 1/2$ ($\uparrow$) on each site. The latter state is in fact a plateau with $m/m_{\text{sat}} = 1/3$. We denote these axial ferromagnetic states with $F3$ and $F1$, respectively. In addition there are two-sublattice states which include the two axial antiferromagnetic states $A3$ and $A1$ and two plateau states $P1$ and $P2$. The staggered magnetization is finite in all four states, furthermore the plateaus exhibit finite uniform magnetization too, that is the 1/3rd and 2/3rd of the saturation value.

In this simple case, the phase boundaries can be determined by comparing the ground state energies. The phases $A1$ and $A3$ are separated by a first order phase boundary at $\Lambda = \zeta J_z/2$, where the lowest lying energy levels cross. We should note that ζ denotes the coordination number of the bipartite lattice. Since the other states are separated by a gap, we expect that the level crossing will persist even for finite values of J. The states $A1$ and $A3$ both are two-fold degenerate, therefore

[1] Note that the single-ion anisotropy is still finite.

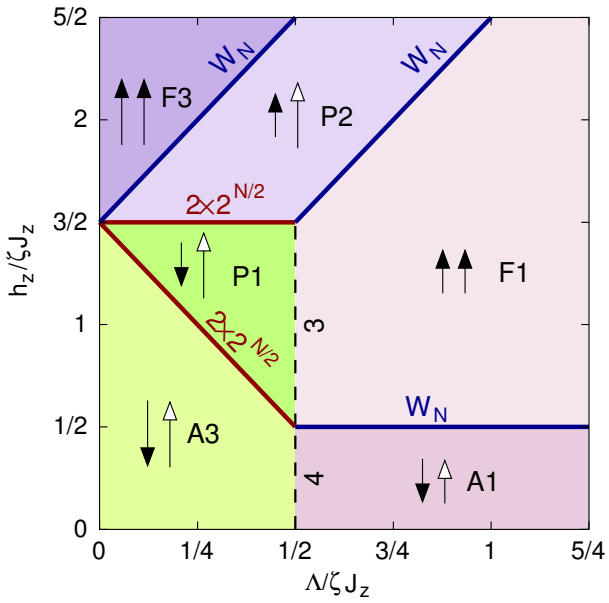

Figure 5.1: Phase diagram in the Ising limit as the function of the anisotropy and magnetic field.The dashed line represents the first order phase boundary. Long arrows denote the $S^z = \pm 3/2$ spin states, while the sort ones the $S^z = \pm 1/2$'s. The coordination number $\zeta = 2$ for the chain and $\zeta = 4$ for the square lattice. $F1$ and $F3$ are uniform phases, while the others break the translational invariance and are two-fold degenerate.

$\lvert S_A^z S_B^z \rangle$	E_0/N	m_z	$m_z^{\rm st}$	$m_z/m_{\rm sat}$	notation
$\lvert \downarrow\uparrow \rangle$	$\frac{1}{4}\Lambda - \frac{1}{8}\zeta J_z$	0	1/2	0	A1
$\lvert \Downarrow\Uparrow \rangle$	$\frac{9}{4}\Lambda - \frac{9}{8}\zeta J_z$	0	3/2	0	A3
$\lvert \uparrow\uparrow \rangle$	$\frac{1}{4}\Lambda + \frac{1}{8}\zeta J_z - \frac{1}{2}h$	1/2	0	1/3	F1
$\lvert \downarrow\Uparrow \rangle$	$\frac{5}{4}\Lambda - \frac{3}{8}\zeta J_z - \frac{1}{2}h$	1/2	1	1/3	P1
$\lvert \uparrow\Uparrow \rangle$	$\frac{5}{4}\Lambda + \frac{3}{8}\zeta J_z - h$	1	1/2	2/3	P2
$\lvert \Uparrow\Uparrow \rangle$	$\frac{9}{4}\Lambda + \frac{9}{8}\zeta J_z - \frac{3}{2}h$	3/2	0	1	F3

Table 5.1: Summary of ground states in the Ising limit. We denote the fully and partially polarized antiferromagnetic states by $A3$ and $A1$, the fully and partially polarized ferromagnetic phases by $F3$ and $F1$, and finally the plateau states by $P2$ and $P1$ corresponding to the 2/3 and 1/3 plateaus respectively. Although, the partially polarized ferromagnetic state $F1$ is actually a plateau with $m/m_{\rm sat} = 1/3$, we prefer to call it ferromagnetic state and refer to the plateaus as states that exhibit both finite m_z and $m_z^{\rm st}$. ζ is the coordination number of the (bipartite) lattice.

at the phase boundary, where they coexist, the degeneracy will be 4-fold.The phase transition between the phases $P1$ and $F1$ is of similar kind.

The second order phase boundary between the two-sublattice states $A3$ and $P1$ is, on the other hand, macroscopically degenerate. As we cross the boundary from the phase $A3$ by increasing the field, the spin state of the sublattice with $S^z = 3/2$ will not change, but the $S^z = -3/2$ spin state of the other sublattice becomes $S^z = -1/2$ in the $P1$ phase. At the boundary, however the spin states $S^z = -1/2$ and $S^z = -3/2$ are equally good, creating a $2^{N/2}$ fold degenerate manifold, if $N/2$ is the number of sublattice sites. For this can occur on either sublattice A or B, there is an additional factor 2. The degeneracy at the phase boundary then is $2 \times 2^{N/2}$. Turning on J, this degeneracy will immediately be lifted, and a gapless phase appears. The same scenario holds for the phase boundary between the phases $P1$ and $P2$. These phase boundaries are shown by thick red line in Fig. 5.1.
Lastly, we examine the phase boundary between the uniform and two–sublattice states. These phase boundaries are shown by thick blue lines in Fig. 5.1 and have a ground state degeneracy W_N. Let us concentrate on the boundary that separates $P2$ and $F3$. The allowed (S^z_A, S^z_B) configurations are $(3/2, 3/2)$, $(3/2, 1/2)$ and $(1/2, 3/2)$, the configuration $(1/2, 1/2)$ is not allowed, though. In the one dimensional chain this rule gives a degeneracy $W_N = F_{N-1} + F_{N+1}$, where F_N is the N-th Fibonacci number ($W_2 = 3$, $W_4 = 7$, $W_6 = 18$, $W_8 = 47$, and so on). [Feiguin 2007] In the case of square lattice, we cannot give an explicit formula for W_N, numerically we find $W_8 = 31$ for the 8–site cluster with D_4 symmetry and $W_{10} = 68$ for the 10–site cluster with C_4 symmetry. We shall mention that the degeneracy depends on the shape of the cluster.

5.2 A perturbation about the Ising limit

In this section, starting from the Ising phase diagram, we study the effect of the off-diagonal exchange J, using perturbation theory. We distinguish among three cases according to the three different types of phase boundaries, discussed above.

5.2.1 Estimating the first order phase transitions

In the Ising limit, we learned that the boundary between $A1$ and $A3$ is of first order, corresponding to the lowest laying level-crossing in the energy spectrum that is otherwise gapped. We assume that for small values of J the first order transition will hold, so that we can estimate the corrections to the phase boundary by comparing the ground state energies now expanded in powers of J. The lowest order corrections appear in the second order:

$$\frac{E_{A1}}{N} = \frac{\Lambda}{4} - \frac{\zeta J_z}{8} - \frac{2\zeta J^2}{(\zeta-1)J_z} - \frac{9\zeta J^2}{32\Lambda - 8(\zeta+1)J_z}, \tag{5.2}$$

$$\frac{E_{A3}}{N} = \frac{9\Lambda}{4} - \frac{9\zeta J_z}{8} - \frac{9\zeta J^2}{(24\zeta-8)J_z - 32\Lambda}. \tag{5.3}$$

Comparing these energies, we get that the first order phase transition between

$A1$ and $A3$ in the square lattice happens when

$$\Lambda = 2J_z - \frac{4J^2}{3J_z} + O(J^4) \tag{5.4}$$

for small J. In the case of the one–dimensional chain we get

$$\Lambda = J_z - \frac{2J^2}{J_z} + O(J^4). \tag{5.5}$$

Similarly, from the second order corrections given in the appendix D, Eqs. (D.4) and (D.3), the boundary between the phases P1 and F1 is

$$\Lambda = 2J_z - \frac{2J^2}{J_z} + O(J^4), \tag{5.6}$$

for a square lattice and

$$\Lambda = J_z - \frac{3J^2}{J_z} + O(J^4), \tag{5.7}$$

for a chain.

5.2.2 Field induced instability of uniform phases

We can think about the field induced instability of Ising phases as a softening of magnetic excitations. The simplest magnetic excitations corresponds to lowering or raising the spins on a site, $S_j^+ \to a_j$ and $S_j^- \to a_j^\dagger$, or the other way around. This excitations become delocalized due to the off-diagonal term J and are gapped in the Ising phases. The size of the gap changes with the value of interaction parameters and that of the magnetic field. When the energy gap vanishes, the excitations can be created in arbitrary number and an off-diagonal long-range order develops. For small values of J we can use perturbation expansion to obtain the dispersion of these excitations. In the case of a uniform order the spins on the two sublattices are equal, and the expansion of the excitation energy is simple. Let us pick one of the uniform phases as an illustration, e.g. the fully polarized phase $F3$ and examine its instability towards the plateau $P2$. In the phase $F3$ the ground state is $\prod_j |\Uparrow_j\rangle$. A spin excitation in this case corresponds to lowering the $\Uparrow$ spin to a $\uparrow$ on a given site, with a diagonal energy cost

$$\Delta E = h - 2\Lambda - \frac{3}{2}\zeta J_z. \tag{5.8}$$

The off-diagonal terms can hop the excitations onto the neighboring sites, as shown in Fig. 5.2(a), with a hopping amplitude

$$\langle \uparrow_i \Uparrow_j |\mathcal{H}| \Uparrow_i \uparrow_j \rangle = \frac{3J}{2}\,. \tag{5.9}$$

This results in the following dispersion:

$$\omega_{\mathbf{k}} = h - 2\Lambda + \frac{3}{2}\zeta\left(J\gamma_{\mathbf{k}} - J_z\right) \tag{5.10}$$

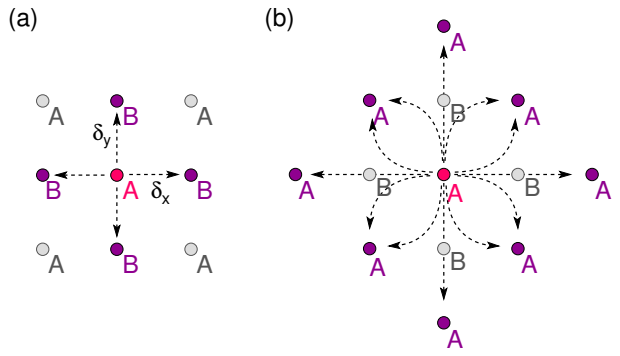

Figure 5.2: (a) Schematic figure for the first order hopping process that occurs during the instability of uniform phases $F1$ and $F3$, where the dispersion is $\propto 4\gamma_{\mathbf{k}}$. (b) Schematic representation of the second neighbor correlated hopping that gives the dipersion $\propto 16\gamma_{\mathbf{k}}^2$. There are 8 neighboring places where the magnon can hop through a virtual state on the B-site.

with $\gamma_{\mathbf{k}} = \frac{1}{\zeta}\sum_{\boldsymbol{\delta}} e^{i\mathbf{k}\cdot\boldsymbol{\delta}}$. The summation is over the vectors $\boldsymbol{\delta}$ pointing toward the ζ nearest neighbor sites. In the one-dimensional model $\gamma_{\mathbf{k}} = \cos k_x$, while in two-dimensions it is $\gamma_{\mathbf{k}} = \frac{1}{2}(\cos k_x + \cos k_y)$. The (5.10) excitation is gapped with a minimum at $\mathbf{k} = \boldsymbol{\pi}$. Lowering the magnetic field the gap closes when

$$h_{\rm sat} = \frac{3}{2}\zeta\,(J_z + J) + 2\Lambda. \tag{5.11}$$

Instabilities of this kind, that is the instability of the phase $F1$ towards the phases $P2$ and $A1$ are summarized in the appendix D in equations (D.7)-(D.9). The corresponding critical fields are collected in Table 5.2, and are plotted in Fig. 5.3 for the parameter value $J/J_z = 0.2$. We note that in the case of the F_3 phase Eqs. (5.10) and (5.11) are exact, while for $F1$ higher order terms in J/J_z appear in the dispersion.

Table 5.2: (color online) Summary of instabilities of uniform phases.

	ΔE	hopping amplitudes	h_c
$F3 \to P2$	$h - 2\Lambda - 6J_z$	$3J/2$	$2\Lambda + 6J_z + 6J$
$F1 \to P2$	$2J_z - h + 2\Lambda$	$6J$	$2\Lambda + 2J_z - 6J$
$F1 \to A1$	$-2J_z + h$	$2J$	$2J_z + 8J$

5.2.3 Dispersion of spin–excitations in translational symmetry breaking states on the square lattice

The softening of the excitations in the two-sublattice gapped phases, ($A1$, $A3$, $P1$, and $P2$) which break the translational symmetry, occur in the second order of the exchange coupling J.As an example, we discuss the lower instability of the 2/3-plateau phase $P2$.

The wave function of the phase $P2$ in the Ising limit is given by

$$|\Psi^{P2}\rangle = \prod_{j\in A}\prod_{j'\in B} |\uparrow_j\rangle|\Uparrow_{j'}\rangle. \tag{5.12}$$

Applying the lowering operator S_j^- on the sublattices A and B, we obtain

$$|\Phi_i^A\rangle = |\downarrow_i\rangle \prod_{\substack{j\in A\\ j\neq i}}\prod_{j'\in B} |\uparrow_j\rangle|\Uparrow_{j'}\rangle, \tag{5.13}$$

$$|\Phi_i^B\rangle = |\uparrow_i\rangle \prod_{j\in A}\prod_{\substack{j'\in B\\ j'\neq i}} |\uparrow_j\rangle|\Uparrow_{j'}\rangle, \tag{5.14}$$

with diagonal excitation energies

$$\Delta E_A = h - 6J_z, \tag{5.15}$$

$$\Delta E_B = h - 2\Lambda - 2J_z, \tag{5.16}$$

respectively. This corresponds to adding an excitation to the system. The two energies are equal when $\Lambda = 2J_z$ which is actually the phase boundary between the phases P_1 and F_1 in the Ising limit (see Fig. 5.1).

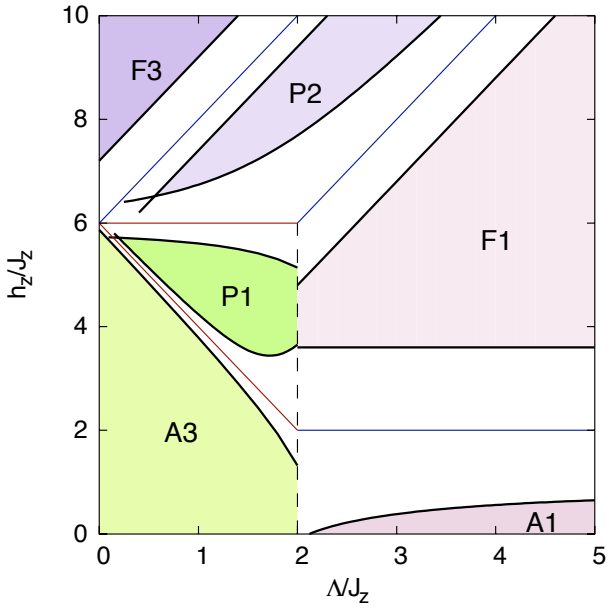

Figure 5.3: Instabilities (thick lines) of the gapped phases in the square lattice as obtained from the perturbation theory for the parameter value $J/J_z = 0.2$. For comparison we show the $J = 0$ Ising phase boundaries of Fig. 5.1 with thin blue, red, and dashed lines.

In this case, the second order perturbation theory fails, as the hopping amplitudes diverge (see appendix D Eqs. (D.15) and (D.16)). Therefore, we shall include both $|\Phi_i^A\rangle$ and $|\Phi_i^B\rangle$ states into the ground state manifold.

Then we need to diagonalize the following 2×2 problem in $\mathbf{k}$ space:

$$\mathcal{H}'_{P2} = \begin{pmatrix} h - 6J_z & 4\sqrt{3}J\gamma_{\mathbf{k}} \\ 4\sqrt{3}J\gamma_{\mathbf{k}} & h - 2J_z - 2\Lambda \end{pmatrix} . \tag{5.17}$$

The 2×2 matrix can be easily diagonalized, leading to the dispersion

$$\omega_{\mathbf{k}} = h - 4J_z - \Lambda \pm \sqrt{(\Lambda - 2J_z)^2 + 48J^2\gamma_{\mathbf{k}}^2} . \tag{5.18}$$

We notice that for $\Lambda = 2J_z$ the dispersion becomes linear in J, while for $J \ll |\Lambda - J_z|$ we can perform an expansion in J and obtain

$$\omega_{\mathbf{k}} = h - 4J_z - \Lambda \pm (\Lambda - 2J_z) \pm \frac{24J^2\gamma_{\mathbf{k}}^2}{\Lambda - 2J_z}. \tag{5.19}$$

which corresponds to the result of the second order perturbation shown in the appendix in Eq. (D.10). Consistently, we shall take into account all the second order processes that contribute to the dispersion. This can be done systematically, and the full expression is given in Eq. (D.20). The critical field at which the gap vanishes can then be determined without difficulty, and the instabilities of this type, given by Eqs. (D.18), (D.19), and (D.20) are shown in Fig. 5.3 for $J/J_z = 0.2$.

5.3 Variational Phase Diagram

In this section we construct the phase diagram variationally, assuming either uniform or two–sublattice ordering. We search for the ground state in the following site–factorized variational form:

$$|\Psi\rangle = \prod_{i \in A} \prod_{j \in B} |\psi_A\rangle_i |\psi_B\rangle_j , \tag{5.20}$$

where

$$|\psi_A\rangle \propto |\Uparrow\rangle + e^{i\xi_1} u_1 |\uparrow\rangle + e^{i\xi_2} u_2 |\downarrow\rangle + e^{i\xi_2} u_3 |\Downarrow\rangle \tag{5.21}$$

and we consider a similar expression for $|\psi_B\rangle$. In the general case, there are 6 independent variational parameters for each sublattice which can be determined by minimizing the ground state energy

$$E = \frac{\langle\Psi|\mathcal{H}|\Psi\rangle}{\langle\Psi|\Psi\rangle} . \tag{5.22}$$

Recalling that the Hamiltonian has $O(2)$ symmetry and commutes with the operator $\hat{S}^z = \sum_i S_i^z$, the state rotated through the angle φ about the z-axis, $\exp(-\varphi\hat{S}^z)|\Psi\rangle$, has the same energy as the state $|\Psi\rangle$. We can therefore reduce the number of independent parameters, say on site A, from 6 to 5, so in total we have 11 variational parameters to determine. It appears, however, that all the phases are coplanar, and after a suitable rotation of the states, the amplitudes in the wave function can all be chosen to be real.

The site–factorized variational wave function (5.20) does not depend on the connectivity of the lattice, only the number of the neighbours, ζ, appears in the energy expression. For simplicity, we discuss the case of the square lattice, however the results can be easily generalized to any bipartite lattice by replacing $J \to \zeta J/4$ and $J_z \to \zeta J_z/4$ in equations to come.

It is useful to note that in the gapped phases the variational wave function is the same as it is in the Ising-limit, when the off-diagonal term is absent. The off-diagonal term $\hat{S}_i^x \hat{S}_j^x + \hat{S}_i^y \hat{S}_j^y$ contributes only if we tilt the spins from the z axis. Consequently, the expressions for the ground state energies of the gapped phases are also equal to those of the Ising limit.

Furthermore, the boundary of the gapped phases, assuming a continuous phase transition, can be determined by studying the stability of the gapped variational wave function $|\Psi_0\rangle$: the 0 eigenvalue of the $\partial^2 E/\partial u_\alpha \partial u_\beta$ indicates a second order phases transition, where u_α and u_β are coefficients of the wave functions orthogonal to $|\Psi_0\rangle$.

5.3.1 Heisenberg exchange with on-site anisotropy

This section is devoted to the phase diagram, as the function of magnetic field and single-ion anisotropy, when the exchange interaction is SU(2) symmetric, i.e. $J = J_z$. The phase diagram outlined in Fig. 5.4(a) was calculated by the variational method introduced above.

On the $h_z = 0$ line the ground state is the planar superfluid phase (SF_0) which will be discussed in chapter 6 in detail. In this phase the spin are confined in the lattice plane, with opposite directions. However, only their relative direction is restricted, and they can freely rotate (together) in the plane as long as their in-plana uniform magnetization remains zero. As the magnetic field becomes finite, the spins tilt out of the plane continuously, and the superfluid ground state SF_F exhibits finite magnetization $m_z^{\rm st} = \frac{1}{2}|S_A^z - S_B^z|$ alongside the finite superfluid order parameter $O_{U(1)} = \frac{1}{2}|\mathbf{S}_A^\perp - \mathbf{S}_B^\perp|$, with $\mathbf{S}_j^\perp = (S_j^x, S_j^y)$. $O_{U(1)}$ is in fact the staggered in-plane order parameter. We show the values of the relevant order parameters in Fig. 5.4(b). A schematic figure of the conical phase SF_F is shown in Fig. 5.4(a) and the ground state wave function can be given as:

$$|\Psi_A\rangle \propto e^{-i\varphi \hat{S}_A^z} \left(|\Uparrow\rangle + u|\uparrow\rangle + v|\downarrow\rangle + w|\Downarrow\rangle\right) \tag{5.23}$$

$$|\Psi_B\rangle \propto e^{-i(\varphi+\pi) \hat{S}_B^z} \left(|\Uparrow\rangle + u|\uparrow\rangle + v|\downarrow\rangle + w|\Downarrow\rangle\right) \tag{5.24}$$

where u, v, and w are all real parametrs.

The ground state energies of the axial ferromagnetic phases and the fully polarized ferromagnetic state are given in Table 5.1,

An analytical expression for the ground state energy of SF_F is beyond our reach, however, the phase boundary with the neighboring $F3$ phase can be given by calculating the critical field for the polarized phase $F3$. By this we recover the exact result of Eq. (5.11). Above the saturation field the fully polarized ferromagnetic

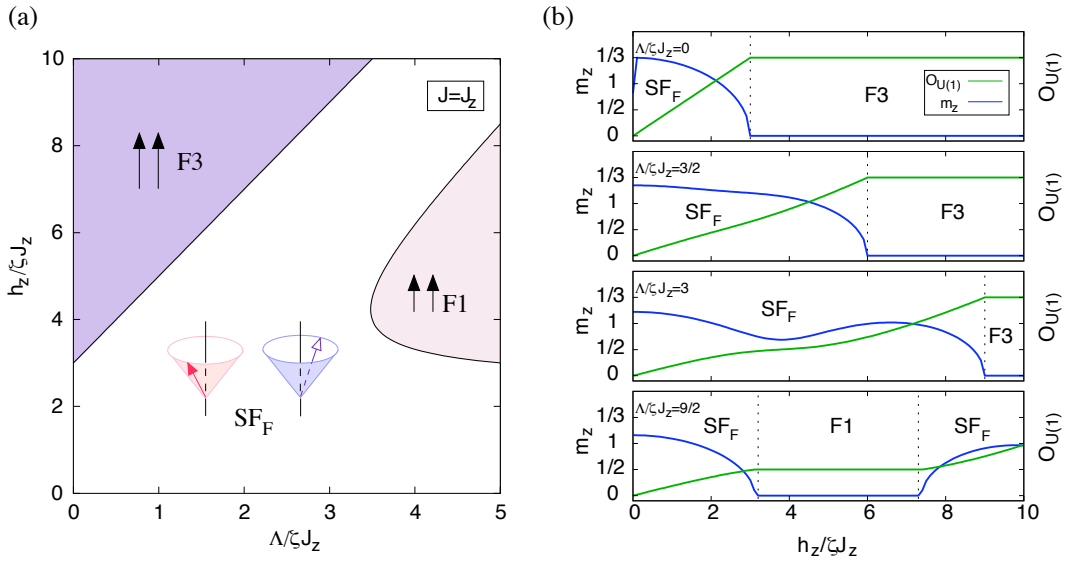

Figure 5.4: (a) Phase diagram in the function of Λ/J and h_z/J ($J_z = J$). (b) Order parameters as the function of magnetic filed for different values of Λ parameter. The fully and partially polarized ferromagnets $F3$ and $F1$ exhibit finite magnetization m_z, while in the conical ferromagnetic phase SF_F the expectation values of both m_z and $O_{U(1)}$ are finite.

phase is stabilized as shown in Fig. 5.4(a). For large enough values of Λ the spins become shorter and the partially polarized axial phase $F1$ emerges. Calculating the instability of $F1$, the phase boundary turns out be

$$h = J + 2J_z + \Lambda \pm \sqrt{J^2 - 14J\Lambda + \Lambda^2}. \tag{5.25}$$

In the Heisenberg limit, there is no evidence for gapped phases that break the translational symmetry.

5.3.2 The effect of exchange anisotropy and the emergence of supersolid phase.

Let us now examine the simultaneous effect of exchange and single-ion anisotropies in finite magnetic field. So far we learned that only the ferro-aligned spins in $F1$ and $F3$ are present as gapped phases in the case of the Heisenberg exchange ($J_z = J$), with a superfluid phase (canted antiferromagnet) between them. As the value of J/J_z is lowered, islands of plateaus and antiferromagnetic phases emerge in the sea of the superfluid phase. We chose a relatively large anisotropy $J/J_z = 0.2$, as in that case we learned from the perturbational expressions that the 2-fold degenerate gapped phases might be stable, as shown in Fig. 5.3. Indeed, the variational phase diagram, shown in Fig. 5.5(a), displays all the phases we were looking for: The

superfluid phase takes place around the axial ferromagnets, and between the plateaus and axial antiferromagnetic phases, i.e. the gapped phases that exhibit staggered diagonal magnetic order, a supersolid phase arises.

The extension of the supersolid around the phases $A1$ and $P2$ is the broadest at their tips, when Λ is not too large. As we increase Λ, the supersolid region decreases, and eventually vanishes for $\Lambda \to +\infty$. Since in this limit the mapping to the XXZ model becomes exact, our finding is also consistent with numerical works on the XXZ model on the square lattice that do not seem to find supersolid.[Kohno 1997, Yunoki 2002, Batrouni 2000]

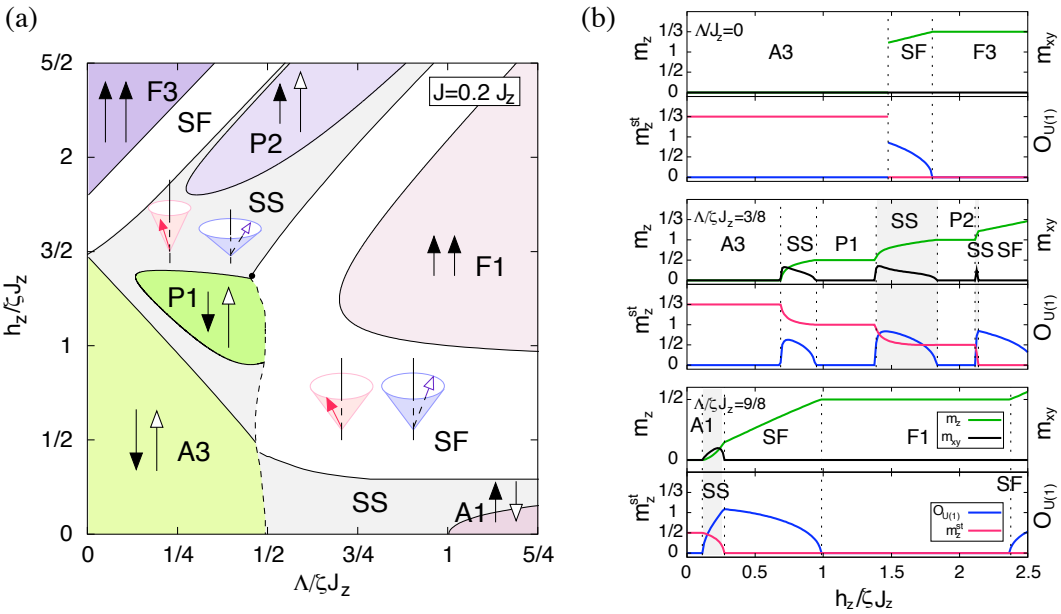

Figure 5.5: (a) Variational phase diagram as function of $\Lambda/\zeta J$ and $h_z/\zeta J$ for large exchange anisotropy $J/J_z = 0.2$ and a bipartite lattice with ζ neighbors. Dashed lines stand for first order, while solid lines denote second order phase transitions. The solid dot ending the first order transition represent a tricritical point. (b) Expectation value of order parameters per site as the function of $h/\zeta J_z$ at different values of $\Lambda/\zeta J_z$. In the axial antiferromagnetic phases $A1$ and $A3$ only the staggered magnetization has finite expectation value. For $\Lambda = 0$ there is a first order phase transition from the completely polarized $A3$ phase to the superfluid phase. All the other field induced transitions are second order transitions. The superfluid phase exhibits finite magnetization m_z and finite staggered in-plane magnetization $O_{U(1)}$. The ferromagnetically ordered phases $F3$ and $F1$ are characterized by finite magnetization m_z, while the plateaus ($P1$ and $P2$) have an additional finite staggered magnetization m_z^{st}. In the supersolid phase all four order parameters have finite expectation values.

Based on variational calculation we find all the phase boundaries to be of second order, except a single first order one around $\Lambda \approx 2J_z$ indicated by dashed line in Fig. 5.5(a). This phase bounday is inherited from the $J = 0$ phase diagram, Fig. 5.1.

The expression of the phase boundaries of the axial ferromagnetic phases are the same as in the Heisenberg limit (see Eqs. (5.11) and (5.25)). We determined the phase boundaries of the plateaus and axial antiferromagnetic states by calculating spin wave instability. The boundary for the 2/3-plateau can be given as

$$\Lambda = \frac{h}{2} - \Theta \pm \sqrt{(\Theta - 3J_z)^2 - 9J^2}, \tag{5.26}$$

with $\Theta = 2J_z + \frac{6J^2}{h/2-3J_z}$. Similar calculations give

$$\begin{aligned} h &= \sqrt{2(J_z^2 - J^2) + 2(J_z - \Lambda)^2 - 2\Sigma}, \\ \Sigma &= \sqrt{(J^2 - \Lambda(\Lambda - 2J_z))^2 + 32J^2\Lambda(2\Lambda - J_z)}, \end{aligned} \tag{5.27}$$

for the phase boundary of the partially polarized axial antiferromagnetic phase $A1$.

$$\Lambda = \Theta - \frac{h}{2} \pm \sqrt{(\Theta - 3J_z)^2 - 9J^2} \tag{5.28}$$

with $\Theta = 2J_z + \frac{h}{2} + \frac{6J^2}{h/2-3J_z}$ is the phase boundary of the plateau $P1$. While

$$\Lambda = 3J_z - \sqrt{\frac{h^2}{4} + 9J^2} \tag{5.29}$$

corresponds to the boundary of the axial antiferromagnetic phase $A3$. When $J = 0$ Eq. (5.28) and (5.29) recover the $h = 6J_z - 2\Lambda$ phase boundary that separates $A3$ and $P1$ in the Ising limit. The ground state energies and phase boundaries for the superfluid and supersolid phases can only be obtained numerically. The ground state wave function of the conical superfluid is given by Eq. (5.24), while that of the supersolid can be expressed as

$$|\Psi_A\rangle \propto e^{-i\varphi\hat{S}_A^z}\left(|\Uparrow\rangle + u|\uparrow\rangle + v|\downarrow\rangle + w|\Downarrow\rangle\right) \tag{5.30}$$

$$|\Psi_B\rangle \propto e^{-i(\varphi+\pi)\hat{S}_B^z}\left(|\Uparrow\rangle + u'|\uparrow\rangle + v'|\downarrow\rangle + w'|\Downarrow\rangle\right), \tag{5.31}$$

where u, u', v, v', w, and w' are all real. Fig. 5.5(b) shows the evolution of the order parameters which can be used to study the nature of the phases as we increase the magnetic field for a few selected values of Λ/J_z.

5.4 Exact Diagonalization studies

In order to gain further insight, we compare the variational results with numerically diagonalized small (8- and 10-site) clusters of spin $S = 3/2$ arranged on the square lattice with periodic boundary condition. The exact diagonalization introduced in this section were carried out by Karlo Penc.

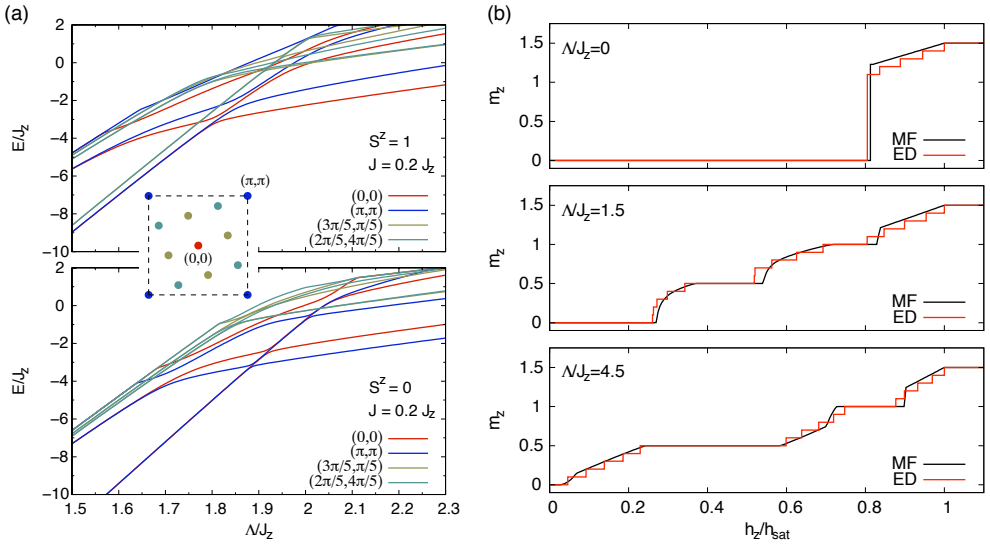

Figure 5.6: (a) The first few lowest lying energy levels of a 10 site cluster for (a) $S^z = 0$ and (b) $S^z = 1$ as a function of Λ/J_z. We set $J = 0.2J_z$. The inset shows the available $\mathbf{k}$–points in the Brillouin zone. (b) Magnetization as a function of magnetic field, as obtained from variational calculation and exact diagonalisation. Here $J = 0.2J_z$, and Λ/J_z =0, 1.5, and 4.5. $h_{\rm sat}$ is the saturation field [Eq. (5.11)].

In the two-sublattice phases the ground states with momentum $\mathbf{k} = (0, 0)$ and (π, π) are degenerate in the thermodynamic limit. In the gapped phases this two-fold degenerate level is well separated from the rest of the states, while in the supersolid state, which is also a translational symmetry breaking two-sublattice state, the rotational symmetry is spontaneously broken and we expect a gapless excitation, a Goldstone-mode. Unfortunately, the large spin makes the finite size scaling difficult, and without a finite size scaling we cannot be sure about the exact nature of the ground state. Nevertheless, even our small cluster gives important support for the variational phase diagram. In Fig. 5.6(a) we show the energy spectrum for the C_4 symmetric 10 site cluster with the choice $J = 0.2J_z$, in the vicinity of $\Lambda = 2J_z$, where we expect the first order transition the supersolid. In zero field the ground state has $S^z = 0$, and in the lower panel of Fig. 5.6(a) we see that the energy levels of lowest lying states corresponding to $\mathbf{k} = (0, 0)$ and (π, π) are essentially indistinguishable and well separated from the higher levels for $\Lambda < 1.88J_z$. This indicates the presence of a gapped, two–sublattice state that we can associate with the $A3$ phase. The sharp level anti-crossing at $\Lambda \approx 1.88J_z$ indicates a first order transition.

In the $S^z = 1$ sector, for $\Lambda < 1.88J_z$, the $\mathbf{k} = (0, 0)$ and (π, π) levels are equally close and reversed in order compared to the $S^z = 0$ case, as shown in the upper panel of Fig. 5.6(a). This behaviour indicates the rotational (U(1)) symmetry breaking, possibly alongside the translational symmetry breaking which is the case in the

supersolid phase.

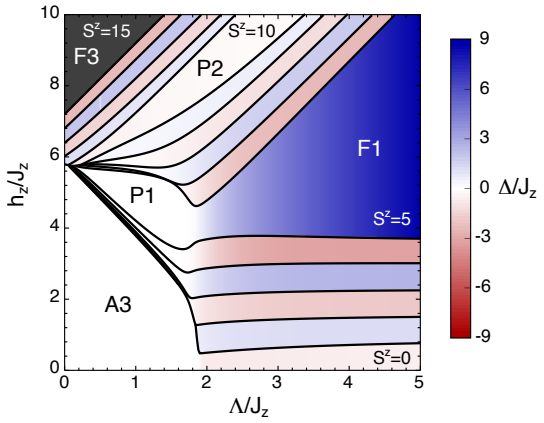

Figure 5.7: The gap $\Delta = E_{(\pi,\pi)} - E_{(0,0)}$ as a function of Λ/J_z and h/J_z for the 10–site cluster. The solid curves separate the different S^z sectors.

In Fig. 5.7 we map out the energy gap between the ground states with momenta $\mathbf{k} = (0,0)$ and (π,π) in the different S^z sectors, as a function of Λ/J_z and magnetic field. This plot can serve as an indicator of the translational symmetry breaking. Aside from $A1$, we can identify the gapped phases whose extensions are even quantitatively in good agreement with the variational phase diagram, shown in Fig. 5.5(a). The consistency between the variational and exact diagonalization result is also supported in Fig. 5.6(a)(lower), where we compare the magnetization calculated by these two methods.

5.5 Supersolid in the one-dimensional model – DMRG

In one-dimension our variational approach can be tested by comparing it with the results of Density Matrix Renormalization Group [White 1992] (DMRG) method. The DMRG calculations shown in this section were carried out by Frank Pollmann.

Quantum Monte Carlo study suggested the presence of a supersolid phase in the anisotropic $S = 1$ spin chain [Sengupta 2007b], which was later confirmed by DMRG calculations. [Peters 2009, Peters 2010, Rossini 2011]. It seems natural, therefore, to expect a supersolid phase to occur in the anisotropic spin-3/2 chain as well. Fig. 5.8 shows the phase diagram in the present finite magnetic field. We can clearly identify the gapped antiferromagnetic and ferromagnetic uniaxial phases with finite values of the staggered (m_z^{st}) and uniform magnetizations (m_z) and small entanglement entropy. The extension of the gapped phases essentially follows the variational phase diagram plotted in Fig. 5.5(a). However, the supersolid phase is more fragile in the one–dimensional case due to strong quantum fluctuations. Consequently, the gapless phase in the phase diagram is predominantly a simple Luttinger liquid with correlations decaying algebraically.

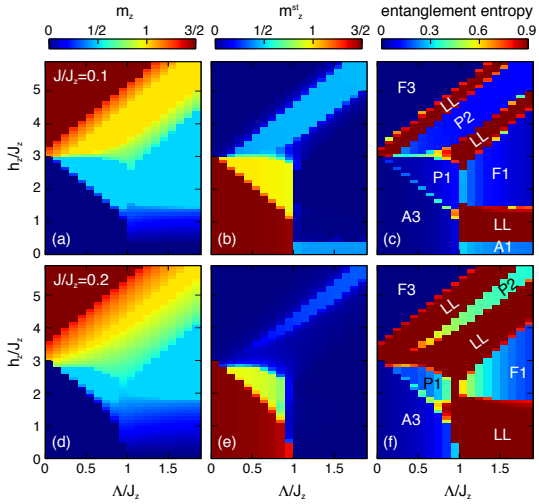

Figure 5.8: Phase diagram as the function of Λ/J_z and h/J_z for (a-c) $J/J_z = 0.1$ and (d-f) $J/J_z = 0.2$. We show the uniform and the staggered magnetization along the z axes, where the plateau phases can be identified. The large increase of the entanglement entropy indicates gapless phases. These results are in good agreement with the variational phase diagram shown in Fig. 5.5(a).

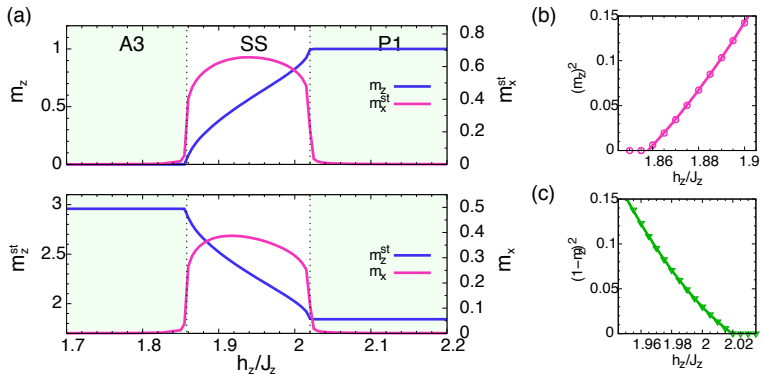

Figure 5.9: (a) The magnetic field dependence of the order parameters as a function of the magnetic field for $J/J_z = 0.2$ and $\Lambda/J_z = 0.5$. In upper panel, the non-vaninshing off-diagonal order parameter $m_x^{\rm st}$ shows the extension of the gapless phases. The finite value of the $m_z^{\rm st}$ and m_x indicate a robust supersolid phases, as seen in the lower panel. (Compare with Fig. 5.5(b).) (b) and (c) The magnetization has a square root singularity at the lower $h_{c,1}/J_z = 1.8579$, and upper $h_{c,2}/J_z = 2.0195$ critical field. The solid lines show the $m_z^2 \approx 2.68(h - h_{c,1})/J_z + 16.9(h - h_{c,1})^2/J_z^2$ and $(1 - m_z)^2 \approx 1.27(h_{c,2} - h)/J_z + 13.2(h_{c,2} - h)^2/J_z^2$ fits to the magnetization curves.

It appears that the supersolid is stable only in a small region, between the gapped phase $A3$ and $P1$. Both the magnetization and the staggered magnetization in the supersolid show a square root like character at the lower and upper critical fields, similarly to the magnetization in the XXZ model, see for example in Ref. [Klanjšek 2008]. This behaviour can be understood by associating the spinons with free fermions, then recalling that the density of states of free fermions shows van Hove singularity at the band edges which manifests as a square root singularity in the magnetization curve of the XXZ model.
This singularity is also inherited for the staggered magnetization at the critical fields. This square root behaviour is shown in Fig. 5.9, where we plotted m_z^2 and $(1-m_z)^2$ in panel (b) and (c) around the critical fields.

From variational calculations, we expect a continuos phase transitions into the supersolid also at the upper edge of the P_1 phase. Numerically, however, we find a first order transition into the LL phase.

5.5.1 The case of S=1

As the spin-1 anisotropic Heisenberg model has been studied earlier, it is useful to perform our variational calculation for the $S = 1$ case and compare our results to the numerical quantum Monte Carlo findings of Ref. [Sengupta 2007a] The variational phase diagrams, for $J = 0$ and $J = 0.2J_z$ are shown in Fig. 5.10(a) and (b), respectively. In the Ising limit, we find two uniform phases, denoted by 00 and 11, where

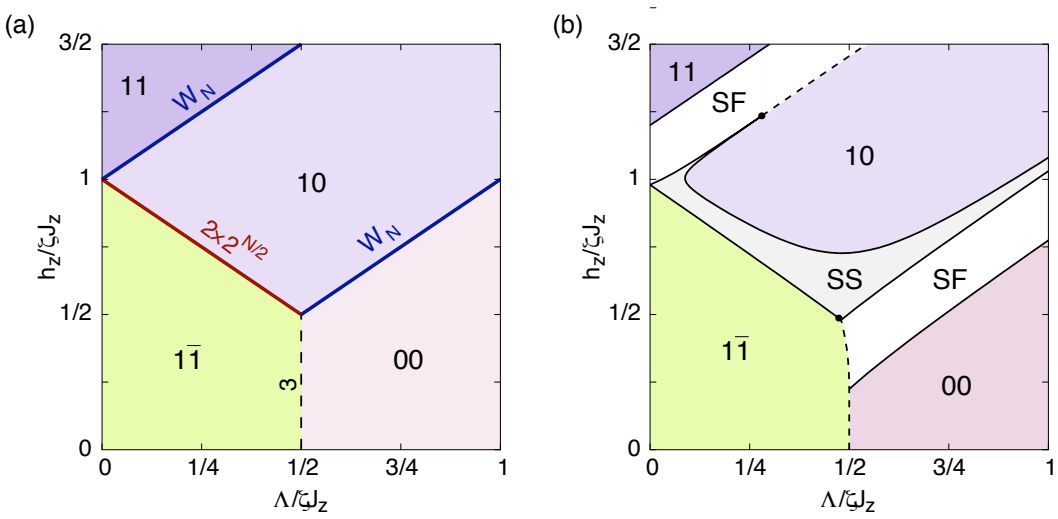

Figure 5.10: The phase diagram of the anisotropic S=1 model in the (a) Ising–limit for a bipartite lattice with coordination number ζ and (b) for the square lattice ($\zeta = 4$) when $J = 0.2J_z$, obtained from the variational calculation.

the numbers 0 and 1 correspond to the expectation value of the S^z. In addition,

there are two translational symmetry breaking phases: $1\bar{1}$ with zero magnetization and 10 which is the 1/2 magnetization plateau. The saturation field is given by $h_{\rm sat} = \Lambda + \zeta J_z + \zeta J$, and from the stability analysis of the gapped phases, $1\bar{1}$, 00, and 10, we obtain the following phase boundaries

$$h^2 = (\zeta J_z - \Lambda - \zeta J)(\zeta J_z - \Lambda + \zeta J), \tag{5.32}$$

$$h^2 = \Lambda(\Lambda - 2\zeta J), \tag{5.33}$$

$$(h - \Lambda)(\zeta J_z + \Lambda - h)(h - \zeta J_z + \Lambda) = 2\zeta^2 J^2 \Lambda, \tag{5.34}$$

respectively.

The XXZ–like physics can be identified for the transition between the phases 11,10, and 00, where the supersolid is fragile. The region between the 10 and $1\bar{1}$ is of different nature, and we expect the supersolid phase to be robust in this part of the phase diagram. This is exactly the region where the supersolid phase was found in Ref. [Sengupta 2007a] . The nature of the phase transitions, is also in qualitative agreement with the numerical results; we recover the first order transition between the upper boundary of the 10 and the superfluid phases.

Chapter 6

Electromagnons and $Ba_2CoGe_2O_7$

They say a little knowledge is a dangerous thing, but it is not one half so bad as a lot of ignorance.

– *Terry Pratchett, Equal Rites*

As we learned in the introductory chapter 2, spin systems of $S > 1/2$ support tensor interactions and may exhibit unconventional, often non-magnetic orders, such as multipolar or nematic order. When one is interested in the dynamical properties of such systems, the conventional quasi particle approaches, such as the Holstein-Primakoff representation, fail and one needs to introduce generalized bosonic operators related not only to the spin but also to higher order operators [Onufrieva 1985]. The idea of the extended spin wave approach is not entirely new; it has been introduced to study magnetic systems with single-ion anisotropy and/or higher order exchange terms [Onufrieva 1985, Papanicolaou 1984, Papanicolaou 1988, Shiina 2003], as well as for spin systems with orbital degeneracy in terms of flavor waves [Joshi 1999].

In this chapter we investigate the momentum and magnetic field dependent spin excitations in the multiferroic compound $Ba_2CoGe_2O_7$ based on the generalized spin wave method, introduced in chapter 3. We will show that this approach is sufficient to describe the higher excitations observed in the far infrared absorption spectra, but would be beyond the reach of the conventional spin wave theory. A word will be added on the spin-induced polarization at zero and finite temperatures, with the aim to reproduce the experimentally observed peculiar behavior of the induced polarization in magnetic field in Ref. [Murakawa 2010] (see Fig. 1.10 in the introductory chapter 1).

Starting from the symmetry analysis in section 2.2.2 we consider the following Hamiltonian

$$\begin{aligned}\mathcal{H} &= J\sum_{\langle i,j\rangle}\left(S_i^xS_j^x+S_i^yS_j^y\right)+J_z\sum_{\langle i,j\rangle}S_i^zS_j^z+\\ &\quad\sum_i\left[\Lambda\left(S_i^z\right)^2+g_{zz}h_zS_i^z+g_{xx}(h_xS_i^x+h_yS_i^y)\right],\end{aligned}\tag{6.1}$$

where $\langle i,j\rangle$ indicates nearest neighbor pairs, and the x, y, and z axes are parallel to the [110], [1$\bar{1}$0], and [001] crystallographic directions, respectively (See Fig. 1.7).

$g_{xx} = g_{yy}$ and g_{zz} are the principal values of the g tensor, and $h_\alpha = \mu_B B_{dc,\alpha}$ are the components of the magnetic field.

6.1 Zero field phase diagram

In this part we give a detailed study on the zero-field excitations of $Ba_2CoGe_2O_7$, considering the effect of single-ion anisotropy, although, for simplicity we neglect the DM interaction which is in fact very small compared to the exchange interaction. On the other hand, we introduce the exchange anisotropy which has a significant effect on the ground state, and subsequently on the excitations, as we have seen in the previous chapter.

We start our investigations with a short discussion of the variational phase diagram as the function of easy-plane and exchange anisotropies. Then, based on these variational findings, we introduce a suitable boson basis and perform the generalized spin wave approach to study the momentum dependent excitation spectrum. We examine the isotropic case ($\Lambda = 0, J_z = J$) separately and consider the limit $\Lambda \to \infty$ in detail. The latter case will be compared the effective spin-1/2 model, discussed in Ref. [Zheludev 2003]. Furthermore, we calculate the dynamical structure factor for the excitation modes so that we can compare our results qualitatively with that of neutron spectroscopy of Ref. [Zheludev 2003].

We search for the ground state in the site-factorized variational form introduced in 5.3:

$$|\Psi\rangle = \prod_{i\in A}\prod_{j\in B} |\psi_A\rangle_i |\psi_B\rangle_j \ , \tag{6.2}$$

where

$$|\psi_A\rangle \propto |3/2\rangle + e^{i\xi_1}u_1|1/2\rangle + e^{i\xi_2}u_2|-1/2\rangle + e^{i\xi_2}u_3|-3/2\rangle \tag{6.3}$$

and with a similar expression for $|\psi_B\rangle$. The variational parameters, as usually, can be determined by minimizing the ground state energy $E = \frac{\langle\Psi|\mathcal{H}|\Psi\rangle}{\langle\Psi|\Psi\rangle}$.

The phase diagram exhibits two, the completely and the partially aligned, axial antiferromagnetic states, $A3$ and $A1$, already familiar from section 5.1. In addition, a superfluid (U(1)) phase emerges between them; this is referred to as a planar state in Ref. [Sólyom 1984], for the spins are aligned in the lattice plane. However, one can call this phase superfluid for the spin-rotation symmetry breaking phases exhibit off-diagonal long-range order, or equivalently finite spin stiffness [Seabra 2011], that is the property of such phases. In the following we refer to this phase as SF_0. Between the planar superfluid SF_0 and the two axial antiferromagnets $A1$ and $A3$ an other superfluid phase appears. The in-plane components of this conical antiferromagnet have the same properties as the planar superfluid but it exhibits finite staggered magnetization too, inheriting the property of the antiferromagnetic phases, $A1$ and $A3$, as well. Therefore we call this phase SF_A.[1] A schematic figure of the various phases is shown in the phase diagram in Fig. 6.1.

[1] As in a superfluid, or conical phase with finite staggered (antiferro) magnetization.

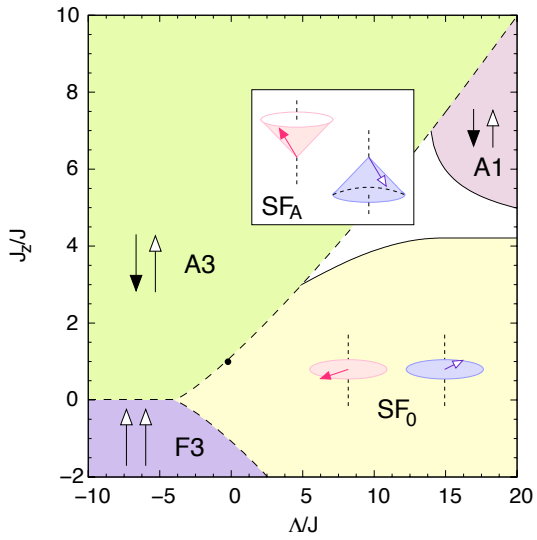

Figure 6.1: Variational phase diagram for $h = 0$ as the function of Λ/J and J_z/J. Solid lines stand for continuous (second order) phase boundaries, while the dashed lines denote the first order phase transition. The black dot represents the SU(2) symmetric isotropic Heisenberg model.

Comparing the ground state energies of $A1$ and $A3$ we find that the first order phase boundary between them is $\Lambda = 2J_z$. The ground state wave functions of sites A and B in the planar superfluid phase SF_0 can be expressed as

$$|\Psi_A\rangle = e^{-i\varphi_A \hat{S}_A^z} |\Psi_{\mathrm{SF}}\rangle, \tag{6.4}$$

$$|\Psi_B\rangle = e^{-i\varphi_B \hat{S}_B^z} |\Psi_{\mathrm{SF}}\rangle, \tag{6.5}$$

where in the absence of in-plane magnetic field the spins are antiparallel, that is $\varphi_A = \varphi$, $\varphi_B = \varphi + \pi$, and the energy depends only on the variational parameter η:

$$|\Psi_{\mathrm{SF}}\rangle = \frac{|\frac{3}{2}\rangle - i\sqrt{3}\eta|\frac{1}{2}\rangle - \sqrt{3}\eta|-\frac{1}{2}\rangle + i|-\frac{3}{2}\rangle}{\sqrt{6\eta^2+2}}. \tag{6.6}$$

The ground state energy as the function of parameter η reads

$$\frac{E_0^{SF_0}(\eta)}{N} = \frac{3}{4}\frac{\eta^2+3}{3\eta^2+1}\Lambda - \frac{18\eta^2(\eta+1)^2}{(3\eta^2+1)^2}J\,. \tag{6.7}$$

In the energy expression the J_z-term is missing, as this wave function has spin components only in the xy plane. The energy in this phase is minimal when the following equation is satisfied:

$$\frac{\Lambda}{J} = \frac{3(\eta^2-1)(3\eta+1)}{3\eta^2+1}\,. \tag{6.8}$$

For small values of Λ the ground state energy can be approximated as:

$$E_0^{SF_0} = -\frac{9}{2}J + \frac{3}{4}\Lambda - \frac{\Lambda^2}{16J} + O(\Lambda^3) \tag{6.9}$$

giving the phase boundary toward the antiferromagnetic phase $A3$

$$J = J_z - \frac{\Lambda}{3} - \frac{\Lambda^2}{72J_z} + O(\Lambda^3) \tag{6.10}$$

as plotted in Fig. 6.1. The parameter φ can take arbitrary value, carrying the U(1) symmetry breaking property of the ground state (we recall that the Hamiltonian commutes with the $\hat{S}^z$ operator), furthermore it determines the angle between the spins and the axis y:

$$\langle\Psi_A|\hat{\mathbf{S}}|\Psi_A\rangle = \frac{3\eta(\eta+1)}{3\eta^2+1}(\sin\varphi_A, -\cos\varphi_A, 0) \tag{6.11}$$

$$\langle\Psi_B|\hat{\mathbf{S}}|\Psi_B\rangle = \frac{3\eta(\eta+1)}{3\eta^2+1}(-\sin\varphi_B, \cos\varphi_B, 0) \tag{6.12}$$

When $\Lambda \to 0$, that is the single-ion anisotropy is absent, $\eta \to 1$ and the Hamiltonian (6.1) has SU(2) symmetry and consequently the ground state corresponds to the spin-3/2 Néel-state. For $\Lambda > 0$ the $S^z = \pm 3/2$ components in the wave function are suppressed. In the large Λ limit $\eta \to \infty$, and the length of the spin is equal to 1. Let us recall that starting from a more general wave function than (6.6), when $\Lambda > 0$ the $S^z = \pm 3/2$ components are suppressed and the wave function is composed of the $S^z = \pm 1/2$ components. Then the tip of the spin can move within an ellipsoid and the length of the spin is maximal (equal to 1) when it lays in the xy-plane and minimal (equal to 1/2) along the z-axis. Therefore a finite antiferromagnetic exchange supports the planar ordering. When the exchange interaction becomes anisotropic, and the $\hat{S}_i^z\hat{S}_j^z$ term becomes strong, this energy can compensate the directional length dependence of the spin, and can choose a spin configuration with a finite z and xy component. This happens in the conical superfluid phase, denoted by SF_A in Fig. 6.1. The parameter η can be expressed in the two limits as it follows:

$$\eta = \begin{cases} 1 + \frac{\Lambda}{6J} + O\left(\frac{\Lambda^2}{J^2}\right) & \Lambda \ll J \\ \frac{\Lambda}{3J} - \frac{1}{3} + O\left(\frac{J}{\Lambda}\right) & \Lambda \gg J \end{cases} \tag{6.13}$$

The phase boundary of the conical superfluid phase (SF_A) towards the planar phase (SF_0) and fully polarized AFM phase ($A3$) are beyond analytical reach, however, the numerically obtained boundaries are shown in Fig. 6.1. Starting from phase $A1$ at a given Λ value, a second order phase transition takes place to the superfluid phase, SF_A. When the exchange coupling J is large enough, in-plane spin components appear continuously as we reach SF_A. The ground state of this conical superfluid phase can be expressed as it follows:

$$|\Psi_A\rangle \propto e^{-i\varphi\hat{S}_A^z}(|3/2\rangle + u|1/2\rangle + v|-1/2\rangle + w|-3/2\rangle) \tag{6.14}$$

$$|\Psi_B\rangle \propto e^{-i(\varphi+\pi)\hat{S}_B^z}(w|3/2\rangle + v|1/2\rangle + u|-1/2\rangle + |-3/2\rangle) \tag{6.15}$$

where the variational parameters u, v and w are all real values.

The instability of the partially aligned AFM phase $A1$ against canting gives the phase boundary between the phases $A1$ and SF_A

$$J = \frac{J_z(J_z - \Lambda)}{J_z - 4\Lambda} \,. \tag{6.16}$$

The same model for one dimension has been treated by mean field calculations in Ref. [Sólyom 1984] for quantum spins 1/2, 1 and 3/2. The phase diagram for the case $S = 3/2$ is similar to ours, however the conical superfluid phase SF_A is missing due to a less general variational wave function.

6.2 Induced polarization in $Ba_2CoGe_2O_7$

In this section we investigate how the induced electric polarization depends on the applied in-plane magnetic field in $Ba_2CoGe_2O_7$. We examine two field settings: $h||[010]$ and $h[\bar{1}10]$. We shall discuss in detail the effect of the Dzyaloshinskii-Moriya interaction on the polarization. In particular, to explain the low field behavior of the polarization observed in Ref. [Murakawa 2010], we introduce an antiferroelectric term in the Hamiltonian that couples the electric polarizations on the neighboring sites. For simplicity we assume that there is no exchange anisotropy: $J = J_z$, as assumed in Ref. [Miyahara 2011] but we consider the out-of plane DM term:

$$\begin{aligned} \mathcal{H} &= J\sum_{\langle i,j\rangle}\left(S_i^xS_j^x + S_i^yS_j^y + S_i^zS_j^z\right) + \sum_i\left[\Lambda\left(S_i^z\right)^2 + \mathbf{h}\mathbf{S}_i\right] \\ &\quad + D_z\sum_{\substack{i\in A\\ j\in B}}(S_i^xS_j^y - S_i^yS_j^x) \,. \end{aligned} \tag{6.17}$$

Again, we consider two-sublattice order and write the variational wave function in the product form of (6.2) and (6.3).

Let us begin our investigations with the familiar case of $D_z = 0$. When the external magnetic field is zero, the variational ground state of (6.17) is the planar antiferromagnetic (or superfluid) phase, SF_0, that breaks rotational symmetry U(1). The planarity is the consequence of the easy-plane single ion anisotropy and the U(1) symmetry breaking is related to the fact that in the absence of an in-plane magnetic field the Hamiltonian commutes with total S^z. φ_A and φ_B determine the angles of the spins with respect to the $[\bar{1}10]$ direction, that is with respect to the y-axis. As shown in the previous section, in zero field $\varphi_A = \varphi$ and $\varphi_B = \varphi + \pi$, i.e. the spins are antiparallel and the U(1) symmetry breaking is manifested in the fact that φ can take arbitrary value.

However, in a finite in-plane magnetic field, φ is not arbitrary any longer and the canted spins turn so that the total magnetization points into the direction of the field. This two sublattice canted order is twofold degenerate because, the Hamiltonian is invariant under the exchange of sites A and B when $D_z = 0$. Increasing the field, the relative angle of the sublattices, $\delta\varphi = \varphi_A - \varphi_B$, decreases from $\delta\varphi = \pi$ to

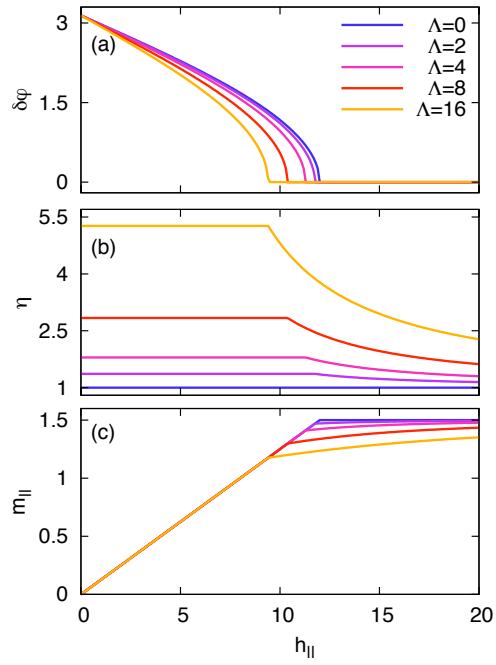

Figure 6.2: (a) The in-plane field dependence of the relative angle $\delta\varphi$ of the spins belonging to the two sublattices. (b) and (c) the field dependence of the parameter η and that of the magnetization.

$\delta\varphi = 0$, while the length of the spins is unchanged, that is, η remains constant in the canted antiferromagnetic phase as indicated in Fig. 6.2(a) and (b). The magnetization increases linearly with the field and its value is independent of the single-ion anisotropy (see Fig. 6.2(c)).It is important to note that the length of the spin is not equal to 3/2, and as we will see in the followings, this implies that there might be an excitation mode corresponding to the longitudinal stretching of the spin length. In the usual spin wave approach, the excitations correspond to tilting the spin away from the quantization axis, that is, they are transversal excitations. The possibility of a spin-stretching mode is the consequence of the single-ion anisotropy (Λ), the exchange anisotropy by itself would not be enough.

At a critical value (h_c) the two spins become aligned and in the place of the two-sublattice order a uniform phase appears. The critical field, however, is not equal to the saturation field, the spins are not fully magnetized yet. With the further increase of the field the magnetization increases slowly as the spins reach their full length, i.e. η decreases to $\eta = 1$ as shown in Fig. 6.2.

The polarization and magnetization for $D_z = 0$ in magnetic fields along the axes $[\bar{1}10]$ and [010] are plotted with black solid lines in Fig. 6.3(c) and (f), respectively. The spin configurations of the twofold degenerate canted order are shown in panel (a),(b) and (d),(e) for the two field settings. In both cases we indicate the canting angle of the spins with respect to the applied field. Conveniently, in the case of

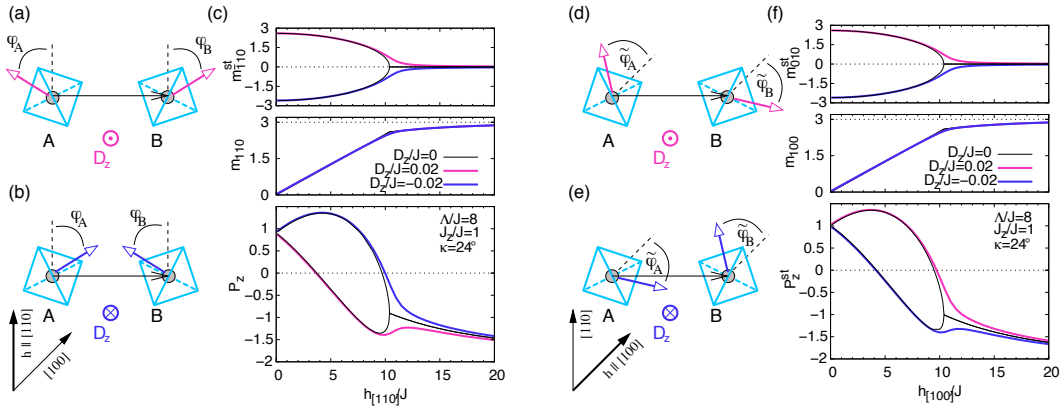

Figure 6.3: (a),(b) Schematic figure of ground states in canted antiferromagnetic phase when $h||[110]$. For $D_z = 0$ (a) and (b) are degenerate. A finite DM coupling lifts the twofold degeneracy, the ground state configuration for $D_z > 0$ is shown in (a) while (b) is selected when $D_z < 0$. (c) The polarization P_z, the magnetization $m_{[110]}$ and the staggered magnetization $m^{\mathrm{st}}_{[\bar{1}10]}$ is shown. Black line indicates the twofold degeneracy of the $D_z = 0$ case below the partially magnetized phase. The colored lines correspond to the $D_z > 0$ and $D_z < 0$ cases in accordance with the coloring of spin states in (a) and (b). (d),(e) the canted antiferromagnetic ground state for $h||[100]$. Similarly to the case of $h||[110]$ (d) and (e) are degenerate when $D_z = 0$. Whereas a finite D_z lifts this degeneracy, and $D_z > 0$ selects the canted state (d) while $D_z < 0$ prefers the configuration of (e). (f) When $h||[100]$ the uniform polarization vanishes ($P_z = P_z^A + P_z^B = 0$) and the staggered polarization $P_z^{\mathrm{st}} = P_z^B - P_z^A$ takes a finite value. The coloring of the cases $D_z > 0$ and $D_z < 0$ follows that of the spin states used in (d) and (e).

$h||[\bar{1}10]$ this canting angle is φ_A and φ_B – following from the definition of the ground state (6.5). However, when $h||[010]$ we need to introduce the canting angles $\tilde{\varphi}_A$ and $\tilde{\varphi}_B$, to measure the angle from the [010]-axis.

Regarding the magnetization it is natural to consider $m_{[\bar{1}10]}$ and its rotated counterpart $m_{[010]}$ as the relevant magnetic order parameters for the two selected field settings $h||[\bar{1}10]$ and $h||[010]$. It is not that easily perceived, however, which component of the polarization will characterize the electric order in the two cases. To get to the bottom of this, we will shortly discuss the connection between $h||[\bar{1}10]$ and $h||[010]$ through a $\pi/4$-rotation of the local basis. In the original basis the spin component S^y is parallel to the y-axis, which corresponds to the $[\bar{1}10]$ direction. Let us choose the new rotated basis so that the component $\tilde{S}^y$ becomes parallel to the crystallographic axis [010]: The effect of the local basis transformation is sketched in Fig. 6.4. As it was pointed out in Ref. [Murakawa 2010], the induced polarization has extremum when the spin is aligned with either the upper or the lower edge of

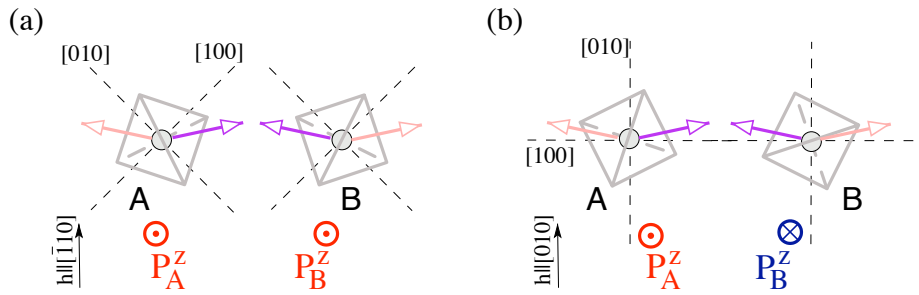

Figure 6.4: The connection between the cases $h||[\bar{1}10]$ and $h||[010]$. In our notation P_j^z takes maximum value for a spin aligned parallel to the lower edge (dashed line) and minimum value along the upper (solid) edge. (a) Schematic spin configuration for $h||[\bar{1}10]$. The two types of vectors indicate the two-fold degeneracy. The spin induced polarization is the same on the two sublattices for the spins are canted by the same angle from either the lower or the upper edge, of the tetrahedra. (b) Spin configuration for $h||[010]$ after rotating the basis by the angle $\pi/4$. Note that due to the rotation of the tetrahedral environment the induced polarization changes. The spins of the two subblatices are now canted from the different edges, consequently the induced polarization on them have different sign.

the surrounding tetrahedra.[2] If P_j^z is maximal for a given spin orientation, then a $\pi/2$-rotation of the spin changes the sign of the polarization, as illustrated by the angular dependence of polarization in Fig. 1.9(e). When the spin lays halfway between these two positions, the polarization is zero. Applying the field in the direction $[\bar{1}10]$, the spins on the two sublattices are tilted by the same angle from the same symmetry plane of the tetrahedra, therefore the induced polarization on A and B has the same sign (and magnitude). However a $\pi/4$ rotation of the local basis rotates the tetrahedral environment in a way that the spins on A and B are now tilted from the different edges, and as a result the induced polarizations have different sign on the two sublattices, as illustrated in Fig. 6.4.

According to this argument, when the field is parallel to $[\bar{1}10]$ the relevant order parameter is the total polarization $P^z = P_A^z + P_B^z$, whereas for $h||[010]$ the staggered component $P_z^{\mathrm{st}} = P_A^z - P_B^z$ will give a finite expectation value. We shall note, that the difference between the two cases is related to the lattice symmetries as well. While along the $[\bar{1}10]$ direction the symmetry operation that connects site A with site B is the mirror plane $\sigma_{[\bar{1}10]}$, along the [010]-direction the sites can be transformed into each-other by a 2_1 screw axis. The lowest panel in Fig. 6.3(c) and (f) shows the induced (staggered) polarization when the field is parallel to the $[\bar{1}10]$ ([010]) crystallographic axis. We find that in the canted antiferromagnetic phase the induced polarization can take two different values corresponding to the twofold degeneracy of the ground state (see Fig. 6.3 (a),(b) and (d),(e)).

[2]The lower and upper edges are those parallel to the Co-plane and correspond to the diagonal in our schematic figures.

6.2.1 The effect of Dzyaloshinsky-Moriya interaction

A finite magnetic field lifts the U(1)-degeneracy of the ground state (6.5) resulting in a twofold degenerate canted antiferromagnetic ground state shown in Fig. 6.4. Similarly to the effect of magnetic field, the DM interaction leads to a canting of the antiferromagnetic state, as the term $\mathbf{D}(\mathbf{S}_i \times \mathbf{S}_j)$ prefers orthogonal spin configuration. When the DM interaction is finite, but the magnetic field is zero, the canting angle depends on the magnitude of D_z. This canted AFM phase, in contrast with the finite $h_{\text{in-plane}}$ and $D_z = 0$ case, breaks the U(1) symmetry too, for D_z controls only the direction of the spins on different sublattices relative to each other, and S^z remains a good quantum number ($[\mathcal{H}, S^z] = 0$) as long as there is no field applied in the plane. Turning on the magnetic field in the case of finite D_z, the $U(1)$ degeneracy is lifted and a non-degenerate ground state develops as the DM coupling is sensitive to the exchange of the sites A and B. Similarly to the case $D_z = 0$, below the critical field the variational parameter η, consequently the spin length, remains constant, as opposed to $h > h_c$, when the spins are partially magnetized and their length increases with the field. The canting angle $\delta\varphi = \varphi_A - \varphi_B$ depends on both the magnetic field and the DM interaction, and the sign of D_z determines which of the two canted states is realized. Comparing our results to the $h||[110]$ measurement of Ref. [Murakawa 2010] (see Fig. 1.10(b)), we find that $D_z < 0$ is the appropriate choice.

A schematic figure of the canted ground states in the case $h||[\bar{1}10]$ is shown in Fig. 6.3(a) and (b) corresponding to $D_z > 0$ and $D_z < 0$, respectively. Similarly, in the case of $h||[010]$ the canted state in Fig. 6.3(d) will be realized for positive while the spin configuration in Fig. 6.3(e) for negative values of D_z. The magnetization and the spin order induced polarization is plotted in Figs. 6.3(c) and (f) for the two field settings. Based on the above argument, when the field is pointing in the direction $[\bar{1}10]$ the total polarization is finite, while for $h||[010]$ the staggered polarization gives non-zero expectation value. We remark that with the choice of $\kappa = \pi/8$, the total polarization for $h||[\bar{1}10]$ and the staggered polarization for $h||[010]$ would match perfectly. A finite D_z interaction chooses different branches of the electric order parameter (P_z and P_z^{st}) for the two settings of magnetic field, e.g. $D_z < 0$ favors the higher branch of the total polarization when $h||[\bar{1}10]$ and the lower branch of the staggered polarization in the case of $h||[010]$.

6.2.2 The effect of an antiferroelectric term

For higher fields the polarization curve is satisfyingly similar to the measurements, however, the low field behavior cannot be explained using only the Hamiltonian (6.17). In order to reproduce the sharp decrease of polarization below $h \approx 1$ T (see Fig. 1.10(b)) we add an anitiferroelectric ($K_z > 0$) coupling term to our model

$$\mathcal{H}_{\text{pol}} = K_z \sum_{(i,j)} P_i^z P_j^z \ , \tag{6.18}$$

where the polarization operator can be written in terms of quadratic spin operators based on the symmetry considerations in chapter 2:

$$\hat{P}_j^z \quad \propto \quad \cos 2\kappa_j \left((\hat{S}_j^y)^2 - (\hat{S}_j^x)^2 \right) - \sin 2\kappa_j \left(\hat{S}_j^x \hat{S}_j^y + \hat{S}_j^y \hat{S}_j^x \right) \tag{6.19}$$

(6.18) is an anisotropic biquadratic term in spin operators whose microscopic origin can e.g. be due to lattice effects. Since $[\mathcal{H}_{\rm pol}, S^z] \neq 0$, the $U(1)$ symmetry is lost with this term in the Hamiltonian.

At low magnetic fields a fourfold degenerate ground state appears which actually corresponds to the one discussed in Ref. [Toledano 2011], where the order parameters in $Ba_2CoGe_2O_7$ were investigated from purely the aspect of symmetries. Let us start our investigation with $D_z = 0$ again. The spin direction is determined by the minimization of (6.18) and (5.1). As discussed above and in Ref. [Murakawa 2010], the orientation of the spins relative to the surrounding tetrahedron determines the induced polarization. When the spin is pointing along the lower (or upper) edge of the tetrahedron, the induced P^z is maximal (or minimal). Therefore, a term $P_A^z P_B^z$ favors a spin configuration in which the spins on sites A and B are parallel to different edges. Note that this is not an orthogonal spin configuration for the tetrahedra of the different sublattices are rotated by $2\kappa \approx 48^\circ$ compared to each other. The polarization term competes with the antiferromagnetic exchange interaction and the resulting ground state is the canted state shown in Fig. 6.5(a). A finite magnetization points along the [100] or [010] axes in these cases. When

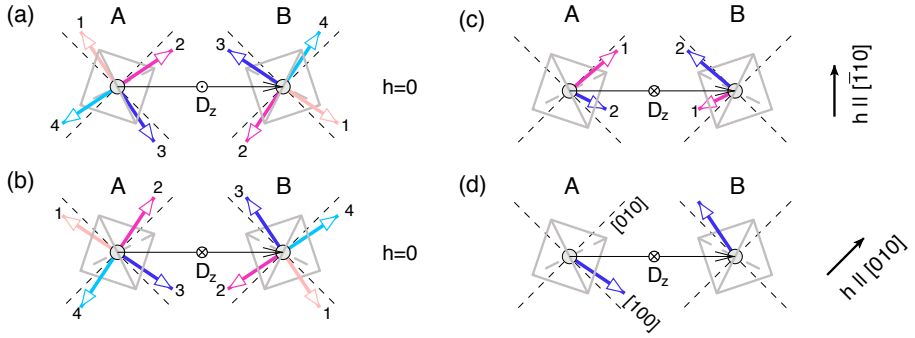

Figure 6.5: Ground state spin configurations when the antiferroelectric is present in the Hamiltonian. (a) and (b) the fourfold degenerate ground state in zero field for different signs of D_z. A spin configuration – with smaller canting angle – shown in (a) would correspond to the case $D_z = 0$, too (c) when $h||[110]$ a canted ferrimagnetic phase emerges below $h_{c2} \approx 1$ T due to the polarization term. (d) for $h||[100]$, since $K_z > 0$, the canted ferrimagnetic phase is missing, and at finite field the ground state is the canted antiferromagnet similar to the case $K_z = 0$. A ferromagnetic polarization term would have the opposite effect.

the DM interaction is finite this spin configuration is favored by $D_z > 0$ that only changes the canting angle. However, a $D_z < 0$ introduces frustration, as it prefers a

reversed spin orientation: if the angle between the spins is $\varphi_A - \varphi_B$ for $D_z > 0$, it is $-\varphi_A + \varphi_B$ for $D_z < 0$ (see Fig. 6.5(b)). We can say that changing the sign of D_z to negative corresponds to the exchange of sites A and B, however with a smaller canting angle arising from the competition of K_z and D_z.

Selecting $D_z < 0$, that recovers the experimental results, we calculated the induced polarization for both orientations of the magnetic field. In the case $h||[\bar{1}10]$ we observed a new phase below $h_{c2} \approx 1$ T. This intervening phase is twofold degenerate. Following from the different spin length on the sublattices A and B, a suitable order parameter is $|\mathbf{S}_A| - |\mathbf{S}_B|$, therefore we refer to this phase as a canted ferrimagnetic phase. The ground state can still be written as (**??**), but here the parameter η, and so the spin length is different for the two sublattices. The angle between the spins on sublattices A and B is determined by the collective effect of K_z, D_z and $h_{[110]}$. A schematic spin configuration of this phase is shown in Fig. 6.5(c). When $h > h_{c2} \approx 1$ T we enter the canted antiferromagnetic phase that was characteristic in the case $K_z = 0$ as well (see Fig. 6.3 (a)). When the field exceeds $h_c \approx 13$ T, the partially magnetized uniform phase emerges. In the rotated field setting, i.e. when $h||[100]$ the intervening canted ferrimagnetic phase is missing, and only three phases are observed. The finite field lifts the fourfold degeneracy of the $h = 0$ ground state and we enter the non-degenerate two sublattice canted antiferromagnetic order shown in Figs. 6.5(d) or 6.3(e). At the critical field the canted antiferromagnet is replaced by the uniform phase.

We shall note that a ferro polarization coupling ($K_z < 0$) would reverse the situation, and it would cause the emergence of the canted ferrimagnetic phase when the field is $h||[010]$, while for $h||[\bar{1}10]$ this phase would not be present. The finite temperature mean field calculations were carried out by Miklós Lajkó [Romhányi 2011]. The variational and the finite temperature mean field results are shown together in Fig. 6.6(a) and (c) for $h||[\bar{1}10]$ and $h||[010]$, respectively. We took the realistic parameter setting: $J = J_z = 1.885$ K, $\Lambda = 15.08$ K according to Ref. [Miyahara 2011], $g = 2.2$ and the values D_z and K_z were set to -0.02 K and 0.01 K respectively. The mean field result for T = 2 K is essentially undistinguishable from the T=0 variational calculation.

For the field applied parallel to $[\bar{1}10]$, we find that below $h_{c2} \approx 1$ T the polarization drops to zero and in this region there is a finite expectation value of $m_{[110]}$ and P_z^{st}, corresponding to the zero temperature canted ferrimagnetic phase. In this region the polarization decreases sharply reproducing qualitatively well the experimental findings in Ref. [Murakawa 2010] (see Fig. 1.10). Above h_{c2} the canted antiferromagnetic phase takes place, in wich the spins rotate according to the increasing field so that at $h_c \approx 13$ T, through a continuous phase transition, they become aligned and the uniform, partially magnetized phase appears. With further increase of $h_{[\bar{1}10]}$ the spins grow to reach $|S| = 3/2$.

For $h||[100]$, however, the canted ferrimagnetic phase is absent, and at finite field only the canted antiferromagnetic and partially magnetized phases can be observed. Changing the polarization-polarization coupling to ferroelectric type, the situation would be reversed: in $h||[\bar{1}10]$ there would be no sign of the canted ferrimagnet,

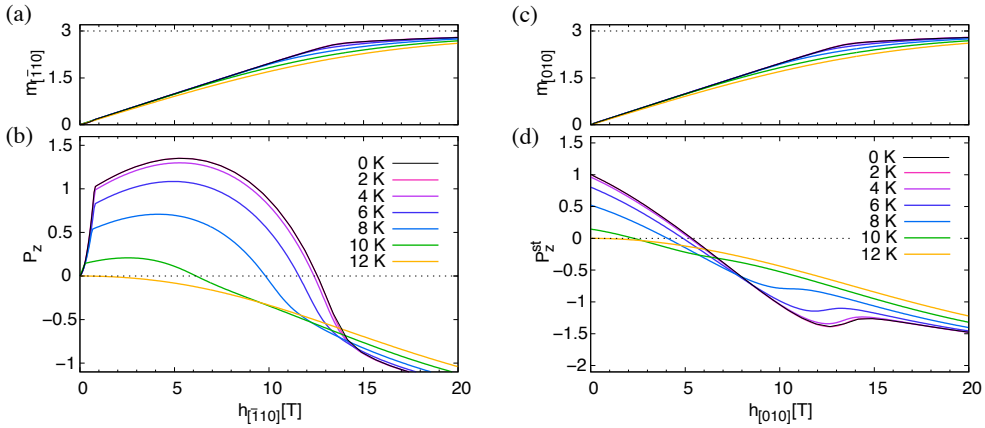

Figure 6.6: Behaviour of magnetization (a) and polarization (b) in external field along the crystallographic axis $[\bar{1}10]$ at various temperature values. (c) staggered polarization and (d) magnetization results at finite temperature when the magnetic field is parallel to the axis [010]. In this setting the canted ferrimagnetic phase is missing, and the lower polarization curve (of Fig. 6.3) is selected when $K_z > 0$. Similarly to the $h||[\bar{1}10]$ case, the staggered polarization depends strongly on the temperature, however the magnetization hardly changes. ($J = J_z = 1.885$ K, $\Lambda = 15.08$ K, $D_z = -0.02$ K, $K_z = 0.01$ K and $g = 2.2$)

while it would appear for $h||[010]$. Taking strictly the Hamiltonian (6.17) extended with the polarization term (6.18), we can recover the main characteristics of the experimental findings in Ref. [Murakawa 2010]. The polarization drops sharply below 1 T and it changes drastically with increasing temperature, whereas the magnetization curve is almost unchanged. Based on our calculations, we believe that relevant information regarding the low field phase could be obtained from torque measurements. Furthermore, extending the magnetization measurements to higher fields can provide information about the partially polarized uniform phase.

Nonetheless, there are yet some properties to account for. The polarization curve in the experiments starts from a small negative value at zero field, while in our model, due to the antiferroelectric term, $P_z = 0$ when $h = 0$. The significance of this small negative polarization, and whether it is intrinsic to the material, is not clear at this moment. Furthermore around h_{c2} the shape of the polarization is softer, in contrast with our findings, that exhibit an edge in P_z when the canted ferrimagnet transforms into the canted antiferromagnetic phase. We shall mention that such anomalies can be reproduced within our model by assuming a finite residual magnetization orthogonal to the applied field in the sample.

6.3 Dynamical properties of $Ba_2CoGe_2O_7$

In this final section we will investigate the excitation spectra in zero and finite magnetic field. Although the Dzyaloshinskii-Moriya interaction played an important role in the understanding of the induced polarization, due to its small magnitude it affects the excitation spectrum negligibly. Therefore we consider the Hamiltonian introduced in Eq. (6.1) which includes the single-ion, the exchange and the g-tensor anisotropies, but omits the Dzyaloshinky-Moriya interaction.

6.3.1 Flavor wave spectrum in zero field

Let us introduce the bosons $\alpha_m^\dagger$ that create the $S^z = m$ states of a spin $S = 3/2$ as $|m\rangle = \alpha_m^\dagger|0\rangle$. In terms of the α bosons, the diagonal spin operators can be written as

$$S^z = \sum_{m=-3/2}^{3/2} m\alpha_m^\dagger\alpha_m, \quad (S^z)^2 = \sum_{m=-3/2}^{3/2} m^2\alpha_m^\dagger\alpha_m. \tag{6.20}$$

and the off-diagonal spin raising operator is

$$S^+ = \sqrt{3}\left(\alpha_{3/2}^\dagger\alpha_{1/2} + \alpha_{-1/2}^\dagger\alpha_{-3/2}\right) + 2\alpha_{1/2}^\dagger\alpha_{-1/2}, \tag{6.21}$$

while the spin lowering operator can be easily achieved by its hermitian conjugation. To conserve the boson number the following condition must be satisfied:

$$\sum_m \alpha_m^\dagger\alpha_m = M\ , \tag{6.22}$$

M being 1 for the spin $S = 3/2$. With this definition the spin operators of 6.20 and 6.21 fulfill the usual spin commutation relations.

As the following step, we apply an SU(4) rotation, that is, a uniform transformation as introduced in chapter 3, in the space of $\alpha_m^\dagger$ bosons in order to set the quantization axis right:

$$(a_j^\dagger, b_j^\dagger, c_j^\dagger, d_j^\dagger)^T = \mathbf{U}_A(e^{\frac{3}{2}i\varphi_j}\alpha_{-3/2}^\dagger, e^{\frac{1}{2}i\varphi_j}\alpha_{-1/2}^\dagger, e^{-\frac{1}{2}i\varphi_j}\alpha_{1/2}^\dagger, e^{-\frac{3}{2}i\varphi_j}\alpha_{3/2}^\dagger)^T \tag{6.23}$$

with

$$\mathbf{U}_A = \begin{pmatrix} \frac{1}{\sqrt{6\eta^2+2}} & \frac{\sqrt{3}\eta}{\sqrt{6\eta^2+2}} & \frac{\sqrt{3}\eta}{\sqrt{6\eta^2+2}} & \frac{1}{\sqrt{6\eta^2+2}} \\ \frac{\sqrt{3}\eta}{\sqrt{14\eta^2-8\eta+2}} & \frac{2\eta-1}{\sqrt{14\eta^2-8\eta+2}} & -\frac{2\eta-1}{\sqrt{14\eta^2-8\eta+2}} & -\frac{\sqrt{3}\eta}{\sqrt{14\eta^2-8\eta+2}} \\ \frac{\sqrt{3}\eta}{\sqrt{6\eta^2+2}} & -\frac{1}{\sqrt{6\eta^2+2}} & -\frac{1}{\sqrt{6\eta^2+2}} & \frac{\sqrt{3}\eta}{\sqrt{6\eta^2+2}} \\ \frac{2\eta-1}{\sqrt{14\eta^2-8\eta+2}} & -\frac{\sqrt{3}\eta}{\sqrt{14\eta^2-8\eta+2}} & -\frac{\sqrt{3}\eta}{\sqrt{14\eta^2-8\eta+2}} & -\frac{2\eta-1}{\sqrt{14\eta^2-8\eta+2}} \end{pmatrix} \tag{6.24}$$

Similar expressions hold for the bosons on the B-sites, where the coefficients are complex conjugates. In this rotated basis the variational solution Eqs. (6.5) and (6.6) correspond to $|\Psi_A\rangle = a_A^\dagger|0\rangle$ and $|\Psi_B\rangle = a_B^\dagger|0\rangle$, and b, c, and d are suitably

chosen bosons that will take the role of the Holstein-Primakoff bosons and describe the excitations of the system. Replacing $a_i^\dagger$ and a_i with $\sqrt{M - b_i^\dagger b_i - c_i^\dagger c_i - d_i^\dagger d_i}$ and performing an expansion in the parameter $1/M$ as outlined in chapter 3, the multiboson spin-wave Hamiltonian up to quadratic order in bosons can be written as:

$$\mathcal{H} = M^2\mathcal{H}^{(0)} + M^{3/2}\mathcal{H}^{(1)} + M\mathcal{H}^{(2)} + O(M^{1/2}) \tag{6.25}$$

where $\mathcal{H}^{(0)}$ is equal to the mean field energy, $\mathcal{H}^{(1)}$ is identically zero when the (6.8) condition for the mean-field solution is satisfied, and the quadratic term has the following form after substituting (6.8):

$$\mathcal{H}^{(2)} = \frac{1}{2}\sum_{\mathbf{k}\in \mathrm{BZ}} \left(\mathcal{H}^{(2)}_{bd,\mathbf{k}} + \mathcal{H}^{(2)}_{c,\mathbf{k}}\right) \tag{6.26}$$

$$\begin{aligned}
\mathcal{H}^{(2)}_{bd,\mathbf{k}} \;=\; & \left[\frac{6(\eta+1)^2\left(9\eta^3-5\eta^2-\eta+1\right)}{\left(3\eta^2+1\right)\left(7\eta^2-4\eta+1\right)}J - \frac{3\left(7\eta^2-4\eta+1\right)}{3\eta^2+1}J\gamma_{\mathbf{k}}\right. \\
& \left. + \frac{12\eta^2(\eta+1)^2}{\left(3\eta^2+1\right)\left(7\eta^2-4\eta+1\right)}J_z\gamma_{\mathbf{k}}\right]\left(b_{\mathbf{k}}^\dagger b_{\mathbf{k}} + b_{-\mathbf{k}}^\dagger b_{-\mathbf{k}}\right) \\
& + \left[\frac{12\eta^2(\eta+1)^2}{\left(3\eta^2+1\right)\left(7\eta^2-4\eta+1\right)}J_z + \frac{3\left(7\eta^2-4\eta+1\right)}{3\eta^2+1}J\right]\gamma_{\mathbf{k}}\left(b_{\mathbf{k}}^\dagger b_{-\mathbf{k}}^\dagger + b_{\mathbf{k}} b_{-\mathbf{k}}\right) \\
& + \frac{72\eta^3(\eta+1)^2}{\left(3\eta^2+1\right)\left(7\eta^2-4\eta+1\right)}J\left(d_{\mathbf{k}}^\dagger d_{\mathbf{k}} + d_{-\mathbf{k}}^\dagger d_{-\mathbf{k}}\right) \\
& + \frac{36\sqrt{3}\eta^2(\eta+1)(\eta-1)^2}{\left(3\eta^2+1\right)\left(7\eta^2-4\eta+1\right)}J\left(b_{\mathbf{k}}^\dagger d_{\mathbf{k}} + b_{-\mathbf{k}}^\dagger d_{-\mathbf{k}} + d_{\mathbf{k}}^\dagger b_{\mathbf{k}} + d_{-\mathbf{k}}^\dagger b_{-\mathbf{k}}\right) \\
& + \frac{9(\eta-1)^4}{\left(3\eta^2+1\right)\left(7\eta^2-4\eta+1\right)}J_z\gamma_{\mathbf{k}}\left(d_{\mathbf{k}}^\dagger d_{-\mathbf{k}}^\dagger + d_{\mathbf{k}} d_{-\mathbf{k}} + d_{\mathbf{k}}^\dagger d_{\mathbf{k}} + d_{-\mathbf{k}}^\dagger d_{-\mathbf{k}}\right) \\
& - \frac{6\sqrt{3}\eta(\eta+1)(\eta-1)^2}{\left(3\eta^2+1\right)\left(7\eta^2-4\eta+1\right)}J_z\gamma_{\mathbf{k}}\left(b_{\mathbf{k}} d_{-\mathbf{k}} + b_{-\mathbf{k}} d_{\mathbf{k}} + b_{\mathbf{k}}^\dagger d_{-\mathbf{k}}^\dagger + b_{-\mathbf{k}}^\dagger d_{\mathbf{k}}^\dagger\right. \\
& \left. + b_{\mathbf{k}}^\dagger d_{\mathbf{k}} + b_{-\mathbf{k}}^\dagger d_{-\mathbf{k}} + d_{\mathbf{k}}^\dagger b_{\mathbf{k}} + d_{-\mathbf{k}}^\dagger b_{-\mathbf{k}}\right),
\end{aligned} \tag{6.27}$$

$$\begin{aligned}
\mathcal{H}^{(2)}_{c,\mathbf{k}} \;=\; & 6J(\eta+1)\left(c_{\mathbf{k}}^\dagger c_{\mathbf{k}} + c_{-\mathbf{k}}^\dagger c_{-\mathbf{k}}\right) \\
& - \frac{3(3\eta+1)^2(\eta-1)^2}{\left(3\eta^2+1\right)^2}J\gamma_{\mathbf{k}}\left(c_{\mathbf{k}}^\dagger c_{-\mathbf{k}}^\dagger + c_{\mathbf{k}} c_{-\mathbf{k}} + c_{\mathbf{k}}^\dagger c_{\mathbf{k}} + c_{-\mathbf{k}}^\dagger c_{-\mathbf{k}}\right).
\end{aligned} \tag{6.28}$$

where

$$b_{\mathbf{k}}^\dagger = \frac{1}{\sqrt{N}}\sum_j e^{-i\mathbf{k}\cdot\mathbf{r}_j} b_j^\dagger \tag{6.29a}$$

$$b_{\mathbf{k}} = \frac{1}{\sqrt{N}}\sum_j e^{i\mathbf{k}\cdot\mathbf{r}_j} b_j \tag{6.29b}$$

correspond to the b-boson in the momentum space, and there are similar Fourier transformations for the bosons $c^\dagger_{\mathbf{k}}$ and $d^\dagger_{\mathbf{k}}$. The geometrical factor $\gamma_{\mathbf{k}}$ can be expressed as:

$$\gamma_{\mathbf{k}} = \frac{1}{2}\left(\cos k_x + \cos k_y\right) \tag{6.30}$$

Eqs. (6.27) and (6.28) can be diagonalized using the generalized Bogoliubov transformation introduced in chapter 3. The eigenvalues of $\mathcal{H}_c^{(2)}$ are independent of J_z and read as:

$$\omega_c = 6J(\eta+1)\sqrt{1 - \frac{(\eta-1)^2(3\eta+1)^2}{(\eta+1)\left(3\eta^2+1\right)^2}\gamma_{\mathbf{k}}}, \tag{6.31}$$

The analytical expression for the eigenvalues of $\mathcal{H}_{bd}^{(2)}$ is, however, beyond our reach. We show the excitation spectrum for various single-ion anisotropy and exchange anisotropy values in Fig. 6.7(a) and (b). The excitation spectrum consists of six modes, three for each Co^{2+} spin in the unit cell.

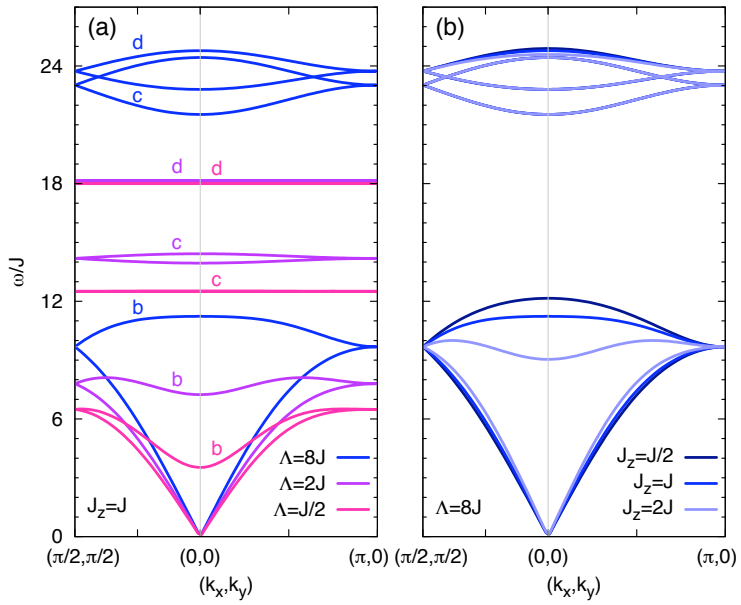

Figure 6.7: (a) Flavor wave dispersion for various single-ion anisotropy values when the exchange interaction is isotropic ($J = J_z$). (b) Dispersions at different exchange anisotropy values for large easy-plane anisotropy, namely $\Lambda/J = 8$.

As noted above, for $\Lambda = 0$ the variational parameter η is equal to 1 and the bosons $a^\dagger_A$ and $a^\dagger_B$ create spin coherent states with maximal spin length $S = 3/2$, that is, the usual antiferromagnetic Néel state is realized as the ground state. The low-energy excitations, b_+ and b_- can be associated with the magnons of the standard

spin wave theory, corresponding to the lowering and raising the $\pm 3/2$ spin states of the sublattices. The high-energy modes, $c_\pm$ and $d_\pm$, can be excited by applying the operators $\hat{S}_j^-$ or $\hat{S}_j^+$ twice and three times, respectively, implying that these transitions can only be excited by quadrupolar or higher order spin operators. As a simple explanation to the excitation energies $12J$ and $18J$ related to $c_\pm$ and $d_\pm$, let us examine what happens to a spin $|\mathbf{S}| = 3/2$ in the Weiss field $h_W = 4 \times \frac{3J}{2}$ of the four neighboring antiparallel spins after applying $\hat{S}_j^- \hat{S}_j^-$ and $\hat{S}_j^- \hat{S}_j^- \hat{S}_j^-$. The energy of the four bonds in the AFM state is $-\frac{9J}{4} \times 4$, while after rotating the middle spin twice it becomes $\frac{3J}{4} \times 4$ resulting in the Zeemann energy $3J - (-9J) = 12J$. Similarly rotating the middle spin three times toward the antiparallel spin, they become actually parallel for the spin length is only $3/2$ and the energy of the four bonds becomes $\frac{9J}{4} \times 4$, providing the energy difference $9J - (-9J) = 18J$. A finite anisotropy Λ reduces the symmetry of the system from O(3) to O(2) decreasing the number of zero energy Goldstone modes from two to one. The zero-energy Goldstone mode associated with turning the order parameter in the xy plane can be given by the self-adjoint operator $b_{\mathrm{GM}}^\dagger = b_{\mathrm{GM}}$

$$b_{\mathrm{GM}}^\dagger \propto b_{(0,0)}^\dagger + b_{(0,0)} - \frac{\sqrt{3}(\eta-1)^2}{2\eta(\eta+1)} \left(d_{(0,0)}^\dagger + d_{(0,0)} \right) \tag{6.32}$$

that commutes with the spin-wave Hamiltonian $\mathcal{H}^{(2)}$. As we turn on Λ, the variational parameter η increases and the spin length in the Néel ground state becomes smaller. The excitation energies in the limit $\Lambda \to 0$ can be written as

$$\omega_b^2 = 12(1-\gamma_{\mathbf{k}})J\left[3J + 3\gamma_{\mathbf{k}} J_z + \Lambda\right] + O(\Lambda^2), \tag{6.33a}$$

$$\omega_c = 12J + \Lambda + (1-2\gamma_{\mathbf{k}})\frac{\Lambda^2}{24J} + O(\Lambda^3/J^2), \tag{6.33b}$$

$$\omega_d = 18J + O(\Lambda^3/J^2), \tag{6.33c}$$

ω_{b_+} shows the square-root behaviour of anisotropy gap, typical for the ordinary spin wave theory in the case of a small exchange ($J \neq J_z$) and/or single-ion (Λ) anisotropies. The d-branch acquires dispersion only in the order Λ^4/J^3.

The intensity of neutrons scattered from the magnetic moments is proportional to the spin-spin correlation function in the following way

$$\frac{d^2\sigma}{d\Omega d\omega} \propto \sum_{\alpha,\beta} (\delta_{\alpha\beta} - \hat{\mathbf{q}}_\alpha \hat{\mathbf{q}}_\beta) S^{\alpha\beta}(\mathbf{q},\omega)\ , \tag{6.34}$$

where $\mathbf{q}$ is the scattering vector defined as the difference between the incoming and outgoing neutron wave vectors. $\hat{\mathbf{q}}$ denotes the normed vector $\mathbf{q}/|\mathbf{q}|$, so that the polarization factor $(\delta_{\alpha\beta} - \hat{\mathbf{q}}_\alpha \hat{\mathbf{q}}_\beta)$ implies that neutrons only couple to magnetization perpendicular to the scattering vector. The scattering function $S^{\alpha\beta}(\mathbf{q},\omega)$, often referred to as the dynamical structure factor, is in fact the Fourier transform of the time and space dependent spin-spin correlation function and can be given as

$$S^{\alpha\beta}(\mathbf{q},\omega) = \frac{2\pi}{N} \sum_f \langle 0|S_{-\mathbf{k}}^\alpha|f\rangle\langle f|S_{\mathbf{k}}^\beta|0\rangle \delta(\omega - \omega_f) \tag{6.35}$$

Therefore, to learn whether a given excitation mode is active, we shall determine the matrix elements $|\langle 0|S^{\alpha}_{\mathbf{k}}|f\rangle|^2$. When Λ is small, the modes $c_{\pm}$ and $d_{\pm}$ are silent in neutron, ESR and FIR spectra.

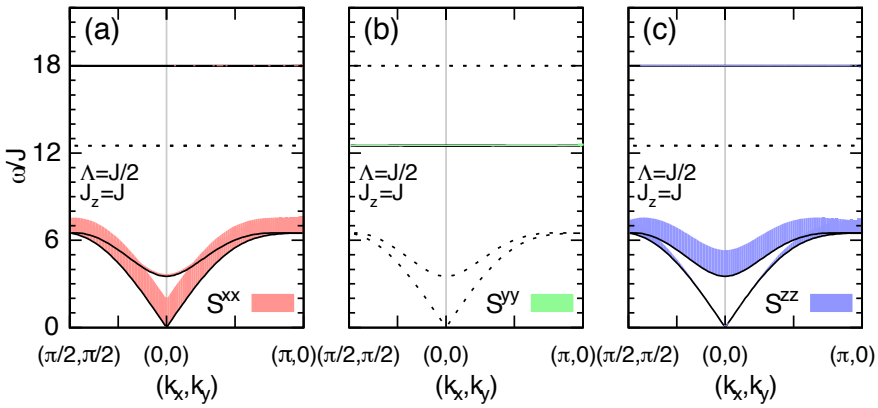

Figure 6.8: Dispersion relation in the for $\Lambda/J = 0.5$, i.e. small Λ limit. The widths of the filled curves above the excitation energies denote the matrix elements $|\langle f|S^{\alpha\alpha}_{\mathbf{k}}|0\rangle|^2$ with $\alpha = x, y$ and z in panel (a), (b) and (c), respectively.

When $\Lambda \to 0$ the matrix elements can be approximated as

$$|\langle 0|S^x|b\rangle|^2 = \frac{3}{4}\sqrt{\frac{J + J_z\gamma_k + \Lambda/3}{J - J\gamma_k}} + O(\Lambda^2) \tag{6.36}$$

$$|\langle 0|S^z|b\rangle|^2 = \frac{3}{4}\sqrt{\frac{J - J\gamma_k}{J + J_z\gamma_k + \Lambda/3}} + O(\Lambda^2) \tag{6.37}$$

$$|\langle 0|S^y|c\rangle|^2 = \frac{\Lambda^2}{48J^2} + O(\Lambda^3)\,. \tag{6.38}$$

$|\langle 0|S^x|d\rangle|^2$ and $|\langle 0|S^z|d\rangle|^2$ are of the fourth order in Λ. The modes $b_{\pm}$ and $d_{\pm}$ correspond to perpendicular fluctuation of the spins, i.e. these modes are transversal modes, similarly to the modes in the standard spin wave theory. The spin length of the modes c_- and c_+ are oscillating synchronously and in opposing phase on the two sublattices, respectively. Therefore we call these modes spin-stretching modes. As a consequence the mode c_-, with the spin length of the sublattices oscillating together, can be excited by the spin operator S^y, with a finite weight in $|\langle 0|S^y|f\rangle|^2$ that vanishes as $(\Lambda/J)^2$ when $\Lambda/J \to 0$.

For a large on-site anisotropy $\eta \to \Lambda/3J$ in the leading order, and the $S^z = \pm 3/2$ states are suppressed in the ground state, reducing the spin length to 1. We recover the spectra of isolated spins with single-ion anisotropy: two modes with energies $\omega/\Lambda \to 0$ and four modes with $\omega \to 2\Lambda$, in agreement with Ref. [Miyahara 2011]. The dispersion relations have the following form

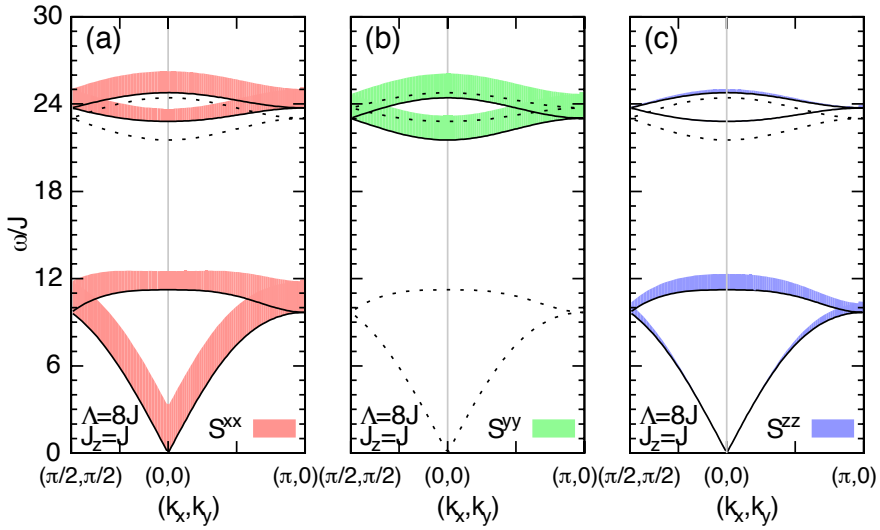

Figure 6.9: Dispersion relation for large easy-plane anisotropy $\Lambda/J = 8$. The widths of the filled curves above the excitation energies denote the matrix elements $|\langle f|S^{\alpha}_{\mathbf{k}}|0\rangle|^2$ with $\alpha = x, y$ and z in panel (a), (b) and (c) respectively. The dotted lines represent the silent modes.

$$\omega_b^2 = 16(1-\gamma_{\mathbf{k}})\,(4J + J_z\gamma_{\mathbf{k}}) + O(1/\Lambda), \tag{6.39}$$

$$\omega_c = 2\Lambda + 4J - 3J\gamma_{\mathbf{k}} + O(1/\Lambda), \tag{6.40}$$

$$\omega_d = 2\Lambda + 4J - 3J\gamma_{\mathbf{k}} + O(1/\Lambda), \tag{6.41}$$

and the matrix elements can be expressed as

$$|\langle 0|S^x|b\rangle|^2 = \frac{\sqrt{4J + J_z\gamma_k}}{2\sqrt{J - J\gamma_k}} + O(1/\Lambda) \tag{6.42}$$

$$|\langle 0|S^z|b\rangle|^2 = \frac{\sqrt{J - J\gamma_k}}{2\sqrt{4J + J_z\gamma_k}} + O(1/\Lambda) \tag{6.43}$$

$$|\langle 0|S^y|c\rangle|^2 = \frac{3}{4} - \frac{24 - 9\gamma_k}{8}\frac{J}{\Lambda} + O(1/\Lambda^2) \tag{6.44}$$

$$|\langle 0|S^x|d\rangle|^2 = \frac{3}{4} - \frac{24 - 9\gamma_k}{8}\frac{J}{\Lambda} + O(1/\Lambda^2) \tag{6.45}$$

$$|\langle 0|S^z|d\rangle|^2 = \frac{3J^2}{\Lambda^2}(1-\gamma_k)^2 + O(1/\Lambda^3)\,. \tag{6.46}$$

The numerically calculated matrix elements in the large Λ spectrum are shown in Fig. 6.9. Similarly to the small Λ limit, the c modes behave differently from the modes b and d; they have finite weight in $S^{yy}(\omega, \mathbf{k})$, while the other two modes are active for the components $S^{xx}(\omega, \mathbf{k})$ and $S^{zz}(\omega, \mathbf{k})$. In the limit $\Lambda \gg J, J_z$, one can project out the states with $m = \pm 3/2$, that is map the problem to an XXZ model. When Λ is large, the essential degrees of freedom are reduced to the $S^z = \pm 1/2$ states of the spin-3/2. These two states can be represented as the

$\sigma^z = \pm 1/2$ states of an effective spin–1/2 model with the Hamiltonian: $\mathcal{H}_{\text{eff}} = \sum_{<i,j>} \left(4J\left(\sigma_i^x\sigma_j^x + \sigma_i^y\sigma_j^y\right) + J_z\sigma_i^z\sigma_j^z\right)$ where the σ_j^α are the spin–1/2 operators on site j that act on the Hilbert space of the effective spins. This provides the dispersion $2\sqrt{(4J \pm 4J|\gamma_{\mathbf{k}}|)(4J \mp J_z|\gamma_{\mathbf{k}}|)}$, in agreement with the result in Ref. [Zheludev 2003].

The scattering function is related to the imaginary part of the dynamical susceptibility $\chi(\mathbf{q},\omega)$ which measures the response of the system, and its imaginary part is related to the energy dissipation.

$$\mathbf{S}^{\alpha\beta}(\mathbf{q},\omega) = \frac{\hbar}{\pi}\left(\frac{1}{e^{\hbar\omega/k_BT}-1}+1\right)\text{Im}\chi(\mathbf{q},\omega)\ , \tag{6.47}$$

Therefore calculating the matrix elements $\text{Im}\chi^{mm}_{\alpha\alpha}(\omega) \propto |\langle 0|S^\alpha_{\mathbf{k}}|f\rangle|^2$ and $\text{Im}\chi^{ee}_{\alpha\alpha}(\omega) \propto |\langle 0|P^\alpha_{\mathbf{k}}|f\rangle|^2$ tells us which mode is active for magnetic and which for electric excitation in optical spectroscopy [Miyahara 2011]. As introduced in chapter 2, when the crystal structure breaks the inversion symmetry, spin quadrupolar and electric dipole (or electric polarization) operators have the same symmetry properties. The polarization P and the spin behave oppositely under the inversion (I) and the time reversal (T) operations: $I\cdot P = -P$ and $T\cdot P = P$, while $I\cdot S = S$ and $T\cdot S = -S$. For there is no inversion center in $Ba_2CoGe_2O_7$, we only have to account for the action of T, and it follows that the polarization can be coupled linearly to operators that are even-order in the spin operator, consequently are invariant under time reversal. Based on symmetry considerations, we showed in chapter 2 that the different components of the polarization vector can be expressed in terms of quadratic spin operators (or in fact quadrupole operators) in the following way

$$\begin{aligned}
\hat{P}^x_j &\propto -\cos 2\kappa_j\left(\hat{S}^x_j\hat{S}^z_j + \hat{S}^z_j\hat{S}^x_j\right) - \sin 2\kappa_j\left(\hat{S}^y_j\hat{S}^z_j + \hat{S}^z_j\hat{S}^y_j\right)\\
\hat{P}^y_j &\propto \cos 2\kappa_j\left(\hat{S}^y_j\hat{S}^z_j + \hat{S}^z_j\hat{S}^y_j\right) - \sin 2\kappa_j\left(\hat{S}^x_j\hat{S}^z_j + \hat{S}^z_j\hat{S}^x_j\right)\\
\hat{P}^z_j &\propto \cos 2\kappa_j\left((\hat{S}^y_j)^2 - (\hat{S}^x_j)^2\right) - \sin 2\kappa_j\left(\hat{S}^x_j\hat{S}^y_j + \hat{S}^y_j\hat{S}^x_j\right)
\end{aligned} \tag{6.48}$$

where j belongs to either sublattice A or B. The different orientation of the neighbouring tetrahedra (see e.g. Fig. 1.7) is accounted for by choosing $\kappa_{j\in A} = \kappa$ and $\kappa_{j\in B} = -\kappa$. Thus, as the consequence of the lack of inversion symmetry, a new channel opens to excite the b, c and d modes. The electric field of the incident light can directly couple to the spin quadrupolar operators (6.48) and the response can be expressed by $\text{Im}\chi^{ee}_{\alpha\alpha}(\omega) \propto |\langle 0|P^\alpha_{\mathbf{k}}|f\rangle|^2$ [Miyahara 2011]. Indeed, d_- and c_+ modes with only magnetic quadrupole moments are excited this way and remain silent for the magnetic component of the exciting light, $\text{Im}\chi^{mm}_{\alpha\alpha}(\omega)$, irrespective of the ratio Λ/J. Form numerical study we learn that most of the weight in $\text{Im}\chi^{mm}_{xx}(\omega)$ comes from the low-energy b_+ mode, while the contribution of d_+ to $\text{Im}\chi^{mm}_{xx}(\omega)$ is proportional to $(\Lambda/J)^4$. $\text{Im}\chi^{mm}_{zz}(\omega)$ is zero for all but the Goldstone mode b_-.
The spectrum as a function of Λ/J in zero magnetic field and for zero momentum is shown in Fig. 6.10(a). The dynamical magnetic and electric susceptibility $\text{Im}\chi^{mm}_{\alpha\alpha}(\omega)$ and $\text{Im}\chi^{ee}_{\alpha\alpha}(\omega)$ are shown in Fig. 6.10(b) and (c), respectively. From the analysis of the dynamic magnetic susceptibility it follows that these unconventional

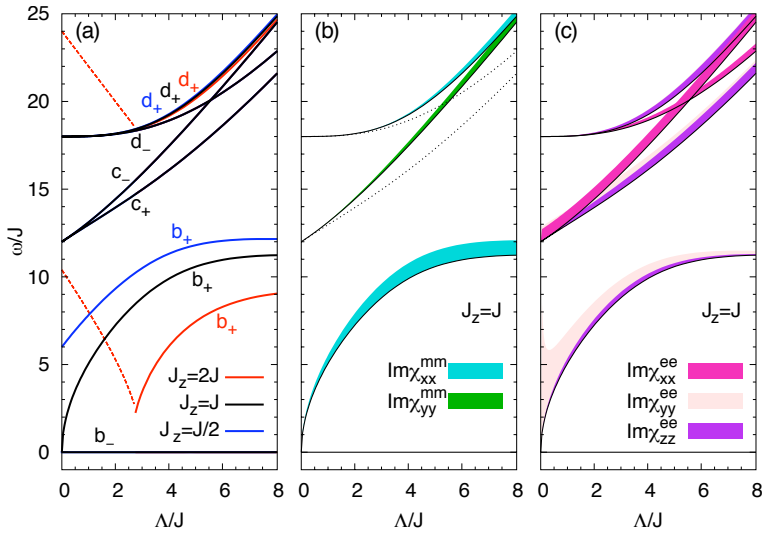

Figure 6.10: (a) The energy of the modes for different values of J_z/J in zero field. b_- denotes the $\omega = 0$ Goldstone mode. Only the b_+ and d_+ modes depend on J_z/J. The dashed lines indicate modes in the easy-axis AF state that forms below $\Lambda \approx 2.7J$ for $J_z = 2$. (b) and (c) shows the imaginary part of the magnetic $\chi^{mm}_{\xi\xi}(\omega)$ and electric $\chi^{ee}_{\xi\xi}(\omega)$ dynamic susceptibilities, respectively, for $J = J_z$. The shaded area above the lines represent the strength of the magnetic and electric response.

spin excitations become observable by ESR, FIR, and neutron scattering as soon as the single-ion anisotropy becomes significant.

6.3.2 Quantitative comparison with experiments

In this part we attempt to interpret the experimentally observed excitation spectra. First let us examine the excitations in finite magnetic field. We shall distinguish beween two settings of the external field $B_{\rm dc}$, namely when it is perpendicular to the tetragonal plane, that is the plane of the cobalt ions, and when it is laying in the plane. The Hamiltonian expressed in terms of the bosons a, b and c, due to its complicated form, has been moved to the appendix E to Eqs. (E.11) and (E.10) The experimental data and the results of our flavor wave calculations are collected in Fig. 6.11. From the fit of the experimental data we obtain the following values $\Lambda = 13.4\,\mathrm{K}$, $J = 2.3\,\mathrm{K}$, $J_z = 1.8\,\mathrm{K}$, $g_{zz} = 2.1$ and $g_{xx} = g_{yy} = 2.3$. We can identify the $\omega \approx 2$ and 4 meV zero field ($B_{\rm dc} = 0$) peaks which correspond to about 0.5 and 1 THz observed in the FIR absorption spectra in Refs. [Kézsmárki 2011, Bordacs 2011]. As discussed in the previous section, the lower mode corresponds to the conventional magnon excitation energy with a gap arising from the anisotropies. The 1 THz branch, however, cannot be described in the usual spin wave picture. These higher excitations are so called electromagnons as they have been shown to respond to both the magnetic and electric component of light [Kézsmárki 2011]. In

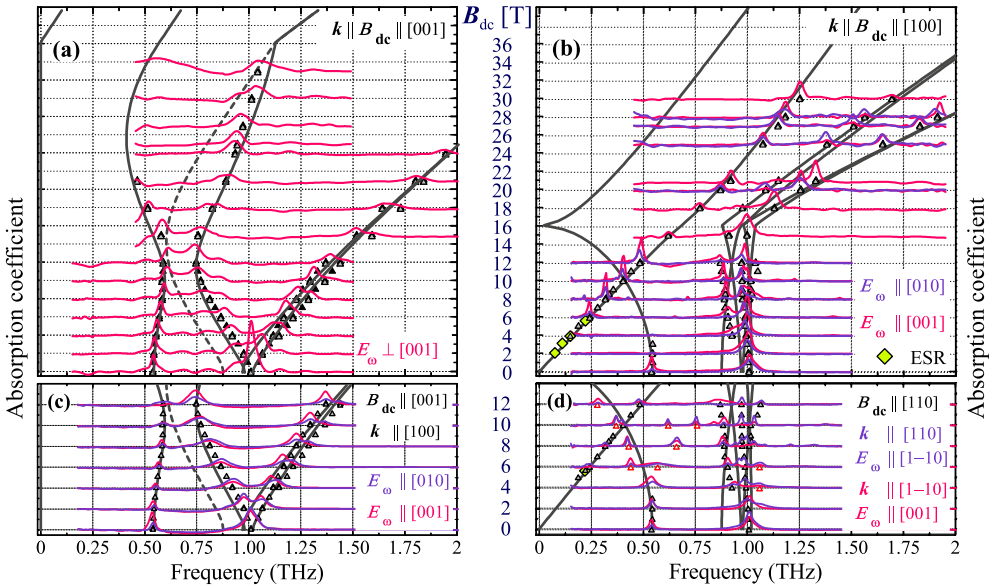

Figure 6.11: Magnetic field dependence of the absorption spectra in $Ba_2CoGe_2O_7$ below 2 THz for a representative set of light polarizations. The spectra are shifted vertically proportional to the magnitude of the field, $B_{\rm dc}$. The distance between horizontal grid lines corresponds to $20\,{\rm cm}^{-1}$ in panels (a) and (c), and $30\,{\rm cm}^{-1}$ in (b) and (d). The direction of $B_{\rm dc}$ is indicated in each panel and the spectra for different polarizations and propagation directions ($\mathbf{k}$) of light are distinguished by the color. Grey triangles and yellow diamonds represent the position of the resonances determined from the FIR and ESR spectra, respectively. The grey lines show the field dependence of the modes obtained in our multi-boson spin wave approach. (d) For $B_{\rm dc} \perp [001]$ in some polarization configurations additional modes have been observed (red triangles) that are not explained by the theory. Two cases, namely when $E \| [1\bar{1}0]$ and $E \| [001]$ are shown here.

our model this branch corresponds to the modes $c_\pm$ and $d_\pm$ which, in accordance with the experimental findings, appear in both the magnetic and electric dynamical susceptibility, as shown previously in Fig. 6.10.

The finite external magnetic field applied perpendicular to the cobalt plane $B_{\rm dc} \| [001]$ splits the 1 THz modes. In this V-shaped splitting the frequencies of two excitations increase, while the other two modes soften with increasing field. The lowest-lying mode of the $\omega \sim 1\,{\rm THz}$ branch is theoretically predicted to be weak and denoted by dashed grey line in Fig. 6.10(a) and (c). This mode does not appear in the experimental spectra. The frequency of the 0.5 THz mode increases with the increasing field until about 12 T where it would cross the lower 1 THz mode. There, after an avoided crossing, its frequency begins to decrease, as indicated in Fig. 6.11(a) and (c). Our theoretical model implies that the ground state is a conical (or superfluid) state, characterized by (5.24) which spontaneously breaks

the $U(1)$ rotational symmetry. As a consequence, a Goldstone mode is present up until the saturation field $h_{sat} = \frac{1}{g_{zz}}\left[\frac{3}{2}\zeta(J + J_z) + 2\Lambda\right]$ introduced in chapter 5 in Eq. 5.11. Inserting our fitting parameters and setting the coordination number ζ to 4, the saturation field can be calculated $B_{\rm dc} \approx 24K$ which corresponds to about 36 T. In the fully saturated phase a gap appears in the Goldstone mode as indicated in Fig. 6.11(a).

Figs. 6.11(b) and (d) show the calculated excitation spectra and the experimental results of ESR and FIR measurements for $B_{\rm dc} \parallel [100]$. As discussed in section 6.2, the finite magnetic field applied in the plane of the cobalt layer lifts the $U(1)$ degeneracy and the ground state is a canted antiferromagnetic state, therefore the Goldstone mode disappears as soon as the field becomes finite. Increasing the magnetic field the canting angle $\delta\varphi = \varphi_A - \varphi_B$ decreases and at about $B_{\rm dc} \approx 16\,\mathrm{T}$ the spins becomes aligned with the magnetic field. This value, however is not equal to the saturation field, although the spins are magnetically polarized, they have not reached their full length. The phase transition from the canted antiferromagnetic phase to the partially polarized phase is indicated by the softening of the $\omega \sim 0.5\,\mathrm{THz}$ mode and by a kink appearing in the 1 THz branch as shown in Figs. 6.11(b) and (d). When $B_{\rm dc}$ is in the cobalt plane, there are more than six resonances observed experimentally in some polarization configurations. Fig. 6.11(d) shows the $E\|[1\bar{1}0]$ and $E\|[001]$ cases. At about $B_{\rm dc} = 5\,\mathrm{T}$, the 0.5 THz mode splits into two, a broader and a sharper, levels and the number of modes is not reduced until about 12 T. This splitting of the 0.5 THz resonance is the only feature not explained by our theoretical model, otherwise it describes satisfyingly the magnetic field dependence of the spin wave excitations in $Ba_2CoGe_2O_7$.

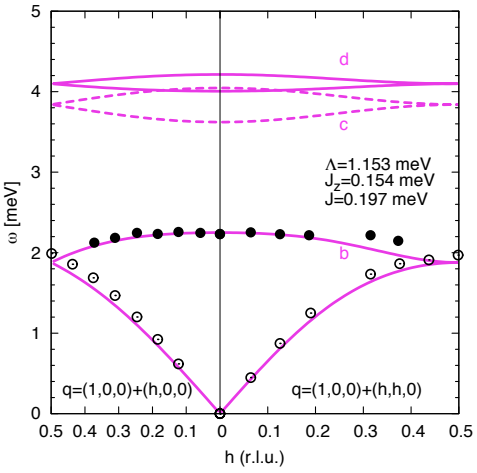

Figure 6.12: Fitting of the inelastic neutron spectrum in Ref. [Zheludev 2003]. We need to mention that the values of the parameters J, J_z and Λ were obtained from the fitting of the excitation spectrum in finite magnetic field which will be discussed in the next section.

Finally, let us point out that with the coupling parameters determined from the fitting of the FIR and ESR spectra, the low lying magnetic excitations observed in inelastic neutron scattering can be reproduced quantitatively. The neutron scattering data from Ref. [Zheludev 2003] and the calculated dispersion relation is shown in Fig. 6.12. We propose that additional four modes are present in the zero field spectrum with weak dispersions, which might be detected by higher energy neutron scattering.

Chapter 7

Conclusion and outlook

Million-to-one chances crop up nine times out of ten.

– Terry Pratchett, The Light Fantastic

We attempted to give a general, yet far from complete, introduction to some of the interesting phenomena one can encounter in the vast field of strongly correlated electron systems. We aimed to show that simple, but appropriately chosen spin models, discussed in terms of variational approach and generalized spin wave technique, can get us quite far in the understanding of some not-so-straightforward properties of real materials. The two materials considered here were the orthogonal dimer system, $SrCu_2(BO_3)_2$ and the multiferroic compound $Ba_2CoGe_2O_7$.

The first step of our approach was the construction of a Hamiltonian that is able to describe the most important features of the given compound. Consequently, we performed a thorough symmetry analysis to learn which terms can actually be included. Naturally, we shall stress that the symmetry considerations by themselves would not have been sufficient; to determine the relevant terms one always has to be aware of the experimental facts. The forms of the different variational wave functions used in our calculations were strongly motivated by measurements too.

In the case of $SrCu_2(BO_3)_2$ the exponentially vanishing magnetic susceptibility measured in Ref. [Kageyama 2000] suggested that the ground state is a magnetically disordered (singlet) state, with properties very similar to quantum spin liquids. Regarding the excitations, inelastic neutron scattering [Gaulin 2004] and electron spin resonance measurements [Nojiri 2003] showed that the triplet excitations split in zero magnetic field, indicating the presence of an anisotropy that can mix the singlet and triplet states of the dimers. Accordingly, we worked in the singlet-triplet dimer basis, allowing for their arbitrary linear combination in the variational wave function.

Considering $Ba_2CoGe_2O_7$, the neutron scattering experiment of Ref. [Zheludev 2003] indicated a two-sublattice canted antiferromagnetic order. The effective spin-half model, introduced on the basis of strong easy-plane single-ion anisotropy, used in Ref. [Zheludev 2003] to fit the spectrum, however is not able to account for the higher excitations observed in the THz absorption spectrum of Ref. [Kézsmárki 2011]. Therefore we chose a site factorized variational wave function in which we include all the four states of the spin-3/2 objects.

To study the relevance of the anisotropies, the Dzyaloshinsky-Moriya interaction in the case of $SrCu_2(BO_3)_2$ and the single-ion and exchange anisotropies in the case

of $Ba_2CoGe_2O_7$, we mapped out the variational phase diagrams as the function of the coupling strengths and external magnetic field applied parallel to different crystallographic directions. Furthermore, we discussed the properties of appearing phases in detail.

Regarding $Ba_2CoGe_2O_7$, we qualitatively reproduced the in-plane field dependence of the magnetic order induced polarization on the basis of the variational approach. Here the inclusion of Dzyaloshinsky-Moriya interaction proved to be essential. The induced polarization does not have dynamics on its own, but follows the spin order. When the field is applied in the cobalt plane, the ground state is two-fold degenerate, thus the induced polarizations of the differently ordered domains would cancel each other which is not what was observed experimentally in Ref. [Murakawa 2010]. A small finite Dzyaloshinsky-Moriya interaction, on the other hand, 'selects' between the two possible states, changing the characteristics of induced polarization drastically.

The dynamical properties were studied using the generalized spin wave method derived in chapter 2. For both material we extensively discussed the effect of the relevant anisotropies on the excitation spectrum, aiming to get an insight to the nature of the different modes. Selecting physically suitable coupling values, we could recover the experimentally obtained excitation spectra with remarkable accuracy. Additionally, we investigated the variational phase diagram of bipartite lattices with $S = 1$ and $3/2$ spins as the function of single-ion anisotropy and magnetic field at various ratios of exchange anisotropy. Although this investigation has less experimental relevance, we found that relatively strong single-ion anisotropy along with Ising-like exchange anisotropy supports the formation of supersolid states in magnetic field.

Needless to say, there is still a lot to do in order to a deeper understanding of the properties of these materials. For example, $SrCu_2(BO_3)_2$ is famous for exhibiting plateau states at various fractions of the saturated magnetization. These plateaus are characterized by magnetic superstructures and – aside from the $1/2$-plateau – break the translational invariance of the lattice as the unit cell contains more than two dimers. To describe i.e. the $1/3$ magnetization plateau, we need to include six dimers in the unit cell, which can be done in different ways. As it turns out, however, the building block of this plateau is probably not a single-dimer, but the brick of three neighbouring dimers that are entangled. At present, these calculations are in progress.

The story of $Ba_2CoGe_2O_7$ requires further considerations as well. Although, our model is able to recover the higher excitations which are beyond the reach of the usual spin wave method, and serves as a tool to understand their electromagnon aspects, there are additional excitations observed in the THz light absorption spectrum that we cannot understand in the framework introduced here. Nevertheless, we believe that the stretching modes we observed in $Ba_2CoGe_2O_7$ shall appear in any $S > 1/2$ material with strong single-ion anisotropy, starting from the related compounds $Ca_xSr_{2-x}CoSi_2O_7$ [Akaki 2009, Akaki 2010] and $Ba_2MnGe_2O_7$[1].

[1] H. Murakawa, private communication

Thesis statements

1. I showed that the generalized spin wave method is suitable to quantitatively reproduce the experimentally observed magnetic field dependent excitation spectrum of the orthogonal dimer compound, $SrCu_2(BO_3)_2$. To obtain the correct spectrum one needs to allow for the singlet state to mix with all three triplet components – this goes beyond the usual perturbation approach, where only two states per dimers are kept. Furthermore, the finite-field gap in the perturbational approach is proportional to the intradimer Dzyaloshinsky-Moriya coupling D, while the generalized spin wave method gives a gap proportional to $\sqrt{D}$, resulting in a spectrum which is in agreement with the experimental results.

2. On bipartite lattices with larger spins (S>1/2) the competition of strong single-ion axial anisotropy, the exchange anisotropies, and the off-diagonal exchange support the formation of magnetic supersolid states in finite magnetic field perpendicular to the easy plane. I determined the phase diagram of such an S=3/2 model: When the off- diagonal exchange is zero the phase diagram is characterized by axial antiferromagnetic, ferromagnetic and plateau phases. The supersolid phase emerges in the vicinity of the translational symmetry breaking axial plateau states when the off-diagonal exchange is finite, but smaller than the diagonal one. Between the supersolid and axial phases spin-rotational symmetry breaking superfluid phase is found. When the exchange interaction is isotropic, but the single-ion anisotropy still breaks the SU(2) symmetry, the plateau islands and their supersolid rim are washed away by the superfluid phase.

3. I pointed out the essential role of the out-of plane Dzyaloshinsky-Moriya interaction for the description of the in-plane magnetic field dependence of the magnetic order induced electric polarization in the multiferroic compound $Ba_2CoGe_2O_7$ at zero temperature. Depending on its direction, one of the two degenerate canted antiferromagnetic states is selected, changing the polarization curve drastically. Furthermore, including an antiferro polarization-polarization term in the Hamiltonian, along with the Dzyaloshinsky-Moriya interaction, can account for the sharp low field ($\lesssim 1$ T) decay in the curve of the induced polarization.

4. I showed that along with the lower lying magnetic excitations, available by the usual Holstein-Primakoff spin wave theory, the high-energy ($\sim$ 1THz) modes observed in $Ba_2CoGe_2O_7$ up to 33 T can be quantitatively reproduced in terms of generalized spin waves. As the Hilbert space of a spin S=3/2 is sufficiently large, these modes exhibit quadrupole and octupole characteristics in a natural way, and the non-centrosymmetric property of $Ba_2CoGe_2O_7$ enables them to be excited by the electric component of the incident light. In the multiferroic ground state the length of the spins is less than 3/2, consequently two of the

high-energy modes are longitudinal excitations, in contrast to the usual spin wave method, where the magnons are associated with transverse fluctuations.

List of publications

1. J. Romhányi, K. Totsuka, K. Penc

   Effect of Dzyaloshinskii-Moriya interactions on the phase diagram and magnetic excitations of $SrCu_2(BO_3)_2$

   Phys. Rev. B **8**3, 024413 (2011)

2. J. Romhányi, F. Pollmann, K. Penc

   Supersolid phase and magnetization plateaus observed in the anisotropic spin-3/2 Heisenberg model on bipartite lattices

   Phys. Rev. B **8**4, 184427 (2011)

3. J. Romhányi, M. Lajkó, K. Penc

   Zero- and finite-temperature mean field study of magnetic field induced electric polarization in $Ba_2CoGe_2O_7$: Effect of the antiferroelectric coupling

   Phys. Rev. B **8**4, 224419 (2011)

4. K. Penc, J. Romhányi, T. Room, U. Nagel, Á. Antal, T. Fehér, A. Jánossy, H. Engelkamp, H. Murakawa, Y. Tokura, D. Szaller, S. Bordács, I. Kézsmárki

   Spin-stretching modes in non-centrosymmetric magnets: spin-wave excitations in the multiferroic Ba2CoGe2O7

   accepted to Phys. Rev. Lett. arXiv:1202.3996 (2012)

5. Judit Romhányi and Karlo Penc

   Multiboson spin-wave theory for Ba2CoGe2O7, a spin-3/2 easy-plane Neel antiferromagnet with strong single-ion anisotropy

   submitted to Phys. Rev. B arXiv:1205.2196 (2012)

Appendix A

The hermiticity of the spin wave Hamiltonian

After the $1/M$ expansion we wrote the Hamiltonian as

$$\mathcal{H} = M^2\mathcal{H}^{(0)} + M^{3/2}\mathcal{H}^{(1)} + M\mathcal{H}^{(2)} + O(\sqrt{M}) \tag{A.1}$$

In this the first corrections appear in $\mathcal{H}^{(2)}$ as $\mathcal{H}^{(1)}$ is identically zero when the mean-field ground state is realized and $\mathcal{H}^{(0)}$ is a constant corresponding to the mean-field energy. After Fourier transformation we brought $\mathcal{H}^{(2)}$ into the following form

$$\mathcal{H}^{(2)}(\mathbf{k}) = \begin{pmatrix} \mathbf{a}_A^\dagger(\mathbf{k}) \\ \mathbf{a}_B^\dagger(\mathbf{k}) \\ \mathbf{a}_B(-\mathbf{k}) \\ \mathbf{a}_A(-\mathbf{k}) \end{pmatrix}^T \begin{pmatrix} \mathbf{H}_{11}(\mathbf{k}) & \mathbf{H}_{12}(\mathbf{k}) & \mathbf{H}_{13}(\mathbf{k}) & \mathbf{H}_{14}(\mathbf{k}) \\ \mathbf{H}_{21}(\mathbf{k}) & \mathbf{H}_{22}(\mathbf{k}) & \mathbf{H}_{23}(\mathbf{k}) & \mathbf{H}_{24}(\mathbf{k}) \\ \mathbf{H}_{31}(\mathbf{k}) & \mathbf{H}_{32}(\mathbf{k}) & \mathbf{H}_{33}(\mathbf{k}) & \mathbf{H}_{34}(\mathbf{k}) \\ \mathbf{H}_{41}(\mathbf{k}) & \mathbf{H}_{42}(\mathbf{k}) & \mathbf{H}_{43}(\mathbf{k}) & \mathbf{H}_{44}(\mathbf{k}) \end{pmatrix} \begin{pmatrix} \mathbf{a}_A(\mathbf{k}) \\ \mathbf{a}_B(\mathbf{k}) \\ \mathbf{a}_B^\dagger(-\mathbf{k}) \\ \mathbf{a}_A^\dagger(-\mathbf{k}) \end{pmatrix} \tag{A.2}$$

Now we will show that due to the hermiticity of the Hamiltonian only six of the $\mathbf{H}_{ij}(\mathbf{k})$ matrices are independent. Applying the bosonic commutation relations we can write:

$$\begin{aligned} \mathbf{a}_A^\dagger(\mathbf{k})\mathbf{H}_{11}(\mathbf{k})\mathbf{a}_A(\mathbf{k}) &= \sum_{nm} [\mathbf{H}_{11}(\mathbf{k})]_{nm}\, a_{A,n}^\dagger(\mathbf{k}) a_{A,m}(\mathbf{k}) \\ &= \sum_{nm} [\mathbf{H}_{11}(\mathbf{k})]_{nm}\, a_{A,m}(\mathbf{k}) a_{A,n}^\dagger(\mathbf{k}) + const. \\ &= \mathbf{a}_A(\mathbf{k})\mathbf{H}_{11}^T(\mathbf{k})\mathbf{a}_A^\dagger(\mathbf{k}) + const. \end{aligned} \tag{A.3}$$

then substituting $\mathbf{k} \to -\mathbf{k}$ and recalling that in the Hamiltonian (A.2) we have $\mathbf{a}_A(-\mathbf{k})\mathbf{H}_{44}(\mathbf{k})\mathbf{a}_A^\dagger(-\mathbf{k})$ it follows that $\mathbf{H}_{44}(\mathbf{k}) = \mathbf{H}_{11}^T(-\mathbf{k})$. Replacing A with B and $\mathbf{H}_{11}(\mathbf{k})$ with $\mathbf{H}_{22}(\mathbf{k})$ we obtain $\mathbf{H}_{33}(\mathbf{k}) = \mathbf{H}_{22}^T(-\mathbf{k})$ in the same way. Similarly

$$\begin{aligned} \mathbf{a}_A^\dagger(\mathbf{k})\mathbf{H}_{12}(\mathbf{k})\mathbf{a}_B(\mathbf{k}) &= \sum_{nm} [\mathbf{H}_{12}(\mathbf{k})]_{nm}\, a_{A,n}^\dagger(\mathbf{k}) a_{B,m}(\mathbf{k}) \\ &= \sum_{nm} [\mathbf{H}_{12}(\mathbf{k})]_{nm}\, a_{B,m}(\mathbf{k}) a_{A,n}^\dagger(\mathbf{k}) \\ &= \mathbf{a}_B(\mathbf{k})\mathbf{H}_{12}^T(\mathbf{k})\mathbf{a}_A^\dagger(\mathbf{k}) \end{aligned} \tag{A.4}$$

with $\mathbf{k} \to -\mathbf{k}$ we get $\mathbf{H}_{34}(\mathbf{k}) = \mathbf{H}_{12}^T(-\mathbf{k})$. Furthermore

$$\begin{aligned} \left(\mathbf{a}_A^\dagger(\mathbf{k})\mathbf{H}_{12}(\mathbf{k})\mathbf{a}_B(\mathbf{k})\right)^\dagger &= \mathbf{a}_B^\dagger(\mathbf{k})\left(\mathbf{a}_A^\dagger(\mathbf{k})\mathbf{H}_{12}(\mathbf{k})\right)^\dagger \\ &= \mathbf{a}_B^\dagger(\mathbf{k})\mathbf{H}_{12}^\dagger(\mathbf{k})\mathbf{a}_A(\mathbf{k}) \end{aligned} \tag{A.5}$$

providing $\mathbf{H}_{21}(\mathbf{k}) = \mathbf{H}_{12}^\dagger(\mathbf{k})$. In fact this derivation is applicable in general: $\mathbf{H}_{ji}(\mathbf{k}) = \mathbf{H}_{ij}^\dagger(\mathbf{k})$, therefore combining our previous result $\mathbf{H}_{34}(\mathbf{k}) = \mathbf{H}_{12}^T(-\mathbf{k})$ with $\mathbf{H}_{43}(\mathbf{k}) = \mathbf{H}_{34}^\dagger(\mathbf{k})$ we obtain $\mathbf{H}_{43}(\mathbf{k}) = (\mathbf{H}_{12}^T)^\dagger(-\mathbf{k}) = \mathbf{H}_{12}^*(-\mathbf{k})$, where the symbol $*$ stands for the complex conjugation. The additional connections between the matrices in $\mathcal{H}^{(2)}(\mathbf{k})$ can be derived in a similar manner, resulting in the Hamiltonian:

$$\mathcal{H}^{(2)}(\mathbf{k}) = \begin{pmatrix} \mathbf{a}_A^\dagger(\mathbf{k}) \\ \mathbf{a}_B^\dagger(\mathbf{k}) \\ \mathbf{a}_B(-\mathbf{k}) \\ \mathbf{a}_A(-\mathbf{k}) \end{pmatrix}^T \begin{pmatrix} \mathbf{H}_{11}(\mathbf{k}) & \mathbf{H}_{12}(\mathbf{k}) & \mathbf{H}_{13}(\mathbf{k}) & \mathbf{H}_{14}(\mathbf{k}) \\ \mathbf{H}_{12}^\dagger(\mathbf{k}) & \mathbf{H}_{22}(\mathbf{k}) & \mathbf{H}_{23}(\mathbf{k}) & \mathbf{H}_{13}^T(-\mathbf{k}) \\ \mathbf{H}_{13}^\dagger(\mathbf{k}) & \mathbf{H}_{23}^\dagger(\mathbf{k}) & \mathbf{H}_{22}^T(-\mathbf{k}) & \mathbf{H}_{12}^T(-\mathbf{k}) \\ \mathbf{H}_{14}^\dagger(\mathbf{k}) & \mathbf{H}_{13}^*(-\mathbf{k}) & \mathbf{H}_{12}^*(-\mathbf{k}) & \mathbf{H}_{11}^T(-\mathbf{k}) \end{pmatrix} \begin{pmatrix} \mathbf{a}_A(\mathbf{k}) \\ \mathbf{a}_B(\mathbf{k}) \\ \mathbf{a}_B^\dagger(-\mathbf{k}) \\ \mathbf{a}_A^\dagger(-\mathbf{k}) \end{pmatrix} \tag{A.6}$$

We shall mention that the hermiticity of $\mathbf{H}^{(2)}(\mathbf{k})$ requires other conditions related to the form of $\mathbf{H}_{11}(\mathbf{k})$, $\mathbf{H}_{22}(\mathbf{k})$, $\mathbf{H}_{14}(\mathbf{k})$ and $\mathbf{H}_{23}(\mathbf{k})$. The first two must be hermitian for they are in the diagonal part of $\mathbf{H}^{(2)}(\mathbf{k})$: $\mathbf{H}_{ii}(\mathbf{k}) = \mathbf{H}_{ii}^\dagger(\mathbf{k})$, the other two on the other hand has to fulfill the following equations: $\mathbf{H}_{14}(\mathbf{k}) = \mathbf{H}_{14}^T(-\mathbf{k})$ and $\mathbf{H}_{23}(\mathbf{k}) = \mathbf{H}_{23}^T(-\mathbf{k})$. To prove this let us take

$$\begin{aligned} \mathbf{a}_A^\dagger(\mathbf{k})\mathbf{H}_{14}(\mathbf{k})\mathbf{a}_A^\dagger(-\mathbf{k}) &= \sum_{nm} \left[\mathbf{H}_{14}(\mathbf{k})\right]_{nm} a_{A,n}^\dagger(\mathbf{k}) a_{A,m}^\dagger(-\mathbf{k}) \\ &= \sum_{nm} \left[\mathbf{H}_{14}(-\mathbf{k})\right]_{nm} a_{A,n}^\dagger(-\mathbf{k}) a_{A,m}^\dagger(\mathbf{k}) \\ &= \sum_{nm} \left[\mathbf{H}_{14}(-\mathbf{k})\right]_{nm} a_{A,m}^\dagger(\mathbf{k}) a_{A,n}^\dagger(-\mathbf{k}) \\ &= \sum_{nm} \left[\mathbf{H}_{14}^T(-\mathbf{k})\right]_{mn} a_{A,m}^\dagger(\mathbf{k}) a_{A,n}^\dagger(-\mathbf{k}) \\ &= \mathbf{a}_A^\dagger(\mathbf{k})\mathbf{H}_{14}^T(-\mathbf{k})\mathbf{a}_A^\dagger(-\mathbf{k}) \end{aligned} \tag{A.7}$$

the condition for the form of $\mathbf{H}_{23}(\mathbf{k})$ can be derived accordingly by changing the sublattice A to B.

Appendix B

Banished phases

B.1 The undiscussed phases in the high symmetry case of $SrCu_2(BO_3)_2$

B.1.1 The Néel phase

When $J = 0$, the Shastry–Sutherland model becomes identical to a square–lattice Heisenberg antiferromagnet, where a Néel–type antiferromagnet with alternating spins is realized. A finite J coupling introduces frustration, as spins on the diagonal of the squares are now antiferromagnetically connected, and we end up with helical states in the semiclassical limit [Shastry 1981, Albrecht 1996]. Considering the quantum $S = 1/2$ case, a twofold degenerate plaquette-singlet state is realized for $0.67 < J'/J < 0.86$ [Koga 2000, Läuchli 2002b]. However, our dimer-product variational wave function is unsuitable to describe the plaquette state: it does not capture the entanglement in the plaquette singlets that is present along the iterdimer bonds.

In the current variational approach , the Néel state can be given as

$$\begin{aligned} \Psi_A &= e^{-i\varphi}|t_u\rangle + \sqrt{2}v|t_0\rangle + v^2 e^{i\varphi}|t_d\rangle \\ \Psi_B &= e^{-i(\varphi+\pi)}|t_u\rangle + \sqrt{2}v|t_0\rangle + v^2 e^{i(\varphi+\pi)}|t_d\rangle \end{aligned} \tag{B.1}$$

We note that since there are four spins in the unit cell, the Néel–type antiferromagnet is a $\mathbf{q} = 0$ state. The singlet component does not contribute and the amplitudes of the triplet components in Eq. (B.1) wave function are such that they describe an $S = 1$ spin coherent state on a dimer. These effective $S = 1$ spins on the A and B dimers form the canted spin configuration of the Néel antiferromagnet in the field.The expectation value of the energy is given by

$$E = \frac{J}{2} + 2J' \frac{\left(1 - 6v^2 + v^4\right)}{(1+v^2)^2} - 2h_z \frac{1-v^2}{1+v^2} \,. \tag{B.2}$$

Minimazing the variational energy with respect to v, we obtain

$$v = \sqrt{\frac{4J' - h_z}{4J' + h_z}} \,, \tag{B.3}$$

and

$$E_{\text{Néel}} = \frac{J}{2} - 2J' - \frac{h_z^2}{4J'} \,. \tag{B.4}$$

The magnetization in the unit cell increases linearly with the field, $m^z = h_z/2J'$. The non-vanishing order parameters are

$$\begin{pmatrix} m^x_{\text{Néel}} \\ m^y_{\text{Néel}} \end{pmatrix} = \frac{\sqrt{16J'^2 - h_x^2}}{2J'} \begin{pmatrix} \cos\varphi \\ -\sin\varphi \end{pmatrix}, \tag{B.5}$$

as defined in Table 2.3.

A first order phase transition takes place at $h = \sqrt{8(J - J')J'}$ between the dimer–singlet and Néel state, as shown in Fig. 4.1. This boundary can be easily obtained from equating the dimer–singlet energy [Eq. (4.19)] and the energy of the Néel–antiferromagnet [Eq. (B.4)].

B.1.2 Half–magnetization plateau

The effective repulsion between the singlets and triplets gives rise to plateaus in the Shastry–Sutherland model [Miyahara 1999, Momoi 2000a, Momoi 2000b] . In our variational approach only the two–fold degenerate (Z_2 symmetry breaking) one–half magnetization plateau state is available, to describe the other plateaus we need to take a larger unit cell. The 1/2 plateau state is formed by alternating singlet and $S^z = 1$ triplet bond. The energy per unit cell reads:

$$E_{\text{PS}} = -\frac{J}{2} - h\,. \tag{B.6}$$

The non-vanishing order parameter is $m^z_{\text{Néel}} = \pm 1$, given in Table (2.3). The phase boundary cab be determined by examining the classical instability, and the boundary to the $O(2) \times Z_2$ phase reads

$$8JD'^{\,2}_{\perp} = (h_z - J)\left[J^2 - (2J' - h_z)^2\right] \tag{B.7}$$

While the first order phase transition to the Néel state occurs when

$$4JJ' = h^2 - 4hJ' + 8J'^2\,. \tag{B.8}$$

B.1.3 The fully polarized phase

In large magnetic fields all the spins become aligned, and a fully polarized ferromagnetic (FM) state with the ground state $\Psi_{A,0} = \Psi_{B,0} = |t_u\rangle$ is realized. The energy per unit cell can be given as

$$E_{\text{FM}} = \frac{J}{2} + 2J' - 2h\,. \tag{B.9}$$

Clearly, this phase reflects all the symmetries of the Hamiltonian, and shows no symmetry breaking. The phase boundaries to the Néel and 1/2-plateau states are $J' = h/4$ and $J' = (h - J)/4$, respectively.

B.2 The Z_2 phases of the low symmetry phase diagram

B.2.1 $Z_2[\mathcal{C}_{2v}]$ phase

For positive values of $D'_\perp$ the $Z_1[\mathcal{D}_{2d}]$ state is connected via a continuous phase transition to a two–fold degenerate $Z_2[\mathcal{C}_{2v}]$. This is the phase that smoothly evolves from the high symmetry $D = 0$ plateau state as we turn on the intradimer DM interaction, which tilts the spins from the direction that is parallel to the field. The variational wave function of this phase is given as

$$\begin{aligned}
\Psi_A &= |s\rangle + \frac{w}{\sqrt{2}}\left(|t_u\rangle + |t_d\rangle\right) \pm \frac{v}{\sqrt{2}}\left(|t_d\rangle - |t_u\rangle\right) \\
&= |s\rangle_A + w|t_y\rangle_A \pm vi|t_x\rangle_A \\
\Psi_B &= |s\rangle + \frac{w}{\sqrt{2}}\left(-i|t_u\rangle + i|t_d\rangle\right) \mp \frac{iv}{\sqrt{2}}\left(|t_d\rangle + |t_u\rangle\right) \\
&= |s\rangle_B - w|t_x\rangle_B \mp vi|t_x\rangle_B
\end{aligned} \tag{B.10}$$

The ground state breaks time–reversal invariance: the dimers have a magnetization along the z direction, alternating between the A and B dimers. At the same time, the staggered magnetization is also finite, with moments pointing along the dimers. In other words, it is characterized by a nonzero value of the $n_{\mathcal{C}_4}$ and $m^z_{\text{Néel}}$ order parameters which were defined in Table (2.3).

Of possible practical interest is the form of the wave function for small values of D/J in the plateau region. To discuss this case, it is conveninet to write the wave function in the following form:

$$\Psi_A = |s\rangle + d_A\,|t_d\rangle + u_A\,|t_u\rangle\ , \tag{B.11}$$

$$\Psi_B = |t_u\rangle - d_B\,|t_d\rangle + is_B\,|s\rangle \tag{B.12}$$

From numerical minimization we learn that d_A, u_A, and s_B grow linearly with D, while $d_B \propto D^2$ and can be neglected. The energy including the leading term in D/J is

$$\begin{aligned}
E &= -h_z - \frac{J}{2} + \frac{D}{\sqrt{2}}\left(u_A + d_A + s_B\right) \\
&\quad + \left(J - 2J' + h_z\right) d_A^2 + 4D'_\perp s_B\left(d_A - u_A\right) \\
&\quad + \left(h_z - J\right) s_B^2 + \left(J + 2J' - h_z\right) u_A^2
\end{aligned} \tag{B.13}$$

This equation can now be easily minimized. Skipping the details, let us only mention the result for the magnetization:

$$m^z = 1 - \frac{D^2}{8}\left[\frac{1}{(h_z - J)^2} - \frac{1}{(h_z + J - 2J')^2} + \frac{1}{(J + 2J' - h_z)^2}\right] \tag{B.14}$$

The deviation from the $m^z = 1$ plateau value is proportional to D^2, and this gives a finite slope intead of a plateau in the magnetization curve.

B.2.2 $Z_2[\mathcal{S}_4]$ phase boundary

At $h = 0$, for negative $D'_\perp$ the states $Z_2[\mathcal{S}_4]$ is realized with the wave functions are

$$\begin{aligned}
\Psi_A &= |s\rangle + \frac{w}{\sqrt{2}} e^{\pm i\varphi} \left(|t_u\rangle + |t_d\rangle\right) \\
&= |s\rangle_A + w e^{\pm i\varphi} |t_y\rangle_A \\
\Psi_B &= |s\rangle + \frac{w}{\sqrt{2}} e^{\pm i\varphi} \left(-i|t_u\rangle + i|t_d\rangle\right) \\
&= |s\rangle_B - w e^{\pm i\varphi} |t_x\rangle_B
\end{aligned} \tag{B.15}$$

Like the previous phase, this also breaks time reversal symmetry: the staggered magnetization has a finite value, and the spins are perpendicular to the dimers in the xy plane and are pointing in opposing directions on the two ends.

As we can see in Fig. 4.2(a), this phase is stable for small magnetic fields only. To find the phase boundary between the I and $Z_2[\mathcal{S}_4]$ phase, we look at the instability of the I phase wave function against a perturbation leading to symmetry breaking found in the $Z_2[\mathcal{S}_4]$ phase:

$$\Psi_A = |s\rangle + (u \pm i\delta)\,|t_u\rangle + (d \pm i\delta)\,|t_d\rangle \tag{B.16}$$

$$\Psi_B = |s\rangle - i(u \pm i\delta)\,|t_u\rangle + i(d \pm i\delta)\,|t_d\rangle \tag{B.17}$$

where δ is small. The variational energy of the state above, keeping the leading term in δ, is

$$E = E_{Z_1[\mathcal{D}_{\in\Gamma}]} + \frac{1}{2} c\delta^2 \tag{B.18}$$

where

$$\begin{aligned}
c = {} & \frac{4J}{\left(u^2+d^2+1\right)^2} - \frac{2\sqrt{2}D(u+d)}{\left(u^2+d^2+1\right)^2} + \frac{4h_z(u^2-d^2)}{\left(u^2+d^2+1\right)^2} \\
& - \frac{8J'(u^2-d^2)^2}{\left(u^2+d^2+1\right)^3} - \frac{16D'_\perp(2ud+1)}{\left(u^2+d^2+1\right)^3}
\end{aligned} \tag{B.19}$$

The instability occurs when it is energetically favorable to introduce a perturbation that happens when $c < 0$. The phase boundary is thus defined by $c = 0$, where the amplitudes u and d minimize the energy $E_{Z_1[\mathcal{D}_{\in\Gamma}]}$. Solving the set of $\partial E_{Z_1[\mathcal{D}_{\in\Gamma}]}/\partial u = 0$, $\partial E_{Z_1[\mathcal{D}_{\in\Gamma}]}/\partial d = 0$ and $c = 0$ equations we get

$$D = \sqrt{2}J \frac{u+d}{u^2+d^2-1} \tag{B.20}$$

$$D'_\perp = -\frac{J}{4} \frac{u^2+d^2+1}{u^2+d^2-1} \tag{B.21}$$

$$h_z = 2J' \frac{u^2-d^2}{u^2+d^2+1} \tag{B.22}$$

at the boundary. Eliminating the u and d, the critical field reads

$$h_c(Z_2[\mathcal{S}_4]) = \sqrt{16{D'_\perp}^2 - D^2 - J^2}\frac{DJ'}{2D'_\perp(J - 4D'_\perp)}. \tag{B.23}$$

The $Z_2[\mathcal{S}_4]$ phase is realized for $h_z < h_c(Z_2[\mathcal{S}_4])$. It is actually a very tiny region, as can be seen on Fig. 4.2.

Appendix C

An effective model of $SrCu_2(BO_3)_2$

C.1 Keeping $|s\rangle$ and $|t_1\rangle$ only

In the case of the field parallel to the z axis it is a usual practice to keep only the low lying singlet and $S^z = 1$ triplet (the component aligned with the field) state of a bond. Here we are interested in the behavior of the gap close to the critical field. For that reason, we restrict the discussion to the dimer–singlet and the $O(2)[S_4]$ phase for $D = 0$ and the $Z_1[\mathcal{D}_{2d}]$ phase in finite D case.

As a first step, we define the following rotated boson operators

$$\tilde{s}^\dagger_{\mathrm{A}}(\mathbf{k}) = \cos\frac{\alpha}{2} s^\dagger_{\mathrm{A}}(\mathbf{k}) + \sin\frac{\alpha}{2} e^{i\varphi} t^\dagger_{1,\mathrm{A}}(\mathbf{k}) \,, \tag{C.1a}$$

$$\tilde{t}^\dagger_{\mathrm{A}}(\mathbf{k}) = \sin\frac{\alpha}{2} s^\dagger_{\mathrm{A}}(\mathbf{k}) - \cos\frac{\alpha}{2} e^{i\varphi} t^\dagger_{1,\mathrm{A}}(\mathbf{k}) \,, \tag{C.1b}$$

$$\tilde{s}^\dagger_{\mathrm{B}}(\mathbf{k}) = \cos\frac{\alpha}{2} s^\dagger_{\mathrm{B}}(\mathbf{k}) - i\sin\frac{\alpha}{2} e^{i\varphi} t^\dagger_{1,\mathrm{B}}(\mathbf{k}) \,, \tag{C.1c}$$

$$\tilde{t}^\dagger_{\mathrm{B}}(\mathbf{k}) = \sin\frac{\alpha}{2} s^\dagger_{\mathrm{B}}(\mathbf{k}) - i\cos\frac{\alpha}{2} e^{i\varphi} t^\dagger_{1,\mathrm{B}}(\mathbf{k}) \,, \tag{C.1d}$$

so that the variational wave–function that comprises the above mentioned phases is given by $|\Psi\rangle_{\mathrm{A}} = \tilde{s}^\dagger_A |0\rangle$ and $|\Psi\rangle_{\mathrm{B}} = \tilde{s}^\dagger_B |0\rangle$, and we fix the phase $\varphi = 0$ for convenience [see also Eq. (4.20) for comparison]. The expectation value of the Hamiltonian is then given by

$$\begin{aligned} E_0 = & -J\left(\frac{1}{2} + \cos\alpha\right) + \frac{J'}{2}(1-\cos\alpha)^2 + D'_\perp \sin^2\alpha \\ & + \frac{1}{\sqrt{2}}\tilde{D}\sin\alpha - g_z h_z (1-\cos\alpha) \,. \end{aligned} \tag{C.2}$$

Here we introduce the $\tilde{D} = D - 2g_s h_z$, as in this section the D and the g_s appear in this combination only. Minimization procedure involves solving a quartic polynomial equation that is tedious. Instead, we concentrate on the case when the anisotropy terms $\tilde{D}$ is small.

We also need the bond–wave Hamiltonian. For that we introduce

$$\tilde{t}^\dagger_\pm(\mathbf{k}) = \frac{1}{\sqrt{2}}\left[\tilde{t}^\dagger_A(\mathbf{k}) \pm \tilde{t}^\dagger_B(\mathbf{k})\right] \tag{C.3}$$

symmetric and antisymmetric combination of the rotated triplet operators that reduce the size of the matrices in the Hamiltonian. Expanding in powers of M, we

get $\mathcal{H} = E_0 M^2 + M\mathcal{H}_2 + \ldots$, where we omitted higher order terms in $1/M$. The bond wave Hamiltonian $\mathcal{H}^{(2)} = \mathcal{H}^{(2)}_+ + \mathcal{H}^{(2)}_-$ is given as

$$\mathcal{H}^{(2)}_{\pm} = \sum_{\mathbf{k}} \begin{pmatrix} \tilde{t}^{\dagger}_{\pm}(\mathbf{k}) \\ \tilde{t}_{\pm}(-\mathbf{k}) \end{pmatrix}^T \begin{pmatrix} a \pm (b + 2D'_{\perp})\gamma_1 & b\gamma_1 \\ b\gamma_1 & a \pm (b + 2D'_{\perp})\gamma_1 \end{pmatrix} \begin{pmatrix} \tilde{t}_{\pm}(\mathbf{k}) \\ \tilde{t}^{\dagger}_{\pm}(-\mathbf{k}) \end{pmatrix}, \tag{C.4}$$

where the a can be conveniently expressed as

$$a = b - E_0 - h_z - \frac{J}{2} \tag{C.5}$$

and

$$b = \frac{1}{2}(J' - 2D'_{\perp}) \sin^2 \alpha \,, \tag{C.6}$$

while γ_1 is defined in Eq. (4.50). The Bogoliubov transformation yields the

$$\omega_{\pm} = \sqrt{(a \pm 2D'_{\perp}\gamma_1)(a \pm 2b\gamma_1 \pm 2D'_{\perp}\gamma_1)} \,. \tag{C.7}$$

C.1.1 High symmetry case

The minimal energy for $\tilde{D} = 0$ of Eq. (C.2) is achieved for

$$\cos \alpha_{O(2)} = \begin{cases} 1 & h_z \leq h_{c1} \,, \\ \frac{h_{c1}+h_{c2}-2h_z}{h_{c2}-h_{c1}} & h_{c1} \leq h_z \leq h_{c2} \,, \\ -1 & h_{c2} \leq h_z \,. \end{cases} \tag{C.8}$$

This solutions correspond the the dimer–singlet, $O(2)[S_4]$ and the fully polarized phase, respectively. Note that the one–half magnetization plateau is missing – the form of the chosen wave function does not allow for the Z_2 breaking.

$$h_{c1} = J - 2|D'_{\perp}| \,, \tag{C.9a}$$

$$h_{c2} = J + 2J' + 2|D'_{\perp}| \,. \tag{C.9b}$$

The variational energy of the unit cell is then

$$E_0 = \begin{cases} -\frac{3J}{2} & h_z \leq h_{c1} \\ -\frac{3J}{2} - \frac{(h_z - h_{c1})^2}{h_{c2}-h_{c1}} & h_{c1} \leq h_z \leq h_{c2} \\ \frac{J}{2} + 2J' - 2g_z h_z & h_{c2} \leq h_z \end{cases} . \tag{C.10}$$

It turns out that the boundary between the dimer singlet phase and the $O(2)$ phase is shifted to the expense of the $O(2)$ phase compared to the case when we keep all the four state of a dimer [see Eq. (4.18)], and the boundaries overlap only in the limit of small $|D'_{\perp}|$ values, when the critical field is close to J.

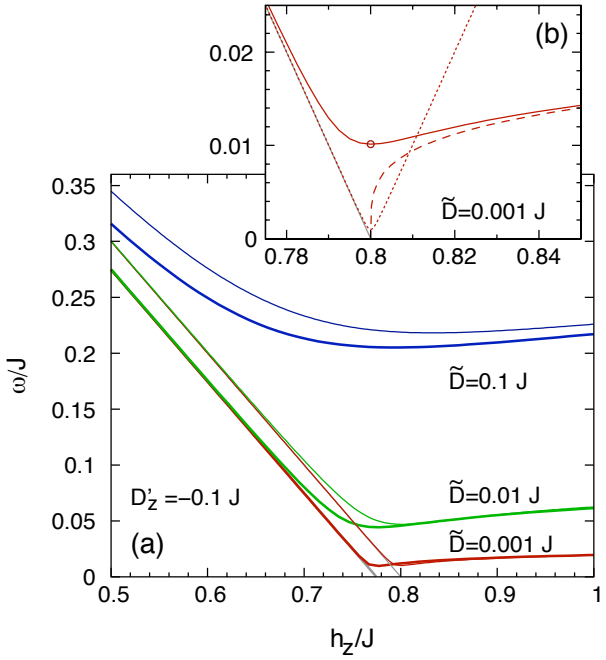

Figure C.1: (a) The lowest lying branch of the excitation spectrum at the $\mathbf{k} = 0$ is shown when keeping 4 (thick) and 2 bosons (thin lines) per dimer for $J' = 0.6J$, $D'_\perp = 0.1J$ and different values of $\tilde{D}$. (b) The bond wave spectrum has a dip at the $h_{c1} = 0.8J$ critical field. The dotted line is the approximation from Ref. [Miyahara 2005], the dashed line and the circle are the approximations given by Eqs. (C.16) and (C.18), respectively.

Now, let us turn to the excitation spectrum. In the dimer–singlet phase $a = J - h_z$ and $b = 0$ in Eq. (C.4), so that the $\mathcal{H}^{(2)}_\pm$ matrices are actually diagonal,

$$\mathcal{H}^{(2)}_\pm \;=\; \sum_{\mathbf{k}} \omega_\pm(\mathbf{k}) \tilde{t}^\dagger_\pm(\mathbf{k}) \tilde{t}_\pm(\mathbf{k}) \;, \tag{C.11}$$

with the excitation energies

$$\omega_\pm(\mathbf{k}) = J - h_z \pm 2D'_\perp \cos\frac{q_a}{2} \cos\frac{q_b}{2} \;. \tag{C.12}$$

This is the same as the small $D'_\perp/J$ limit of the dispersions given by Eqs. (4.51), when we kept all the four bosons per dimer.

In the $O(2)[S_4]$ phase the $a = J - h_{c1} = -2D'_\perp$ and

$$b = \frac{(h_z - h_{c1})(h_{c2} - h_z)}{(h_{c2} - h_{c1})} \;, \tag{C.13}$$

and from Eq. (C.7) we get

$$\omega^\pm(\mathbf{k}) = 2\sqrt{1 \mp \cos\frac{\mathbf{a}}{2}\cos\frac{\mathbf{b}}{2}}\sqrt{D'_\perp\left(D'_\perp \mp \left(D'_\perp + b\right)\cos\frac{\mathbf{a}}{2}\cos\frac{\mathbf{b}}{2}\right)} \;. \tag{C.14}$$

We note that $\omega^+(\mathbf{k}) \to 0$ as $\mathbf{k} \to 0$, thus it becomes the Goldstone mode associated with the continuous symmetry breaking in the $O(2)$ phase.

C.1.2 Low symmetry case

In the presence of the $\tilde{D}$ anisotropies the ω_+ Goldstone mode acquires a finite gap in the presence of anisotropies. In the case of small $\tilde{D}$ we include the first order correction in $\tilde{D}$ to the α given by Eq. (C.8),

$$\cos\alpha = \left(1 + \frac{\tilde{D}}{\sqrt{2(h_z - h_{c1})(h_{c2} - h_z)}}\right) \cos\alpha_{O(2)} \ , \tag{C.15}$$

and we end up with

$$\omega_+ = \tilde{D}^{1/2} \left[\frac{(h_z - h_{c1})(h_{c2} - h_z)}{2}\right]^{1/4} \tag{C.16}$$

in the leading order in $\tilde{D}$. This approximation is shown with dotted line in Fig. C.1(b). It clearly fails as $h \to h_{c1}$, as in the limit $\alpha_{O(2)} \to 0$ the Eq. (C.15) is not valid any more. Instead, at the critical field h_{c1} and in the $\alpha \to 0$ limit the energy expression Eq. (C.2) simplifies considerably, in leading order

$$\alpha = -\frac{2^{1/6}\tilde{D}^{1/3}}{(J' - 2D'_\perp)^{1/3}} \ , \tag{C.17}$$

and for the gap we get

$$\omega_{c1} = \frac{\sqrt{3}\tilde{D}^{2/3}\,(J' - 2D'_\perp)^{1/3}}{2^{2/3}} \ . \tag{C.18}$$

This approximation is shown with circle in Fig. C.1(b). We find that on the boundary between the dimer–singlet and the $O(2)$ phase the gap closes faster than $\tilde{D}^{1/2}$, namely with a power 2/3. Such a behavior at the quantum critical point has been discussed for quantum antiferromagnets in Refs. [Fouet 2004] and [Chernyshev 2005]. We also note that the perturbational $\sqrt{(h - h_{c1})^2 + \tilde{D}^2}$ result of Ref. [Miyahara 2005] does not capture the quantum fluctuation effects close to the critical field h_{c1}.

Appendix D

Perturbation expansion

Here we are presenting the results of the Rayleigh-Scrödinger perturbation theory applied to states and excitations in the $J \to 0$ limit.

D.1 Second order corrections in J to the ground-state energy

The second order correction to the energy/(per site) of the different phases are as follows:

$$\varepsilon^{(2)}_{A1} = -\frac{8J^2}{3J_z} - \frac{9J^2}{2(4\Lambda - 5J_z)} \tag{D.1}$$

$$\varepsilon^{(2)}_{A3} = -\frac{9J^2}{2(11J_z - 4\Lambda)} \tag{D.2}$$

$$\varepsilon^{(2)}_{F1} = -\frac{12J^2}{2\Lambda - J_z} \tag{D.3}$$

$$\varepsilon^{(2)}_{P1} = -\frac{6J^2}{7J_z - 2\Lambda} \tag{D.4}$$

$$\varepsilon^{(2)}_{P2} = -\frac{3J^2}{2J_z} \tag{D.5}$$

$$\varepsilon^{(2)}_{F3} = 0 \tag{D.6}$$

D.2 First order degenerate perturbation theory for excitation spectrum of the uniform F1 and F2 phases

$$\omega_{F1\to P2} = -h + 2J_z + 2\Lambda + 6J\gamma_{\mathbf{k}} \tag{D.7}$$

$$\omega_{F1\to A1} = h - 2J_z + 8J\gamma_{\mathbf{k}} \tag{D.8}$$

$$\omega_{F3\to P2} = h - 6J_z - 2\Lambda + 6J\gamma_{\mathbf{k}} \tag{D.9}$$

where $\gamma_{\mathbf{k}} = \frac{1}{\zeta}\sum_{\boldsymbol{\delta}} e^{i\mathbf{k}\cdot\boldsymbol{\delta}}$.

D.3 Second order degenerate perturbation for the excitation spectrum of the staggered phases

The softening of the excitations in the two-sublattice gapped phases, $A1$, $A3$, $P1$, and $P2$, occur in the second order of J. The on-site excitations have dif-

ferent energies on the two sublattices, and depending on this energy discrepancy one should follow different strategies for the degenerate perturbation calculations. As an example, we discuss the lower instability of the 2/3-plateau phase $P2$ in more detail. The wave function of the phase $P2$ in the Ising limit is given by $|\Psi^{P2}\rangle = \prod_{j\in A}\prod_{j'\in B}|\uparrow_j\rangle|\Uparrow_{j'}\rangle$, and the effect of the lowering operator S_j^- results in $|\Phi_i^A\rangle = |\downarrow_i\rangle\prod_{\substack{j\in A\\ j\neq i}}\prod_{j'\in B}|\uparrow_j\rangle|\Uparrow_{j'}\rangle$ and $|\Phi_i^B\rangle = |\uparrow_i\rangle\prod_{j\in A}\prod_{\substack{j'\in B\\ j'\neq i}}|\uparrow_j\rangle|\Uparrow_{j'}\rangle$ with the diagonal excitation energies $\Delta E_A = h - 6J_z$ and $\Delta E_B = h - 2\Lambda - 2J_z$, respectively, as it was noted in section 5.2.3. When the energy difference on the sublattices is larger than J, that is, when $\Delta E_B - \Delta E_A = 4J_z - 2\Lambda \gg J$, the ground state manifold is given by the states $|\Phi_i^A\rangle$. Since $\langle\Phi_i^B|\mathcal{H}|\Phi_{i'}^A\rangle = \sqrt{3}J$ for neighboring i and i' sites and $\langle\Phi_i^A|\mathcal{H}|\Phi_{i'}^A\rangle = 0$, the $|\downarrow\rangle$ excitation acquires dispersion in a second order process in J, where the $|\uparrow\rangle$ excitations on the B sublattice can be viewed as virtual state [see Fig. 5.2(b)]. This leads to

$$\omega_{P2\to P1}(\mathbf{k}) = h - 6J_z - \frac{3J^2}{4J_z - 2\Lambda}16\gamma_{\mathbf{k}}^2 + \omega_{P2\to P1}^{(2)} \tag{D.10}$$

where the $\omega_{P2\to P1}^{(2)}$ denotes additional second order contributions in J that are independent of $\mathbf{k}$ — the full form of the dispersion is given in Eq. (D.16). In other words, the gap closes quadratically for small values of J. A similar calculation can be done for the case $\Delta E_A - \Delta E_B = 2\Lambda - 4J_z \gg J$, when the ground state manifold is given by the $|\Phi_i^B\rangle$ states, and we obtain the dispersion, Eq. (D.15), where the hopping amplitude is quadratic in J (we note that a new virtual state assists the hopping).

$$\omega_{P1\to A3} = h + 2\Lambda - 6J_z - \frac{36J^2}{8J_z - 2\Lambda} - \frac{9J^2}{4(8J_z - 4\Lambda)}16\gamma_{\mathbf{k}}^2 + \frac{48J^2}{7J_z - 2\Lambda} \tag{D.11}$$

$$\omega_{P1\to P2} = -h + 6J_z - \frac{3J^2}{2J_z} + \frac{48J^2}{7J_z - 2\Lambda} - \frac{3J^2}{6J_z - 2\Lambda}(16\gamma_{\mathbf{k}}^2 + 8) \tag{D.12}$$

$$\omega_{A1\to F1} = -h + 2J_z - \frac{27J^2}{4\Lambda - 4J_z} - \frac{12J^2}{2\Lambda - 2J_z} + \frac{64J^2}{3J_z} + \frac{36J^2}{4\Lambda - 5J_z} - \frac{2J^2}{J_z}(16\gamma_{\mathbf{k}}^2 + 8) - \frac{3J^2}{2\Lambda - 4J_z}16\gamma_{\mathbf{k}}^2 \tag{D.13}$$

$$\omega_{P2\to F3} = -h + 6J_z + 2\Lambda - \frac{9J^2}{8J_z}(16\gamma_{\mathbf{k}}^2 + 8) + 12\frac{J^2}{J_z} \tag{D.14}$$

$$\omega_{P2\to F1} = h - 2J_z - 2\Lambda - \frac{12J^2}{2J_z + 2\Lambda} - \frac{9J^2}{8J_z}16\gamma_{\mathbf{k}}^2 - \frac{3J^2}{2\Lambda - 4J_z}16\gamma_{\mathbf{k}}^2 + \frac{3J^2}{J_z} \tag{D.15}$$

$$\omega_{P2\to P1} = h - 6J_z + \frac{21J^2}{4J_z} - \frac{3J^2}{4J_z - 2\Lambda}16\gamma_{\mathbf{k}}^2 \tag{D.16}$$

$$\begin{aligned}\omega_{A3\to P1} &= -h+6J_z-2\Lambda-\frac{12J^2}{10J_z-2\Lambda}+\frac{36J^2}{11J_z-4\Lambda}\\ &\quad -\frac{9J^2}{8(5J_z-2\Lambda)}(16\gamma_{\mathbf{k}}^2+8)\end{aligned} \tag{D.17}$$

When we include the excitations on both sublattices, the S_i^- excitations from the phase $A1$ in the $\mathbf{k}$ space are the eigenvalues of the matrix

$$\mathcal{H}_{A1}=\begin{pmatrix}\Sigma_1 & 4\sqrt{3}J\gamma_{\mathbf{k}}\\ 4\sqrt{3}J\gamma_{\mathbf{k}} & \Sigma_2\end{pmatrix}-8\varepsilon_{A1}^{(2)} \tag{D.18}$$

where $\Sigma_1=2J_z-h-\frac{2J^2}{J_z}(16\gamma_{\mathbf{k}}^2+8)-\frac{27J^2}{4\Lambda-4J_z}-\frac{12J^2}{2\Lambda-2J_z}$ and $\Sigma_2=2\Lambda-2J_z-h-\frac{12J^2}{J_z}-\frac{9J^2}{4(4\Lambda-6J_z)}(16\gamma_{\mathbf{k}}^2+8)$. If we expand in J up to the second order, we recover Eq. D.13, the corrections to the dispersion directly to the F1 phase.

Similarly, for the phase $P1$

$$\mathcal{H}_{P1}=\begin{pmatrix}2\Lambda+h-6J_z-\frac{36J^2}{8J_z-2\Lambda} & 6J\gamma_{\mathbf{k}}\\ 6J\gamma_{\mathbf{k}} & 2J_z+h-2\Lambda-\frac{8J^2}{3J_z}-\frac{3J^2}{6J_z-2\Lambda}(16\gamma_{\mathbf{k}}^2+8)\end{pmatrix}-8\varepsilon_{P1}^{(2)}, \tag{D.19}$$

and for the P2 phase:

$$\mathcal{H}_{P2}=\begin{pmatrix}-6J_z+h-\frac{27J^2}{4J_z} & 4\sqrt{3}J\gamma_{\mathbf{k}}\\ 4\sqrt{3}J\gamma_{\mathbf{k}} & -2J_z+h-2\Lambda-\frac{12J^2}{2J_z+2\Lambda}-\frac{9J^2}{8J_z}(16\gamma_{\mathbf{k}}^2+8)\end{pmatrix}-8\varepsilon_{P2}^{(2)}. \tag{D.20}$$

Appendix E

Flavor waves in finite magnetic field

In the rotated basis the variational wave functionn corresponds to the $a_A^\dagger|0\rangle$ and $a_B^\dagger|0\rangle$. The energy per site, as a function of the two variational parameters η and $\varphi = \varphi_A = -\varphi_B$, reads

$$\frac{E(\eta,\varphi)}{N} = \frac{3}{4}\frac{\left(\eta^2+3\right)}{(3\eta^2+1)}\Lambda + \frac{18\eta^2(\eta+1)^2}{(3\eta^2+1)^2}J\cos 2\varphi - \frac{3\eta(\eta+1)}{3\eta^2+1}g_{xx}h_x\cos\varphi. \tag{E.1}$$

Minimizing the $E(\eta,\varphi)$ with respect to η and φ, we get two solutions: (i) the canted Néel-state, defined via the following set of equations:

$$\Lambda = \frac{3(3\eta+1)\left(\eta^2-1\right)}{3\eta^2+1}J, \tag{E.2a}$$

$$g_{xx}h_x = \frac{24\eta(\eta+1)}{(3\eta^2+1)}J\cos\varphi. \tag{E.2b}$$

The spins cant in the direction of the field keeping the η parameter unchanged. The limiting cases for η are

$$\eta = \begin{cases} 1+\dfrac{\Lambda}{6J}+O\left(\Lambda^2/J^2\right), & \text{if } \Lambda \ll J; \\ \dfrac{\Lambda}{3J}-\dfrac{1}{3}+O\left(J/\Lambda\right), & \text{if } \Lambda \gg J. \end{cases} \tag{E.3}$$

(ii) For high enough magnetic field, the spins in the A and B sublattice become equal and parallel to the field, setting $\varphi = 0$, and η is obtained from:

$$\Lambda = \frac{(\eta-1)(3\eta+1)}{4\eta}g_{xx}h_x - \frac{3(3\eta+1)\left(\eta^2-1\right)}{3\eta^2+1}J. \tag{E.4}$$

$\eta \to 1$ as the field $h_x \to \infty$.

The b_j, c_j, and d_j (i.e. $a_{\nu,j}$, with $j = A, B$) bosons in (6.24) take the role of the Holstein-Primakoff bosons. After the $1/M$ expansion, the spin dipole operators are

$$
\begin{aligned}
S_j^x &= M\frac{3\eta(\eta+1)}{3\eta^2+1}\cos\varphi_j + \sqrt{M}\left[-\frac{i\sqrt{3}\sqrt{7\eta^2-4\eta+1}}{2\sqrt{3\eta^2+1}}\sin\varphi_j\left(b_j^\dagger - b_j\right)\right. \\
&\left. + \frac{\sqrt{3}(\eta-1)(3\eta+1)}{2\left(3\eta^2+1\right)}\cos\varphi_j\left(c_j^\dagger + c_j\right)\right], \qquad \text{(E.5)} \\
S_j^y &= M\frac{3\eta(\eta+1)}{3\eta^2+1}\sin\varphi_j + \sqrt{M}\left[\frac{i\sqrt{3}\sqrt{7\eta^2-4\eta+1}}{2\sqrt{3\eta^2+1}}\cos\varphi_j\left(b_j^\dagger - b_j\right)\right. \\
&\left. + \frac{\sqrt{3}(\eta-1)(3\eta+1)}{2\left(3\eta^2+1\right)}\sin\varphi_j\left(c_j^\dagger + c_j\right)\right], \qquad \text{(E.6)} \\
S_j^z &= \sqrt{M}\left[-\frac{\sqrt{3}\eta(\eta+1)}{\sqrt{3\eta^2+1}\sqrt{7\eta^2-4\eta+1}}\left(b_j^\dagger + b_j\right)\right. \\
&\left. + \frac{3(\eta-1)^2}{2\sqrt{3\eta^2+1}\sqrt{7\eta^2-4\eta+1}}\left(d_j^\dagger + d_j\right)\right], \qquad \text{(E.7)}
\end{aligned}
$$

The multiboson spin-wave Hamiltonian up to quadratic order in bosons reads:

$$
\mathcal{H} \approx M^2\mathcal{H}^{(0)} + M^{3/2}\mathcal{H}^{(1)} + M\mathcal{H}^{(2)} \qquad \text{(E.8)}
$$

where $\mathcal{H}^{(0)}$ is equal to mean field energy (E.1), $\mathcal{H}^{(1)}$ is identically zero when (6.8) is satisfied, and the quadratic term has the following form for the solution given by Eqs. (E.2):

$$
\begin{aligned}
\mathcal{H}^{(2)} \;=\;& +\frac{6(\eta+1)^2\left(9\eta^3-5\eta^2-\eta+1\right)}{\left(3\eta^2+1\right)\left(7\eta^2-4\eta+1\right)}J\left(b_A^\dagger b_A+b_B^\dagger b_B\right)\\
&+\frac{72\eta^3(\eta+1)^2}{\left(3\eta^2+1\right)\left(7\eta^2-4\eta+1\right)}J\left(d_A^\dagger d_A+d_B^\dagger d_B\right)\\
&+\frac{9(\eta-1)^4}{\left(3\eta^2+1\right)\left(7\eta^2-4\eta+1\right)}J_z\left(d_A^\dagger d_B^\dagger+d_Ad_B+d_A^\dagger d_B+d_B^\dagger d_A\right)\\
&-\frac{6\sqrt{3}\eta(\eta+1)(\eta-1)^2}{\left(3\eta^2+1\right)\left(7\eta^2-4\eta+1\right)}J_z\left(d_Ab_B+d_Bb_A+b_A^\dagger d_B+b_A^\dagger d_B^\dagger+b_B^\dagger d_A\right.\\
&\left.+b_B^\dagger d_A^\dagger+d_A^\dagger b_B+d_B^\dagger b_A\right)\\
&+\frac{36\sqrt{3}\eta^2(\eta+1)(\eta-1)^2}{\left(3\eta^2+1\right)\left(7\eta^2-4\eta+1\right)}J\left(b_A^\dagger d_A+b_B^\dagger d_B+d_A^\dagger b_A+d_B^\dagger b_B\right)\\
&+\left[\frac{12\eta^2(\eta+1)^2}{\left(3\eta^2+1\right)\left(7\eta^2-4\eta+1\right)}J_z-\frac{3\left(7\eta^2-4\eta+1\right)}{3\eta^2+1}J\cos 2\varphi\right]\\
&\times\left(b_A^\dagger b_B^\dagger+b_Ab_B+b_A^\dagger b_B+b_B^\dagger b_A\right)\\
&+\frac{3(3\eta+1)(\eta-1)\sqrt{7\eta^2-4\eta+1}}{\left(3\eta^2+1\right)^{3/2}}iJ\sin 2\varphi\left(b_Ac_B+b_Ac_B^\dagger+b_B^\dagger c_A+b_B^\dagger c_A^\dagger\right.\\
&\left.-b_A^\dagger c_B-b_A^\dagger c_B^\dagger-b_Bc_A-b_Bc_A^\dagger\right)\\
&+\frac{3(3\eta+1)^2(\eta-1)^2}{\left(3\eta^2+1\right)^2}J\cos 2\varphi\left(c_A^\dagger c_B^\dagger+c_Ac_B+c_A^\dagger c_B+c_Ac_B^\dagger\right)\\
&+6J(\eta+1)\left(c_A^\dagger c_A+c_B^\dagger c_B\right). \qquad \text{(E.9)}
\end{aligned}
$$

We note that in zero field ($\varphi=\pm\pi/2$) and parallel spins the Hamiltonian separates into two parts, one involving b and d bosons, the other only the c bosons. Similarly, for the uniform state in high fields, where the variational parameters are given by Eq. (E.4) we get $\mathcal{H}^{(2)}=\mathcal{H}_{bd}^{(2)}+\mathcal{H}_c^{(2)}$ with

$$
\begin{aligned}
\mathcal{H}_c^{(2)} \;=\;& +\left(\frac{g_{xx}h_x\left(3\eta^2+1\right)}{2\eta}-6J(\eta+1)\right)\left(c_A^\dagger c_A+c_B^\dagger c_B\right)\\
&+\frac{3J(3\eta+1)^2(\eta-1)^2}{\left(3\eta^2+1\right)^2}\left(c_Bc_A+c_A^\dagger c_B+c_A^\dagger c_B^\dagger+c_B^\dagger c_A\right). \qquad \text{(E.10)}
\end{aligned}
$$

and

$$
\begin{aligned}
\mathcal{H}_{bd}^{(2)} \;=\;& \frac{9J_z(\eta-1)^4}{(3\eta^2+1)\,(7\eta^2-4\eta+1)}\left(d_Bd_A+d_A^\dagger d_B+d_A^\dagger d_B^\dagger+d_B^\dagger d_A\right)\\
&-\frac{6\sqrt{3}J_z\eta(\eta+1)d_Ab_B(\eta-1)^2}{(3\eta^2+1)\,(7\eta^2-4\eta+1)}\left(d_Ab_B+d_Bb_A+b_A^\dagger d_B+b_A^\dagger d_B^\dagger\right.\\
&\left.+b_B^\dagger d_A+b_B^\dagger d_A^\dagger+d_A^\dagger b_B+d_B^\dagger b_A\right)\\
&+\left(\frac{12J_z\eta^2(\eta+1)^2}{(3\eta^2+1)\,(7\eta^2-4\eta+1)}-\frac{3J\left(7\eta^2-4\eta+1\right)}{3\eta^2+1}\right)\left(b_Bb_A+b_A^\dagger b_B^\dagger\right)\\
&+\left(\frac{12J_z\eta^2(\eta+1)^2}{(3\eta^2+1)\,(7\eta^2-4\eta+1)}+\frac{3J\left(7\eta^2-4\eta+1\right)}{3\eta^2+1}\right)\left(b_A^\dagger b_B+b_B^\dagger b_A\right)\\
&+\left(\frac{g_{xx}h_x(\eta+1)\left(9\eta^3-5\eta^2-\eta+1\right)}{2\eta\,(7\eta^2-4\eta+1)}-\frac{6J(\eta+1)^2\left(9\eta^3-5\eta^2-\eta+1\right)}{(3\eta^2+1)\,(7\eta^2-4\eta+1)}\right)\\
&\times\left(b_A^\dagger b_A+b_B^\dagger b_B\right)\\
&+\left(\frac{3\sqrt{3}g_{xx}h_x(\eta-1)^2\eta}{7\eta^2-4\eta+1}-\frac{36\sqrt{3}J(\eta-1)^2\eta^2(\eta+1)}{(3\eta^2+1)\,(7\eta^2-4\eta+1)}\right)\\
&\times\left(b_A^\dagger d_A+b_B^\dagger d_B+d_A^\dagger b_A+d_B^\dagger b_B\right)\\
&+\left(\frac{6g_{xx}h_x\eta^2(\eta+1)}{7\eta^2-4\eta+1}-\frac{72J\eta^3(\eta+1)^2}{(3\eta^2+1)\,(7\eta^2-4\eta+1)}\right)\left(d_A^\dagger d_A+d_B^\dagger d_B\right) \qquad \text{(E.11)}
\end{aligned}
$$

Bibliography

[A. Bencini 1990] D. Gatteschi A. Bencini. Electron paramagnetic resonance of exchange coupled systems. Springer-Verlag, Berlin, 1990.

[Abendschein 2008] A. Abendschein and S. Capponi. *Effective Theory of Magnetization Plateaux in the Shastry-Sutherland Lattice.* Phys. Rev. Lett., vol. 101, no. 22, pages 227201–, November 2008.

[Akaki 2009] M. Akaki, J. Tozawa, D. Akahoshi and H. Kuwahara. *Gigantic magnetoelectric effect caused by magnetic-field-induced canted antiferromagnetic-paramagnetic transition in quasi-two-dimensional Ca2CoSi2O7 crystal.* Applied Physics Letters, vol. 94, no. 21, page 212904, 2009.

[Akaki 2010] M Akaki, J Tozawa, M Hitomi, D Akahoshi and H Kuwahara. *Magnetoelectric properties of Cax Srx-2 CoSi 2 O 7 Crystals.* Journal of Physics: Conference Series, vol. 200, no. 1, page 012003, 2010.

[Albrecht 1996] M. Albrecht and F. Mila. *First-order transition between magnetic order and valence bond order in a 2D frustrated Heisenberg model.* EPL (Europhysics Letters), vol. 34, no. 2, page 145, 1996.

[Alet 2000] F. Alet and E. S. Sørensen. *Magnetization profiles and NMR spectra of doped Haldane chains at finite temperatures.* Phys. Rev. B, vol. 62, pages 14116–14121, Dec 2000.

[Allen 1938] J. F. Allen and A. D. Misener. *Flow of Liquid Helium II.* Nature, vol. 141, page 75, Jan 1938.

[Anderson 1952] P. W. Anderson. *An Approximate Quantum Theory of the Antiferromagnetic Ground State.* Phys. Rev., vol. 86, pages 694–701, Jun 1952.

[Anderson 1973] P.W. Anderson. *Resonating valence bonds: A new kind of insulator?* Materials Research Bulletin, vol. 8, no. 2, pages 153 – 160, 1973.

[Anderson 2007] P. W. Anderson. *Two new vortex liquids.* Nature Phys., vol. 3, pages 160–162, 2007.

[Anderson 2008] P. W. Anderson. *Bose Fluids Above Tc: Incompressible Vortex Fluids and "Supersolidity".* Phys. Rev. Lett., vol. 100, no. 21, page 215301, May 2008.

[Anderson 2009] P. W. Anderson. *A Gross-Pitaevskii Treatment for Supersolid Helium.* Science, vol. 324, no. 5927, pages 631–632, 2009.

[Andreev 1971] A. F. Andreev and I. M. Lifshitz. *Quantum Theory of Defects in Crystals.* Sov. Phys. Usp., vol. 13, page 670, 1971.

[Andreev 1984] A. F. Andreev and I. A. Grishchuk. *Spin Nematics.* Zh Eksp. Teor. Fiz., vol. 87, no. 2, pages 467–475, 1984.

[Aoki 2007] Y. Aoki, J. C. Graves and H. Kojima. *Oscillation Frequency Dependence of Nonclassical Rotation Inertia of Solid $He4$.* Phys. Rev. Lett., vol. 99, no. 1, page 015301, Jul 2007.

[Arima 2011] Takahisa Arima. *Spin-Driven Ferroelectricity and Magneto-Electric Effects in Frustrated Magnetic Systems.* Journal of the Physical Society of Japan, vol. 80, no. 5, page 052001, 2011.

[Balents 2010] Leon Balents. *Spin liquids in frustrated magnets.* Nature, vol. 464, pages 199–208, Mar 2010.

[Bardeen 1957] J. Bardeen, L. N. Cooper and J. R. Schrieffer. *Theory of Superconductivity.* Phys. Rev., vol. 108, pages 1175–1204, Dec 1957.

[Batrouni 2000] G. G. Batrouni and R. T. Scalettar. *Phase Separation in Supersolids.* Phys. Rev. Lett., vol. 84, no. 7, pages 1599–1602, Feb 2000.

[Bert 2005] F. Bert, D. Bono, P. Mendels, F. Ladieu, F. Duc, J.-C. Trombe and P. Millet. *Ground State of the Kagomé-Like $S = 1/2$ Antiferromagnet Volborthite $Cu_3V_2O_7(OH)_2 \cdot 2H_2O$.* Phys. Rev. Lett., vol. 95, page 087203, Aug 2005.

[Bogoliubov 1947] N. N. Bogoliubov. *On the theory of superßuidity.* J. Phys. (USSR), vol. 11, page 23, 1947.

[Bordacs 2011] S. Bordacs, I. Kezsmarki, D. Szaller, L. Demko, N. Kida, H. Murakawa, Y. Onose, R. Shimano, T. Room, U. Nagel, S. Miyahara, N. Furukawa and Y. Tokura. *Chirality of Matter Shows Up via Spin Excitations.* ArXiv e-prints, September 2011.

[Cépas 2001] O. Cépas, K. Kakurai, L. P. Regnault, T. Ziman, J. P. Boucher, N. Aso, M. Nishi, H. Kageyama and Y. Ueda. *Dzyaloshinski-Moriya Interaction in the 2D Spin Gap System $SrCu_2(BO_3)_2$.* Phys. Rev. Lett., vol. 87, no. 16, pages 167205–, October 2001.

[Chapon 2006] L. C. Chapon, P. G. Radaelli, G. R. Blake, S. Park and S.-W. Cheong. *Ferroelectricity Induced by Acentric Spin-Density Waves in* YMn_2O_5. Phys. Rev. Lett., vol. 96, page 097601, Mar 2006.

[Cheng 2007] Y. F. Cheng, O. Cépas, P. W. Leung and T. Ziman. *Magnon dispersion and anisotropies in $SrCu_2(BO_3)_2$.* Phys. Rev. B, vol. 75, no. 14, pages 144422–, April 2007.

[Cheong 2007] Sang-Wook Cheong and Maxim Mostovoy. *Multiferroics: a magnetic twist for ferroelectricity.* Nature Materials, vol. 6, page 13, Jan 2007.

[Chernyshev 2005] A. L. Chernyshev. *Effects of an external magnetic field on the gaps and quantum corrections in an ordered Heisenberg antiferromagnet with Dzyaloshinskii-Moriya anisotropy.* Phys. Rev. B, vol. 72, no. 17, pages 174414–, November 2005.

[Chester 1970] G. V. Chester. *Speculations on Bose-Einstein Condensation and Quantum Crystals.* Phys. Rev. A, vol. 2, no. 1, pages 256–258, Jul 1970.

[Coldea 2001] R. Coldea, S. M. Hayden, G. Aeppli, T. G. Perring, C. D. Frost, T. E. Mason, S.-W. Cheong and Z. Fisk. *Spin Waves and Electronic Interactions in* La_2CuO_4. Phys. Rev. Lett., vol. 86, pages 5377–5380, Jun 2001.

[Colman 2011] R. H. Colman, F. Bert, D. Boldrin, A. D. Hillier, P. Manuel, P. Mendels and A. S. Wills. *Spin dynamics in the* $S = \frac{1}{2}$ *quantum kagome compound vesignieite,* $Cu_3Ba(VO_5H)_2$. Phys. Rev. B, vol. 83, page 180416, May 2011.

[Darriet 1993] J. Darriet and L.P. Regnault. *The compound Y2BaNiO5: A new example of a haldane gap in A S = 1 magnetic chain.* Solid State Communications, vol. 86, no. 7, pages 409 – 412, 1993.

[de Vries 2009] M. A. de Vries, J. R. Stewart, P. P. Deen, J. O. Piatek, G. J. Nilsen, H. M. Rønnow and A. Harrison. *Scale-Free Antiferromagnetic Fluctuations in the* $s = 1/2$ *Kagome Antiferromagnet Herbertsmithite.* Phys. Rev. Lett., vol. 103, page 237201, Dec 2009.

[Dorier 2008] J. Dorier, K. P. Schmidt and F. Mila. *Theory of Magnetization Plateaux in the Shastry-Sutherland Model.* Phys. Rev. Lett., vol. 101, no. 25, pages 250402–, December 2008.

[Dzyaloshinsky 1958] I. Dzyaloshinsky. *A thermodynamic theory of "weak" ferromagnetism of antiferromagnetics.* Journal of Physics and Chemistry of Solids, vol. 4, no. 4, pages 241–255, 1958. cited By (since 1996) 927.

[Einstein 1924] A. Einstein. *Quantentheorie des einatomigen idealen Gases.* Sitzber preuss Akad. Wiss. Physik-Math. Kl., pages 261–267, 1924.

[El Shawish 2005] S. El Shawish, J. Bonca, C. D. Batista and I. Sega. *Electron spin resonance of* $SrCu_2(BO_3)_2$ *at high magnetic fields.* Phys. Rev. B, vol. 71, no. 1, pages 014413–, January 2005.

[Fazekas 1999] P. Fazekas. Lecture notes on electron correlation and magnetism. World Scientific, Singapore, 1999.

[Feiguin 2007] Adrian Feiguin, Simon Trebst, Andreas W. W. Ludwig, Matthias Troyer, Alexei Kitaev, Zhenghan Wang and Michael H. Freedman. *Interacting Anyons in Topological Quantum Liquids: The Golden Chain.* Phys. Rev. Lett., vol. 98, no. 16, page 160409, Apr 2007.

[Fiebig 2005] Manfred Fiebig. *Revival of the magnetoelectric effect.* Journal of Physics D: Applied Physics, vol. 38, no. 8, page R123, 2005.

[Fouet 2004] J.-B. Fouet, O. Tchernyshyov and F. Mila. *Field-induced gap in ordered Heisenberg antiferromagnets.* Phys. Rev. B, vol. 70, no. 17, pages 174427–, November 2004.

[Fukunaga 2009] M. Fukunaga, Y. Sakamoto, H. Kimura, Y. Noda, N. Abe, K. Taniguchi, T. Arima, S. Wakimoto, M. Takeda, K. Kakurai and K. Kohn. *Magnetic-Field-Induced Polarization Flop in Multiferroic* $TmMn_2\mathbf{O}_5$. Phys. Rev. Lett., vol. 103, page 077204, Aug 2009.

[Gaulin 2004] B. D. Gaulin, S. H. Lee, S. Haravifard, J. P. Castellan, A. J. Berlinsky, H. A. Dabkowska, Y. Qiu and J. R. D. Copley. *High-Resolution Study of Spin Excitations in the Singlet Ground State of* $SrCu_2(BO_3)_2$. Phys. Rev. Lett., vol. 93, no. 26, pages 267202–, December 2004.

[Gelfand 1989] M.P. Gelfand, R.R.P. Singh and D.A. Huse. Phys. Rev. B, vol. 40, page 10801, 1989.

[Gozar 2005] A. Gozar, B. S. Dennis, H. Kageyama and G. Blumberg. *Symmetry and light coupling to phononic and collective magnetic excitations in* $SrCu_2(BO_3)_2$. Phys. Rev. B, vol. 72, no. 6, pages 064405–, August 2005.

[Gross 1995] David J. Gross. *Symmetry in Physics: Wigner's Legacy.* Physics Today, vol. 48, no. 12, pages 46–50, 1995.

[Gutzwiller 1963] Martin C. Gutzwiller. *Effect of Correlation on the Ferromagnetism of Transition Metals.* Phys. Rev. Lett., vol. 10, pages 159–162, Mar 1963.

[Hase 1993a] Masashi Hase, Ichiro Terasaki and Kunimitsu Uchinokura. *Observation of the spin-Peierls transition in linear* Cu^{2+} *(spin-1/2) chains in an inorganic compound* $CuGeO_3$. Phys. Rev. Lett., vol. 70, pages 3651–3654, Jun 1993.

[Hase 1993b] Masashi Hase, Ichiro Terasaki and Kunimitsu Uchinokura. *Observation of the spin-Peierls transition in linear* Cu^{2+} *(spin-1/2) chains in an inorganic compound* $CuGeO_3$. Phys. Rev. Lett., vol. 70, pages 3651–3654, Jun 1993.

[Heidarian 2005] Dariush Heidarian and Kedar Damle. *Persistent Supersolid Phase of Hard-Core Bosons on the Triangular Lattice.* Phys. Rev. Lett., vol. 95, page 127206, Sep 2005.

[Helton 2007] J. S. Helton, K. Matan, M. P. Shores, E. A. Nytko, B. M. Bartlett, Y. Yoshida, Y. Takano, A. Suslov, Y. Qiu, J.-H. Chung, D. G. Nocera and Y. S. Lee. *Spin Dynamics of the Spin-*1/2 *Kagome Lattice Antiferromagnet* $ZnCu_3(OH)_6Cl_2$. Phys. Rev. Lett., vol. 98, page 107204, Mar 2007.

[Holstein 1940] T. Holstein and H. Primakoff. *Field Dependence of the Intrinsic Domain Magnetization of a Ferromagnet.* Phys. Rev., vol. 58, pages 1098–1113, Dec 1940.

[Hubbard 1963] J. Hubbard. *Electron Correlations in Narrow Energy Bands.* Proceedings of the Royal Society of London. Series A. Mathematical and Physical Sciences, vol. 276, no. 1365, pages 238–257, 1963.

[Hutanu 2011] V. Hutanu, A. Sazonov, H. Murakawa, Y. Tokura, B. Náfrádi and D. Chernyshov. *Symmetry and structure of multiferroic $Ba_2CoGe_2O_7$.* Phys. Rev. B, vol. 84, page 212101, Dec 2011.

[Ishida 1994] Kenji Ishida, Yoshio Kitaoka, Kunisuke Asayama, Masaki Azuma, Zenji Hiroi and Mikio Takano. *Spin Gap Behavior in Ladder-Type of Quasi-One-Dimensional*
Spin ($S = 1/2$) System $SrCu_2O_3$. Journal of the Physical Society of Japan, vol. 63, no. 9, pages 3222–3225, 1994.

[Jia 2006] Chenglong Jia, Shigeki Onoda, Naoto Nagaosa and Jung Hoon Han. *Bond electronic polarization induced by spin.* Phys. Rev. B, vol. 74, page 224444, Dec 2006.

[Jia 2007] Chenglong Jia, Shigeki Onoda, Naoto Nagaosa and Jung Hoon Han. *Microscopic theory of spin-polarization coupling in multiferroic transition metal oxides.* Phys. Rev. B, vol. 76, page 144424, Oct 2007.

[Joshi 1999] A. Joshi, M. Ma, F. Mila, D. N. Shi and F. C. Zhang. *Elementary excitations in magnetically ordered systems with orbital degeneracy.* Phys. Rev. B, vol. 60, pages 6584–6587, Sep 1999.

[Kageyama 1999a] H. Kageyama, K. Yoshimura, R. Stern, N. V. Mushnikov, K. Onizuka, M. Kato, K. Kosuge, C. P. Slichter, T. Goto and Y. Ueda. *Exact Dimer Ground State and Quantized Magnetization Plateaus in the Two-Dimensional Spin System $SrCu_2(BO_3)_2$.* Phys. Rev. Lett., vol. 82, no. 15, page 3168, April 1999.

[Kageyama 1999b] Hiroshi Kageyama, Kenzo Onizuka, Touru Yamauchi, Yutaka Ueda, Shingo Hane, Hiroyuki Mitamura, Tsuneaki Goto, Kazuyoshi Yoshimura and Koji Kosuge. *Anomalous Magnetizations in Single Crystalline $SrCu_2(BO_3)_2$.* J. Phys. Soc. Jpn., vol. 68, no. 6, pages 1821–1823, 1999.

[Kageyama 2000] H. Kageyama, M. Nishi, N. Aso, K. Onizuka, T. Yosihama, K. Nukui, K. Kodama, K. Kakurai and Y. Ueda. *Direct Evidence for the Localized Single-Triplet Excitations and the Dispersive Multitriplet Excitations in $SrCu_2(BO_3)_2$.* Phys. Rev. Lett., vol. 84, no. 25, pages 5876–, June 2000.

[Kageyama 2002] Hiroshi Kageyama, Yutaka Ueda, Yasuo Narumi, Koichi Kindo, Masashi Kosaka and Yoshiya Uwatoko. *Crossbreeding between Experiment and Theory on Orthogonal Dimer Spin System.* Progress of Theoretical Physics Supplement, vol. 145, pages 17–22, 2002.

[Kanamori 1963] Junjiro Kanamori. *Electron Correlation and Ferromagnetism of Transition Metals.* Progress of Theoretical Physics, vol. 30, no. 3, pages 275–289, 1963.

[Kapitza 1938] P. Kapitza. *Viscosity of Liquid Helium below the Lambda-Point.* Nature, vol. 141, page 74, Jan 1938.

[Katsura 2005] Hosho Katsura, Naoto Nagaosa and Alexander V. Balatsky. *Spin Current and Magnetoelectric Effect in Noncollinear Magnets.* Phys. Rev. Lett., vol. 95, page 057205, Jul 2005.

[Kézsmárki 2011] I. Kézsmárki, N. Kida, H. Murakawa, S. Bordács, Y. Onose and Y. Tokura. *Enhanced Directional Dichroism of Terahertz Light in Resonance with Magnetic Excitations of the Multiferroic* $Ba_2CoGe_2O_7$ *Oxide Compound.* Phys. Rev. Lett., vol. 106, page 057403, Feb 2011.

[Kim 2004] E. Kim and M. H. W. Chan. *Probable observation of a supersolid helium phase.* Nature, vol. 427, no. 6971, pages 225–227, Jan 2004.

[Kimura 2003] T. Kimura, T. Goto, H. Shintani, K. Ishizaka, T. Arima and Y. Tokura. *Magnetic control of ferroelectric polarization.* Nature, vol. 426, page 55, Nov 2003.

[Kimura 2006] T. Kimura, J. C. Lashley and A. P. Ramirez. *Inversion-symmetry breaking in the noncollinear magnetic phase of the triangular-lattice antiferromagnet* $CuFeO_2$. Phys. Rev. B, vol. 73, page 220401, Jun 2006.

[Kimura 2008] T. Kimura, Y. Sekio, H. Nakamura, T. Siegrist and A. P. Ramirez. *Cupric oxide as an induced-multiferroic with high-TC.* Nature Materials, vol. 7, page 291, Apr 2008.

[Klanjšek 2008] M. Klanjšek, H. Mayaffre, C. Berthier, M. Horvatić, B. Chiari, O. Piovesana, P. Bouillot, C. Kollath, E. Orignac, R. Citro and T. Giamarchi. *Controlling Luttinger Liquid Physics in Spin Ladders under a Magnetic Field.* Phys. Rev. Lett., vol. 101, page 137207, Sep 2008.

[Knetter 2000] Christian Knetter, Alexander Bühler, Erwin Müller-Hartmann and Götz S. Uhrig. *Dispersion and Symmetry of Bound States in the Shastry-Sutherland Model.* Phys. Rev. Lett., vol. 85, no. 18, pages 3958–, October 2000.

[Kodama 2002] K. Kodama, M. Takigawa, M. Horvatic, C. Berthier, H. Kageyama, Y. Ueda, S. Miyahara, F. Becca and F. Mila. *Magnetic Superstructure*

in the Two-Dimensional Quantum Antiferromagnet $SrCu_2(BO_3)_2$. Science, vol. 298, no. 5592, pages 395–399, 2002.

[Kodama 2005] K Kodama, S Miyahara, M Takigawa, M Horvatićand C Berthier, F Mila, H Kageyama and Y Ueda. *Field-induced effects of anisotropic magnetic interactions in $SrCu_2(BO_3)_2$.* J. Phys.: Condensed Matt, vol. 17, no. 4, page L61, 2005.

[Koga 2000] Akihisa Koga and Norio Kawakami. *Quantum Phase Transitions in the Shastry-Sutherland Model for $SrCu_2(BO_3)_2$.* Phys. Rev. Lett., vol. 84, no. 19, pages 4461–, May 2000.

[Kohno 1997] Masanori Kohno and Minoru Takahashi. *Magnetization process of the spin-$\frac{1}{2}$ XXZ models on square and cubic lattices.* Phys. Rev. B, vol. 56, pages 3212–3217, Aug 1997.

[Kondo 2007] M. Kondo, S. Takada, Y. Shibayama and K. Shirahama. *Observation of Non-Classical Rotational Inertia in Bulk Solid 4 He.* J. Low Temp. Phys., vol. 148, pages 695–699, 2007. 10.1007/s10909-007-9471-1.

[Kubo 1952] Ryogo Kubo. *The Spin-Wave Theory of Antiferromagnetics.* Phys. Rev., vol. 87, pages 568–580, Aug 1952.

[Laflorencie 2007] Nicolas Laflorencie and Frédéric Mila. *Quantum and Thermal Transitions Out of the Supersolid Phase of a 2D Quantum Antiferromagnet.* Phys. Rev. Lett., vol. 99, no. 2, page 027202, Jul 2007.

[Läuchli 2002a] A. Läuchli, S. Wessel and M. Sigrist. *Phase diagram of the quadrumerized Shastry-Sutherland model.* Phys. Rev. B., vol. 66, page 014401, 2002.

[Läuchli 2002b] Andreas Läuchli, Stefan Wessel and Manfred Sigrist. *Phase diagram of the quadrumerized Shastry-Sutherland model.* Phys. Rev. B, vol. 66, no. 1, pages 014401–, June 2002.

[Läuchli 2005] A. Läuchli, J. C. Domenge, C. Lhuillier, P. Sindzingre and M. Troyer. *Two-Step Restoration of SU(2) Symmetry in a Frustrated Ring-Exchange Magnet.* Phys. Rev. Lett., vol. 95, no. 13, page 137206, 2005.

[Lawes 2005] G. Lawes, A. B. Harris, T. Kimura, N. Rogado, R. J. Cava, A. Aharony, O. Entin-Wohlman, T. Yildrim, M. Kenzelmann, C. Broholm and A. P. Ramirez. *Magnetically Driven Ferroelectric Order in* $Ni_3V_2O_8$. Phys. Rev. Lett., vol. 95, page 087205, Aug 2005.

[Leggett 1970] A. J. Leggett. *Can a Solid Be "Superfluid"?* Phys. Rev. Lett., vol. 25, no. 22, pages 1543–1546, Nov 1970.

[Leggett 2004] Tony Leggett. *Superfluidity in a Crystal?* Science, vol. 305, no. 5692, pages 1921–1922, 2004.

[Liu 1973] Kao-Shien Liu and Michael E. Fisher. *Quantum lattice gas and the existence of a supersolid.* Journal of Low Temperature Physics, vol. 10, pages 655–683, 1973. 10.1007/BF00655458.

[London 1938] F. London. *The Lambda-Phenomenon of Liquid Helium and the Bose-Einstein Degeneracy.* Nature, vol. 141, pages 643–644, Apr 1938.

[Majumdar 1969] Chanchal K. Majumdar and Dipan K. Ghosh. *On Next-Nearest-Neighbor Interaction in Linear Chain. I.* Journal of Mathematical Physics, vol. 10, no. 8, pages 1388–1398, 1969.

[Masuda 2002] T. Masuda, K. Uchinokura, T. Hayashi and N. Miura. *Impurity-induced antiferromagnetic phase in a doped Haldane system* $\mathrm{Pb(Ni_{1-x}Mg_x)_2\%mathrmV_2O_8}$. Phys. Rev. B, vol. 66, page 174416, Nov 2002.

[Matsuda 1970] Hirotsugu Matsuda and Toshihiko Tsuneto. *Off-Diagonal Long-Range Order in Solids.* Progress of Theoretical Physics Supplement, vol. 46, pages 411–436, 1970.

[Mazurenko 2008] V. V. Mazurenko, S. L. Skornyakov, V. I. Anisimov and F. Mila. *First-principles investigation of symmetric and antisymmetric exchange interactions of* $SrCu_2(BO_3)_2$. Phys. Rev. B, vol. 78, no. 19, pages 195110–, November 2008.

[Melko 2005] R. G. Melko, A. Paramekanti, A. A. Burkov, A. Vishwanath, D. N. Sheng and L. Balents. *Supersolid Order from Disorder: Hard-Core Bosons on the Triangular Lattice.* Phys. Rev. Lett., vol. 95, no. 12, page 127207, Sep 2005.

[Mila 2000] F. Mila. *Quantum spin liquids.* European Journal of Physics, vol. 21, no. 6, page 499, 2000.

[Misguich 2005] G. Misguich and C. Lhuillier. Frustrated spin systems, chapitre 5. World Scientific, Singapore, 2005.

[Miyahara 1999] Shin Miyahara and Kazuo Ueda. *Exact Dimer Ground State of the Two Dimensional Heisenberg Spin System* $SrCu_2(BO_3)_2$. Phys. Rev. Lett., vol. 82, no. 18, pages 3701–, May 1999.

[Miyahara 2000] Shin Miyahara and Kazuo Ueda. *Superstructures at magnetization plateaus in* $SrCu_2(BO_3)_2$. Phys. Rev. B, vol. 61, no. 5, pages 3417–, February 2000.

[Miyahara 2003] Shin Miyahara and Kazuo Ueda. *Theory of the orthogonal dimer Heisenberg spin model for* $SrCu_2(BO_3)_2$. J. Phys.: Condens. Matter, vol. 15, no. 9, page R327, 2003.

[Miyahara 2005] Shin Miyahara and Frédéric Mila. *The Effects of Dzyaloshinsky-Moriya Interaction in the Orthogonal Dimer Heisenberg Model for $SrCu_2(BO_3)_2$.* Prog. Theor. Phys. Suppl., vol. 159, pages 33–38, 2005.

[Miyahara 2011] Shin Miyahara and Nobuo Furukawa. *Theory of Magnetoelectric Resonance in Two-Dimensional $S = 3/2$ Antiferromagnet $Ba_2CoGe_2O_7$ via Spin-Dependent Metal-Ligand Hybridization Mechanism.* Journal of the Physical Society of Japan, vol. 80, no. 7, page 073708, 2011.

[Mochizuki 2010] Masahito Mochizuki, Nobuo Furukawa and Naoto Nagaosa. *Spin Model of Magnetostrictions in Multiferroic Mn Perovskites.* Phys. Rev. Lett., vol. 105, page 037205, Jul 2010.

[Momoi 2000a] Tsutomu Momoi and Keisuke Totsuka. Phys. Rev. B, vol. 61, pages 3231–, 2000.

[Momoi 2000b] Tsutomu Momoi and Keisuke Totsuka. *Magnetization plateaus of the Shastry-Sutherland model for $SrCu_2(BO_3)_2$: Spin-density wave, supersolid, and bound states.* Phys. Rev. B, vol. 62, no. 22, pages 15067–, December 2000.

[Moriya 1960] Tôru Moriya. *Anisotropic Superexchange Interaction and Weak Ferromagnetism.* Phys. Rev., vol. 120, pages 91–98, Oct 1960.

[Motoyama 1996] N. Motoyama, H. Eisaki and S. Uchida. *Magnetic Susceptibility of Ideal Spin 1 /2 Heisenberg Antiferromagnetic Chain Systems,* Sr_2CuO_3 *and* $SrCuO_2$. Phys. Rev. Lett., vol. 76, pages 3212–3215, Apr 1996.

[Murakawa 2010] H. Murakawa, Y. Onose, S. Miyahara, N. Furukawa and Y. Tokura. *Ferroelectricity Induced by Spin-Dependent Metal-Ligand Hybridization in* $Ba_2CoGe_2\mathbf{O}_7$. Phys. Rev. Lett., vol. 105, page 137202, Sep 2010.

[Ng 2006] Kwai-Kong Ng and T. K. Lee. *Supersolid Phase in Spin Dimer XXZ Systems under a Magnetic Field.* Phys. Rev. Lett., vol. 97, no. 12, page 127204, Sep 2006.

[Nilsen 2011] G. J. Nilsen, F. C. Coomer, M. A. de Vries, J. R. Stewart, P. P. Deen, A. Harrison and H. M. Rønnow. *Pair correlations, short-range order, and dispersive excitations in the quasi-kagome quantum magnet volborthite.* Phys. Rev. B, vol. 84, page 172401, Nov 2011.

[Noda 2008] Y Noda, H Kimura, M Fukunaga, S Kobayashi, I Kagomiya and K Kohn. *Magnetic and ferroelectric properties of multiferroic RMn 2 O 5.* Journal of Physics: Condensed Matter, vol. 20, no. 43, page 434206, 2008.

[Nojiri 1999] Hiroyuki Nojiri, Hiroshi Kageyama, Kenzo Onizuka, Yutaka Ueda and Mitsuhiro Motokawa. *Direct Observation of the Multiple Spin Gap Excitations in Two-Dimensional Dimer System $SrCu_2(BO_3)_2$.* J. Phys. Soc. Jpn., vol. 68, no. 9, pages 2906–2909, 1999.

[Nojiri 2003] Hiroyuki Nojiri, Hiroshi Kageyama, Yutaka Ueda and Mitsuhiro Motokawa. *ESR Study on the Excited State Energy Spectrum of $SrCu_2(BO_3)_2$ —A Central Role of Multiple-Triplet Bound States—.* J. Phys. Soc. Jpn., vol. 72, no. 12, pages 3243–3253, 2003.

[Okamoto 1992] Kiyomi Okamoto and Kiyohide Nomura. *Fluid-dimer critical point in S = 12 antiferromagnetic Heisenberg chain with next nearest neighbor interactions.* Physics Letters A, vol. 169, no. 6, pages 433 – 437, 1992.

[Okamoto 2007] Yoshihiko Okamoto, Minoru Nohara, Hiroko Aruga-Katori and Hidenori Takagi. *Spin-Liquid State in the $S = 1/2$ Hyperkagome Antiferromagnet $Na_4Ir_3O_8$.* Phys. Rev. Lett., vol. 99, page 137207, Sep 2007.

[Olariu 2008] A. Olariu, P. Mendels, F. Bert, F. Duc, J. C. Trombe, M. A. de Vries and A. Harrison. *^{17}O NMR Study of the Intrinsic Magnetic Susceptibility and Spin Dynamics of the Quantum Kagome Antiferromagnet $ZnCu_3(OH)_6Cl_2$.* Phys. Rev. Lett., vol. 100, page 087202, Feb 2008.

[Onizuka 2000] Kenzo Onizuka, Hiroshi Kageyama, Yasuo Narumi, Koichi Kindo, Yutaka Ueda and Tsuneaki Goto. *1/3 Magnetization Plateau in $SrCu_2(BO_3)_2$- Stripe Order of Excited Triplets* -. J. Phys. Soc. Jpn., vol. 69, no. 4, pages 1016–1018, 2000.

[Onufrieva 1985] F.P. Onufrieva. *LOW-TEMPERATURE PROPERTIES OF SPIN SYSTEMS WITH TENSOR ORDER PARAMETERS.* ZHURNAL EKSPERIMENTALNOI I TEORETICHESKOI FIZIKI, vol. 89, no. 6, pages 2270–2287, DEC 1985.

[Papanicolaou 1984] N. Papanicolaou. *Pseudospin approach for planar ferromagnets.* Nuclear Physics B, vol. 240, no. 3, pages 281 – 311, 1984.

[Papanicolaou 1988] N. Papanicolaou. *Unusual phases in quantum spin-1 systems.* Nuclear Physics B, vol. 305, no. 3, pages 367 – 395, 1988.

[Park 2007] S. Park, Y. J. Choi, C. L. Zhang and S-W. Cheong. *Ferroelectricity in an $S = 1/2$ Chain Cuprate.* Phys. Rev. Lett., vol. 98, page 057601, Jan 2007.

[Penc 2012] K. Penc, J. Romhányi, T. Rõõm, U. Nagel, Á. Antal, T. Fehér, A. Jánossy, H. Engelkamp, H. Murakawa, Y. Tokura, D. Szaller, S. Bordács and I. Kézsmárki. *Spin-stretching modes in anisotropic magnets: spin-wave excitations in the multiferroic Ba2CoGe2O7.* ArXiv e-prints, February 2012.

[Penrose 1951] O. Penrose. *CXXXVI. On the quantum mechanics of helium II.* Philosophical Magazine Series 7, vol. 42, no. 335, pages 1373–1377, 1951.

[Penrose 1956] Oliver Penrose and Lars Onsager. *Bose-Einstein Condensation and Liquid Helium.* Phys. Rev., vol. 104, no. 3, pages 576–584, Nov 1956.

[Peters 2009] D. Peters, I. P. McCulloch and W. Selke. *Spin-one Heisenberg antiferromagnetic chain with exchange and single-ion anisotropies.* Phys. Rev. B, vol. 79, page 132406, Apr 2009.

[Peters 2010] D Peters, I P McCulloch and W Selke. *Quantum Heisenberg antiferromagnetic chains with exchange and single-ion anisotropies.* Journal of Physics: Conference Series, vol. 200, no. 2, page 022046, 2010.

[Picon 2008] J.-D. Picon, A. F. Albuquerque, K. P. Schmidt, N. Laflorencie, M. Troyer and F. Mila. *Mechanisms for spin supersolidity in $S = \frac{1}{2}$ spin-dimer antiferromagnets.* Phys. Rev. B, vol. 78, page 184418, Nov 2008.

[Quilliam 2011] J. A. Quilliam, F. Bert, R. H. Colman, D. Boldrin, A. S. Wills and P. Mendels. *Ground state and intrinsic susceptibility of the kagome antiferromagnet vesignieite as seen by ^{51}V NMR.* Phys. Rev. B, vol. 84, page 180401, Nov 2011.

[Rõõm 2000] T. Rõõm, U. Nagel, E. Lippmaa, H. Kageyama, K. Onizuka and Y. Ueda. *Far-infrared study of the two-dimensional dimer spin system $SrCu_2(BO_3)_2$.* Phys. Rev. B, vol. 61, no. 21, pages 14342–, June 2000.

[Rõõm 2004] T. Rõõm, D. Hüvonen, U. Nagel, J. Hwang, T. Timusk and H. Kageyama. *Far-infrared spectroscopy of spin excitations and Dzyaloshinskii-Moriya interactions in the Shastry-Sutherland compound $SrCu_2(BO_3)_2$.* Phys. Rev. B, vol. 70, no. 14, pages 144417–, October 2004.

[Ramirez 1994] A. P. Ramirez, S-W. Cheong and M. L. Kaplan. *Specific heat of defects in Haldane systems Y_2BaNiO_5 and NENP: Absence of free spin-1/2 excitations.* Phys. Rev. Lett., vol. 72, pages 3108–3111, May 1994.

[Rittner 2006] Ann Sophie C. Rittner and John D. Reppy. *Observation of Classical Rotational Inertia and Nonclassical Supersolid Signals in Solid $He4$ below 250 mK.* Phys. Rev. Lett., vol. 97, no. 16, page 165301, Oct 2006.

[Romhányi 2011] Judit Romhányi, Miklós Lajkó and Karlo Penc. *Zero- and finite-temperature mean field study of magnetic field induced electric polarization in $Ba_2CoGe_2O_7$: Effect of the antiferroelectric coupling.* Phys. Rev. B, vol. 84, page 224419, Dec 2011.

[Rossini 2011] Davide Rossini, Vittorio Giovannetti and Rosario Fazio. *Spin-supersolid phase in Heisenberg chains: A characterization via matrix product states with periodic boundary conditions.* Phys. Rev. B, vol. 83, page 140411, Apr 2011.

[Sachdev 1990] Subir Sachdev and R. N. Bhatt. *Bond-operator representation of quantum spins: Mean-field theory of frustrated quantum Heisenberg antiferromagnets.* Phys. Rev. B, vol. 41, no. 13, pages 9323–9329, 1990.

[Sato 2003] T. Sato, T. Masuda and K. Uchinokura. *Magnetic property of Ba2CoGe2O7.* Physica B: Condensed Matter, vol. 329Ð333, Part 2, no. 0, pages 880 – 881, 2003. <ce:title>Proceedings of the 23rd International Conference on Low Temperature Physics</ce:title>.

[Schmidt 2008] K. P. Schmidt, J. Dorier, A. M. Läuchli and F. Mila. *Supersolid Phase Induced by Correlated Hopping in Spin-1/2 Frustrated Quantum Magnets.* Phys. Rev. Lett., vol. 100, page 090401, Mar 2008.

[Seabra 2011] Luis Seabra and Nic Shannon. *Competition between supersolid phases and magnetization plateaus in the frustrated easy-axis antiferromagnet on a triangular lattice.* Phys. Rev. B, vol. 83, no. 13, page 134412, Apr 2011.

[Sengupta 2005] Pinaki Sengupta, Leonid P. Pryadko, Fabien Alet, Matthias Troyer and Guido Schmid. *Supersolids versus Phase Separation in Two-Dimensional Lattice Bosons.* Phys. Rev. Lett., vol. 94, no. 20, page 207202, May 2005.

[Sengupta 2007a] P. Sengupta and C. D. Batista. *Field-Induced Supersolid Phase in Spin-One Heisenberg Models.* Phys. Rev. Lett., vol. 98, no. 22, page 227201, May 2007.

[Sengupta 2007b] P. Sengupta and C. D. Batista. *Spin Supersolid in an Anisotropic Spin-One Heisenberg Chain.* Phys. Rev. Lett., vol. 99, page 217205, Nov 2007.

[Sergienko 2006] I. A. Sergienko and E. Dagotto. *Role of the Dzyaloshinskii-Moriya interaction in multiferroic perovskites.* Phys. Rev. B, vol. 73, page 094434, Mar 2006.

[Shastry 1981] S. Shastry and B. Sutherland. Physica B&C, vol. 108, page 1069, 1981.

[Shiina 2003] Ryousuke Shiina, Hiroyuki Shiba, Peter Thalmeier, Atsushi Takahashi and Osamu Sakai. *Dynamics of Multipoles and Neutron Scattering Spectra in Quadrupolar Ordering Phase of CeB_6.* Journal of the Physical Society of Japan, vol. 72, no. 5, pages 1216–1225, 2003.

[Shimizu 2003] Y. Shimizu, K. Miyagawa, K. Kanoda, M. Maesato and G. Saito. *Spin Liquid State in an Organic Mott Insulator with a Triangular Lattice.* Phys. Rev. Lett., vol. 91, page 107001, Sep 2003.

[Smirnov 2002] A. I. Smirnov, V. N. Glazkov, H.-A. Krug von Nidda, A. Loidl, L. N. Demianets and A. Ya. Shapiro. *Paramagnetic and antiferromagnetic resonances in the diamagnetically diluted Haldane magnet* $PbNi_2V_2O_8$. Phys. Rev. B, vol. 65, page 174422, May 2002.

[Smith 1991] R.W. Smith and D.A. Keszler. J. Solid State Chem., vol. 93, page 430, 1991.

[Sólyom 1984] J. Sólyom and T. A. L. Ziman. *Ground-state properties of axially anisotropic quantum Heisenberg chains.* Phys. Rev. B, vol. 30, no. 7, pages 3980–3992, Oct 1984.

[Sparta 2001] K. Sparta, G.J. Redhammer, P. Roussel, G. Heger, G. Roth, P. Lemmens, A. Ionescu, M. Grove, G. Güntherodt, F. Hüning, H. Lueken, H. Kageyama, K. Onizuka and Y. Ueda. *Structural phase transition in the 2D spin dimer compound* $SrCu_2(BO_3)_2$. Eur. Phys. J. B, vol. 19, no. 4, pages 507–516, 2001.

[Takigawa 2010] Masashi Takigawa, Takeshi Waki, Mladen Horvatić and Claude Berthier. *Novel Ordered Phases in the Orthogonal Dimer Spin System* $SrCu_2(BO_3)_2$. J. Phys. Soc. Jpn., vol. 79, no. 1, page 011005, 2010.

[Taniguchi 1995] Satoshi Taniguchi, Takashi Nishikawa, Yukio Yasui, Yoshiaki Kobayashi, Masatoshi Sato, Takashi Nishioka, Masaaki Kontani and Kazuhiro Sano. *Spin Gap Behavior of* $S = 1/2$ *Quasi-Two-Dimensional System* CaV_4O_9. Journal of the Physical Society of Japan, vol. 64, no. 8, pages 2758–2761, 1995.

[Taniguchi 2006] K. Taniguchi, N. Abe, T. Takenobu, Y. Iwasa and T. Arima. *Ferroelectric Polarization Flop in a Frustrated Magnet* $MnWO_4$ *Induced by a Magnetic Field.* Phys. Rev. Lett., vol. 97, page 097203, Aug 2006.

[Toledano 2011] Pierre Toledano, Dmitry D. Khalyavin and Laurent C. Chapon. *Spontaneous toroidal moment and field-induced magnetotoroidic effects in* $Ba_2CoGe_2O_7$. Phys. Rev. B, vol. 84, page 094421, Sep 2011.

[Ueda 1998] Yutaka Ueda. *Vanadate Family as Spin-Gap Systems.* Chemistry of Materials, vol. 10, no. 10, pages 2653–2664, 1998.

[Ueda 2010] Hiroaki T. Ueda and Keisuke Totsuka. *Supersolid phase of three-dimensional spin- and hardcore-boson models.* Phys. Rev. B, vol. 81, no. 5, page 054442, Feb 2010.

[Wessel 2005] Stefan Wessel and Matthias Troyer. *Supersolid Hard-Core Bosons on the Triangular Lattice.* Phys. Rev. Lett., vol. 95, no. 12, page 127205, Sep 2005.

[White 1992] S. R. White. Phys. Rev. Lett., vol. 69, page 2863, 1992.

[Yamamoto 2009] Keisuke Yamamoto, Synge Todo and Seiji Miyashita. *Successive phase transitions at finite temperatures toward the supersolid state in a three-dimensional extended Bose-Hubbard model.* Phys. Rev. B, vol. 79, page 094503, Mar 2009.

[Yamasaki 2006] Y. Yamasaki, S. Miyasaka, Y. Kaneko, J.-P. He, T. Arima and Y. Tokura. *Magnetic Reversal of the Ferroelectric Polarization in a Multiferroic Spinel Oxide.* Phys. Rev. Lett., vol. 96, page 207204, May 2006.

[Yang 1962] C. N. Yang. *Concept of Off-Diagonal Long-Range Order and the Quantum Phases of Liquid He and of Superconductors.* Rev. Mod. Phys., vol. 34, no. 4, pages 694–704, Oct 1962.

[Yi 2008] H. T. Yi, Y. J. Choi, S. Lee and S.-W. Cheong. *Multiferroicity in the square-lattice antiferromagnet of Ba2CoGe2O7.* vol. 92, no. 21, page 212904, 2008.

[Yoshida 2009] M. Yoshida, M. Takigawa, H. Yoshida, Y. Okamoto and Z. Hiroi. *Phase Diagram and Spin Dynamics in Volborthite with a Distorted Kagome Lattice.* Phys. Rev. Lett., vol. 103, page 077207, Aug 2009.

[Yunoki 2002] Seiji Yunoki. *Numerical study of the spin-flop transition in anisotropic spin-$\frac{1}{2}$ antiferromagnets.* Phys. Rev. B, vol. 65, page 092402, Jan 2002.

[Zheludev 2003] A. Zheludev, T. Sato, T. Masuda, K. Uchinokura, G. Shirane and B. Roessli. *Spin waves and the origin of commensurate magnetism in* $Ba_2CoGe_2O_7$. Phys. Rev. B, vol. 68, page 024428, Jul 2003.

[Zorko 2008] A. Zorko, S. Nellutla, J. van Tol, L. C. Brunel, F. Bert, F. Duc, J.-C. Trombe, M. A. de Vries, A. Harrison and P. Mendels. *Dzyaloshinsky-Moriya Anisotropy in the Spin-1/2 Kagome Compound* $ZnCu_3(OH)_6Cl_2$. Phys. Rev. Lett., vol. 101, page 026405, Jul 2008.